

**UNIVERSITE DE STRASBOURG**

UMR 7357 – Laboratoire des sciences de l'ingénieur, de l'informatique et de l'imagerie - ICube

**ÉCOLE DOCTORALE MATHÉMATIQUES SCIENCES DE L'INFORMATION ET DE L'INGÉNIEUR**

**THESE**

En vue de l'obtention du grade de

**Docteur de l'Université de Strasbourg**

**Discipline** : Science pour l'ingénieur

**Spécialité** : Génie des Procédés et Energétique

Présentée par

**Boutheina Merad**

**Experimental Study of the Mechanical Behavior of Organoclay-Stabilized Pickering Emulsions**

Soutenue publiquement le 19/04/2021

**JURY**

Président du jury	Chérif NOUAR, Directeur de Recherches — CNRS	LEMTA / CNRS
Rapporteur	Yacine HEMAR, Professeur	Guangdong Technion Israel Institute
Rapporteur	Philippe COUSSOT, Professeur	Laboratoire Navier / IFSTTAR
Examinatrice	Dominique DUPUIS, Professeure, Émérite	Université de Haute-Alsace — ENSISA
Examineur	Pierre FRANÇOIS, MC - HDR	Université de Strasbourg / ICUBE, UMR 7357
Examineur	René MULLER, Professeur	Université de Strasbourg — Institut Charles Sadron
Directeur de thèse	Karim BEKKOUR, MC-CE- HDR	Université de Strasbourg / ICUBE, UMR 7357
Co-directeur de thèse	Mourad GARECHE, MC A	Université M'hamed Bougara / LGPH



*The challenge is not to be perfect, it's to be whole.*

Jane Fonda

*I am always busy, which is perhaps the chief reason why I am always well.*

Elizabeth Candy Stanton



To my parents

To my brothers and sister

To my beloved husband



## Acknowledgements

First and foremost, I would like to thank my supervisors, Karim Bekkour and Mourad Gareche for their continuous support and inestimable advice during all the ups and downs of my PhD study. Thank you for believing in me, for giving me this invaluable opportunity, and for sharing with me a part of your scientific knowledge.

I cannot write this page without thanking Pierre François and Fabrice Lawniczak for their technical and scientific support. Without your help, I would never have accomplished the two final chapters of this project. Thank you, Fabrice, for the extra time that you spent with me working on the flow loop, and thank you, Pierre, for the Saturdays that we spent together trying to explain the weird behavior of the Pickering emulsions.

I would also like to thank Pr. Coussot and Pr. Hemar, my thesis referees, for giving me some of their precious time, for their pertinent comments, and for their tremendous help to enhance the quality of the present manuscript. My deepest gratitude goes also to Dr. Nouar, for accepting to chair the jury committee, and to Pr. Muller and Pr. Dupuis for their valuable advice and for the nice scientific discussions.

During the three years spent at ICube, I had the chance to meet many inspiring personalities, Yannick, the person that you should go to if you need anything and who's also our lab manager, Michael, our IT savior, Catherine, to whom I would like to send a special thanks for supporting the insupportable odor of gasoil for over 9 months, and all my doctoral colleagues at ICube (the list of names would be endless).

There are no words to express my gratitude to all of you who were part of this journey, I will therefore simply say thank you!

Ce dernier paragraphe est dédié à ma famille, sans laquelle je n'aurais jamais pu arriver jusqu'ici. Merci à ma chère maman qui m'a appris le vrai sens du dévouement et de la persévérance. Merci à mon héros, mon cher papa, qui a, depuis ma naissance, cru en moi. Et je ne peux pas écrire ces lignes sans remercier mon meilleur ami et mon mari qui m'a appris à ne jamais baisser les bras.

Boutheina Merad

May, 2021



## Déclaration sur l'honneur

### *Declaration of Honour*

J'affirme être informé que le plagiat est une faute grave susceptible de mener à des sanctions administratives et disciplinaires pouvant aller jusqu'au renvoi de l'Université de Strasbourg et passible de poursuites devant les tribunaux de la République Française.

Je suis conscient(e) que l'absence de citation claire et transparente d'une source empruntée à un tiers (texte, idée, raisonnement ou autre création) est constitutive de plagiat.

Au vu de ce qui précède, **j'atteste sur l'honneur que le travail décrit dans mon manuscrit de thèse est un travail original et que je n'ai pas eu recours au plagiat ou à toute autre forme de fraude.**

*I affirm that I am aware that plagiarism is a serious misconduct that may lead to administrative and disciplinary sanctions up to dismissal from the University of Strasbourg and liable to prosecution in the courts of the French Republic.*

*I am aware that the absence of a clear and transparent citation of a source borrowed from a third party (text, idea, reasoning or other creation) is constitutive of plagiarism.*

*In view of the foregoing, I hereby certify that the work described in my thesis manuscript is original work and that I have not resorted to plagiarism or any other form of fraud.*

**Nom : Merad Prénom : Boutheina**

**Ecole doctorale : [Mathématiques Sciences de l'Information et de l'Ingenieur](#)**

**Laboratoire : [Laboratoire des sciences de l'ingénieur, de l'informatique et de l'imagerie - ICube](#)**

**Date : 19-05-2021**

**Signature :**



# **TABLE OF CONTENTS**

## TABLE OF CONTENTS

INTRODUCTION .....	2
CHAPTER 1 REVIEW OF THE LITERATURE .....	10
1.1 Introduction.....	13
1.2 Basics of rheology.....	13
1.2.1 Simple shear flow .....	13
1.2.2 Newtonian behavior .....	15
1.2.3 Non-Newtonian behavior .....	16
1.3 Pipe-flow of non-Newtonian fluids .....	26
1.3.1 Flow regimes in circular pipes .....	27
1.3.2 Fundamental background on Poiseuille flow of yield fluids.....	28
1.4 Organoclays .....	34
1.4.1 Microstructure of clay minerals .....	35
1.4.2 Smectite clays.....	36
1.4.3 Composition, preparation and swelling of organoclays.....	37
1.5 Pickering emulsions.....	42
1.6 Summary to Chapter .....	43
1.7 References.....	44
CHAPTER 2. MATERIALS AND METHODS.....	53
2.1 Introduction.....	56
2.2 Rheological measurement techniques .....	56
2.2.1 Measuring geometry .....	57
2.2.2 Experimental problems inducing measuring errors.....	58
2.3 Hydraulic loop.....	59
2.3.1 Pump calibration .....	63
2.3.2 Testing system .....	64
2.3.3 Emulsification system.....	70
2.4 Fluid preparation protocol .....	70
2.5 Summary to Chapter .....	71
2.6 References.....	73

CHAPTER 3. RHEOLOGICAL BEHAVIOR OF ORGANO-HECTORITE DISPERSIONS.....	76
3.1 Introduction.....	79
3.2 Literature review .....	79
3.3 Experimental protocol.....	81
3.4 Aging behavior.....	82
3.5 Shear flow experiments.....	83
3.5.1 Macrostructural behavior.....	84
3.5.2 Microstructural behavior.....	86
3.5.3 Yielding behavior .....	91
3.6 Viscoelastic properties .....	95
3.6.1 Oscillatory shear experiments.....	95
3.6.2 Creep and recovery experiments .....	100
3.6.3 Evolution of the viscoelastic properties .....	104
3.7 Visual aspects .....	106
3.8 Summary to chapter.....	107
3.9 References.....	109
CHAPTER 4. RHEOLOGICAL AND FLOW BEHAVIOR OF ORGANO-HECTORITE BASED EMULSIONS..	113
4.1 Introduction.....	116
4.2 Literature review .....	116
4.3 Experimental Protocol.....	120
4.4 Rheological behavior .....	121
4.4.1 Shear flow experiments.....	121
4.4.2 Viscoelastic Properties .....	124
4.4.3 Limitations of rheological measurements.....	127
4.5 Pipe-flow behavior .....	129
4.5.1 Chronological sequence of measurements.....	129
4.5.2 Flow parameters during the emulsification process.....	130
4.5.3 Flow parameters during the homogenization process .....	132
4.5.4 Verification of the flow regimes.....	133
4.5.5 Comparison between flow measurements and rheology.....	136
4.5.6 Emulsion stability .....	140
4.6 Visual aspects .....	145
4.7 Summary to chapter.....	146
4.8 References.....	148
CHAPTER 5. FLOW BEHAVIOR OF CONCENTRATED ORGANO-HECTORITE BASED EMULSIONS....	154
5.1 Introduction.....	157

5.2	Literature review .....	157
5.3	Experimental Protocol .....	161
5.3.1	Emulsification process .....	161
5.3.2	Homogenization process .....	164
5.3.3	Verification of oil/water fractions .....	166
5.4	Flow behavior of concentrated Pickering emulsions .....	168
5.4.1	Stable emulsion .....	170
5.4.2	Unstable emulsion .....	173
5.5	Attenuation measurements .....	179
5.6	Summary to chapter .....	181
5.7	References .....	182
CONCLUSIONS AND PERSPECTIVES .....		186



# **INTRODUCTION**

## INTRODUCTION

## INTRODUCTION

The present work was co-financed by the ICube Laboratory - University of Strasbourg, the Laboratory of Génie Physique des Hydrocarbures - University of Boumerdes, and the Franco-Algerian scholarship Profas B +. This thesis is a contribution to the experimental study of rheological and flow behaviors of Pickering emulsions. Moreover, the preparation of these systems through an in-line continuous circulation as well as the study of their pipe-flow behavior are important added values of this work, as it remains an under-studied subject to date.

A vinaigrette, a moisturizing cream, an infusion solution, a sealing joint or even an inverse emulsion drilling fluid, are all emulsion-based products widely used in our everyday life and by industrials. These emulsions are generally stabilized by surfactants (also called surface active agents), and their preparation as well as their mechanical characteristics are already well documented in the literature. Furthermore, the market share of surfactants is one of the highest within the chemicals market with a value of 42120,3 M€, and a global consumption of 380 kg per second\*. Beyond its economic impact, massive use of surfactants is dangerous to the environment and to the human being (Zoller, 2019), hence the increasing demand to alternative emulsion stabilizers.

What if we can produce emulsions with strong long-term stability, using less expensive materials while, simultaneously, controlling and optimizing the dispersing phase droplet size, wouldn't that be interesting?

In the last 2 decades, an increasing interest in emulsions stabilized by solid particles has been noticed. Also known as "Pickering", these emulsions are stabilized through the adsorption of solid particles, with both hydrophobic and hydrophilic characteristics, on the oil/water interface. Depending on the nature, wettability and surface modification of the used solid particles, the prepared emulsion can be direct (oil in water) or inverse (water in oil).

The main objective of this work is to prepare and optimize the composition of a surfactant-free inverse emulsion, stabilized using a modified hectorite, with a comparable mechanical behavior to that of inverse emulsion drilling fluids.

Inverse emulsion drilling fluids are usually used to drill the reservoir rock (porous and permeable medium). In addition to their high cost and toxicity (Fig. 1), surfactants, used to stabilize drilling fluids, are the cause of an important damage to the reservoir rock, by reversing its wettability from water-wet to oil-wet (Donaldson et al., 1969; McDonald and Buller, 1992; Jiao and Sharma, 1993; Masalmeh, 2002; Wang et al., 2012; Hou et al., 2015). An oil-wet rock

would naturally repulse water and thus reduce the productivity of the reservoir. This damage is irreversible, hence, the advantage of using a Pickering inverse emulsion drilling fluid.



Fig. 1 Toxicity of oil-based drilling fluids. Left: soil contamination, Texaco – Ecuador\* Right: consequences of water contamination, Hassi-Messaoud – Algeria (Leila and Benabbou, 2016).

Furthermore, this type of drilling fluids usually contains high oil contents (diesel, gasoil, and synthetic oils). The hydrocarbon content in a drilling fluid can easily exceed 90 % of the fluid total volume. Worse, in many cases, used drilling fluids are disposed in nature without any prior treatment. Therefore, another goal of the present work is to study the flow behavior of highly concentrated inverse Pickering emulsions.

To resume, the main problematics related to the currently used classical inverse emulsion drilling fluids are:

- Long-term stability.
- Low water content (about 10%).
- Environmental toxicity because of:
  - The used surfactants.
  - High hydrocarbons ratio in their formulation.
- Damaging effects of free surfactants on the reservoir rock.

An optimum solution should be:

- Surfactant-free.
- With a long-term stability.
- And a higher water content.

Within this context, large quantities (70 L) of inverse emulsions were prepared and stabilized using organophilic clay particles, by the means of 2 diaphragms placed near the outlet of a circulation flow loop. The same system was as well used to study the mechanical behavior of the emulsions, using an ultrasound pulsed doppler velocimeter and 7 pressure sensors. In the following, the five chapters of this manuscript will be presented:

In **Chapter 1**, some mathematical and physical tools, used to study the rheological as well as pipe-flow behaviors of non-Newtonian fluids, were given. Then, a theoretical background on clays, organoclays and Pickering emulsions was presented.

The aim of **Chapter 2** was to give a detailed description of the experimental set-up and methods used in this work, starting by a brief description of the AR2000 rheometer and its used geometries, followed by a detailed description of the flow loop, its components and its measuring and emulsification systems. Finally, before concluding this chapter, preparation protocols of the studied organoclay dispersions and Pickering emulsions were detailed.

As it was mentioned earlier, Pickering emulsions, studied in the current work, were stabilized using organo-hectorite particles. Looking at the scarcity of the literature discussing the rheological behavior of organo-hectorite dispersions, **Chapter 3** was dedicated to studying the rheological behavior of a commercial hectorite, modified with dimethyldialkyl ammonium cations, dispersed in gasoil. The viscous and elastic properties of the organo-hectorite dispersions, at concentrations ranging from 3 to 10 wt%, and at ambient pressure and temperature conditions, were studied using a stress-controlled rheometer (AR 2000). The suspensions were found to be shear thinning with a yield stress value, proportional to the concentration of organo-hectorite clay. Moreover, the flow curves of these suspensions were fitted using both Herschel-Bulkley and Carreau-Yasuda models, and their creep-recovery measurements were modeled using the mechanical model of Burger and the Weibull distribution function. Finally, the existence of a critical concentration, influencing on the microstructure of the dispersions, was put into evidence. The results of this chapter were published in the *Journal of Applied Clay Science*.

In **Chapter 4**, a 3 wt% organo-hectorite-in-gasoil dispersion was used to prepare water-in-oil inverse emulsions at different water mass concentrations (0 % to 50 %). These emulsions were prepared and studied by the means of the flow loop presented in Chapter 2. Besides their long-term stability (until 12 months under ambient pressure and temperature conditions), the studied emulsions exhibited a similar rheological and flow behaviors to those of drilling fluids (shear-

thinning with yield stress following the model of Herschel-Bulkley and exhibiting strong viscoelastic characteristics). Furthermore, local velocity and pressure results were used to validate the in-line emulsification system and to study the evolution of flow parameters (velocity profiles, wall shear stress and friction factor). After that, we concluded the chapter with a comparison between the rheological and the flow results, that showed a satisfying agreement between the two experimental procedures. A paper discussing the results of this chapter was published in the *Journal of Petroleum Science and Engineering*.

Finally, the last chapter of this work (**Chapter 5**), was dedicated to study Pickering emulsions with high water concentrations (60 wt% to 80 wt%), presenting static and/or dynamic instabilities. The aim of this chapter was to understand the structural mechanisms responsible for the dynamic stability of the studied concentrated emulsions. Rheological measurements being impossible because of the slipping phenomenon at the rheometer geometry walls, velocity and pressure measurements were the only available means to studying these systems. Finally, an attempt to explain the structural interactions responsible of the dynamic stability was presented, using some visualization experiments.

This thesis dissertation is concluded with a general conclusion listing the main findings and results established during the present work, followed by some perspectives and propositions that I, personally, wish to be the subject of future research projects.

## References

- Donaldson, E.C., Thomas, R.D., Lorenz, P.B., 1969. Wettability Determination and Its Effect on Recovery Efficiency. *SPE J.* 13–20. <https://doi.org/10.2118/2338-PA>
- Hou, B., Wang, Y., Huang, Y., 2015. Mechanistic study of wettability alteration of oil-wet sandstone surface using different surfactants. *Appl. Surf. Sci.* 330, 56–64. <https://doi.org/10.1016/j.apsusc.2014.12.185>
- Jiao, D., Sharma, M.M., 1993. Dynamic Filtration of Invert-Emulsion Muds. *SPE Drill. Complet.* 8. <https://doi.org/10.2118/24759-PA>
- Leila, L., Benabbou, S., 2016. Les Effets Des Rejets Petroliers Sur La Region De Hassi Messaoud. *Rev. algérienne d'économie Gest.* 9, 164–184.
- Masalmeh, S.K., 2002. Studying the effect of wettability heterogeneity on the capillary pressure curves using the centrifuge technique. *J. Pet. Sci. Eng.* 33, 29–38. [https://doi.org/10.1016/S0920-4105\(01\)00173-5](https://doi.org/10.1016/S0920-4105(01)00173-5)
- McDonald, J.A., Buller, D.C., 1992. The significance of formation damage caused by the adsorption oil-based mud surfactant. *J. Pet. Sci. Eng.* [https://doi.org/10.1016/0920-4105\(92\)90062-6](https://doi.org/10.1016/0920-4105(92)90062-6)
- Wang, D., Butler, R., Zhang, J., 2012. Wettability Survey in Bakken Shale Using Surfactant Formulation Imbibition. *Eighteenth SPE Improv. Oil Recover. Symp.* 1–13. <https://doi.org/10.2118/153853-PA>
- Zoller, U., 2019. *Handbook of Detergents, Part B: Environmental Impact*, First. ed. CRC Press.



CHAPTER 1  
**REVIEW OF THE LITERATURE**

## CHAPTER 1

**TABLE OF CONTENTS**

1.1	Introduction.....	13
1.2	Basics of rheology.....	13
1.2.1	Simple shear flow .....	13
1.2.2	Newtonian behavior .....	15
1.2.3	Non-Newtonian behavior .....	16
1.3	Pipe-flow of non-Newtonian fluids .....	26
1.3.1	Flow regimes in circular pipes .....	27
1.3.2	Fundamental background on Poiseuille flow of yield fluids.....	28
1.4	Organoclays .....	34
1.4.1	Microstructure of clay minerals .....	35
1.4.2	Smectite clays.....	36
1.4.3	Composition, preparation and swelling of organoclays.....	37
1.5	Pickering emulsions.....	42
1.6	Summary to Chapter .....	43
1.7	References.....	44

## 1.1 Introduction

This work is an experimental attempt to understand the mechanical behavior of organoclay stabilized Pickering emulsions. To do so, rheological, and pipe-flow experiments were performed to measure the mechanical parameters of these systems.

Before discussing the latter measurements, we will present, in the current chapter, some definitions as well as mathematical and physical basics of the experimental methods. In addition, a brief literature review on organoclays and Pickering emulsions will be presented.

## 1.2 Basics of rheology

Rheology is the discipline which studies the flow and the deformation of materials. The term rheology originated from the Greek words “rheo” which translates to *flow* and “logia” meaning *the study of*. Although it studies all states of matter, in this chapter, we will only focus on the rheology of fluids, especially clay suspensions and colloids. The study of rheology is particularly interesting in the case of non-Newtonian materials, where the response of a deformation can be influenced by several parameters such as shear rate, time, and micromolecular interactions. In this section, some rheology notions will be briefly defined then the basics of rheology will be detailed.

### 1.2.1 Simple shear flow

In the case of a simple shear flow, the fluid is placed between two parallel plates with a gap equal to “ $e$ ”. The lower plate is kept immobile, and the upper plate moves with a velocity,  $V_0$ , (Fig. 1.1). In the case of a laminar flow (the fluid flows in parallel layers, with no mixing between two adjacent layers), the layers of the fluid slide one over another and each layer exhibits a higher velocity than the one beneath it. The upper layer moves with a maximum velocity while the bottom one (at  $x=0$ ) is immobile. The force causing the velocity  $V_0$  is the origin of a shear stress,  $\sigma$ , which is defined as a force,  $F$ , per unite area,  $A$ :

$$\sigma = \frac{dF}{dA} \quad 1.1$$

The unit of shear stress is Pascal [Pa].

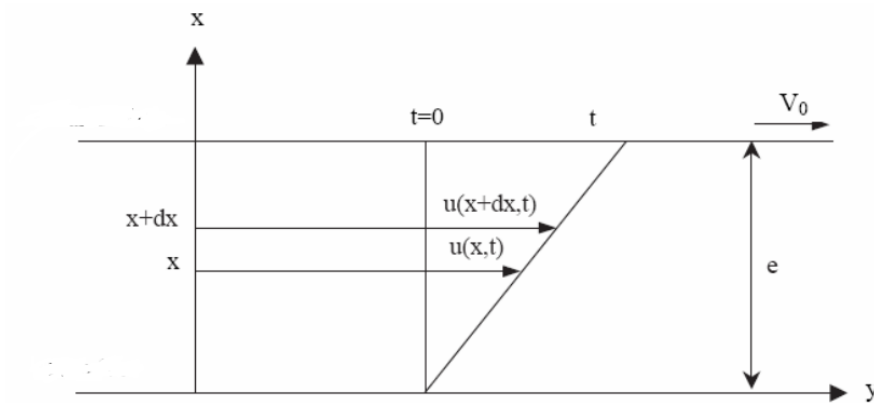


Fig. 1.1. Schematic representation of a simple shear flow.

As a result of the applied force, the upper layer moves to a finite distance  $y$  while the bottom layer stays immobile. The ratio of this displacement to the distance from the bottom plate is termed the shear strain,  $\gamma$ :

$$\gamma = \frac{dy(x,t)}{dx} \quad 1.2$$

From Eq. 1.2, it can be noticed that in the case of a Hookean solid, the deformation will be finite, hence no flow will occur. For a liquid material, shear strain will continually increase if the shear stress is applied, resulting in a velocity gradient called shear rate or strain rate,  $\dot{\gamma}$ :

$$\dot{\gamma} = \frac{d\gamma}{dt} = \frac{d}{dt} \frac{dy}{dx} = \frac{d}{dx} \frac{dy}{dt} \quad 1.3$$

Because  $[du(x,t)/dt]$  represents the velocity,  $v(x,t)$ , of a layer at a distance,  $x$ , from the bottom plate and an instant,  $t$ , the shear rate can be written as follows:

$$\dot{\gamma}(x,t) = \frac{dv(x,t)}{dx} \quad 1.4$$

The unit of shear rate is  $[s^{-1}]$ .

The shear stress and the shear rate are always related through a constitutive equation. The ratio of these two parameters is termed the viscosity coefficient,  $\eta$ . In the simplest case, this coefficient is independent of the shear rate and the fluid is called Newtonian. In the case of a non-Newtonian fluid, the behavior is much more complicated.

The viscosity of a fluid is defined by the following expression:

$$\eta(\dot{\gamma}) = \frac{f(\dot{\gamma})}{\dot{\gamma}} \quad 1.5$$

The unit of viscosity is [Pa.s].

### 1.2.2 Newtonian behavior

For Newtonian fluids, the relationship between shear stress and shear rate is linear. Typical Newtonian fluids are those made of low molecular weight components with low polymer/insoluble solids concentrations (water, vegetable oil, honey, sugar syrup, glycerin, etc.) (Barnes et al., 1989; Anandha, 2002). Isaac Newton was the first to mathematically describe the behavior of an ideal fluid by assuming that the ratio of the shear stress to the shear rate is constant (Schramm, 1998). In this case, the shear rate is described using the equation (Fig. 1.1):

$$\dot{\gamma} = \frac{V}{e} \quad 1.6$$

With a corresponding constitutive equation:

$$\sigma = \eta \cdot \dot{\gamma} \quad 1.7$$

As it can be noticed, the viscosity of a Newtonian fluid is independent of the applied shear stress.

However, the Newtonian model fails to describe most of industrial materials. An example of a more complex fluids is clay suspensions, where the viscosity is shear rate and time dependent. Moreover, clay suspensions do not flow until the shear stress reaches a critical value below which the suspension behaves like a solid. Above this critical stress, the dynamic viscosity of these suspensions declines with the increase in shear rate. In addition to that, after an applied shear, if a clay suspension is left at rest, the viscosity starts to increase until reaching a maximum viscosity at which the fluid is *fully structured* (Bekkour and Kherfellah, 2002; Bekkour et al., 2005; Azouz et al., 2010; Benslimane et al., 2016).

### 1.2.3 Non-Newtonian behavior

In nature, most fluids are non-Newtonians, and the viscosity depends on different parameters such as shear rate, time, etc. The behavior of non-Newtonian fluids is either non-linear or linear exhibiting a yield point (Anandha, 2002). They can also have different behaviors when increasing and decreasing the applied shear stress. In which case the non-Newtonian fluid is time-dependent, and the viscosity depend on both shear rate and time. Non-Newtonian fluids can also be classified according to their elasticity. A fluid that has both elastic and viscous components is called viscoelastic. More details on viscoelastic fluids will be given in next sections.

#### 1.2.3.1. Time-independent fluids

For this category, the viscosity of the fluid depends only on the applied shear rate and does not evolve with time. If a constant shear stress step is applied on a time independent fluid, the value of the viscosity would stay constant in time. In this case, shear stress and shear rate are related with the following equation:

$$\sigma = f(\dot{\gamma}) \quad 1.8$$

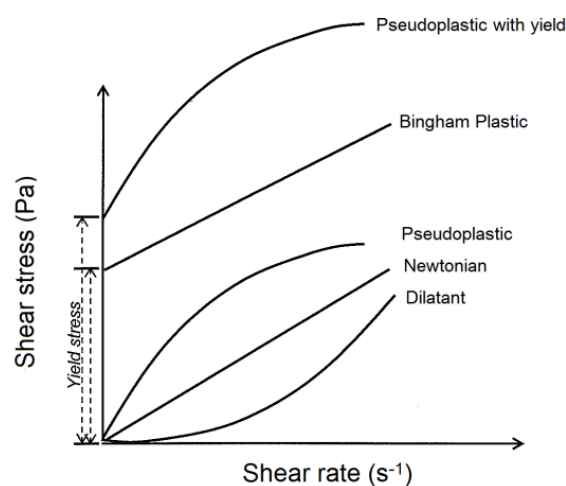


Fig. 1.2 Time independent rheological behaviors (G. Vieira and E. C. Peres, 2012).

According to Eq. 1.8, three main behaviors can be described using the shapes of the flow curves (shear stress as a function of shear rate curves) shown in Fig. 1.2:

- i. A shear thinning behavior (pseudoplastic): where the viscosity of the fluid decreases when the shear rate increases. Shear thinning fluids are the most frequent in nature. Their flow curves are best represented by the viscosity as a function of shear rate, in order to observe the Newtonian plateaus at low and high shear rates (Coussot and Grossiord, 2002). Using viscosity values at the Newtonian plateaus ( $\eta_0$ ,  $\eta_\infty$ ), the behavior of a shear thinning fluid can be easily described using a four or a three parameters' model (Fig. 1.3). The main cause of a shear thinning behavior is the internal organization of the fluid particles. When the shear rate increases, the particles tend to rearrange in the flow direction, as a result the friction between fluid particles, thus the viscosity, decreases.
- ii. Shear thickening behavior (dilatant): where the viscosity increases with the increase in shear rate. This type of fluids is rare and less studied than the first one.
- iii. Fluids with yield stress (plastic): where the fluid behaves like a solid at low shear rates and starts to flow when the shear stress exceeds a critical shear stress termed yield stress  $\sigma_0$ . The yield stress is causally related to the viscoelastic properties of the material. If an applied stress is lower than the yield stress, the viscoelastic material behaves as a Hookean solid, and its experimental data can be fitted using a Kelvin-Voight model. Once the applied stress exceeds the yield stress, the Kelvin-Voight model becomes inadequate to predict the behavior of the viscous part of the fluid's behavior. In the latter case, it has been shown that the Jeffrey model describes well the viscoelastic behavior of the fluid (Benmouffok-Benbelkacem et al., 2010). Barnes (1999), in his papers, doubted the existence of a *real* yield stress because the latter depends on the time during which a stress is applied, for example, for the same material, several values of yield stress can be obtained depending on the applied stress and the time length of its application (Barnes and Walters, 1985). "Everything flows" is a true statement if the material is given a sufficient time to rearrange its internal structure and flow. Practically though, industrial processes take place in relatively short times and thus a practical definition of yield stress is needed indeed.

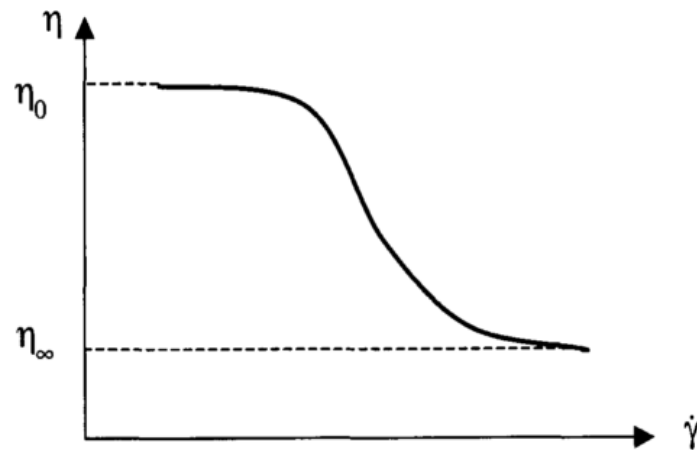


Fig. 1.3 Viscosity as a function of shear rate in the case of a shear thinning fluid (Coussot and Grossiord, 2002).

In the current work, and for practical purposes, yield stress will be defined as follows:

- It is the minimal detectable shear stress above which a drop of viscosity as a function of time can be observed.

Several models were proposed to describe the mentioned behaviors. A brief presentation of the most known models will be given.

#### 1.2.3.1.1. Rheological models

Several mathematical equations, relating shear stress  $\sigma$  to shear rate  $\dot{\gamma}$ , are used to describe the rheological behavior of fluids. These equations could be termed “constitutive laws” or “rheological models”.

- a) **Phenomenological models:** used to describe shear-thickening as well as shear-thinning fluids. A parameter can be added to take into consideration the yield stress of the fluid. This type of models describes the macrostructural properties of non-Newtonian fluids without investigating the change of its inner structure, which makes them convenient in industrial applications. In the following, some of the most used phenomenological models are listed:

- i. **The Ostwald model (1925):** also known as the power law model. Used to describe shear-thinning and shear-thickening behaviors of non-Newtonian fluids. Its equation is:

$$\sigma = K\dot{\gamma}^n \quad 1.9$$

where  $\dot{\gamma}$  ( $s^{-1}$ ) is the shear rate at any given shear stress  $\sigma$  (Pa),  $K$  is the consistency coefficient ( $Pa.s^n$ ), and  $n$  is the flow behavior index (dimensionless).

The viscosity using the power law could be described as follows:

$$\eta(\dot{\gamma}) = K\dot{\gamma}^{n-1} \quad 1.10$$

According to Eq. 1.10, the fluid is Newtonian if  $n = 1$ , shear-thinning if  $n < 1$  and shear-thickening if  $n > 1$

The power law was used to describe the flow behavior of some fluids such as polymeric solutions (Razavi and Karazhiyan, 2009), organoclay suspensions (Bhatt et al., 2013), nanotube dispersions (Kinloch et al., 2002), and blood (Wang and Ho, 2011).

- ii. **The Bingham model (1922):** one of the first rheological models in the literature. In addition to shear-thinning and shear-thickening behaviors of non-Newtonian fluids, the Bingham model describes the yield behavior as well, by adding a yield stress parameter to the equation of the Newtonian fluid:

$$\sigma = \sigma_y + \eta_p \dot{\gamma} \quad 1.11$$

where  $\eta_p$  (Pa.s) is the plastic viscosity and  $\sigma_y$  (Pa) is the yield stress.

The Bingham model was used to describe the flow behavior of drilling fluids (Maxey, 2007), organoclay suspensions (Moraru, 2001; Zhuang et al., 2018) and cement (Nehdi and Rahman, 2004).

- iii. **The Herschel-Bulckley model (1926):** a modified Bingham model combining the terms of Ostwald and Bingham models. It describes shear-thinning, shear-thickening and yield behaviors of non-Newtonian fluids. The Herschel-Bulckley model is described as follows:

$$\sigma = \sigma_y + K\dot{\gamma}^n \quad 1.12$$

Where  $\sigma_y$  (Pa) is the yield stress,  $K$  (Pa.s<sup>n</sup>) is the consistency index and  $n$  (dimensionless) is the flow index.

The Herschel-Bulckley model was used to describe the flow behavior of drilling fluids (Kelessidis et al., 2006; Maxey, 2007; Baba Hamed and Belhadri, 2009; Rooki et al., 2012), bentonite dispersions (Bekkour et al., 2005; Benslimane et al., 2016), bentonite and polymer dispersions (Benyounes et al., 2010), and concrete (Güneyisi et al., 2016).

**b) Microstructural models:** unlike phenomenological models, microstructural models can be used to discuss the internal structure of the material. They describe the viscosity as a function of shear rate, by giving the values of viscosity at low and/or high shear rates (Newtonian plateaus), as well as the evolution of viscosity in the shear thinning region (Fig. 1.3). Several microstructural models were reported in the literature:

- i. Cross model (1965):** which describes the transition from the first Newtonian behavior ( $\eta_0$ ) to the shear thinning region and then to the second Newtonian behavior ( $\eta_\infty$ ).

$$\frac{\eta(\dot{\gamma})-\eta_\infty}{\eta_0-\eta_\infty} = \frac{1}{1+(\tau\dot{\gamma})^m} \quad 1.13$$

Where  $\eta$  (Pa) is the viscosity at any given shear rate  $\dot{\gamma}$  (s<sup>-1</sup>),  $\eta_0$  and  $\eta_\infty$  are the zero-shear-rate and the infinite-shear-rate viscosities, respectively,  $\tau$  (s) is a time constant, and  $m$  is a dimensionless rate constant indicating the dependence degree of the viscosity on shear rate in the shear-thinning region.

The cross model was mainly used to describe the flow behavior of polymer solutions (Ebagnin et al., 2009; Bahlouli et al., 2013).

- ii. Carreau-Yasuda (1987):** a five parameters model used to describe the flow behavior of polymers (Andrade et al., 2007), blood (Boyd et al., 2007; Wang and Ho, 2011), and nanocomposites (Zare et al., 2019):

$$\frac{\eta(\dot{\gamma})-\eta_\infty}{\eta_0-\eta_\infty} = [1 + (\tau\dot{\gamma})^a]^{\frac{n-1}{a}} \quad 1.14$$

where  $\eta(\dot{\gamma})$  is the viscosity at any given shear rate  $\dot{\gamma}$ ,  $\eta_0$  and  $\eta_\infty$  are the zero and the infinite shear rate viscosities,  $\tau$  is a time constant describing the transition

between the first Newtonian plateau and the shear thinning behavior,  $n$  is the power law exponent which indicates the dependency of the viscosity on the shear rate, and  $a$  is a dimensionless transition factor, describing the width of the transition zone between the first Newtonian plateau and the power law behavior (a low value of  $a$  lengthens the transition while a high value leads to a sharp transition).

### 1.2.3.2. Linear viscoelasticity

Ideal materials have either an elastic behavior where a solid is deformed and stores energy under external forces, then restores its original form once the force is removed, or a viscous behavior where a liquid is permanently deformed under external forces because of the energy dissipation.

Viscoelastic fluids are non-Newtonian fluids that have both elastic, where the strain is proportional to the shear stress, and viscous, where the shear rate is proportional to the shear stress, properties.

The linear viscoelasticity theory is based on the superposition principal which indicates that the ratio of the response (e.g. the strain) to the initial signal (e.g. the stress) is constant (Barnes, 1997). This constant is termed the compliance  $J(t)$ :

$$J(t) = \frac{\gamma(t)}{\sigma} \quad 1.15$$

where  $\gamma(t)$  is the measured strain and  $\sigma$  is the applied stress.

In the following, viscoelastic properties, characterized using oscillatory shear and creep measurements, as well as three of the most used mechanical models will be discussed.

#### 1.2.3.2.1. Oscillatory shear

In oscillatory shear measurements, a sinusoidal stress (or deformation), that varies as a function of time at a given frequency, is applied in the viscoelastic linear domain of the fluid, and the sinusoidal deformation (or stress) at the same frequency is measured. If we consider, for instance, an applied oscillatory stress:

$$\sigma(t) = \sigma_0 \cos(\omega t) \quad 1.16$$

where  $\sigma_0$  is the amplitude of the applied stress and  $\omega$  is the oscillation frequency. In the case of a linear response, the deformation follows the following equation:

$$\gamma(t) = \gamma_0 \cos(\omega t + \delta) \quad 1.17$$

where  $\gamma_0$  is the amplitude of the deformation and  $\delta$  is the phase shift.

Based on the phase shift value, the material can be:

- i. Hookean solid or purely elastic if  $\delta = 0$ .
- ii. Purely viscous if  $\delta = \pi/2$ .
- iii. Viscoelastic if  $0 < \delta < \pi/2$ .

The phase shift can be related to the viscous and elastic properties of the material:

$$\tan(\delta) = \frac{G''}{G'} \quad 1.18$$

where  $G''$  (Pa) is the loss modulus and  $G'$  (Pa) is the storage modulus, related to the viscous and the elastic properties of the material, respectively.

Furthermore, the complex shear modulus,  $G^*$ , can be defined as:

$$G^* = G' + iG'' \quad 1.19$$

#### 1.2.3.2.2. Creep-Recovery measurements

Creep measurements are one of the most important tests to be performed on viscoelastic materials to study their properties in a near to rest state. During the test, a fixed stress,  $\sigma_0$ , inferior to the yield stress of the material is applied, and the resulting deformation is measured as a function of time. The recovery test is as important as the creep test, as it allows to measure the viscoelastic behavior of the material after the suppression of the applied stress. The creep and recovery tests can give a qualitative and a quantitative description of the material. The quantitative description of viscoelastic materials will be discussed in the next section. Regarding the qualitative description, elasticity and viscosity of the material can be described using deformation measurements during the creep and recovery tests (Fig.1.4).

- i. If the deformation diminishes instantaneously to zero, the material has fully recovered after the suppression of the applied stress and is said to be an elastic solid.

- ii. If the deformation stays constant after the removal of the applied stress, the material is said to be viscous.
- iii. If the deformation decreases gradually until a non-zero value, the material is viscoelastic. In this case, the elasticity of the material allows a partial recovery of its initial structure while its viscosity causes the dissipation of a part of its deformation energy.

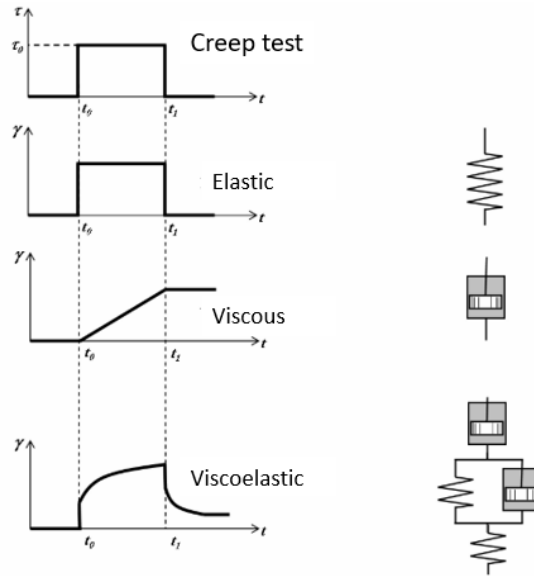


Fig. 1.4 Creep-Recovery tests in the case of: an elastic material, a viscous material, and a viscoelastic material (Benchabane, 2006).

### 1.2.3.2.3. Viscoelastic mechanical models

Many mechanical analogues are used to describe viscoelastic models, they serve as a representation of viscous and elastic responses in each fluid. In the following, three of the most used mechanical viscoelastic models are discussed:

#### a) Maxwell model

The Maxwell mechanical model (Fig. 1.5), a two-elements model, represents the viscoelastic fluid as an assembly, in-series, of a spring with a stiffness  $E$ , representing the elastic response, and a dashpot with a constant  $\eta$ , representing the viscous response.

The stress-strain relations are respectively:

$$\sigma = E \varepsilon_2 \tag{1.20}$$

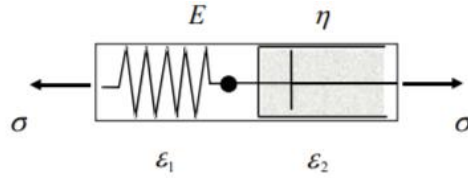


Fig. 1.5 Mechanical model of Maxwell (Papanicolaou and Zaoutsos, 2011).

$$\sigma = \eta \frac{d\varepsilon_1}{dt} \quad 1.21$$

The total strain of the system is:

$$\varepsilon = \varepsilon_1 + \varepsilon_2 \quad 1.22$$

Using Eq. 1.20 and 1.21 in Eq. 1.22, the constitutive Maxwell equation can be derived:

$$\frac{d\varepsilon}{dt} = \frac{1}{E} \frac{d\sigma}{dt} + \frac{\sigma}{\eta} \quad 1.23$$

### b) Kelvin-Voight model

The kelvin Voight model (Fig. 1.6) is the second two-elements mechanical model, that describes viscoelastic materials as an assembly, in-parallel, of a spring with a stiffness  $E$  and a dashpot with a constant  $\eta$ . In this case the following equations are used:

$$\varepsilon = \frac{1}{E} \sigma_1 \quad 1.24$$

$$\frac{d\varepsilon}{dt} = \frac{1}{\eta} \sigma_2 \quad 1.25$$

The total stress of the system is expressed using the equation:

$$\sigma = \sigma_1 + \sigma_2 \quad 1.26$$

By replacing the values of  $\sigma_1$  (Eq. 1.24) and  $\sigma_2$  (Eq. 1.25) in Eq. 1.26, the differential equation of Kelvin-Voight could be written as:

$$\sigma = \varepsilon E + \eta \frac{d\varepsilon}{dt} \quad 1.27$$

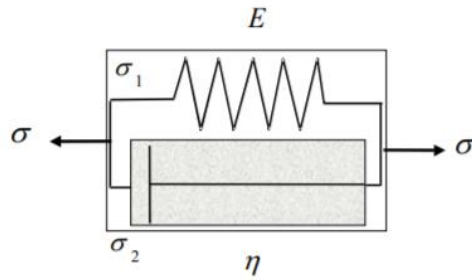


Fig. 1.6 Mechanical model of Kelvin-Voigt.

### c) Burger model

The Maxwell and the Kelvin-Voigt models are two simple mechanical models. In the case of real fluids, more complex models are used. For instance, three elements' models, the generalized Maxwell and Kelvin-Voigt models, or non-linear models can be used.

In this section, the Burger model, which is a combination, in-series, of a Maxwell unit and a Kelvin Voigt unit (Fig.1.7) will be presented. The Burger model was used to describe the viscoelastic behavior of the organo-hectorite suspensions studied in Chapter 3. This model is mainly used to model the viscoelasticity of polymeric materials like nanocomposites (Jia et al., 2011; Yao et al., 2013). It was also used to model the behavior of food emulsions (Dolz et al., 2008), and organoclay dispersions (Merad et al., 2019).

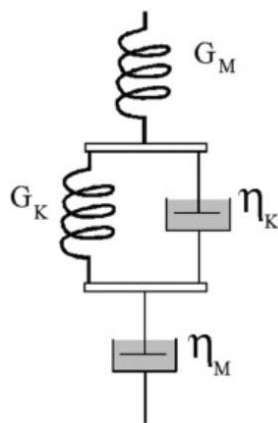


Fig. 1.7 The Burger mechanical model.

In this model, the compliance of the system, which is the total deformation per stress unit, is expressed as follows:

$$J(t) = \frac{1}{G_M} + \frac{1}{G_K} \left[ 1 - \exp\left(\frac{-tG_K}{\eta_K}\right) \right] + \frac{t}{\eta_M} \quad 1.28$$

where  $G_M$  and  $G_K$  are the elastic moduli of the Maxwell and the Kelvin-Voigt units of the model, respectively.  $\eta_M$  the residual viscosity related to the dashpot of the Maxwell unit and  $\eta_K$  the internal viscosity associated with the Kelvin-Voigt model.

The recovery experimental data, on the other hand, can be correlated using the Weibull distribution function (Jia et al., 2011):

$$J(t) = J_\infty + J_{KV} \exp(-Bt^C) \quad 1.29$$

where  $J_\infty$  is the full recovery of the material,  $J_{KV}$  is the proper recovery of the material occurring after the instantaneous elastic recovery, and the parameters  $B$  and  $C$  describe the recovery speed of the material (Fig.1.8).

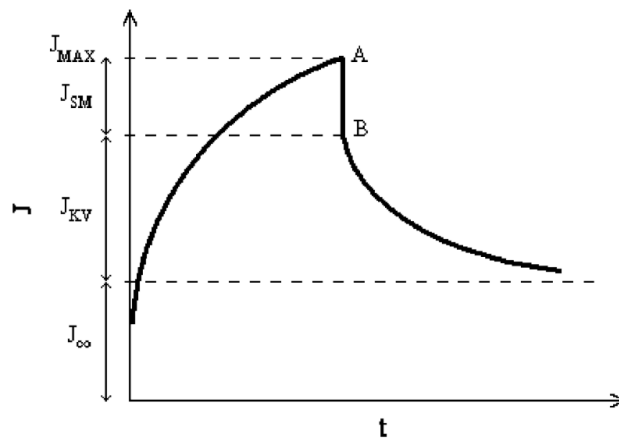


Fig. 1.8 Compliance as a function of time in a creep and recovery test.

### 1.3 Pipe-flow of non-Newtonian fluids

As it was mentioned in last section, most of industrial fluids are non-Newtonian. The need to transport these fluids explains the importance of understanding their flow behavior. In the current work, pipe-flow of Pickering emulsions, which are the principal component of our model drilling fluid, will be studied. Drilling fluids were found to follow the rheological law of Hershel-Bulckley. Therefore, we will mainly focus on the pipe-flow of Hershel-Bulckley fluids.

### 1.3.1 Flow regimes in circular pipes

When pipe fluid velocity is relatively small, the fluid layers tend to move in straight parallel lines and the regime is termed laminar. In this case, the velocity profile is parabolic, and the velocity is maximal at the pipe center and is equal to zero at the wall. Yield stress fluids, on the other hand, are characterized by the presence of two velocity zones:

- i. A block flow at a constant velocity at the centerline of the pipe, where the shear stress is lower than the yield stress.
- ii. A velocity gradient near to the wall, where the shear stress is greater than the fluid's yield stress.

Once velocity exceeds a certain critical value, the distribution of the streamlines becomes random throughout the pipe, and the flow regime becomes turbulent. Turbulence can be defined as the presence of an infinite number of eddies interacting with each other at all timescales. Unlike the laminar regime, in a turbulent flow, each streamline fluctuates in all directions in a random distribution (Fig. 1.9). In this case, the velocity profile is divided into three regions:

- i. A thin viscous laminar sublayer at the pipe wall, where the shear stress is dominant.
- ii. An overlap layer where the flow is turbulent with a very sharp velocity gradient.
- iii. An outer turbulent layer with a uniform velocity profile.

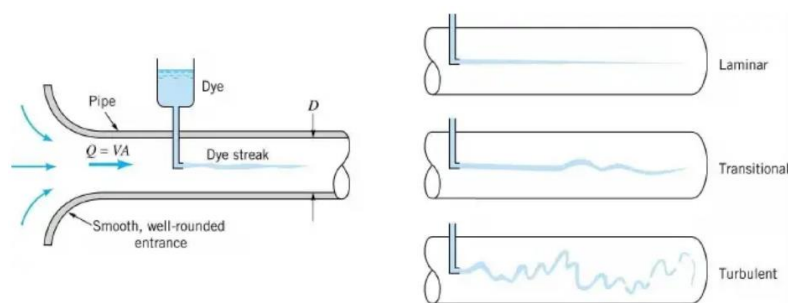


Fig. 1.9 Trajectory of a dye streak injected in a pipe flow at different flow regimes (Purushothmann, 2017).

The transition between laminar and turbulent flows is not instantaneous. Under a certain critical velocity, the flow regime is laminar and above a second critical velocity, the flow regime becomes fully turbulent. When the fluid velocity ranges between the two latter critical velocities, the flow regime is said to be transitional. The transition between laminar and turbulent regimes is not fully understood yet. Several experimental works were performed in order to identify the parameters influencing the flow during the transitional regime (Escudier et al., 2005; Güzel et al., 2009; Vajargah Karimi et al., 2017).

### 1.3.2 Fundamental background on Poiseuille flow of yield fluids

#### 1.3.2.1 Reynolds Number

The transition from laminar to turbulent regimes in circular pipes depends on the velocity and the properties of the fluid as well as the diameter of the used geometry. The Reynolds number is a dimensionless value characterizing the limits of the laminar, transitional and the turbulent regimes. For Newtonian fluids, the Reynolds number can be expressed as follows:

$$Re = \frac{\rho U D}{\eta} \quad 1.30$$

$U$  is the average velocity,  $D$  is the pipe diameter,  $\rho$  is the density of the fluid, and  $\eta$  is the dynamic viscosity of the fluid.

In the case of a non-Newtonian fluid, five definitions of the Reynold number can be found in the literature (Cho and Harnett, 1982):

- i. The generalized Reynold number introduced by Metzner and Reed (1955):

$$Re' = \frac{\rho U^{2-n'} R^{n'}}{8^{n'-1} k'} \quad 1.31$$

where the generalized index flow behavior  $n'$  and the generalized consistency index  $k'$  depend on the flow parameters. Many definitions of  $n'$  and  $k'$  can be found:

- o Kozicki et al (1966) defined  $n'$  and  $k'$  for a power law fluid as follows:

$$n' = n \quad 1.32$$

$$k' = k \left( \frac{3n+1}{4n} \right)^n \quad 1.34$$

with  $n$  and  $k$  the parameters of the power law model.

- Peixinho et al (2005) defined  $n'$  and  $k'$  for a Hershel-Bulkley fluid as a function of the rheological model parameters as well as the plug zone:

$$n' = \frac{(1-a) + \frac{2a(1-a)(1+m)}{2+m} + \frac{(1-a)^2(1+m)}{3+m}}{m+1-3(1-a) \left[ a^2 + \frac{2a(1-a)(1+m)}{2+m} + \frac{(1-a)^2(1+m)}{(3+m)} \right]} \quad 1.35$$

With  $m = 1/n$  and  $a$  is numerically calculated using the Newton's method.

$$k' = \left( \frac{k^m}{4} \right)^{n'} \left( \frac{\sigma_y}{a} \right)^{\&-n'm} \left\{ (1-a)^{1+m} \left[ 1 + \frac{2(1-a)(1+m)}{a(2+m)} + \frac{(1-a)^2(m+1)}{a^2(3+m)} \right] \right\}^{-n'} \quad 1.36$$

- ii. The wall Reynolds number, which has a similar expression to the Newtonian Reynolds number with replacing the dynamic viscosity by the apparent viscosity at the pipe wall  $\eta_w$  (Cho and Harnett, 1982):

$$Re_w = \frac{\rho U D}{\eta_w} \quad 1.37$$

The apparent viscosity at the pipe wall for a Hershel-Bulckley fluid is calculated using the expression (Chilton and Stainsby, 1998):

$$\eta_w = \frac{\sigma_w}{\dot{\gamma}_w} = \sigma_w^{(n-1)/n} \left( \frac{k}{1-X} \right)^{(1/n)} \quad 1.38$$

And 
$$X = \frac{\sigma_y}{\sigma_w} = \frac{4L\sigma_y}{D\Delta P} \quad 1.39$$

- iii. The generalized Reynold number derived from the dimensionless momentum equation:

$$Re_g = \frac{\rho U^{2-n'} R^{n'}}{8^{n'-1} k'} \quad 1.40$$

- iv. The effective Reynolds number:

$$Re_{eff} = \frac{\rho U D}{\eta_{eff}} \quad 1.41$$

with: 
$$\eta_{eff} = \sigma_w \frac{D}{8U} \quad 1.42$$

### 1.3.2.2. Friction factor

#### 1.3.2.2.1. Laminar regime

In case of flows at low Reynold numbers, the friction parameter depends only on the Reynolds number and is independent of the internal conditions of the pipe (pipe roughness). It is given by the following equation:

$$f_D = \frac{64}{Re} \quad 1.43$$

where  $f_D$  is the Darcy friction parameter and  $Re$  is the Reynolds number.

We should note that sometimes a similar definition of the friction parameter, using the Fanning friction parameter  $f$ , can be found:

$$f = \frac{f_D}{4} \quad 1.44$$

It is worth mentioning that the same formula of the friction parameter is used for both Newtonian and non-Newtonian fluids, while the formula of Reynolds number would differ.

#### 1.3.2.2.2. Turbulent regime

In turbulent regime, many correlations can be found in the literature. These correlations depend either on the internal conditions of the pipe (rough or smooth) or on the type of fluid (Newtonian or non-Newtonian). One of the most used correlations is the phenomenological Colebrook-White equation expressed as follows:

$$\frac{1}{\sqrt{f}} = -2 \log \left[ \left( \frac{e}{3.7D} \right) + \left( \frac{2.51}{Re\sqrt{f}} \right) \right] \quad 1.45$$

where  $e$  is the absolute pipe roughness,  $D$  is the pipe internal diameter.

If the pipe is assumed to be fully smooth, the friction factor would only depend on the Reynolds number, and the following Prandtl equation can be used (Brkić, 2011):

$$\frac{1}{\sqrt{f}} = -2 \log \left[ \frac{2.51}{Re\sqrt{f}} \right] \quad 1.46$$

In the case of a fully rough pipe, the friction factor appears to be less dependent on the Reynolds number and the von Karman's relation is usually used (Brkić, 2011):

$$\frac{1}{\sqrt{f}} = -2 \log \left[ \frac{e}{3.7D} \right] \quad 1.47$$

As it can be noticed, the Colebrook-White equation is implicit and thus can only be solved numerically. Several explicit approximations of the Colebrook equation exist in the literature, some of them can be applied in the case of laminar and turbulent flows (Churchill, 1977), and most of them are only developed for turbulent flows (Brkić, 2011).

### 1.3.2.2.3. Friction parameter for Herschel-Bulckley fluids

In the following, some of the most used friction factor equations for the pipe flow of Herschel-Bulckley fluids will be presented. Usually, authors use correlations originally developed for power law fluids to correlate the experimental data of Herschel-Bulckley fluids (Peixinho et al., 2005; Benslimane et al., 2016). Friction parameter equations are, in general, either semi-theoretical like the well-known Dodge and Metzner (1959) equation, or purely empirical like the Blasius equation (Chilton and Stainsby, 1998).

- Dodge and Metzner equation (1959):

A major step in the study of non-Newtonian fluids was made by Dodge and Metzner after the introduction of their equation initially developed using the Ostwald model for purely viscous, time independent fluids. In addition to the power law fluids, the Dodge and Metzner equation was used to describe the Herschel-Bulckley fluids (Peixinho et al., 2005; Benslimane et al., 2016).

The Dodge and Metzner friction factor is expressed as follows:

$$\frac{1}{\sqrt{f}} = \frac{4}{(nr)^{0.75}} \log \left[ R_e' \left( f^{1-\frac{n'}{2}} \right) \right] - \frac{0.4}{(nr)^{1.2}} \quad 1.48$$

where  $R_e'$  is the generalized Dodge and Metzner Reynolds number introduced in Eq. 1.31.

Benslimane (2013) used in his work the Dodge and Metzner friction factor expression using the wall Reynolds' number to model the experimental results of a Herschel-Bulckley fluid turbulent pipe-flow. It is obvious that the calculations would be easier and more accurate when using the wall Reynolds' number because of the consideration of the yield stress in its

calculations. The expression of the Dodge and Metzner friction factor using the wall Reynolds' number is as follows:

$$\frac{1}{\sqrt{f}} = 1,737n^{0,25} \ln \left( \frac{4n}{3n+1} Re_w \sqrt{f} \right) + \frac{4,8164}{n^{0,75}} (1 - n) - \frac{0,4}{n^{1,2}} \quad 1.49$$

- Blasius equation (1913):

Many empirical equations were developed to model the Darcy friction factor for turbulent flows (Blasius, Lees, Hermann, Nikuradse). Generally, the form of this type of correlations is:

$$f = A + B(R_e)^C \quad 1.50$$

where  $A$ ,  $B$  and  $C$  are defined empirically.

One of the most used empirical equations is the Blasius equation because of its simplicity. This equation does not include a term for the geometry roughness, and is valid up to a Reynolds number of  $10^5$  (Chilton and Stainsby, 1998). The Blasius equation is expressed as follows:

$$f = \frac{0,079}{(R_e)^{0,25}} \quad 1.51$$

Although the original Blasius equation was developed for Newtonian fluids, the generalized Reynolds number  $R_e'$  can be used for non-Newtonian fluids.

In addition to the Dodge and Metzner and Blasius equations, Peixinho (2005) and (Benslimane et al., 2016) used the Virk equation to model the turbulence of Hershel-Bulckley fluids. In both cases the Virk model did not show good results to model the experimental data. Virk equation, on the other hand, showed good results on polymeric viscoelastic non-Newtonian fluids (Cho and Harnett, 1982).

### 1.3.2.3. Velocity profiles

Pipe-flow velocity profiles depend highly on the rheological behavior of the studied fluid. A constitutive equation can be used to describe the pipe-flow behavior of non-Newtonian fluids. In our case, the phenomenological model of Herschel-Bulckley was used to describe the pipe-flow of the studied Pickering emulsions. Herschel-Bulckley model is widely used in the literature to model the pipe-flow of industrial fluids (Maxey, 2007; Kelessidis et al., 2011; Karimi and VanOort, 2015). Benslimane et al. (2016) studied the pipe-flow behavior of

bentonite suspensions using the same hydraulic loop used in our work. Bentonite suspensions were found to follow the Herschel-Bulckley model.

The Herschel-Bulckley model is composed of two parts, a first part describing the yield behavior and a second part describing the power law behavior for shear stresses superior to the yield stress. Hence, two distinct regions, in laminar regime, are observed in a cylindrical pipe (Fig. 1.10):

- i.  $r < R_c$  ( $R_c$  being the critical radius): a solid like behavior at the centerline of the pipe where the fluid flows as a plug with a constant velocity. In this region, the applied stress is lower than the yield stress and the fluid is not sheared.
- ii.  $r > R_c$ : a velocity gradient when the applied shear stress is higher than the yield stress. In this region the fluid is fully sheared, and it behaves as a power law fluid.

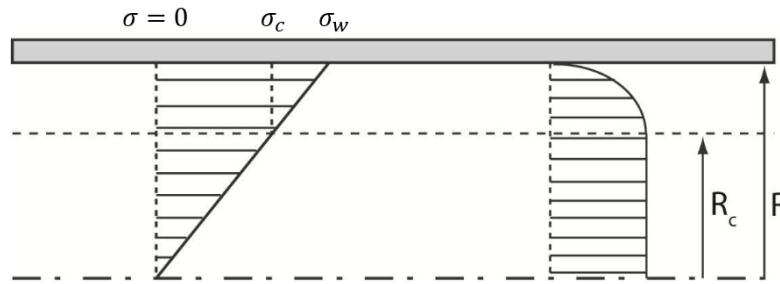


Fig. 1.10 Laminar pipe-flow of a Herschel-Bulckley fluid (Benslimane, 2012).

In the following, a brief description of the most used equations is presented:

The Hagen-Poiseuille pipe-flow of a Herschel-Bulckley fluid is given by the equation:

$$\frac{1}{r} \frac{d}{dr} (r\sigma) - \frac{dP}{dx} = 0 \quad 1.52$$

where the shear stress  $\sigma$  is given by the constitutive equation of Herschel-Bulckley:

$$\begin{cases} \sigma = \sigma_y + K \left( \frac{du}{dr} \right)^n & \text{if } \sigma > \sigma_y \\ \frac{du}{dr} = 0 & \text{if } \sigma < \sigma_y \end{cases} \quad 1.53$$

Furthermore, the laminar velocity profile can be calculated using the equations:

$$u(r) = \begin{cases} \frac{R}{\sigma_w k^{\frac{1}{n}} (\frac{1}{n} + 1)} \left[ (\sigma_w - \sigma_y)^{\frac{1}{n} + 1} - \left( \frac{\sigma_w r}{R} - \sigma_y \right)^{\frac{1}{n} + 1} \right], & \sigma_y < \sigma \\ \frac{R}{k^{\frac{1}{n}} (\frac{1}{n} + 1)} \left[ (\sigma_w - \sigma_y)^{\frac{1}{n} + 1} \right] & , \sigma_y \geq \sigma \end{cases} \quad 1.54$$

where the first expression is used for  $R_c \leq r \leq R$ ,  $R_c$  being the plug radius corresponding to an applied shear stress higher than the yield stress, and the second expression is used for  $r \leq R_c$  where the applied shear stress is smaller than the yield stress, and the fluid has a solid-like behavior.

It should be noted that this model assumes a no slip boundary condition.

Using Eq. 1.53, the expression of shear rate can be written:

$$\dot{\gamma} = f(\tau) = \left( \frac{\sigma - \sigma_y}{K} \right)^{\frac{1}{n}} \quad 1.55$$

Replacing Eq. 1.55 in Eq. 1.54 gives the expression of the wall shear rate (shear rate at  $R$ ) as a function of the Herschel-Bulckley parameters:

$$\dot{\gamma}_w = \left( - \frac{du(r)}{dr} \right)_{r=R} = \frac{nR}{n+1} \left( \frac{(\sigma_w - \sigma_y)}{K} \right)^{\frac{1}{n}} \left( 1 - \frac{\sigma_y}{\sigma_w} - \frac{n+1}{nR} \right) \quad 1.56$$

This expression is used to calculate the Reynolds' wall number.

## 1.4 Organoclays

Clays are studied in many domains such as geology, civil and petroleum engineering. Their fluid formulations are of a big interest in industrial applications due to their relatively low price and highly viscosifying characteristics. Among their several applications as rheological modifiers, they can be found in drilling fluids, cosmetics (creams), paints, food technology (wine), and water treatment (adsorbents).

In the following, a brief review on clay structure, clay suspensions and the preparation of organoclays will be presented.

### 1.4.1 Microstructure of clay minerals

Clay minerals are basically structured of an octahedral sheet and one or more tetrahedral sheets. The combinations of these two basic units (each with two dimensions) form the different types of clay minerals. The octahedral sheet is composed of a central atom (aluminum, magnesium, iron, or lithium) surrounded by hydrogens and hydroxyls, so that their final structure is an octahedron (Fig. 1.11). The tetrahedral sheet on the other hand, is composed of a central silicon atom surrounded by four oxygens and/or hydroxyls (Fig. 1.12). The repetition of tetrahedrons form a 2D horizontal plane named “silica tetrahedral sheet” (Fig. 1.11) (Bergaya et al., 2006).

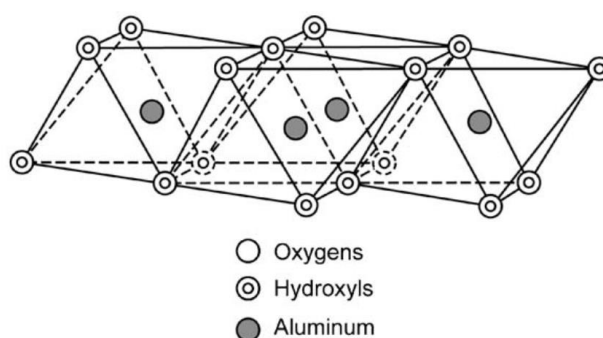


Fig. 1.11 Atomic structure of an octahedral sheet (Murray, 2007)

Octahedral and tetrahedral sheets are linked together by sharing axial oxygen and hydroxyl atoms to form either a 1:1 clay layer (e.g., Kaolinite) or a 2:1 clay layer (e.g., smectite). Even though all industrial clays have the same basic units (octahedral and tetrahedral sheets), they have quite different atomic compositions and structures. Moreover, physicochemical properties of clay minerals are determined by the arrangement and the types of atoms composing each sheet (Murray, 2007).

In this work, we are particularly interested in the structure of smectite minerals.

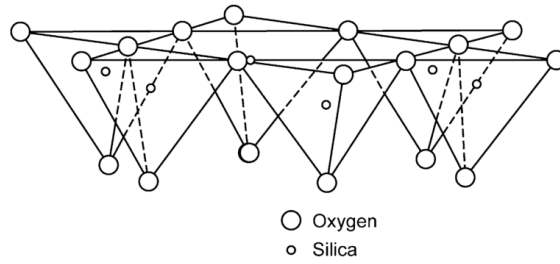


Fig. 1.12 Atomic structure of the tetrahedral sheet (Murray, 2007)

### 1.4.2 Smectite clays

Many types of smectite clays can be found in nature such as sodium montmorillonite, calcium montmorillonite, magnesium montmorillonite (saponite), iron montmorillonite (nontronite), aluminum montmorillonite (beidellite) and lithium montmorillonite (hectorite). Each type is named after the central atom of its octahedral sheet or the type of the cations existing in the interlayer space.

The most used smectite clays in the industry are the so called “bentonites” (Grim, 1968). They are predominantly comprised of sodium montmorillonite, calcium montmorillonite and in a lower percentage, hectorite (Murray, 1991). Smectites are composed of an octahedral sheet located between two tetrahedral sheets, where the notation 2:1 (Fig. 1.13). Different cations can occupy the space between the 2:1 smectite layers.

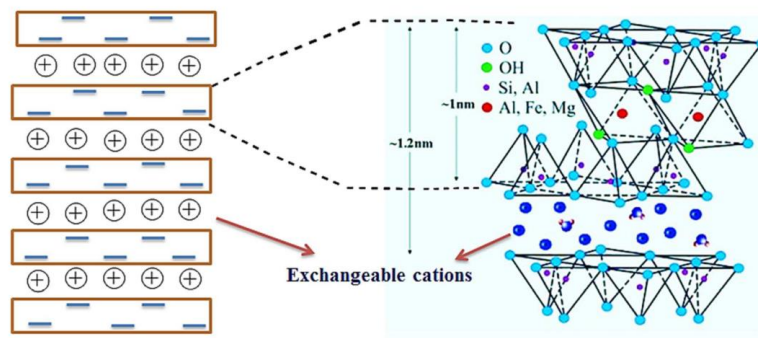


Fig. 1.13 schematic representation of the structure of smectites (Hebbar et al., 2014).

Finding an exact composition of smectites is impossible as it varies from a mineral to another. Different compositions of the tetrahedral and the octahedral sheets may be found. In the octahedral sheet, many substitutions of the aluminum atom are possible (e.g. magnesium or lithium in the case of hectorite) which cause a charge deficiency in the smectite layer (Murray, 1991). In the tetrahedral sheet, a substitution of the silicon atoms by aluminum occurs in 15% of the cases (Grim, 1968). Negative charges on the clay surface are balanced by interlayer cations and water (Fig.1.13). In the case of calcium montmorillonite for example, this charge deficiency is balanced by calcium cations and two layers of water (Murray, 2007).

#### **1.4.2.1. Physicochemical properties of smectites**

Smectites represent all types of hydrated silicate minerals. As it was previously mentioned, smectites are three sheets' minerals: two tetrahedral silicon sheets ( $\text{Si}^{4+}$ ) and one octahedral aluminum sheet. Aluminum could be replaced with  $\text{Fe}^{3+}$ ,  $\text{Fe}^{2+}$ ,  $\text{Mg}^{2+}$ ,  $\text{Li}^{2+}$  and silicon by aluminum. These replacements are the cause of the deficiency in positive charges which makes the surfaces of the clay charged negatively. This negative charge is compensated by the presence of hydrated cations in the interlayer space such as  $\text{Ca}^{2+}$ ,  $\text{Na}^+$ ,  $\text{Mg}^{2+}$ .

Among bentonites mentioned earlier, sodium montmorillonite and hectorite have higher cation exchange capacities (CEC) compared to calcium montmorillonite. CEC is the number of positive charges (cations) that can be exchanged by a clay surface. The high CEC values of sodium montmorillonite and hectorite makes easier the replacement of the hydrated cations by polar organic molecules such as ethylene glycol, quaternary amines and polyalcohols (Murray, 2007). High CEC clays are of a big industrial interest as they can be used to produce organic clays using natural or industrial hydrophilic clays. These modified clays are termed «organoclay».

#### **1.4.3 Composition, preparation and swelling of organoclays**

Modified clays or organoclays are usually made using smectite clays, in particular sodium montmorillonite and hectorite because of their high cation exchange capacity (Murray, 2007). In this modification process, cations present in the interlayer space ( $\text{Na}^+$ ,  $\text{K}^+$ , ...) are replaced by organic cations such as quaternary ammoniums (Jordan, 1949). Organoclays are widely used

in several applications as adsorbents of organic molecules in water/soil/air treatment, rheology control agents in paints, cosmetics, greases, oil-based drilling fluids and more recently in nanocomposites where organoclays, called in this case nanoclays with a size smaller than 0.5  $\mu\text{m}$ , are mixed with polymers to make high temperature resistant materials (de Paiva et al., 2008; Cavalcanti et al., 2012).

#### **1.4.3.1. Organic modification of clay minerals**

Organic modification of the clay surfaces (from hydrophilic to organophilic) is getting attention recently because of the application of organoclays in nanocomposites, one of the most advanced areas of nanotechnology. Modified clays are also used in other applications such as adsorbents of organic contaminants and in drilling fluids. Some of the methods used to organically modify clay minerals are (Bergaya and Lagaly, 2002; Jaber and Miehé-Brendlé, 2009):

- Adsorption or ion exchange of interlayer cations with organic molecules or cations.
- Binding of inorganic and organic anions on the edges of clay mineral layers.
- Grafting of organic molecules.

Many studies were published on the intercalation of organic molecules into the interlayer of clay minerals after the discovery of X-Ray diffraction in 1913 (Merinska et al., 2002). Modification of clay surfaces by the use of ion exchange was first introduced by Okada et al. (1988) for polymer nanocomposite preparation (Okada et al., 1988).

Among clay minerals, smectites especially montmorillonites are the most used to prepare organoclays due to their high cation exchange capacity and swelling properties. Hectorites are also suitable for organoclay preparation because of their high cation exchange capacity. However, only a few studies could be found on their modification and swelling properties in organic media.

The method used to prepare the organoclay used in our work is ion exchange of interlayer cations with alkylammonium ions, which is one of the most studied and applied clay modification methods (Bergaya and Lagaly, 2002; Merinska et al., 2002; Ragouilliaux et al., 2008).

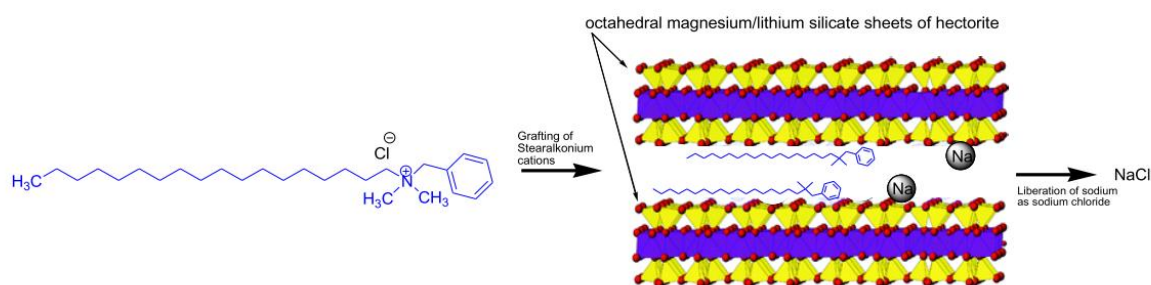


Fig. 1.14 Synthesis of organo-silicate mineral by cation exchange. The organic modifier used in this case is a quaternary ammonium salt (Becker, 2012).

#### 1.4.3.1.1. Preparation of organoclays by cation exchange

In this type of organic modification, inorganic cations present in the interlayer space, for instance  $\text{Na}^+$ ,  $\text{K}^+$  and  $\text{Ca}^+$ , are replaced with organic cations such as quaternary ammonium cations (Jaber and Miehé-Brendlé, 2009) (Fig.1.14). Modification of clays using cationic surfactants was reported in many works in the literature (Xi et al., 2004; Hu et al., 2013; Zhuang et al., 2017b, 2018). Different cationic surfactants were used in the literature such as tetradecyltrimethylammonium bromide (Hu et al., 2013), cetyl trimethyl ammonium bromide (Zhuang et al., 2016), and lauryl trimethyl ammonium chloride (Zhuang et al., 2017a). Organoclays are usually prepared by mixing aqueous clay suspension and solutions of the chosen surfactant. In some cases, alkylammonium salts are added directly to the clay suspension (Moraru, 2001). Clay-alkylammonium salt mixture is then stirred under heat (Zhu et al., 2005). After that, organoclay is extracted by centrifugation or filtration than washed several times with deionized water or a mixture of deionized water-alcohol to remove resulting anions (Moraru, 2001; Zhu et al., 2005). At last, organoclay is dried under moderate temperature (between 60 and 100°C) then milled and sieved (Gorrasi et al., 2003; Jaber and Miehé-Brendlé, 2009; Zhuang et al., 2017a).

#### 1.4.3.2. Structure of organoclays

The microscopic structure of organoclays depends on the cation density of the basal spacing, the nature of the silicate clay mineral, and the alkyl chain length used in the modification process. In a specific type of silicates, the basal spacing depends on the number of the carbon

atoms present in the cationic surfactant alkyl chains. Three organizations of the alkylammonium cations in the interlayer space are possible:

- i. Monolayers.
- ii. Bilayers.
- iii. Pseudo-trimolecular layers which are observed in highly charged smectites.

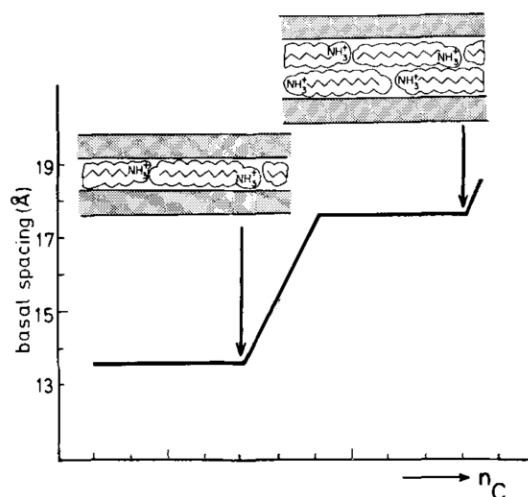


Fig. 1.15 Representation of the basal spacing in alkylammonium smectites as a function of the carbon atoms number in the alkyl chain (Lagaly et al., 1976).

As it is illustrated in Fig. 1.15, the type of alkyl chains organization controls the basal spacing of the organoclay. Monolayer arrangement takes place if the equivalent area ( $A_e$ ) i.e., the available clay surface for a monolayer cation configuration is larger than the area of the surfactant cation ( $A_c$ ). In this case, organoclay have a basal spacing of 13,6 Å. If the area of the alkylammonium ions becomes larger than the available clay surface, a bilayer arrangement takes place with an interlayer of 17,7 Å (Lagaly et al., 1976). If the surfactant cation area becomes larger than twice the equivalent area, three layers structure of alkylammonium is observed. Since the latter structure is energetically unstable, the alkyl chains in this case form a paraffin type structure (Fig.1.16) where the basal spacing depends on the angle between the clay surface and the axes of the alkyl chains. This angle increases with the increase in charge density of the basal spacing (de Paiva et al., 2008).

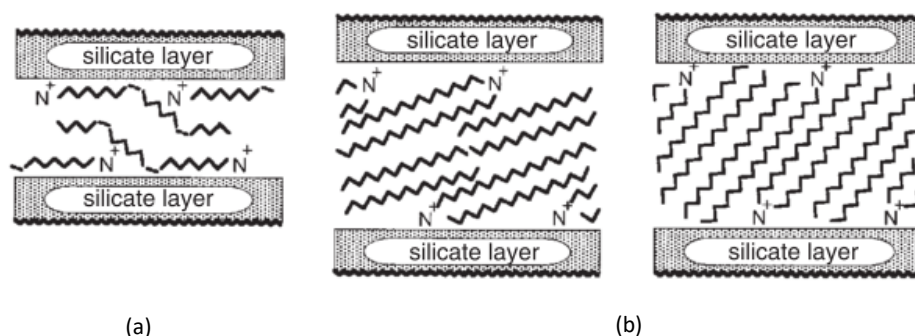


Fig. 1.16 Arrangement of alkylammonium chains in the basal spacing of silicate clay: (a) pseudo-trimolecular layers and (b) paraffin type structure with different angles (Bergaya et al., 2006).

#### 1.4.3.3. Quaternary alkylammonium salts

The most used organic compounds in clay modification are quaternary alkyl ammonium salts which are cationic surfactants.

These surfactants replace the basal spacing cations, which are bonded to the negative surface, due to weak electrostatic forces (Fig.1.14). Quaternary alkylammonium salts are synthesized by a complete alkylation of ammonia ( $\text{NH}_3$ ) or ammonium ( $\text{NH}_4^+$ ). A significant amount of work studying the organic modification of clay minerals using quaternary alkylammonium chlorides and bromides can be found in the literature (Dekany et al., 1986; Hu et al., 2013; Zhuang et al., 2017a).

#### 1.4.3.4. Organoclay swelling in organic media

Organoclays are characterized by their high hydrophobicity as well as swelling and forming time dependent gels when dispersed in organic media. Gel formation of organoclays is usually explained using the model of montmorillonite swelling in water. When clay loading in dispersant becomes sufficiently high, the distance separating clay particles diminishes and interactions between them become possible. This results in the formation of a microscopic structure where three possible configurations can be noticed: (i) face-to-face (FF); (ii) edge-to-edge (EE) and (iii) edge-to-face (EF). A literature review as well as an experimental study on the microstructural and rheological behavior of swelled organoclays in organic media are presented in Chapter 3.

## 1.5 Pickering emulsions

Drilling fluids (or drilling muds) are the fluids used to drill petroleum wells. The main purposes behind the use of a drilling fluid are:

- i. Maintaining the well walls by applying a back pressure slightly higher than the drilled rock pressure.
- ii. Stabilizing the borehole by the formation of thin impermeable layer called *the cake*.
- iii. Cleaning the well bottom from the cuttings resulting from the drilling process through a continuous circulation of the drilling fluid.
- iv. Maintaining the cuttings in suspension when the drilling process is paused.
- v. Lubricating the drilling tools.
- vi. Cooling the drilling tool and string.

Many types of drilling fluids can be found in the literature. The most used drilling fluids are the water-based drilling fluids, mainly composed of water, bentonite and polymers, and oil-based drilling fluids, composed of a surfactant stabilized inverse emulsion and organoclays. Water-based drilling fluids are usually used to drill the non-reservoir layers. Oil-based drilling fluids, on the other hand, are used to drill the petroleum reservoir layer (Schramm, 2000; Quintero, 2002). This is the reason why the components of oil-based drilling fluids should not be damaging to the reservoir layer.

Despite their major role in the stabilization of inverse emulsion drilling fluids, surfactants were early found to change the wettability of reservoir rocks from water-wet to oil-wet. The wettability alteration of the reservoir rock was found to decrease the productivity of petroleum reservoirs (Menezes et al., 1989; McDonald and Buller, 1992; Yan et al., 1993).

In this work, a new inverse emulsion drilling fluid is proposed, and surfactant stabilized inverse emulsions are replaced by Pickering emulsions.

Pickering emulsions are solid particles stabilized emulsions (Fig. 1.17). They can be water-in-oil or oil-in-water emulsions. The type of the emulsion depends on the wettability of the stabilizing solid particles (Wang and Ho, 2011). In general, water-wet solid-particles stabilize oil in water emulsions while oil-wet solid-particles stabilize water-in-oil (or inverse) emulsions. Because we wanted to develop inverse emulsion model drilling fluid, organoclays were used to replace surfactants in the preparation of Pickering emulsions.

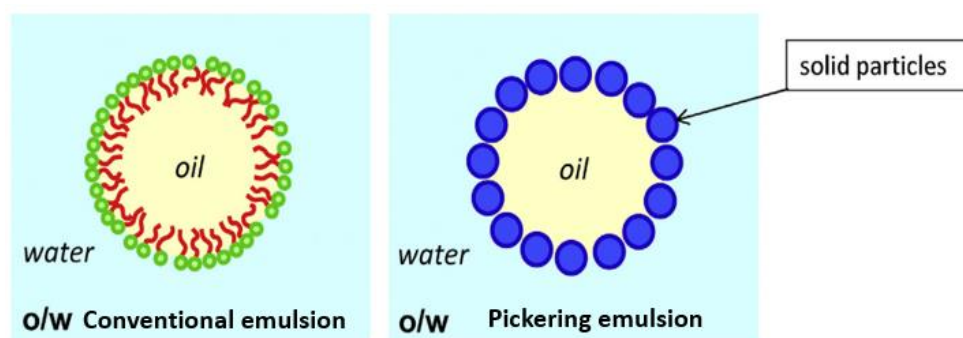


Fig. 1.17 Difference between a surfactant-based emulsion and a Pickering emulsion (Chevalier and Bolzinger, 2013).

Solid-particles stabilized emulsions can have the same characteristics as surfactant-based emulsions if the solid particles do not self-interact. If interactions are possible between the solid particles, the characteristics and behavior of Pickering emulsions may vary from those of conventional emulsions. In the current study, Pickering emulsions are prepared using organoclays. Organoclay suspensions were found to have a shear-thinning, yielding, and viscoelastic behavior. Their use to stabilize water in oil emulsions may result in a fluid with a complex behavior. The rheological and the flow behavior of Pickering emulsions will be discussed in Chapters 4 and 5.

## 1.6 Summary to Chapter

The aim of this chapter was to present some of the required background to help understanding the research work reported in this manuscript.

In the first part, some mathematical and physical tools used to study rheological and pipe-flow behaviors of non-Newtonian fluids were given. In the second part, a literature review on the material used in this work was presented.

In the following chapter, the used experimental apparatus and protocols will be detailed.

## 1.7 References

- Anandha, M., 2002. Rheology of Fluid, Semisolid, and Solid Foods, Statistical Methodology.
- Andrade, L.C.F., Petronílio, J.A., Maneschy, C.E. de A., Cruz, D.O. de A., 2007. The carreau-yasuda fluids: a skin friction equation for turbulent flow in pipes and kolmogorov dissipative scales. *J. Brazilian Soc. Mech. Sci. Eng.* 29, 162–167.  
<https://doi.org/10.1590/S1678-58782007000200005>
- Azouz, K. Ben, Dupuis, D., Bekkour, K., 2010. Rheological characterizations of dispersions of clay particles in viscoelastic polymer solutions. *Appl. Rheol.* 20.  
<https://doi.org/10.3933/ApplRheol-20-13041>
- Baba Hamed, S., Belhadri, M., 2009. Rheological properties of biopolymers drilling fluids. *J. Pet. Sci. Eng.* 67, 84–90. <https://doi.org/10.1016/J.PETROL.2009.04.001>
- Bahlouli, M.I., Bekkour, K., Benchabane, A., Hemar, Y., Nemdili, A., 2013. The effect of temperature on the rheological behavior of polyethylene oxide (PEO) solutions. *Appl. Rheol.* 23. <https://doi.org/10.3933/ApplRheol-23-13435>
- Barnes, H., Hutton, J., Walters F.R.S, K., 1989. Rheology series 3: An introduction to rheology, ELSEVIER. ed. Elsevier B.V.
- Barnes, H.A., 1999. The yield stress—a review or ‘*παντα ρει*’—everything flows? *J. Nonnewton. Fluid Mech.* 81, 133–178. [https://doi.org/10.1016/S0377-0257\(98\)00094-9](https://doi.org/10.1016/S0377-0257(98)00094-9)
- Barnes, H.A., 1997. Thixotropy—a review. *J. Nonnewton. Fluid Mech.* 70, 1–33.  
[https://doi.org/10.1016/S0377-0257\(97\)00004-9](https://doi.org/10.1016/S0377-0257(97)00004-9)
- Barnes, H.A., Walters, K., 1985. The yield stress myth? *Rheol. Acta* 24, 323–326.  
<https://doi.org/10.1007/BF01333960>
- Becker, L.C., 2012. Final Report On the Safety Assessment of Ammonium Hectorites as Used in Cosmetics.
- Bekkour, K., Kherfellah, N., 2002. Linear Viscoelastic Behavior of Bentonite-Water Suspensions Abstract : *Appl. Rheol.* 12, 234–240.
- Bekkour, K., Leyama, M., Benchabane, A., Scrivener, O., 2005. Time-dependent rheological behavior of bentonite suspensions: An experimental study. *J. Rheol. (N. Y. N. Y.)* 49,

1329–1345. <https://doi.org/10.1122/1.2079267>

- Benchabane, A., 2006. Etude du comportement rhéologique de mélanges argiles - polymères. Effets de l'ajout de polymères. Thèse. Université Louis Pasteur, Strasbourg.
- Benmouffok-Benbelkacem, G., Caton, F., Baravian, C., Skali-Lami, S., 2010. Non-linear viscoelasticity and temporal behavior of typical yield stress fluids: Carbopol, Xanthan and Ketchup. *Rheol. Acta* 49, 305–314. <https://doi.org/10.1007/s00397-010-0430-4>
- Benslimane, A., 2013. Rhéologie et écoulement de fluides chargés : application aux réseaux d'assainissement urbains : étude expérimentale et modélisation. Thèse. Université de Strasbourg.
- Benslimane, A., 2012. Rhéologie et écoulement de fluides chargés : application aux réseaux d'assainissement urbains : étude expérimentale et modélisation. Université de Strasbourg.
- Benslimane, A., Bekkour, K., François, P., Bechir, H., 2016. Laminar and turbulent pipe flow of bentonite suspensions. *J. Pet. Sci. Eng.* 139, 85–93.  
<https://doi.org/10.1016/j.petrol.2015.12.020>
- Benyounes, K., Mellak, A., Benchabane, A., 2010. The effect of carboxymethylcellulose and xanthan on the rheology of bentonite suspensions. *Energy Sources, Part A Recover. Util. Environ. Eff.* 32, 1634–1643. <https://doi.org/10.1080/15567030902842244>
- Bergaya, F., Lagaly, G., 2002. Surface modification of clay minerals. *Appl. Clay Sci.* 19, 1–3. [https://doi.org/10.1016/s0169-1317\(01\)00063-1](https://doi.org/10.1016/s0169-1317(01)00063-1)
- Bergaya, F., Theng, B.K.G., Lagaly, G., 2006. Handbook of Clay Science, JavaWorld: IDG's magazine for the Java community.
- Bhatt, J., Somani, R.S., Mody, H.M., Bajaj, H.C., 2013. Rheological study of organoclays prepared from Indian bentonite: Effect of dispersing methods. *Appl. Clay Sci.* 83–84, 106–114. <https://doi.org/10.1016/J.CLAY.2013.08.012>
- Boyd, J., Buick, J.M., Green, S., 2007. Analysis of the Casson and Carreau-Yasuda non-Newtonian blood models in steady and oscillatory flows using the lattice Boltzmann method. *Phys. Fluids* 19. <https://doi.org/10.1063/1.2772250>
- Brkić, D., 2011. Review of explicit approximations to the Colebrook relation for flow friction.

- J. Pet. Sci. Eng. 77, 34–48. <https://doi.org/10.1016/j.petrol.2011.02.006>
- Cavalcanti, J.V.F.L., Abreu, C. a. M., Carvalho, M.N., Sobrinho, M. a. M., Benachour, M., Baraúna, O.S., 2012. Removal of Effluent from Petrochemical Wastewater by Adsorption Using Organoclay. *J. intech Open Sci.* 14, 277–295. <https://doi.org/10.5772/37200>
- Chevalier, Y., Bolzinger, M.-A., 2013. Emulsions stabilized with solid nanoparticles: Pickering emulsions. *Colloids Surfaces A Physicochem. Eng. Asp.* 439, 23–34. <https://doi.org/10.1016/J.COLSURFA.2013.02.054>
- Chilton, R.A., Stainsby, R., 1998. Pressure Loss Equations For Laminar And Turbulent Non-Newtonian Pipe Flow. *J. Hydraul. Eng.* 124, 522–529.
- Cho, Y.I., Harnett, J.P., 1982. Non-Newtonian Fluids in Circular Pipe Flow. *Adv. Heat Transf.* 15, 59–141. [https://doi.org/10.1016/S0065-2717\(08\)70173-4](https://doi.org/10.1016/S0065-2717(08)70173-4)
- Churchill, S., 1977. Friction-factor equation spans all fluid-flow regimes. *Chem. Eng. Sci.* 84, 91–92.
- Coussot, P., Grossiord, J., 2002. Comprendre la rhéologie, de la circulation du sang à la prise du béton, EDP science.
- de Paiva, L.B., Morales, A.R., Valenzuela Díaz, F.R., 2008. Organoclays: Properties, preparation and applications. *Appl. Clay Sci.* 42, 8–24. <https://doi.org/10.1016/J.CLAY.2008.02.006>
- Dekany, I., Szanto, F., Weiss, A., Lagaly, G., 1986. Interactions of Hydmpdk Layer Silicates with AlcoholBenzene Mixtures I. *Adsorption Isotherms* 422–427.
- Dodge, D.W., Metzner, A.B., 1959. Turbulent flow of non-newtonian systems. *AIChE J.* 5, 189–204. <https://doi.org/10.1002/aic.690050214>
- Dolz, M., Hernández, M.J., Delegido, J., 2008. Creep and recovery experimental investigation of low oil content food emulsions. *Food Hydrocoll.* 22, 421–427. <https://doi.org/10.1016/J.FOODHYD.2006.12.011>
- Ebagninin, K.W., Benchabane, A., Bekkour, K., 2009. Rheological characterization of poly(ethylene oxide) solutions of different molecular weights. *J. Colloid Interface Sci.* 336, 360–367. <https://doi.org/10.1016/J.JCIS.2009.03.014>

- Escudier, M.P., Poole, R.J., Presti, F., Dales, C., Nouar, C., Desaubry, C., Graham, L., Pullum, L., 2005. Observations of asymmetrical flow behaviour in transitional pipe flow of yield-stress and other shear-thinning liquids. *J. Nonnewton. Fluid Mech.* 127, 143–155. <https://doi.org/10.1016/J.JNNFM.2005.02.006>
- G. Vieira, M., E. C. Peres, A., 2012. Effect of Reagents on the Rheological Behavior of an Iron Ore Concentrate Slurry. *Int. J. Min. Eng. Miner. Process.* 1, 38–42. <https://doi.org/10.5923/j.mining.20120102.03>
- Gorrasi, G., Tortora, M., Vittoria, V., Kaempfer, D., Mülhaupt, R., 2003. Transport properties of organic vapors in nanocomposites of organophilic layered silicate and syndiotactic polypropylene. *Polymer (Guildf).* 44, 3679–3685. [https://doi.org/10.1016/S0032-3861\(03\)00284-2](https://doi.org/10.1016/S0032-3861(03)00284-2)
- Grim, R.E., 1968. *Clay mineralogy*, 2d ed. ed. McGraw-Hill, New York.
- Güneyisi, E., Gesoglu, M., Naji, N., İpek, S., 2016. Evaluation of the rheological behavior of fresh self-compacting rubberized concrete by using the Herschel–Bulkley and modified Bingham models. *Arch. Civ. Mech. Eng.* 16, 9–19. <https://doi.org/10.1016/J.ACME.2015.09.003>
- Güzel, B., Burghilea, T., Frigaard, I.A., Martinez, D.M., 2009. Observation of laminar-turbulent transition of a yield stress fluid in Hagen-Poiseuille flow. *J. Fluid Mech.* 627, 97–128. <https://doi.org/10.1017/S0022112009005813>
- Hebbar, R.S., Isloor, A.M., Ismail, A.F., 2014. Preparation and evaluation of heavy metal rejection properties of polyetherimide/porous activated bentonite clay nanocomposite membrane. *RSC Adv.* 4, 47240–47248. <https://doi.org/10.1039/c4ra09018g>
- Hu, Z., He, G., Liu, Y., Dong, C., Wu, X., Zhao, W., 2013. Effects of surfactant concentration on alkyl chain arrangements in dry and swollen organic montmorillonite. *Appl. Clay Sci.* 75–76, 134–140. <https://doi.org/10.1016/J.CLAY.2013.03.004>
- Jaber, M., Miehe-Brendlé, J., 2009. *Organoclays. Preparation, Properties and Applications. Ordered Porous Solids* 31–49. <https://doi.org/10.1016/B978-0-444-53189-6.00002-0>
- Jia, Y., Peng, K., Gong, X., Zhang, Z., 2011. Creep and recovery of polypropylene/carbon nanotube composites. *Int. J. Plast.* 27, 1239–1251. <https://doi.org/10.1016/J.IJPLAS.2011.02.004>

- Jordan, J.W., 1949. Organophilic bentonites. I: Swelling in organic liquids. *J. Phys. Colloid Chem.* 53, 294–306. <https://doi.org/10.1021/j150467a009>
- Karimi, V.A., VanOort, E., 2015. Determination of drilling fluid rheology under downhole conditions by using real-time distributed pressure data. *J. Nat. Gas Sci. Eng.* 24, 400–411. <https://doi.org/10.1016/J.JNGSE.2015.04.004>
- Kelessidis, V.C., Dalamarinis, P., Maglione, R., 2011. Experimental study and predictions of pressure losses of fluids modeled as Herschel–Bulkley in concentric and eccentric annuli in laminar, transitional and turbulent flows. *J. Pet. Sci. Eng.* 77, 305–312. <https://doi.org/10.1016/J.PETROL.2011.04.004>
- Kelessidis, V.C., Maglione, R., Tsamantaki, C., Aspirtakis, Y., 2006. Optimal determination of rheological parameters for Herschel–Bulkley drilling fluids and impact on pressure drop, velocity profiles and penetration rates during drilling. *J. Pet. Sci. Eng.* 53, 203–224. <https://doi.org/10.1016/J.PETROL.2006.06.004>
- Kinloch, I.A., Roberts, S.A., Windle, A.H., 2002. A rheological study of concentrated aqueous nanotube dispersions. *Polymer (Guildf)*. 43, 7483–7491. [https://doi.org/10.1016/S0032-3861\(02\)00664-X](https://doi.org/10.1016/S0032-3861(02)00664-X)
- Kozicki, W., Chou, C.H., Tiu, C., 1966. Non-Newtonian flow in ducts of arbitrary cross-sectional shape. *Chem. Eng. Sci.* 21, 665–679. [https://doi.org/10.1016/0009-2509\(66\)80016-7](https://doi.org/10.1016/0009-2509(66)80016-7)
- Lagaly, G., Gonzalez, F., Weiss, A., 1976. Problems in layer-charge determination of montmorillonites. *Clay Miner.* 11, 173.
- Maxey, J., 2007. Thixotropy and Yield Stress Behavior in Drilling Fluids. *Am. Assoc. Drill. Eng.* 07.
- McDonald, J.A., Buller, D.C., 1992. The significance of formation damage caused by the adsorption oil-based mud surfactant. *J. Pet. Sci. Eng.* [https://doi.org/10.1016/0920-4105\(92\)90062-6](https://doi.org/10.1016/0920-4105(92)90062-6)
- Menezes, J., Yan, J., Sharma, M.M., 1989. The Mechanism of Wettability Alteration Due to Surfactants in Oil-Based Muds. *Soc. Pet. Eng. SPE* 18460, 17–29.
- Merad, B., Bekkour, K., Gareche, M., 2019. Rheological and structural characterization of organo-hectorite dispersions: Influence of the organoclay loading. *Appl. Clay Sci.*

105321. <https://doi.org/10.1016/j.clay.2019.105321>

Merinska, D., Malac, Z., Pospisil, M., Weiss, Z., Chmielova, M., Capkova, P., Simonik, J., 2002. Polymer/clay nanocomposites based on MMT/ODA intercalates. *Compos. Interfaces* 9, 529–540. <https://doi.org/10.1163/15685540260494100>

Moraru, V.N., 2001. Structure formation of alkylammonium montmorillonites in organic media. *Appl. Clay Sci.* 19, 11–26. [https://doi.org/10.1016/S0169-1317\(01\)00053-9](https://doi.org/10.1016/S0169-1317(01)00053-9)

Murray, H.H., 2007. *Applied Clay Mineralogy Occurrence Processing and Application of Kaolins Bentonites Palygorskite Sepiolite and Common Clays*, Elsevier. ed.

Murray, H.H., 1991. Overview — clay mineral applications. *Appl. Clay Sci.* 5, 379–395. [https://doi.org/10.1016/0169-1317\(91\)90014-Z](https://doi.org/10.1016/0169-1317(91)90014-Z)

Nehdi, M., Rahman, M.-A., 2004. Estimating rheological properties of cement pastes using various rheological models for different test geometry, gap and surface friction. *Cem. Concr. Res.* 34, 1993–2007. <https://doi.org/10.1016/J.CEMCONRES.2004.02.020>

Okada, A., Fukushima, Y., Kawasumi, M., Inagaki, S., 1988. Composite material and process for manufacturing same. US Patent.

Papanicolaou, G.C., Zaoutsos, S.P., 2011. Viscoelastic constitutive modeling of creep and stress relaxation in polymers and polymer matrix composites. *Creep Fatigue Polym. Matrix Compos.* 3–47. <https://doi.org/10.1533/9780857090430.1.3>

Peixinho, J., Nouar, C., Desaubry, C., Théron, B., 2005. Laminar transitional and turbulent flow of yield stress fluid in a pipe. *J. Nonnewton. Fluid Mech.* 128, 172–184. <https://doi.org/10.1016/J.JNNFM.2005.03.008>

Purushothmann, K.V., 2017. *Laminar and Turbulent flows in pipes*. Online course.

Quintero, L., 2002. An Overview of Surfactant Applications in Drilling Fluids for the Petroleum Industry. *J. Dispers. Sci. Technol.* 23, 1–3. <https://doi.org/10.1080/01932690208984212>

Ragouilliaux, A., Pierre, L.U., Marie, E.T., 2008. Etude rhéophysique de systèmes émulsions inverses / argile organophile . Applications au boues de forage pétrolier. Thèse.

Razavi, S.M.A., Karazhiyan, H., 2009. Flow properties and thixotropy of selected hydrocolloids: Experimental and modeling studies. *Food Hydrocoll.* 23, 908–912.

<https://doi.org/10.1016/J.FOODHYD.2008.05.010>

- Rooki, R., Ardejani, F.D., Moradzadeh, A., Mirzaei, H., Kelessidis, V., Maglione, R., Norouzi, M., 2012. Optimal determination of rheological parameters for herschel-bulkley drilling fluids using genetic algorithms (GAs). *Korea-Australia Rheol. J.* 24, 163–170. <https://doi.org/10.1007/s13367-012-0020-3>
- Schramm, G., 1998. *A Practical Approach to Rheology and Rheometry*, Gebrueder. ed.
- Schramm, L.L., 2000. *Surfactants: Fundamentals and Applications in the petroleum industry*, Cambridge. ed.
- Vajargah Karimi, A., Sullivan, G., Johnson, M., Oort, E. Van, 2017. *Transitional and Turbulent Flow of Drilling Fluids in Pipes : An Experimental Investigation*. Am. Assoc. Drill. Eng.
- Wang, C.-H., Ho, J.-R., 2011. A lattice Boltzmann approach for the non-Newtonian effect in the blood flow. *Comput. Math. with Appl.* 62, 75–86. <https://doi.org/10.1016/J.CAMWA.2011.04.051>
- Xi, Y., Ding, Z., He, H., Frost, R.L., 2004. Structure of organoclays—an X-ray diffraction and thermogravimetric analysis study. *J. Colloid Interface Sci.* 277, 116–120. <https://doi.org/10.1016/J.JCIS.2004.04.053>
- Yan, J.N., Menezes, J.L., Sharma, M.M., 1993. Wettability Alteration Caused by Oil-Based Muds and Mud Components. *SPE Drill. Complet.* 35–44.
- Yao, Z., Wu, D., Chen, C., Zhang, M., 2013. Creep behavior of polyurethane nanocomposites with carbon nanotubes. *Compos. Part A Appl. Sci. Manuf.* 50, 65–72. <https://doi.org/10.1016/J.COMPOSITESA.2013.03.015>
- Zare, Y., Park, S.P., Rhee, K.Y., 2019. Analysis of complex viscosity and shear thinning behavior in poly (lactic acid)/poly (ethylene oxide)/carbon nanotubes biosensor based on Carreau–Yasuda model. *Results Phys.* 13, 102245. <https://doi.org/10.1016/J.RINP.2019.102245>
- Zhu, J., He, H., Zhu, L., Wen, X., Deng, F., 2005. Characterization of organic phases in the interlayer of montmorillonite using FTIR and <sup>13</sup>C NMR. *J. Colloid Interface Sci.* 286, 239–244. <https://doi.org/10.1016/J.JCIS.2004.12.048>

- Zhuang, G., Zhang, H., Wu, H., Zhang, Z., Liao, L., 2017a. Influence of the surfactants' nature on the structure and rheology of organo-montmorillonite in oil-based drilling fluids. *Appl. Clay Sci.* 135, 244–252. <https://doi.org/10.1016/J.CLAY.2016.09.033>
- Zhuang, G., Zhang, Z., Jaber, M., Gao, J., Peng, S., 2017b. Comparative study on the structures and properties of organo-montmorillonite and organo-palygorskite in oil-based drilling fluids. *J. Ind. Eng. Chem.* 56, 248–257. <https://doi.org/10.1016/J.JIEC.2017.07.017>
- Zhuang, G., Zhang, Z., Sun, J., Liao, L., 2016. The structure and rheology of organo-montmorillonite in oil-based system aged under different temperatures. *Appl. Clay Sci.* 124–125, 21–30. <https://doi.org/10.1016/J.CLAY.2016.01.051>
- Zhuang, G., Zhang, Z., Yang, H., Tan, J., 2018. Structures and rheological properties of organo-sepiolite in oil-based drilling fluids. *Appl. Clay Sci.* 154, 43–51. <https://doi.org/10.1016/j.clay.2017.12.048>

## REVIEW OF THE LITTERATURE

**CHAPTER 2.**  
**MATERIALS AND METHODS**

## CHAPTER 2

**TABLE OF CONTENTS**

2.1	Introduction.....	56
2.2	Rheological measurement techniques.....	56
2.2.1	Measuring geometry.....	57
2.2.2	Experimental problems inducing measuring errors.....	58
2.3	Hydraulic loop.....	59
2.3.1	Pump calibration.....	63
2.3.2	Testing system.....	64
2.3.3	Emulsification system.....	70
2.4	Fluid preparation protocol.....	70
2.5	Summary to Chapter.....	71
2.6	References.....	73

## 2.1 Introduction

In the precedent chapter, the theory used in our study was detailed. Two different aspects were discussed, the rheology and the pipe-flow of non-Newtonian fluids. It can be noticed that some measurement techniques are necessary to obtain the needed experimental data. Furthermore, the preparation procedure of the studied organoclay suspensions and Pickering emulsions is still ambiguous.

In the following, the rheological measurement techniques will be detailed as well as the experimental set used in the study of the flow of Pickering emulsions. This experimental setup is termed “hydraulic loop” or “flow loop” and is equipped with pressure and velocity measuring devices that will also be described. Finally, the preparation protocols of organoclay suspensions and Pickering emulsions will be presented.

## 2.2 Rheological measurement techniques

The rheological measurements were conducted using an AR2000 stress applied rheometer, purchased from TA Instruments, France (Fig. 2.1). AR2000 is a rotative rheometer where the geometry is formed of a rotating unit and a fixed unit (Fig. 2.2). The shearing torque is applied on the fluid via the rotating part of the geometry, and therefore the studied material deforms and flows, if the applied stress is higher than its yield stress value. In the case of the current study, a cone and a plate geometry was used with different angles ( $2^\circ$  and  $4^\circ$ ). The expressions of shear stress and shear rate are written as follows (Ben Azouz Ahmed, 2012):

$$\sigma = \frac{3}{2\pi R^3} M \quad 2.1$$

$$\dot{\gamma} = \frac{1}{\alpha} \omega \quad 2.2$$

where  $\dot{\gamma}$  is the resulting shear rate,  $\alpha$  is the cone angle,  $\omega$  is the angular velocity,  $\sigma$  is the applied shear stress,  $R$  is the cone radius and  $M$  is the applied couple.



Fig. 2.1 AR2000 rheometer.

### 2.2.1 Measuring geometry

There is no precise procedure to define the proper measuring geometry for rheological measurements. Our choice was purely based on previous works, where the rheological behavior of different colloidal systems was studied (Benchabane and Bekkour, 2008; Ebagninin et al., 2009; Bahlouli et al., 2013; Benslimane, 2013).

Cone and plate geometry was then chosen with a cone angle of  $2^\circ$  and  $4^\circ$ . The same geometry was used in our lab to measure the rheological behavior of clay dispersions (Benchabane, 2006), polymer solutions (Ebagninin et al., 2009) and clay-polymer dispersions (Ben Azouz Ahmed, 2012). The choice of the cone angle was based on two considerations:

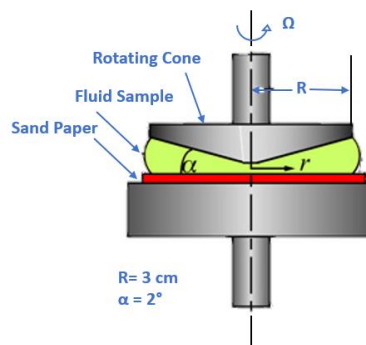


Fig. 2.2 Measuring geometry (Benchabane, 2006).

- i. Attend a maximum shear rate. According to Eq. 2.2, shear rate is inversely proportional to the cone angle, so a maximum shear rate is reached when using a geometry with the lowest possible cone angle.
- ii. The ratio between the geometry gap and the size of the measured particles should be greater than 10 (Benslimane, 2013). In the case of organo- Hectorite dispersions, for example, the maximal size after swelling, was 18  $\mu\text{m}$ .

## 2.2.2 Experimental problems inducing measuring errors

### 2.2.2.1. Sample evaporation

Sample evaporation can take place if the sample, during the measurement, is in a direct contact with air. In this case, a volume of the continuous phase would evaporate and thus the mass concentration of the dispersion and its apparent viscosity increase.

To prevent this problem and minimize the measurements errors, two types of practical solutions are usually used:

- i. Proceed the rheological measurements in a saturated environment (Benchabane, 2006; Benslimane, 2013).
- ii. Adding a thin oil film to prevent the direct contact between the studied material and air, in the case of cylindrical measurement geometries (Ouaer and Gareche, 2018).

In our study, and to prevent the continuous phase evaporation, all the measurements were conducted in an oil-saturated environment (Fig. 2.3).

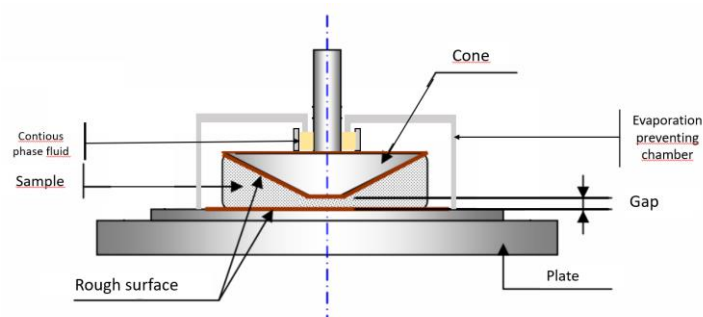


Fig. 2.3 Sample evaporation apparatus (Benchabane, 2006).

### 2.2.2.2. Wall slip

This phenomenon could be encountered when working with colloidal materials such as polymer solutions, particle suspensions, and emulsions (Barnes, 1995). Wall slipping takes place when using geometries with smooth surfaces and results in a preferential shearing in the layers adjacent to the wall. This phenomenon can cause different measurement errors especially at low shear rates, where an underestimation of the yield stress can take place. The presence of wall slipping can be suspected if a sudden decrease of the viscosity is noticed at the beginning of the flow. In order to eliminate, or at least minimize, wall slipping effects, the plate of the geometry was covered by a rough surface (sandpaper) with a roughness of  $30,2 \mu\text{m}$ .

## 2.3 Hydraulic loop

Experiments during pipe-flow were realized using an assembly of a pump, pipes, and measuring tools called the “hydraulic loop”. The hydraulic loop was fully designed and built by the Mecafllu team in ICube laboratory. A schematic diagram of the flow loop used in the current study is represented in Fig. 2.4.

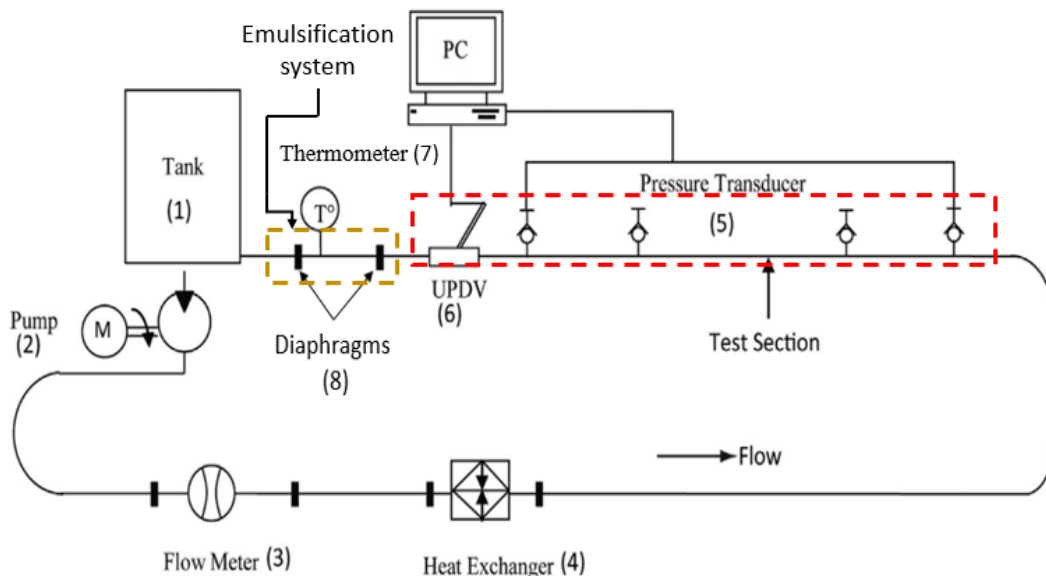


Fig. 2.4 Schematic diagram of the hydraulic loop.

The apparatus is composed of a 50 L tank (1), where the organoclay in gasoil suspension and water are initially added. After that, the studied fluid passes through a volumetric pump (PCM-Moineau, France) (2), that can generate flow rates up to  $9 \text{ m}^3 \cdot \text{h}^{-1}$ . The flow rate at the outlet of the pump is regulated and can be measured using a flow meter (3). The loop consists of an assemblage of transparent smooth Plexiglas tubes of two diameters: 20 mm and 50 mm. In the current study, all the experiments were conducted in the 20 mm tubes. The total length of the pipes is 16 m. Both pressure and velocity measurements are possible at different positions of the hydraulic loop. Moreover, the design was made in a way that different sections of the loop can be easily interchanged at any time, even without draining the tank, to measure pressure and velocity profiles at any point. This allows to study different flow effects such as entry effects and singularities. The measuring system is composed of pressure sensors (GS SensorsXPM) (5) and an Ultrasound Pulsed Doppler Velocimeter (6). The flow loop is equipped with 7 pressure sensors, located at different distances from the inlet and used to measure linear pressure losses. Unless mentioned otherwise, the used pressure sensors are located at 4.36 m and 8 m from the inlet of the flow loop, with a maximum measured absolute pressure of 2.5 bars. Furthermore, the pressure sensors are calibrated before and after each experiment. Velocity profiles are obtained using a non-intrusive Ultrasound Pulsed Doppler Velocimetry (UPDV). As it can be noticed from Fig. 2.4, the UPD velocimeter is located far from the loop entry and before the diaphragms, which allows to measure steady-state flow velocity profiles. The temperature of the fluid was monitored using a thermometer (7) near to the loop outlet.

Our in-line emulsification system is composed of two diaphragms (8), placed after the measuring system. This sudden diameter restriction leads to an increase in the local velocity and thus to the appearance of turbulence.

Several valves are integrated into the loop giving the possibility to customize the wanted flow circuit. For instance, a simple manipulation of these valves allows to choose measuring either structured or unstructured fluid. This can be very important when studying fluids with high thixotropy effects such as bentonite suspensions. Benslimane (2012) in his work, studied pressure losses and velocity profiles of structured bentonite suspensions. To do so, the valves were manipulated in a way that the fluid flows directly to the loop without passing by the pump. This experiment was not conducted in our study because of the absence of time dependency effects in the case of the studied fluids. Our fluid circulation trajectory is illustrated in Fig. 2.5.

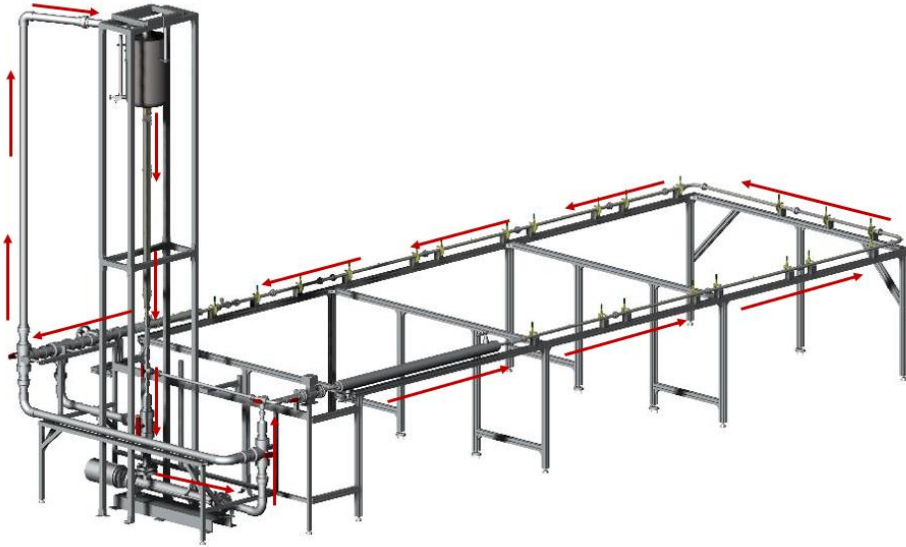


Fig. 2.5 Fluid circuit in the hydraulic loop.

A sealing joint is used to attach two pipes together (Fig. 2.6), and two resistance seals were placed at the beginning and at the end of the flow loop to limit the vibrations caused by the pump (Fig. 2.7). The pipe assembly is put on a U-shaped aluminum frame, and special clips were used to fix the pipes to the frame (Fig. 2.8). Two 90° elbows (Fig.2.9) were especially designed to obtain the U shape of the loop.



Fig. 2.6 Sealing joints.

CHAPTER 2



Fig. 2.7 Operating principle of the volumetric pump.



Fig. 2.8 Fixing clips.

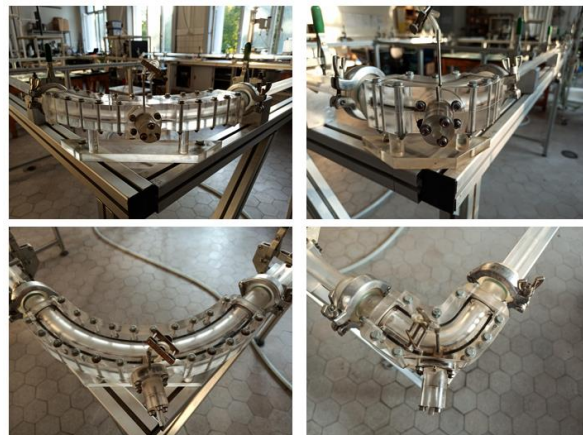


Fig. 2.9 90° in-house designed elbows.

### 2.3.1 Pump calibration

A verification of the volumetric flow rate given by the pump was conducted to ensure that the real given flow rate is equal to the one indicated by the flow meter, and to establish a relationship between the pump rotation and the given flow rate. Water was used in this calibration process. Several rotation speeds were imposed, and the flow rate values given by the flow meter were registered. At the same time, a container, a scale, and a timer were used to measure the needed time to fill the container and its corresponding mass. These measurements were used to calculate the flow rate for each pump rotation speed.

As it can be noticed from Fig. 2.10, where flow rates calculated using the mass and time measurements were plotted as a function of the flow rate values given by the flow meter, both technics give similar values, and the data can be fitted using an  $x$  graph. The latter allowed to confirm the performance of our pump.

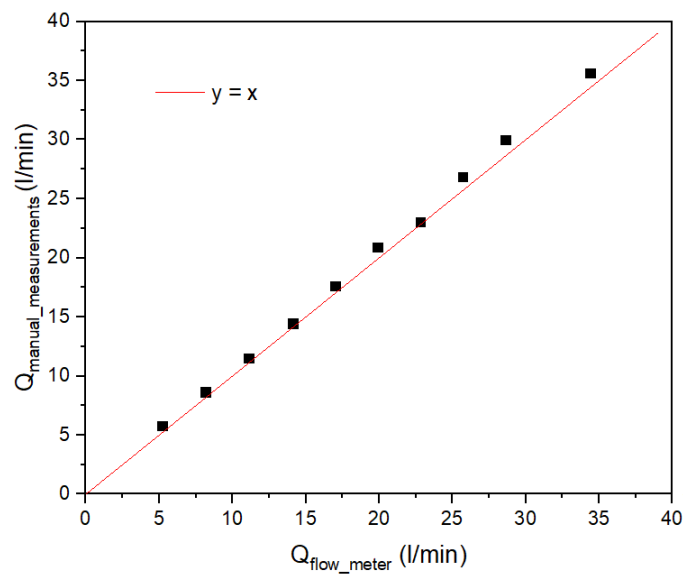


Fig. 2.10 Verification of the flow rate given by the pump.

## 2.3.2 Testing system

### 2.3.2.1. Pressure measuring system

Pressure measurements are performed using pressure sensors, conditioners, and a data acquisition card.

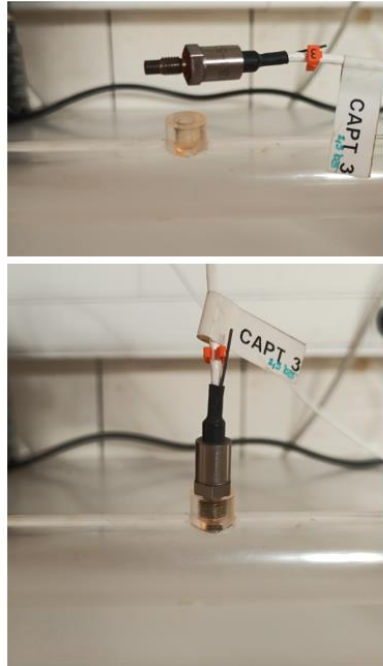


Fig. 2.11 Pressure sensors.

Pressure sensors are strain gaged. This type of sensors is equipped with a flexible foil that deforms as the pressure changes. The latter induces a change in the electrical resistance of the foil that is used to calculate the applied strain and thus the pressure of the fluid. The pressure reference of the used sensors, in other words the reference shape of the foil, is the atmospheric pressure. All sensors are equipped with a small capillary open to ambient air (Fig. 2.11). It should be noticed that the applied pressure should be within the elastic domain of the foil. In our case, two pressure sensors with a maximum possible applied pressure of 2,5 bars were used. Operating temperature of the sensors ranges between (-40°C and +120°C). A calibration of these sensors should be conducted before and after each measurement campaign because of their sensibility to temperature changes.

The second element in our pressure measurement chain is the conditioners. They are responsible to supply the pressure sensors with electricity, receive their transmitted signals, and send it to the data acquisition card. The data acquisition card is responsible of the digitization of the electrical signal (Fig. 2.12).

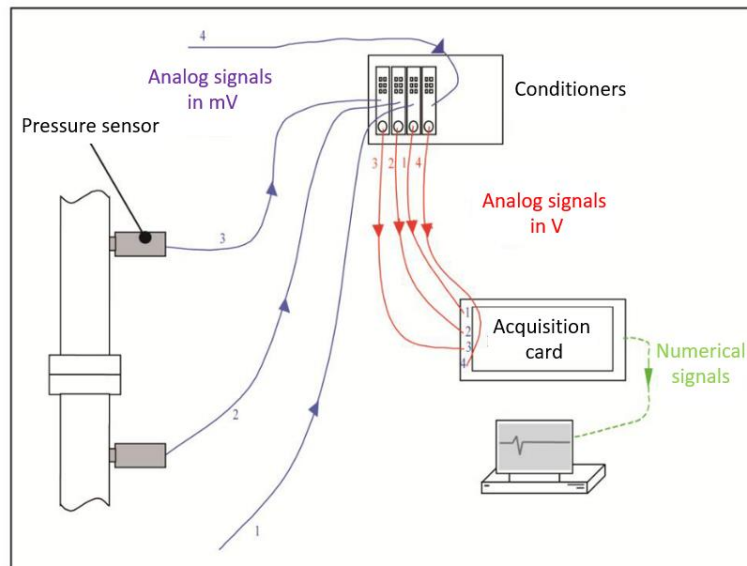


Fig. 2.12 Pressure measurement chain (Benslimane, 2012).

#### 2.3.2.1.1. Pressure calibration

As it was mentioned in the previous section, pressure sensors are very sensible to temperature changes. Therefore, a pressure calibration was necessary before and after pressure measurements. The main reason behind this process is to define a relationship between the tension measured by the sensors and the pressure values.

In the current study, two types of pressure calibration procedures were used. For fluids with low concentrations and small yield stress values, a pressure controller was used. The calibration process starts with reducing the pressure inside the loop to the atmospheric pressure (Fig. 2.13). The pressure controller is then connected to the loop via a rigid plastic tubing. The latter allows to manually impose a known hydraulic pressure value. The response of the pressure sensors is then registered and the relationships between the signals given by the sensors and the hydraulic pressure is deduced. The used pressure controller can measure pressures ranging from 2,5 mbar to 700 bars.

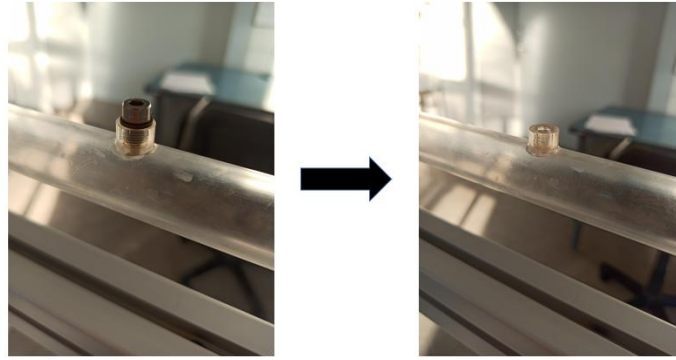


Fig. 2.13 Pressure purging.

At high concentrations, on the other hand, the fluids exhibited remarkably high yield stress values. Consequently, introducing a hydraulic pressure from one entry is no more sufficient to calibrate the pressure sensors. In this case, only the sensors near to the pressure controller would sense the real applied pressure. To overcome this limitation, the following procedure was proposed:

- i. Isolate the flow loop by closing two valves at its inlet and outlet.
- ii. Start recording the pressure data.
- iii. Purge the flow loop at all possible levels (Fig. 2.13) and wait until the equilibration of the measured data.
- iv. Consider the minimum registered value equivalent to the atmospheric pressure.
- v. Deduce the relationships between the registered values and the hydraulic pressure.

#### 2.3.2.1.2. Verification of the pressure measuring system

A Newtonian fluid (gasoil) was used to verify the pressure measuring system. Because of the absence of a yield stress in the case of gasoil, the pressure controller was used to calibrate the pressure sensors. A flow rate ramp was imposed, pressure at different sensors was measured and the friction factor was calculated. The following equation was used to calculate the friction factor:

$$f = \frac{2\sigma_w}{\rho U^2} \quad 2.2$$

where  $f$  is the fanning friction factor,  $\sigma_w$  is the wall shear stress,  $\rho$  is the density and  $U$  is the mean velocity.

Wall shear stress was calculated using the equation:

$$\sigma_w = \frac{R \Delta P}{2 L} \quad 2.3$$

where  $R$  (m) is the pipe radius,  $\Delta P/L$  (Pa/m) is the pressure loss over a pipe length  $L$ .

Fig. 2.14 shows the experimental values of friction factor as a function of the Reynolds number. To verify the validity of the pressure measurements, theoretical models were used to calculate the friction factor both in laminar (the Hagen-Poiseuille equation) and turbulent regimes (the Blasius equation). It is evident from Fig. 2.14 that the theoretical models agree well with the experimental data. It should be noticed that both models were developed for Newtonian fluids, which is the case of gasoil.

Pressure sensors were also verified after each test. To do so, the linearity of the values indicated by the pressure sensors at a constant mean velocity was confirmed. An example of this verification is illustrated in Fig. 2. 15.

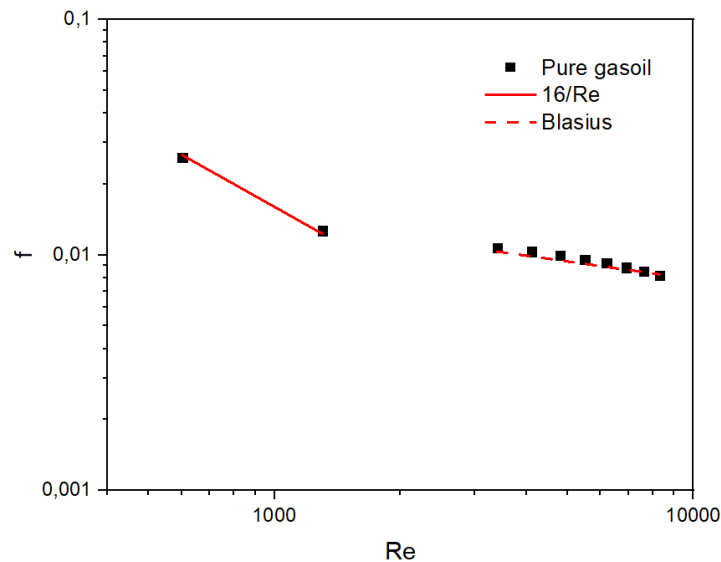


Fig. 2.14 Friction factor as a function of Reynolds number for gasoil.

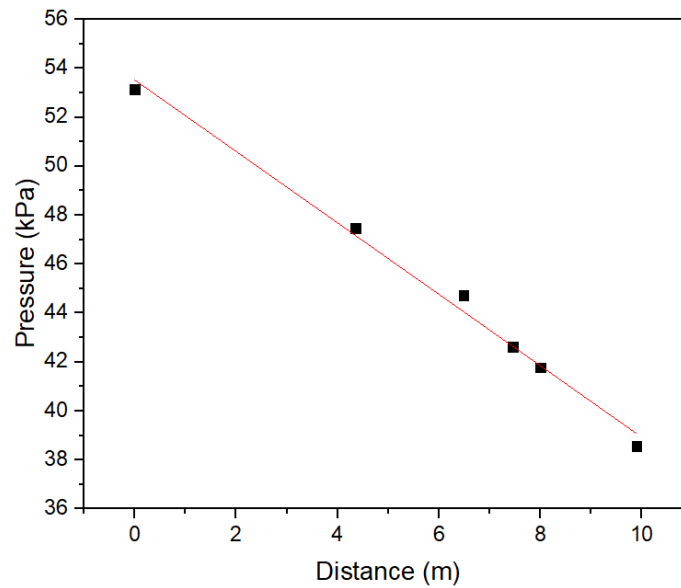


Fig. 2.15 Values of pressure given by the different sensors at a constant mean velocity.

### 2.3.2.2. Velocity measuring system

Ultrasound pulsed Doppler velocimetry (UPDV) was used to measure the steady state velocity profiles as a function of time. This technique comes with two main advantages: it is non-intrusive and therefore does not disturb the fluid flow during the measurements and, unlike optical techniques, it is applicable in the case of opaque fluids. The UPDV technique has been widely used especially in fluid mechanics because of its non-intrusive properties (Teufel et al., 1992; Nowak, 2002; Cramer et al., 2004; Jaafar et al., 2009; Benslimane et al., 2016; Achard et al., 2018; Nauber et al., 2018). Along with being a non-intrusive technique and the possibility of studying opaque fluids, the UPDV technique was also chosen to measure velocity profiles at high temperatures and using chemically aggressive fluids (Eckert and Gerbeth, 2002).

A UPDV technique or a pulsed ultrasound echography method is based on the emission of ultrasounds and the reception of their echoes. A sinusoidal ultrasound beam is emitted from a transducer with an imposed frequency ( $f_E$ ). When the path of the ultrasound wave is interrupted by a particle, its echo is reflected and detected by the same transducer. The repetition of the ultrasound beams (emission-reception cycles) is controlled via the PRF i.e., pulse repetition frequency.

The velocimeter used in this work was initially designed and developed by Fisher during his PhD in the ICube laboratory (ex. IMFS) (Fischer, 2014). Some modifications were eventually

carried out by other researchers. It is now possible to control all the measuring parameters ( $f_E$ ,  $f_D$ , PRF, number of the wanted values in a profile, and the measuring distance). Both Jaafar (2009) and Benslimane (2012) used the same velocimeter in their works to measure the instantaneous velocity profiles of charged fluid flows and found that the experimental results given by the velocimeter coincide well with the theoretical calculations.

A velocimetric transducer is responsible of the emission and the reception of ultrasound waves. It has a diameter of 5 mm and placed in a probe holder. The latter was made with the same Plexiglas used for the flow tubes. Both the transducer and the holder are presented in Fig. 2.16. A thin plastic film was placed inside the tubular part of the holder to create the same internal diameter as that of the tubes. The holder is also equipped with a valve which permits the elimination of air bubbles. The transducer is placed at an opposite direction to the main flow with an angle of  $73,8^\circ$  to the horizontal. A large angle was chosen to increase the range of the possible measured velocity values. Particle velocity is calculated using the following expression:

$$u = \frac{c_w f_D}{2 f_E \cos \theta} \quad 2.4$$

where  $c_w$  is the acoustic celerity in water at a given temperature,  $f_D$  is the Doppler shift frequency induced by the particle motion,  $f_E$  is the emission frequency, and  $\theta$  is the angle between the axis of the UPDV transducer and the flow direction.

The performance of the velocity measuring system was tested using Newtonian fluids (water and gasoil).

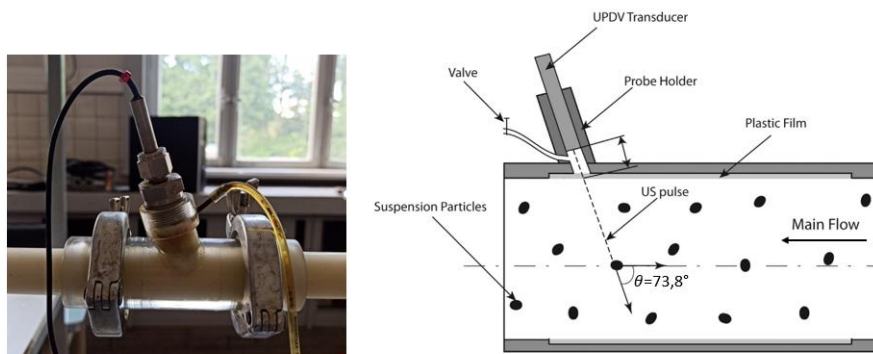


Fig. 2.16 UPDV transducer and its holder.

### 2.3.3 Emulsification system

An emulsification system was designed to prepare Pickering emulsions inside the flow loop. The reason behind choosing an in-line emulsification instead of a selection of turbines is the need of large fluid quantities (70 L) to insure the absence of air bubbles in the flow loop during measurements. The emulsification system was composed of two diaphragms (Fig. 2.17) placed at the end of the flow loop and after the testing system (see Fig. 2.4). This placement was carefully chosen to assure having a steady state flow during measurements. The sudden diameter restriction leads to an increase in the shear rate and thus in the emulsification of the fluid. The efficacy of the latter system to produce homogenous and stable Pickering emulsions was confirmed and will be discussed in chapters 4 and 5. It should be noticed that the pump, the pipe-flow, and the singularities of the flow loop contribute, as well, to the emulsification process. However, no experiments were conducted to study the influence of each of these elements on the emulsification of the fluid.

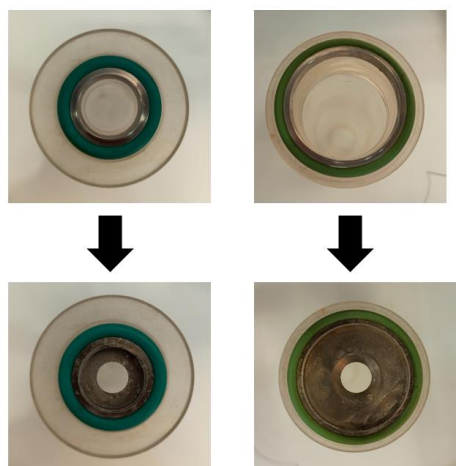


Fig. 2.17 20 mm (left) and 50 mm (right) Plexiglass tubes with and without the diaphragms.

## 2.4 Fluid preparation protocol

Shear history can be of a big influence on the rheological properties of the studied fluids. Therefore, their preparation protocol can have a high impact on their inner structure. Different preparation protocols were tested and two were chosen to prepare the organoclay suspensions

and the Pickering emulsions. A preparation protocol is chosen if the fluid is stable and allows to have reproducible data.

- Organoclay suspensions: Organo-hectorite powder was first dispersed in gasoil and homogenized under a constant mechanical agitation at 500 rpm, which was found to be the optimum speed for the preparation of organoclay dispersions (Bhatt et al., 2013), for 24 h. The prepared dispersions were then left at rest for 24 h at 20° C and stirred at low speed for 1 h before each experiment to ensure their homogenization.
- Pickering emulsions: first, an organo-hectorite in gasoil suspension was prepared with a constant concentration of 3 wt% (B3). A constant organoclay concentration in gasoil was kept for all emulsions. The preparation of the organoclay suspensions was achieved using a continuous mechanical stirring for 24 H. After that, the suspension was placed in the tank (1) of the hydraulic loop (Fig. 2.4) and water was added to reach the wanted gasoil/water ratio. Then, the emulsification was achieved through a continuous in-line circulation at the maximum pump rate. The emulsification is achieved when both the measured local pressure and the velocity profile reach their equilibrium values. It should be noticed that the needed emulsification time depends on the gasoil/water ratio of the emulsion. The prepared Pickering emulsions are termed as follows:  
 $B_x\text{-}yy\text{H}_2\text{O}$  where  $x$  is the Organo-Hectorite (Oht) mass concentration in gasoil and  $yy$  is the water mass concentration in the emulsion.

## 2.5 Summary to Chapter

The aim of this chapter was to give a detailed description of the experimental apparatus used to conduct the different experimental measurements as well as to present the preparation methods of the organoclay suspensions and Pickering emulsions.

First, a brief presentation of the AR2000 rheometer, its used geometries and the encountered experimental problems was given. After that, a detailed description of the flow loop, its components and its measuring and emulsification systems were discussed. Finally, the different preparation protocols of the studied suspensions and emulsions were detailed.

## CHAPTER 2

It should be noticed that the implemented in-line emulsification system was tested and verified. More results will be presented in Chapter 4 where the rheological and the pipe-flow results are compared.

## 2.6 References

- Achard, J.L., Jarry, P., Taina, F., 2018. Ultrasonic Doppler Velocimetry in Liquid Aluminum, in: Minerals, Metals and Materials Series. Springer International Publishing, pp. 879–884. [https://doi.org/10.1007/978-3-319-72284-9\\_114](https://doi.org/10.1007/978-3-319-72284-9_114)
- Bahlouli, M.I., Bekkour, K., Benchabane, A., Hemar, Y., Nemdili, A., 2013. The effect of temperature on the rheological behavior of polyethylene oxide (PEO) solutions. *Appl. Rheol.* 23. <https://doi.org/10.3933/ApplRheol-23-13435>
- Barnes, H.A., 1995. A review of the slip (wall depletion) of polymer solutions, emulsions and particle suspensions in viscometers: its cause, character, and cure. *J. Nonnewton. Fluid Mech.* 56, 221–251. [https://doi.org/10.1016/0377-0257\(94\)01282-M](https://doi.org/10.1016/0377-0257(94)01282-M)
- Ben Azouz Ahmed, K., 2012. Relations entre propriétés rhéologiques et structure microscopique de dispersions de particules d' argile dans des solutions de polymères. Thèse. Université de Haute Alsace.
- Benchabane, A., 2006. Etude du comportement rhéologique de mélanges argiles - polymères. Effets de l'ajout de polymères. Thèse. Université Louis Pasteur, Strasbourg.
- Benchabane, A., Bekkour, K., 2008. Rheological properties of carboxymethyl cellulose (CMC) solutions. *Colloid Polym. Sci.* 286, 1173–1180. <https://doi.org/10.1007/s00396-008-1882-2>
- Benslimane, A., 2013. Rhéologie et écoulement de fluides chargés : application aux réseaux d'assainissement urbains : étude expérimentale et modélisation. Thèse. Université de Strasbourg.
- Benslimane, A., 2012. Rhéologie et écoulement de fluides chargés : application aux réseaux d'assainissement urbains : étude expérimentale et modélisation. Université de Strasbourg.
- Benslimane, A., Bekkour, K., François, P., Bechir, H., 2016. Laminar and turbulent pipe flow of bentonite suspensions. *J. Pet. Sci. Eng.* 139, 85–93. <https://doi.org/10.1016/j.petrol.2015.12.020>
- Bhatt, J., Somani, R.S., Mody, H.M., Bajaj, H.C., 2013. Rheological study of organoclays prepared from Indian bentonite: Effect of dispersing methods. *Appl. Clay Sci.* 83–84,

106–114. <https://doi.org/10.1016/J.CLAY.2013.08.012>

Cramer, A., Zhang, C., Eckert, S., 2004. Local flow structures in liquid metals measured by ultrasonic Doppler velocimetry. *Flow Meas. Instrum.* 15, 145–153.

<https://doi.org/10.1016/j.flowmeasinst.2003.12.006>

Ebagninin, K.W., Benchabane, A., Bekkour, K., 2009. Rheological characterization of poly(ethylene oxide) solutions of different molecular weights. *J. Colloid Interface Sci.* 336, 360–367. <https://doi.org/10.1016/J.JCIS.2009.03.014>

Eckert, S., Gerbeth, G., 2002. Velocity measurements in liquid sodium by means of ultrasound Doppler velocimetry. *Exp. Fluids* 32, 542–546.

<https://doi.org/10.1007/s00348-001-0380-9>

Fischer, S., 2014. Développement d'une instrumentation ultrasonore pour la mesure des vitesses des liquides au-delà de la limite de Nyquist par une approche spectrale. Thèse. Université Louis Pasteur - Strasbourg I.

Jaafar, W., Fischer, S., Bekkour, K., 2009. Velocity and turbulence measurements by ultrasound pulse Doppler velocimetry. *Meas. J. Int. Meas. Confed.* 42, 175–182.

<https://doi.org/10.1016/j.measurement.2008.05.004>

Nauber, R., Büttner, L., Eckert, K., Fröhlich, J., Czarske, J., Heitkam, S., 2018. Ultrasonic measurements of the bulk flow field in foams. *Phys. Rev. E* 97, 013113.

<https://doi.org/10.1103/PhysRevE.97.013113>

Nowak, M., 2002. Wall shear stress measurement in a turbulent pipe flow using ultrasound doppler velocimetry. *Exp. Fluids* 33, 249–255. [https://doi.org/10.1007/s00348-002-0407-](https://doi.org/10.1007/s00348-002-0407-x)

x

Ouaer, H., Gareche, M., 2018. The rheological behaviour of a water-soluble polymer (HEC) used in drilling fluids. *J. Brazilian Soc. Mech. Sci. Eng.* 40, 1–8.

<https://doi.org/10.1007/s40430-018-1301-7>

Teufel, M., Trimis, D., Lohmüller, A., Takeda, Y., Durst, F., 1992. Determination of velocity profiles in oscillating pipe-flows by using laser Doppler velocimetry and ultrasonic measuring devices. *Flow Meas. Instrum.* 3, 95–101. [https://doi.org/10.1016/0955-5986\(92\)90006-Q](https://doi.org/10.1016/0955-5986(92)90006-Q)



**CHAPTER 3.**  
**RHEOLOGICAL BEHAVIOR OF**  
**ORGANO-HECTORITE**  
**DISPERSIONS**



**TABLE OF CONTENTS**

3.1	Introduction.....	79
3.2	Literature review .....	79
3.3	Experimental protocol.....	81
3.4	Aging behavior.....	82
3.5	Shear flow experiments.....	83
3.5.1	Macrostructural behavior.....	84
3.5.2	Microstructural behavior.....	86
3.5.3	Yielding behavior .....	91
3.6	Viscoelastic properties .....	95
3.6.1	Oscillatory shear experiments.....	95
3.6.2	Creep and recovery experiments .....	100
3.6.3	Evolution of the viscoelastic properties .....	104
3.7	Visual aspects .....	106
3.8	Summary to chapter.....	107
3.9	References.....	109

### 3.1 Introduction

As it was already discussed in the first chapter, the rheological behavior of fluids is of a major influence on their pipe-flow behavior. Hence the choice of discussing the rheological behavior of the studied fluids before their pipe-flow behavior seemed to be evident. The fact that very few detailed scientific studies, dealing with the rheological behavior of organoclays dispersed in organic media (Geng et al., 2019), could be found in the literature was also a reason to work on the current chapter.

The aim of this chapter is to deeply investigate the rheological behaviors of organoclay dispersions. As it was discussed in chapter 1, organoclay used in this study is an organically modified hectorite which will be termed Oht, for simplicity purposes. The AR2000 rheometer, presented in chapter 2, was used to conduct the experiments discussed in the current chapter.

### 3.2 Literature review

The swelling of modified clays in organic media has been largely studied by several authors (Jordan, 1949; Dekany et al., 1986; Vaia et al., 1994; Moraru, 2001; Burgentzlé et al., 2004). The work of Jordan (1949) was one of the first investigations on the swelling of organoclays, where it was found that the factors controlling the swelling of organoclays in organic media are the surface of the clay platelets, the degree of saturation in organic cations and the nature of the dispersing medium. Slabaugh et al. (1968) and Gherardi et al. (1996) found that several parameters can influence the gelling of the organoclay in organic media such as the nature of clay, the nature of the surfactant used in the modification process, the dielectric constant of the couple clay/solvent and the presence of an alcohol or water. Lagaly and Malberg (1990) in their work showed that the presence of a polar activator in the dispersing medium has a major effect on the aggregation and the stability of organoclay dispersions. Same remarks were made by Bhatt et al. (2013) where it was found that a mixture of methanol/H<sub>2</sub>O (95/5) may be added to organo-bentonite dispersions to generate a larger hydrogen bonds network.

Unlike organoclays, lots of studies have been carried out on the rheological behavior of water-wet clay dispersions in aqueous media in which clay particles show a shear thinning behavior with yield stress and a gel behavior at low clay concentrations (Jhon et al., 1996; Mouchid and Levitz, 1998; Karim et al., 2001; Bekkour and Kherfellah, 2002; Bekkour et al., 2005; Azouz

et al., 2010). Bekkour et al. (2005) investigated the time dependency of the bentonite dispersions in water where it was observed that bentonite dispersions, whose behavior was correlated with the Hershel-Bulkley model, exhibit a shear thinning thixotropic behavior. The authors showed that the thixotropy of these dispersions, which is clay concentration dependent, is due to the buildup and the breakdown of the inner structure of the dispersion. Depending on the pH of the dispersing medium, three possible clay platelets configurations are possible in clay dispersions (Benna et al., 1999): face-to-face, edge-to-face, and edge-to-edge. Many authors attributed the gelling of the clay dispersions to the configuration of the clay platelets where the electrostatic attraction between the negatively charged faces and the positively charged edges leads to the formation of a 3D network termed “house-of-cards” (Benna et al., 1999; Luckham and Rossi, 1999; Ramos-Tejada et al., 2001; Bekkour and Kherfellah, 2002; Azouz et al., 2010). Ramsay (1986) in his work on synthetic hectorite clay dispersions attributed the gelation and the viscoelastic properties of the dispersion to the swelling and the repulsion between clay platelets in the dispersing medium. One of the few studies on clays dispersed in non-aqueous media was that of Zhang et al. (2003), where the authors studied two montmorillonite clay dispersions (KSF and K10) in silicone oil. Dynamic rheological experiments showed that, depending on the type and the concentration of the clay, both dispersions exhibited a viscoelastic behavior. Shear experiments illustrated that K10 clay dispersions exhibited both a Newtonian and a shear thinning behavior depending on their clay loading.

The rheological behavior of organoclay in organic media, on the other hand, has been less studied (Zhang et al., 2003; Hato et al., 2011; Bhatt et al., 2013; Zhuang et al., 2016, 2017a, 2018b; Geng et al., 2019). Hato et al. (2011) investigated the rheological behavior of three commercial organo-montmorillonites (Cloisite 15A, 25A, and 30B), modified by three different quaternary ammonium salts, dispersed in silicone oil. Cloisite 15A showed the best compatibility with the silicone oil and all the dispersions exhibited a non-Newtonian, shear thinning solid-like behavior. The study has also shown that the viscoelastic characteristics of the dispersions depend on the level of hydrophobicity of the surfactant used in the clay modification process, as the elastic characteristics were higher for the dispersions containing organoclays modified with surfactants representing higher hydrophobicity. The rheological behavior of exfoliated Cloisite 15 A dispersed in xylene was also reported by Zhong and Wang (2003) in one of the most detailed studies on the rheology of organoclay dispersions, where the yield behavior and viscoelastic properties of organoclay dispersions were studied at different

concentrations. Dynamic shear measurements showed that the dispersions exhibit a gel behavior at loadings as low as 1 wt%. Furthermore, controlled stress measurements illustrated a positive correlation between the storage modulus  $G'$  and the yield stress, as a function of clay loading. Zhuang et al. (2016) studied the influence of temperature on the structure and rheology of montmorillonite modified with (cetyl trimethyl ammonium bromide) dispersed in diesel oil and heated in a rotatory oven for 16 hours at four different temperatures. Up to a critical temperature, thixotropic characteristics were found to be increasing. Beyond this critical temperature, gradual destruction of the gel structure in the dispersions was noticed, due to the desorption of the surfactants. The gelling was explained by the formation of edge-to-edge and face-to-edge configurations. The temperature was seen to affect the swelling of the organoclay where the swelling increases with the temperature until exfoliation then shrinking of the basal spacing. The same rheological behavior as a function of temperature was noticed for modified sepiolite dispersed in white oil (Zhuang et al., 2018b). Several phenomenological models were used to correlate the rheological behavior of organoclay dispersions such as the Power law model, the Casson model (Bhatt et al., 2013) and the Bingham model (Zhuang et al., 2016).

Because the organoclay concentration in the organic media has a crucial influence on the rheological behavior of the dispersion, OHt suspensions at loadings going from 3 wt%, at which OHt dispersions in gasoil exhibit a Newtonian behavior, up to 10 wt% were studied in this chapter.

### 3.3 Experimental protocol

As it was mentioned in Chapter. 2, the suspensions were prepared using gasoil, purchased from Total and Bentone 38, which is an organically modified hectorite clay, manufactured by Elementis Specialties UK. The organoclay, termed OHt, was gradually added to the gasoil, at a predefined concentration, under a constant mechanical agitation. An agitation speed of 500 rpm, which was found to be the optimum agitation velocity to homogenize organoclay dispersions (Bhatt et al., 2013), was used in this work. After that, all the suspensions were left under a constant agitation for 24 H followed by a 24 H of rest inside a laboratory oven at a constant temperature of 20 °C. Before each experiment, the OHt dispersions were homogenized for 1 H under the same mechanical agitation of 500 rpm.

The rheological properties were then investigated using the AR2000, which is a stress-controlled rheometer equipped with a cone-and-plate geometry (diameter: 60 mm; angle: 2°). All the rheological measurements were conducted under a constant temperature of 20 °C using a Peltier system. Furthermore, looking at the great impact of the sample concentration on its rheological behavior, all the measurements were conducted in a gasoil-saturated environment to avoid the evaporation of the continuous phase. The plate surface was also covered by a rough surface (sandpaper) with a roughness of 30,2 µm to prevent the undesirable phenomenon of wall slipping.

Before each experiment, a small volume (2 ml) of the sample is carefully placed in the geometry, trying to not to disturb its “at rest” structure. Afterwards, the sample is kept at rest under the geometry for 10 min for a temperature regulation. A preshear of 100 s<sup>-1</sup> is then applied for 1 min followed by a rest of 2 min. Once the conditioning procedure is finished, the sample is ready for the different rheological experiments. The latter protocol was applied before the rheological experiments to ensure having a comparable structural state for all the dispersions and to avoid adding other variables to the equation such as memory effects.

### 3.4 Aging behavior

Our knowledge on the rheological behavior of organoclay dispersions is very limited because of the recent interest in this type of materials (Zhuang et al., 2016, 2017b, 2017a, 2018a). Furthermore, even in one of the most detailed works on the rheology of organoclay dispersions, their age effect was not studied (Zhong and Wang, 2003).

Clay, especially bentonite, dispersions were deeply studied in our laboratory. It has been shown in many works that the age of clay dispersions has a high impact on their rheological behavior (Bekkour and Kherfellah, 2002; Bekkour et al., 2005; Benchabane, 2006; Azouz et al., 2010; Benslimane et al., 2016). Yield stress, viscosity and storage modulus of bentonite dispersions were found to increase with time. Therefore, a rest period of 10 to 15 days was found to be necessary for bentonite dispersions to reach the equilibrium state and thus having reproducible experimental data.

In this section, we wanted to investigate the effect of aging on the rheological behavior of OHT dispersions. To do so, flow shear experiments were conducted on OHT dispersions at different ages. A continuous increasing shear stress ramp with a slope of 0,034 Pa.s<sup>-1</sup> was applied on all

the samples. Experimental results obtained from two OHt dispersions (3 wt% and 5 wt%) are represented in Fig. 3.1.

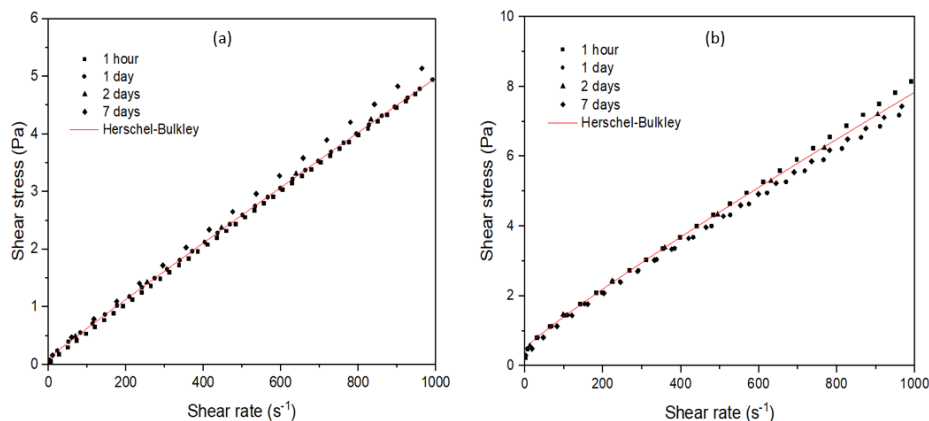


Fig. 3.1 Flow curves of OHt dispersions at different ages, correlated using the Herschel-Bulkley model. (a): 3 wt%, (b): 5 wt%.

Flow curves presented in Fig. 3.1 show that, for both concentrations and unlike bentonite dispersions, the age of the OHt dispersions does not affect their rheological behavior. The overlapping of the flow curves for each concentration indicates that no major changes in both viscosity and yield stress took place even after 7 days of rest. All the curves, for each concentration, were successfully correlated using a master Herschel-Bulkley curve. Moreover, the same tendency was noticed for the range of the concentrations. This unexpected result can be an indicator that the behavior of organoclays can be very different from that of bentonites. The equilibrium state of OHt dispersions is then reached immediately after their preparation.

Even though the experiments showed that the age has no impact on the structural state of the OHt dispersions and thus on their rheological behavior, for the sake of prudence, all the experiments were conducted in the 10 days following the preparation of the samples.

### 3.5 Shear flow experiments

Shear flow measurements were conducted to characterize the behavior of OHt dispersions. Seven different organoclay loadings were studied in this section (3 wt%, 4 wt%, 5wt%, 6 wt%,

7 wt%, 8 wt%, and 10 wt%). Furthermore, flow curves were obtained by applying a continuous increasing shear stress ramp with a constant slope of  $0,034 \text{ Pa}\cdot\text{s}^{-1}$  for all concentrations.

Two graphical representations were used to study both the macrostructural and the microstructural behaviors of organoclay dispersions in gasoil.

### 3.5.1 Macrostructural behavior

Fig. 3.2 represents the flow curves of OHt dispersions in a linear plot. All the measurements were obtained using the same experimental protocol detailed in section (3.3). It should be noticed that the 10 wt% concentration is not presented in the linear plot for clarity purposes.

It can be noticed from Fig. 3.2 that the OHt dispersions exhibit a shear thinning behavior, with yield stress. For the two lowest concentrations (3 wt% and 4 wt%), the yield stress is near to zero. The same observation was made on the behavior of bentonite dispersions (Benslimane, 2012), and it can be related to the inner state of the dispersion. At low loadings, the dispersed state of the particles leads to a behavior near to that of the dispersing medium (Luckham and Rossi, 1999). At concentrations higher than 4 wt%, the yielding behavior becomes more important and increases with the OHt concentration. Once the dispersions become concentrated, i. e. 7 wt%, 8 wt% and 10 wt%, the yielding behavior becomes much important and a small increase in the OHt loading can lead to a jump in the yield stress.

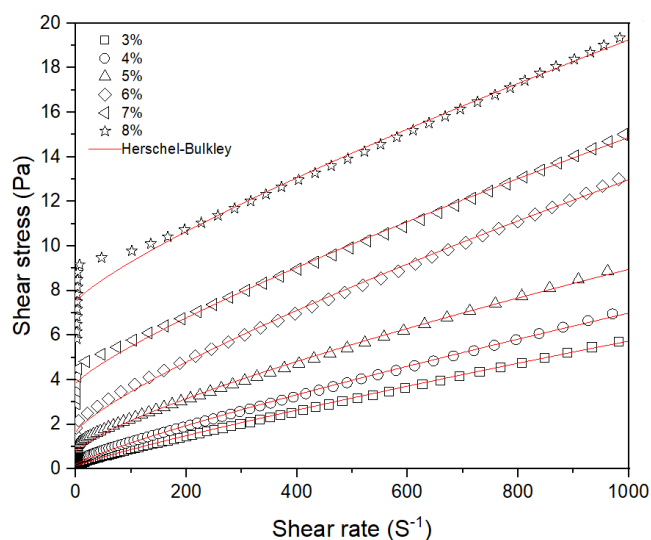


Fig. 3.2 Flow curves of Organo-Hectorite dispersions, correlated using the Herschel-Bulkley model.

This change in the yield stress can be explained by the increase of the interactions between the organo-clay platelets which leads to the formation of a 3D structure, especially at high concentrations. In fact, this structure is the cause of the solid-like behavior of the dispersion at low shear rates (Bekkour and Kherfellah, 2002; Azouz et al., 2010; Bhatt et al., 2013).

The experimental data were correlated using the Herschel-Bulckley phenomenological model, which is widely used to model the rheological behavior of the drilling fluids (Kelessidis et al., 2006; Baba Hamed and Belhadri, 2009; Rooki et al., 2012):

$$\sigma = \sigma_y + K\dot{\gamma}^n \quad 3.1$$

where  $\sigma_y$  (Pa) is the yield stress,  $K$  ( $\text{Pa s}^n$ ) is the consistency index and  $n$  (dimensionless) is the flow index.

The fits to the experimental data using the Hershel-Bulckley model were reported as solid lines in Fig. 3.2, and the corresponding parameters of the model were listed in Table 3.1. It can be noticed that the Hershel-Bulckley model best fits the experimental data of the dispersions where the loading is lower than 6 wt%. Above this concentration, the linear plot of the shear flow measurements tends more towards a linear configuration (Bingham model).

<b>Concentration</b>	<b><math>n</math> [-]</b>	<b><math>K</math> [Pa s<sup>n</sup>]</b>	<b><math>\sigma_y</math> [Pa]</b>	<b><math>R^2</math></b>
<b>3%</b>	0.877 ± 0.00	0.013 ± 0.00	0.128 ± 0.00	0.99
<b>4%</b>	0.847 ± 0.00	0.020 ± 0.00	0.21 ± 0.01	0.99
<b>5%</b>	0.77 ± 0.01	0.040 ± 0.00	0.77 ± 0.03	0.99
<b>6%</b>	0.80 ± 0.02	0.047 ± 0.00	1.65 ± 0.09	0.99
<b>7%</b>	0.82 ± 0.03	0.039 ± 0.00	3.8 ± 0.1	0.99
<b>8%</b>	0.82 ± 0.05	0.04 ± 0.01	7.5 ± 0.2	0.99
<b>10%</b>	0.91 ± 0.05	0.04 ± 0.01	20.9 ± 0.4	0.99

Table 3.1 Rheological parameters of the Herschel-Bulckley model.

From Table 3.1, we can notice that, for concentrations higher than 4 wt%, the value of yield stress increases with the concentration of OHt, whereas the consistency index,  $K$ , increases up to a 5 wt% concentration and then remains constant at around  $0,4 \text{ Pa}\cdot\text{s}^n$ . At the same time, the flow index,  $\alpha$ , remains constant, and it tends towards the unity at highly concentrated OHt dispersions.

### 3.5.2 Microstructural behavior

Even though the Hershel-Bulckley model is widely used for its simplicity and its satisfying results, it did not give enough information on the structural state of the studied dispersions. Furthermore, it could be noticed that it did not fit well at low shear rates and high concentrations. To take a deeper look into the inner structure of the OHt dispersions, precisely at low shear rates and at near to rest state, the experimental data were plotted over a log-log scale. Figure 3.3 plots the same data as in Fig.3.2 in terms of the apparent viscosity as a function of shear rate.

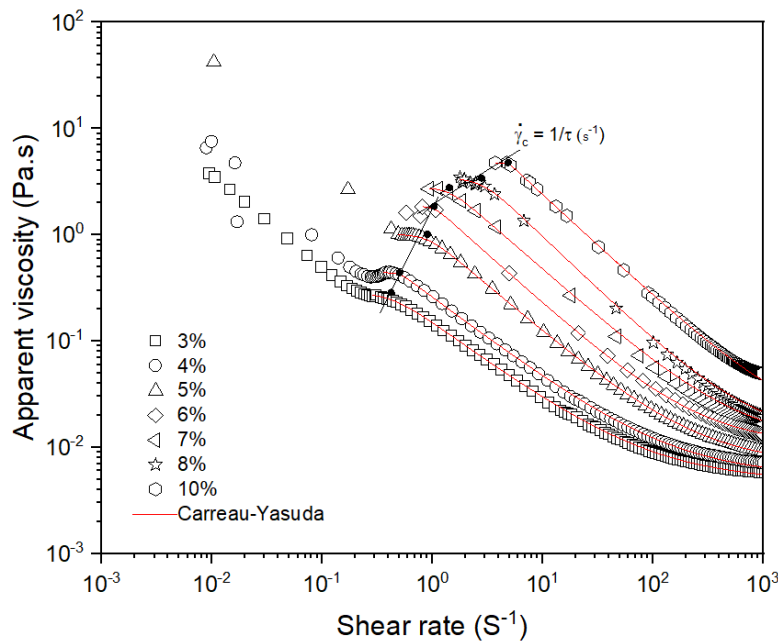


Fig. 3.3 Flow curves of Organo-Hectorite dispersions, correlated using the Carreau-Yasuda model.

Four different regions could be noticed:

- i. First region: wall slipping phenomena at low shear rates, only noticeable at the lowest OHt loadings (3, 4 and 5 wt%), with an inflection point separating it from the second region. This behavior was related to the wall slipping of the less concentrated dispersions. One possible explanation is of the absence of roughness on the cone surface. As it was explained in earlier chapters, it was only possible to add roughness via glass paper to the plate surface. The influence of the surface roughness on the flow of OHt dispersions was not studied. As the OHt dispersions becomes more concentrated i.e., above 5 wt%, a higher friction is applied on the smooth cone surface which leads to the elimination of the wall slipping phenomena. More details on wall slipping for the lowest concentrations will be given in the next section.
- ii. Second region: first Newtonian plateau at low shear rates. In their work on oil-based drilling fluids, Herzhaft et al. (2003), showed that this quasi-Newtonian behavior is due to the high level of elasticity of the fluid at low shear rates. At rest, the fluid develops a solid-like structure which makes it move as a single bloc at low shear rates.
- iii. Third region: power law region with a power low index inferior to 1. The latter shows that the dispersion starts to flow beyond the transition zone. It is admitted that the shear thinning behavior of clay dispersions is due to the breakdown of connections between clay platelets, which lead to the destruction of the inner 3D structure. This shear thinning behavior continues until the destruction of the inner structure of the OHt dispersions and the orientation of clay platelets in the direction of the flow.
- iv. Fourth region: second Newtonian plateau at high shear rates corresponding to the totally broken inner structure of the dispersion. It should be noted that a second Newtonian plateau was not fully developed for all concentrations. The transition from a power law shear thinning behavior to the second Newtonian plateau occurred at higher shear rates as the loading of the OHt dispersions increased.

Above a specific shear rate  $\dot{\gamma}_c$ , termed *critical shear rate*, and plotted in black dots in Fig. 3.3, the flow curves corresponding to all the OHt concentrations show the same tendency i.e., two Newtonian plateaus separated by a power law behavior. This tendency was successfully correlated using the Carreau-Yasuda Structural model (solid lines in Fig. 3.3). The Carreau-Yasuda model is expressed as follows:

$$\frac{\eta(\dot{\gamma}) - \eta_{\infty}}{\eta_0 - \eta_{\infty}} = [1 + (\tau\dot{\gamma})^a]^{\frac{n-1}{a}} \quad 3.2$$

where  $\eta(\dot{\gamma})$  is the viscosity at any given shear rate  $\dot{\gamma}$ ,  $\eta_0$  and  $\eta_{\infty}$  are the zero and the infinite shear rate viscosities,  $\tau$  is a time constant describing the transition between the first Newtonian plateau and the shear thinning behavior,  $n$  is the power law exponent which indicates the dependency of the viscosity on the shear rate, and  $a$  is a dimensionless transition factor, describing the width of the transition zone between the first Newtonian plateau and the power law behavior (a low value of  $a$  lengthens the transition while a high value leads to a sharp transition).

The values corresponding to the Carreau-Yasuda parameters for each Oht loading are reported in Table 3.2.

Since the Carreau-Yasuda model was not developed for yield stress fluids, it was made sure to apply it after the fluid start getting sheared i.e., after yielding. As the second Newtonian plateau was not fully developed for all the concentrations, the viscosity at a shear rate of  $1000 \text{ s}^{-1}$  was considered the infinite shear rate viscosity  $\eta_{\infty}$ . Furthermore, the reciprocal of the time constant,  $1/\tau$ , was found to be equal to the critical shear rate,  $\dot{\gamma}_c$ , mentioned earlier and from which a shear thinning behavior is observed.

Concentration	$\tau$ [s]	$n$ [-]	$a$ [-]	$\eta_0$ [Pa.s]	$\eta_{\infty}$ [Pa.s]	$R^2$
3%	$2.35 \pm 0.02$	$0.235 \pm 0.007$	$3.3 \pm 0.2$	$0.286 \pm 0.002$	$0.004 \pm 0.001$	0.99
4%	$1.99 \pm 0.01$	$0.219 \pm 0.006$	$12.6 \pm 1.5$	$0.439 \pm 0.001$	$0.005 \pm 0.001$	0.99
5%	$1.11 \pm 0.01$	$0.12 \pm 0.01$	$4.9 \pm 0.2$	$1.010 \pm 0.003$	$0.007 \pm 0.001$	0.99
6%	$0.964 \pm 0.004$	$0.063 \pm 0.003$	$10.3 \pm 0.5$	$1.854 \pm 0.001$	$0.010 \pm 0.001$	0.99
7%	$0.70 \pm 0.01$	$0.083 \pm 0.002$	$5.3 \pm 0.7$	$2.79 \pm 0.03$	$0.011 \pm 0.002$	0.99
8%	$0.36 \pm 0.03$	$0.070 \pm 0.005$	$4.3 \pm 1.2$	$3.42 \pm 0.09$	$0.01 \pm 0.01$	0.99
10%	$0.204 \pm 0.001$	$0.039 \pm 0.004$	$34.5 \pm 4.3$	$4.76 \pm 0.01$	$0.014 \pm 0.001$	0.99

Table 3.2 Rheological parameters of the Carreau-Yasuda model.

Table 3.2 shows that zero and infinite shear rate viscosities  $\eta_0$  and  $\eta_\infty$  increase with OHt concentration. This could be explained by the rise in the interactions between organoclay platelets as the concentration increases. The time constant  $\tau$  was found to be decreasing with the increase in the concentration of OHt, which indicated that the viscosity become a stronger function of the shear rate as the concentration increases. A possible explanation of this phenomenon is the fact that the formation of an inner structure between clay platelets, and thus the energy needed to break this structure, increase with OHt concentration. Similarly, as the OHt concentration declines, less energy is needed to break the solid-like structure and a small change in the shear rate could cause high deformation to the structure.

Moreover, the power law exponent  $n$ , was found to be decreasing with the increase in the OHt concentration. This decrease is due to the presence of a more important shear thinning behavior as the OHt concentration increases.

One of the most interesting behaviors from Fig. 3.3 is that of the reciprocal of the Carreau-Yasuda time constant  $1/\tau$ . This parameter (which was also considered a critical shear rate  $\dot{\gamma}_c$ ), separates the Newtonian and the shear thinning behaviors, and was noticed to shift towards higher shear rates as the OHt concentration increases. Furthermore, a slope change of the  $\dot{\gamma}_c$  curve was noticed at a OHt concentration of 6 wt%. To our knowledge, this behavior was not reported before in the literature in the case of clay dispersions. A similar behavior was recorded on polymer solutions correlated using the Cross model (Benchabane and Bekkour, 2008; Ebagninin et al., 2009), where the corresponding concentration was a critical concentration separating two types of polymer solution structural behaviors:

- i. A semi-diluted entangled network solution.
- ii. A concentrated network solution.

### 3.5.2.1. Carreau-Yasuda model parameters

In order to ensure the existence of a similar behavior in the case of organoclay dispersions, and to understand the significance of this slope change in the critical shear rate curve, the parameters of the Carreau-Yasuda model were plotted as a function of the OHt concentration.

In Fig. 3.4, the reciprocal of the time parameter of the Carreau-Yasuda model was plotted as a function of the OHt loading. On the same figure, and for clarity purposes, the reciprocal of the zero-shear-rate viscosity was as well plotted. Both  $1/\tau$  and  $1/\eta_0$  curves, as a function of the OHt

concentration, exhibit a slope change at the same concentration reported above, i.e., 6 wt%. Up to this concentration, the change rate of both zero-shear-rate viscosity and time constant seems to be higher than that of concentrations above 6 wt%. The latter concentration can be considered as critical for the OHt in Gasoil dispersions.

One possible explanation is that this concentration,  $c^*$ , corresponds to the one at which the OHt platelets swell and absorb all the available dispersing media. As of this concentration, all the continuous media, i.e., the gasoil, is absorbed by the OHt platelets and the dispersion becomes overcrowded which allows the swelled OHt platelets to form a more complex 3D solid-like structure.

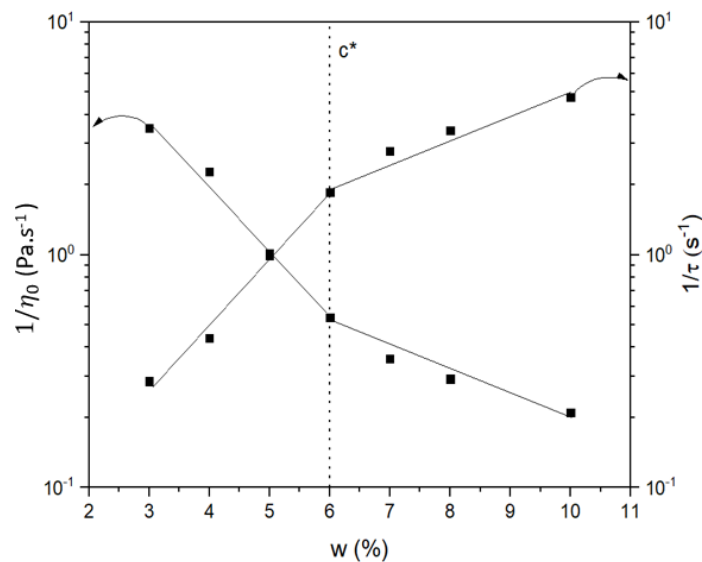


Fig. 3.4 Critical shear rate and the reciprocal of the zero-shear-rate viscosity as a function of organoclay loading.

Fig. 3.5 illustrates the evolution of the power law exponent of the Carreau-Yasuda model as a function of the OHt concentration. It can be noticed that, similarly to critical shear rate and to the zero-shear-rate viscosity, the power law exponent evolves differently prior to and after what was termed as “the critical concentration”. The power law exponent indicates the dependency of the viscosity on the shear rate. Furthermore, this dependency is directly related to the microstructure of the material, which indicates that a major change in the OHt platelets’s structure takes place at the critical concentration,  $c^* = 6 \text{ wt}\%$ .

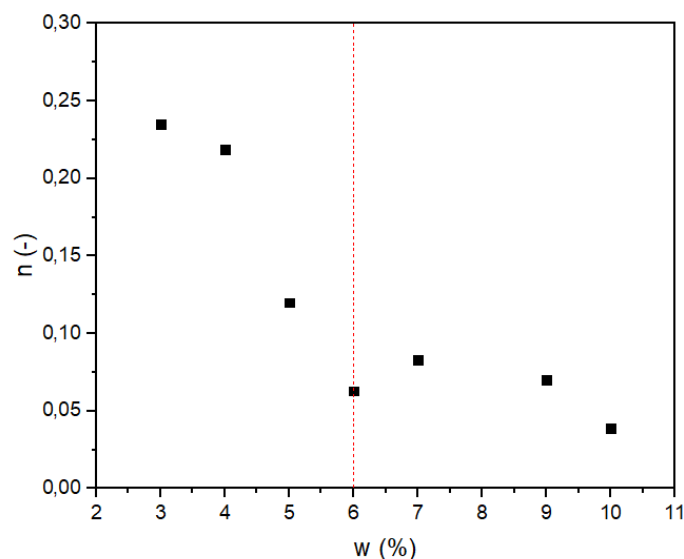


Fig. 3.5 The power law exponent of the Carreau-Yasuda model as a function of organoclay loading.

Using the Carreau-Yasuda model parameters mentioned in Table 3.2, the dimensionless viscosity,  $(\eta - \eta_{\infty})/(\eta_0 - \eta_{\infty})$ , was plotted as a function of the dimensionless shear rate,  $\tau\dot{\gamma}$ .

It was noticed that, starting from a 6 wt% OHt loading, all the curves of the dimensionless viscosity as a function of the dimensionless shear rate overlap (Fig. 3.6). The latter observation indicates that all the OHt dispersions with concentrations higher than the critical concentration,  $c^*$ , have a similar microstructural behavior, which is different from the behavior of those with loadings lower than  $c^*$ . Furthermore, it was possible to fit all the experimental data with a Carreau-Yasuda model master curve at shear rates lower than  $100 \text{ s}^{-1}$  (Fig. 3.6).

### 3.5.3 Yielding behavior

As it was illustrated in the previous section, the microstructure of OHt dispersions seems to play a major role in their rheological behavior. Fig. 3.2 shows that the studied dispersions exhibit a yield stress that increases with the organoclay loading. In addition to that, the values of the critical shear rate increase as the concentration increases. This critical shear rate is related to the flow of the dispersions, and thus to their yield stress.

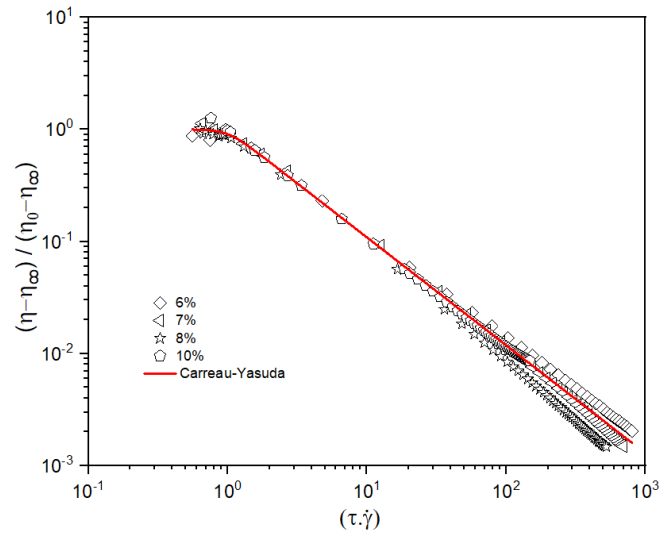


Fig. 3.6 Dimensionless viscosity as a function of dimensionless shear rate, using the Carreau-Yasuda model parameters.

### 3.5.2.2. Measuring yield stress values

To better understand the behavior of these dispersions at the beginning of the flow, it was chosen to study their yielding behavior. Shear flow measurements were used to plot the next two graphical representations.

First, strain and shear rate were plotted as a function of time for each OHT concentration, at a linear constant stress ramp. Fig. 3.7 shows the experimental data for two different OHT concentrations (a: 6 wt% and b: 8 wt%). It should be noticed that in this part, we are only interested by the beginning of the flow as the goal is studying the yielding behavior.

The yield stress was determined as the stress corresponding to the drastic change of the curves representing the strain and the shear rate as a function of time. When the shear rate and the deformation increase suddenly, the sample is considered to start flowing and the yield stress is reached. Before yield stress, though the sample deformed, the shear rate stays constant. In this domain of stresses, the sample does not flow and behaves like a solid due to its elastic properties. After reaching the yield stress, the sample flows and the deterioration of its inner structure begins. Repeating the same protocol for all clay loadings, yield stresses  $\sigma_y$  as a function of OHT loading were obtained. To ensure the validity of these values, apparent viscosity  $\eta = \sigma/\dot{\gamma}$  was plotted as a function of the applied stress for all the OHT concentrations in Fig. 3.8.

RHEOLOGICAL BEHAVIOR OF ORGANO-HECTORITE DISPERSIONS

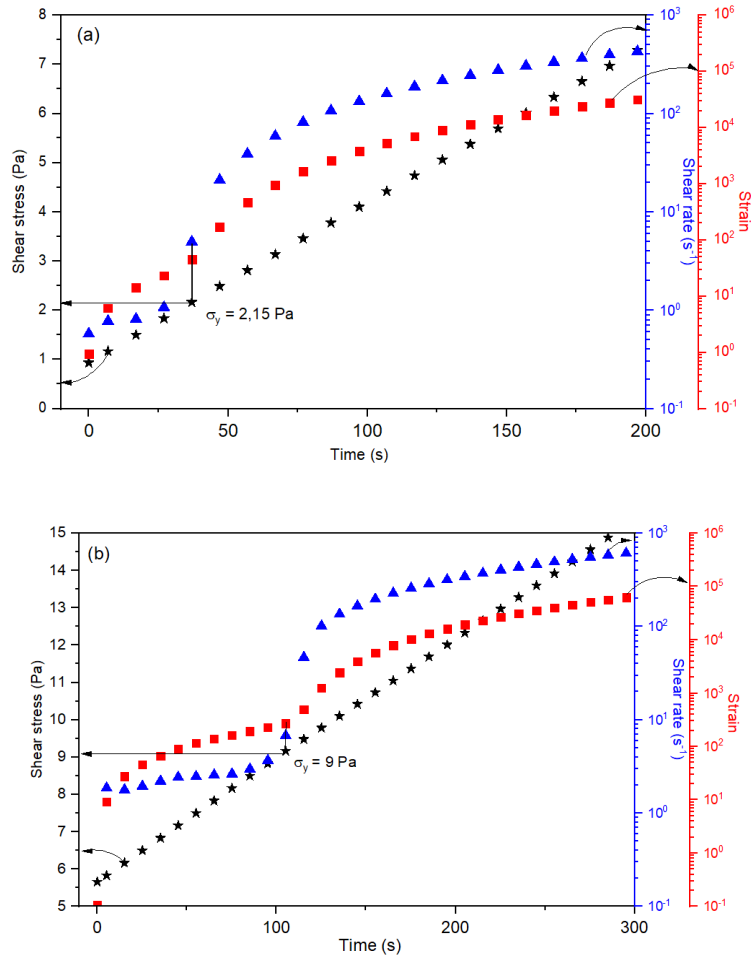


Fig. 3.7 Determination of yield stress by plotting shear stress, shear rate and strain as a function of time for OHT dispersions: 6 wt% (a) and 8 wt% (b).

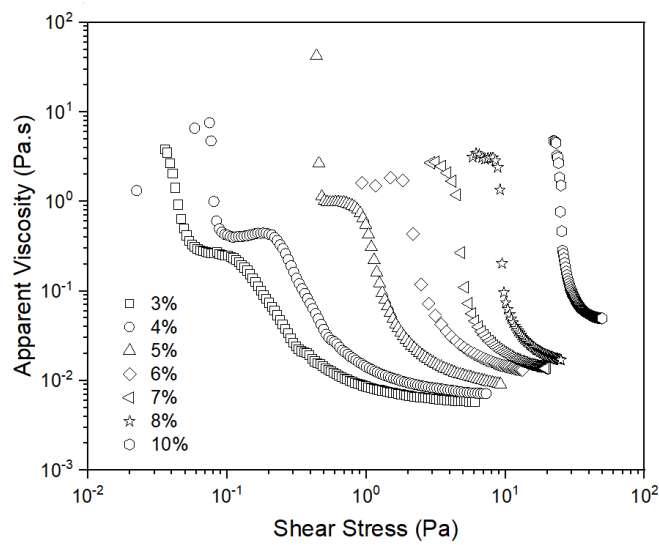


Fig. 3.8 Apparent viscosity as a function of Shear stress.

In Fig. 3.8, we can notice the same flow regions illustrated in Fig. 3.3 and discussed in section (3.5.2). In the apparent viscosity plot, the shear stress value corresponding to the transition from the first Newtonian plateau (the first constant apparent viscosity plateau at increasing shear stress) to the shear thinning region, was the yield stress. In the range of the measured viscosities, it could be noticed that the apparent viscosity exhibited a Newtonian plateau with the increasing shear stress up to the point of yield in Fig. 3.8, where the viscosity dropped as much as 2 orders of magnitude as the shear stress kept increasing until reaching the second Newtonian plateau. The transition occurs at higher shear stresses as the OHt concentration increases.

### 3.5.3.2. Comparing experimental and numerical yield stress values

In a second part, yield stress values obtained from the flow measurements and the Herschel-Bulckley model were plotted on the same graph in Fig. 3.9. Unexpectedly, a small difference can be noticed between yield stress values from the Herschel-Bulckley model and those from the experimental data. Flow measurement yield point values were slightly higher than those of Herschel-Bulckley except for the two lowest concentrations, i.e., 3 wt% and 4 wt%. This result can be considered as a validation for the use of the simple Herschel-Bulckley model as a method to rapidly obtain the yield point values. It is noteworthy that the curve of the measured yield point stresses on Fig. 3.9 exhibits a slope change at  $w = 6 \text{ wt}\%$ . This change of slope confirms the observations made in section (3.5.2.1).

Zhong and Wang (2003) in their work, attributed the cause of the viscosity difference, between the rest and the fully broken states of organoclay dispersions at high clay loadings, to the formation of a network between clay platelets due to their confinement in the dispersing media, which leads to a gel behaving as an elastic solid. The formation of Hydrogen bonds between organoclay platelets, on the other hand, was seen to be unlikely to happen because of the high distances between clay platelets due to the presence of long quaternary ammonium chains on the modified clay surfaces.

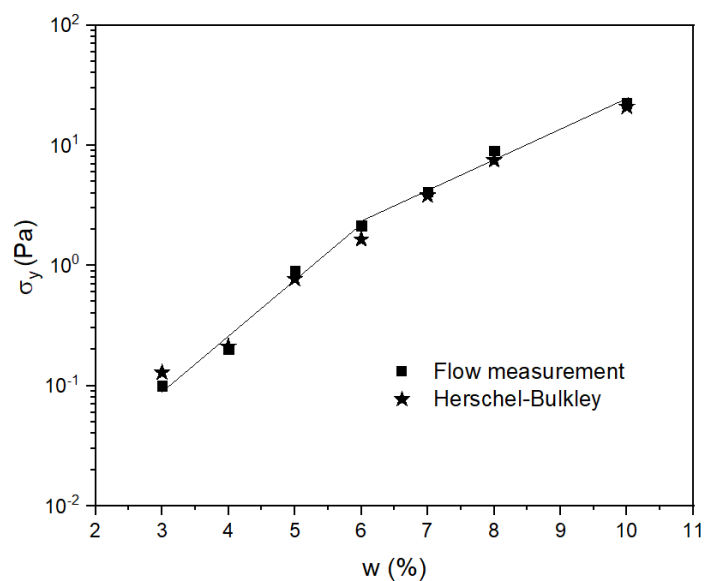


Fig. 3.9 Yield stress values obtained from the flow measurements and the Herschel-Bulkley model as a function of OHt loading.

### 3.6 Viscoelastic properties

In the previous sections, the existence of a critical concentration,  $c^*$ , was suggested. It was hypothetically related to the formation of an inner network between OHt platelets due to the absorbance of free dispersing media and the decreasing spaces between clay platelets as the OHt concentration increases.

To investigate the latter hypothesis, both dynamic and creep experiments were performed, as they allow to study the viscoelastic properties of the OHt dispersion under conditions near to at-rest state. In other words, these tests deform the OHt dispersions without breaking their inner structure. Furthermore, it was made sure that all the tests are carried out in the linear domain of the OHt dispersions.

#### 3.6.1 Oscillatory shear experiments

Oscillatory measurements were performed to study the viscoelastic behavior of OHt dispersions. The AR2000 rheometer equipped with the same geometry was used to carry out all the experiments. Furthermore, because oscillatory measurements can be time consuming, it

was made sure that all the experiments are conducted in a gasoil saturated environment to prevent sample evaporation. All organoclay loadings were studied in this section (3 wt%, 4 wt%, 5wt%, 6 wt%, 7 wt%, 8 wt% and 10 wt%).

The experimental protocol used to proceed dynamic measurements was slightly different than the one previously used in shear flow measurements. In the following, conditioning, and measuring protocols will be detailed:

- i. Sample conditioning protocol: a small volume (2 ml) of the sample is carefully placed in the geometry, trying to not to disturb its “at-rest” structure. Afterwards, the sample is kept at rest under the geometry for 10 min for a temperature regulation. A preshear of  $100 \text{ s}^{-1}$  is then applied for 5 min followed by a 10 min of rest.
- ii. Stress sweep experiment protocol: an oscillatory stress, ranging from  $10^{-3} \text{ Pa}$  to  $10 \text{ Pa}$ , is applied at a constant frequency ( $10^{-3} \text{ Hz}$ ,  $10^{-2} \text{ Hz}$ ,  $10^{-1} \text{ Hz}$ ,  $10^0 \text{ Hz}$ ,  $10^1 \text{ Hz}$ ,  $10^2 \text{ Hz}$ ). This test is performed to study the linearity of the sample.
- iii. Frequency sweep experiment protocol: a frequency, ranging from  $10^{-3} \text{ Hz}$  to  $10^2 \text{ Hz}$ , is applied at a constant oscillatory stress belonging to the linear domain.

### 3.6.1.1. Stress sweep measurements

As it was mentioned previously, stress sweep measurements are conducted mainly to define the linear viscoelasticity domain of the sample. Within this domain, the applied stress deforms the material without changing its inner structure. It should be noticed that, for the same sample, a different linear domain can be found for each applied frequency. Therefore, several stress sweep experiments are performed on each concentration in order to cover the studied frequency range.

Fig. 3.10 is an example illustrating the conducted measurements to define the linear viscoelasticity domain for the OHt concentrations: 4 wt%, 6 wt%, and 8 wt%. A stress sweep, ranging from  $2 \cdot 10^{-3} \text{ Pa}$  to  $10 \text{ Pa}$ , was performed at a fixed frequency,  $f = 0,1 \text{ Hz}$ . Storage,  $G'$ , and loss,  $G''$ , moduli were measured and plotted as a function of oscillatory shear. Viscoelastic linearity domain can be defined as the range for which  $G'$  and  $G''$  are independent of the applied oscillatory shear.

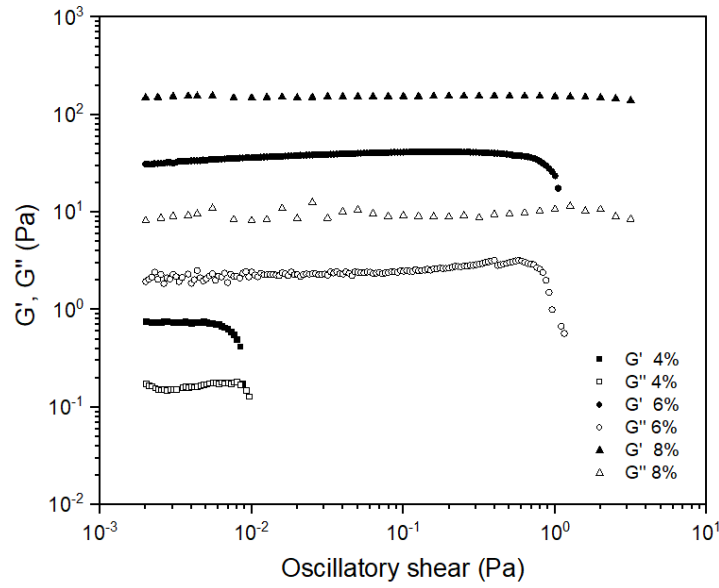


Fig. 3.10 Storage and loss moduli as a function of oscillatory shear at 0,1 Hz.

Moreover, the strain curve as a function of the applied shear (Fig. 3.11) can be used to define the viscoelastic linearity domain ( $slope = 1$  in a log-log scale). In this case, the linear domain corresponds to the elastic behavior of the material whereas the non-linear domain corresponds to its viscous behavior. For instance, both elastic and viscous behaviors are illustrated in the strain curve at  $f = 10^{-1} Hz$ , where the transition occurs at  $\sigma \approx 10^{-1} Pa$ .

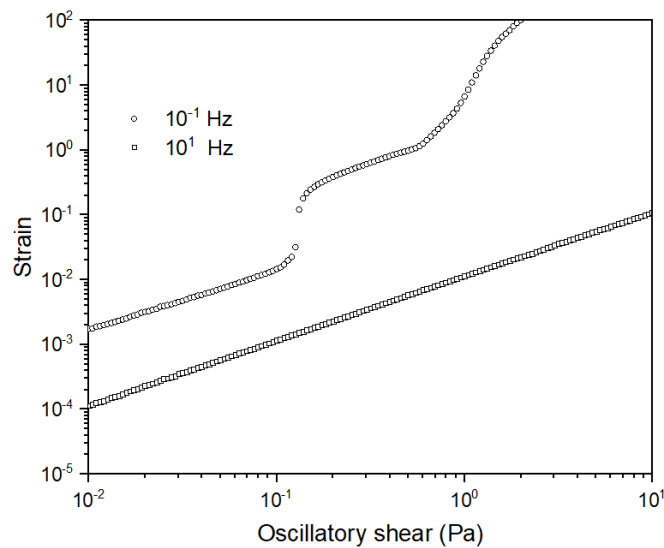


Fig. 3.11 Strain as a function of oscillatory shear at 0,1 Hz and 100 Hz (5 wt% OHt).

### 3.6.1.2. Frequency sweep measurements

Given the viscoelastic linear domain previously defined, elasticity modulus,  $G'$ , and viscous modulus,  $G''$ , are measured by applying a constant stress, belonging to the linear domain of each concentration, and a continuous descending frequency sweep along five decades ( $10^2$  to  $10^{-3}$  Hz). Fig. 3.12 illustrates the variations of  $G'$  for the entire range of the studied OHT concentrations (a) and compares  $G'$  and  $G''$  for three different OHT concentrations (b), as a function of the applied frequency.

It was quite interesting to observe the tendency of the storage modulus,  $G'$ , curves of the OHT dispersions. Two observations can be made from Fig. 3.12, (a):

- i. Depending on the OHT concentration, the curves of  $G'$  show two different behaviors. First, for the lowest OHT concentrations (3 and 4 wt%), where the storage modulus values increase without reaching a plateau. One possible explanation is that, at low concentrations, OHT dispersions do not reach a gel structure at rest. Second, for organoclay loadings higher than 5 wt%, a gel behavior, with constant plateaus of  $G'$  on large frequency ranges, takes place. In this case, the fluid behaves as an elastic solid under low stresses. It is worth noting that a solid-like structure can only be the result of a particular OHT platelets inner architecture, in a way that the energy, needed to separate clay particles, becomes higher than the energy resulting from the applied oscillatory shear.

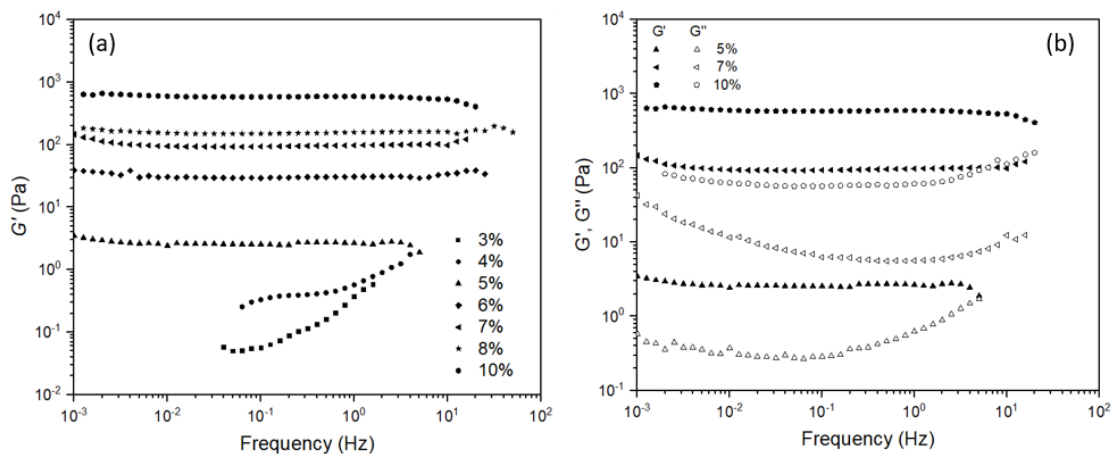


Fig. 3.12 Storage and loss moduli as a function of frequency.

- ii. Although its gel behavior, 5 wt% OHt dispersion exhibits, remarkably, a narrower linearity domain comparing to higher concentrations; it can also be noticed that its corresponding storage modulus was near, in value, to those of 3 and 4 wt% organoclay dispersions.

Fig. 3.12 (b), shows the evolution of  $G'$  and  $G''$  as a function of the frequency for the 5 wt%, 7 wt%, and 10 wt% OHt dispersions. The elastic modulus is higher, in value, than the viscous modulus for the entire range of the studied frequencies for the 7 wt% and the 10 wt% suspensions and up to about 1 Hz for the 5 wt% suspension. This behavior is similar to that of bentonite suspensions (Benchabane, 2006; Paumier, 2007; Benslimane, 2012).

It should also be noticed that the elastic properties become more dominant and the  $G'$  plateaus become flatter as the clay concentration increase. At lower concentrations, on the other hand, the viscous behavior is dominant on a wide range of the explored frequencies. Fig. 3.13 shows the evolution of the storage and the loss moduli as a function of the clay concentration at  $f = 10^{-1} \text{ Hz}$ . It can be observed from the figure that, at 0,1 Hz, except for the 3 wt% loading, the elastic properties are dominant for the range of the studied concentrations ( $G' > G''$ ), and that the difference between these two moduli increases with the clay loading.

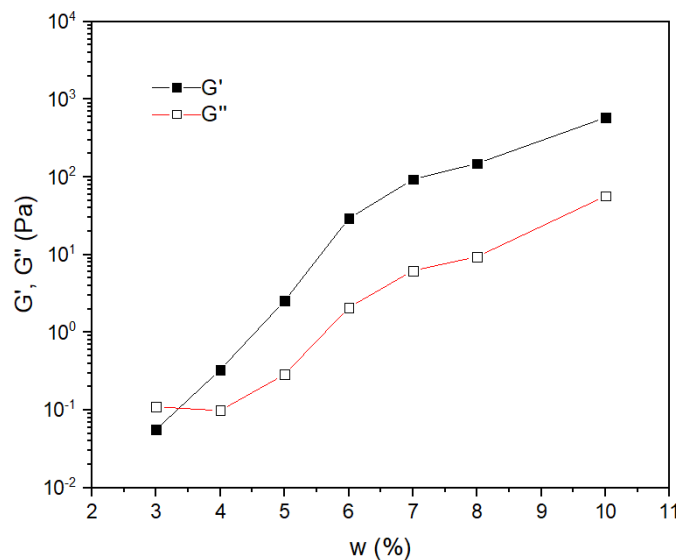


Fig. 3.13 Storage and loss moduli at 0,1 Hz as a function of OHt loading.

### 3.6.2 Creep and recovery experiments

In addition to the oscillatory properties discussed above, creep tests were carried out. Each sample was first crept, for 180 s within its linear domain, then it could recover for an additional 180 s. The strain was measured for each experiment and compliance,  $J(t)$ , values were calculated:

$$J(t) = \frac{\gamma(t)}{\sigma} \quad 3.3$$

where  $\gamma(t)$  is the measured strain and  $\sigma$  is the applied stress.

#### 3.6.3.1. Linear domain

To confirm the linear behavior of the dispersions, at least three tests were performed on each concentration, using different stress values belonging to its linear domain. As it was discussed in section (3.6.1.1), the viscoelastic linear domain takes place when the strain curve as a function of the applied stress, on a log-log scale, is an affine function. Using the latter definition and Eq. 3.3, the linear domain can be verified by superposing compliance curves as a function of time, and at different applied stresses, for each concentration. The applied stresses belong to the linear domain of the fluid if the creep compliance curves overlap.

Fig. 3.14 (a) shows the strain measurements for a creep-recovery experiment conducted on a 7 wt% OHT dispersion, at three different stresses (0,5 Pa, 0,7 Pa, and 1 Pa). It should be mentioned that these stress values were chosen based on the results of the stress sweep experiments. Fig. 3.14 (b) on the other hand, illustrates the evolution of the creep and the recovery compliance as a function of time.  $J_c$  curves overlap for the applied stresses, which confirms the viscoelastic linearity domain defined through the oscillatory measurements.

#### 3.6.2.2. Mechanical approach

Two different models were used to model the deformation and the recovery behaviors of the OHT dispersion at different concentrations. A stress belonging to its linear viscoelasticity domain was applied on each organoclay loading.

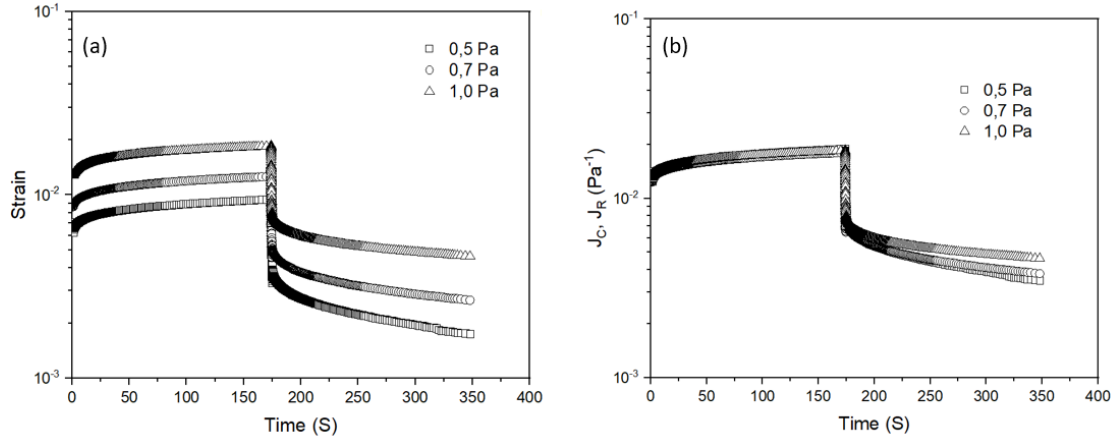


Fig. 3.14 Strain (a) and compliance (b) as a function of time, at the applied stresses  $\sigma = 0,5$ ,  $0,7$  and  $1$  Pa, for a  $7$  wt% OHt suspension.

First, the elastic properties of the dispersions were studied by fitting the experimental creep test results using the Burger model, which associates in series a Maxwell and a Kelvin Voigt models (Dolz et al., 2008):

$$J(t) = \frac{1}{G_M} + \frac{1}{G_K} \left[ 1 - \exp\left(\frac{-tG_K}{\eta_K}\right) \right] + \frac{t}{\eta_M} \quad 3.4$$

where  $G_M$  and  $G_K$  are the elastic moduli of the Maxwell and the Kelvin-Voigt units of the model, respectively.  $\eta_M$  the residual viscosity related to dashpot of the Maxwell unit and  $\eta_K$  the internal viscosity associated with the Kelvin-Voigt model.

Fig. 3.15 illustrates the results of the creep tests at the applied stresses:  $\sigma = 0,005$  Pa,  $0,02$  Pa,  $0,02$  Pa,  $0,60$  Pa,  $1,00$  Pa,  $1,20$  Pa, and  $3$  Pa, respectively, for the  $3$  wt%,  $4$  wt%,  $5$  wt%,  $6$  wt%,  $7$  wt%,  $8$  wt%, and  $10$  wt% OHt suspensions fitted using the above mentioned ‘‘Burger model’’. For all the studied concentrations, the use of the Burger model yielded values of  $R^2 \geq 0,98$ , which is considered satisfactory. The values of  $G_M$ ,  $G_K$ ,  $\eta_M$ , and  $\eta_K$  are reported in Table 3.3, and it shows that all the parameters display an increasing trend with the OHt concentration.

Regarding the Maxwell representation, the instantaneous elastic modulus,  $G_M$ , which is associated with the strain that would be immediately recovered after stress elimination seems to increase with the OHt loading. Furthermore, the residual viscosity,  $\eta_M$ , which represents the irrecoverable deformation, also increases with OHt loading, and is much higher than  $\eta_K$  for all the concentrations.

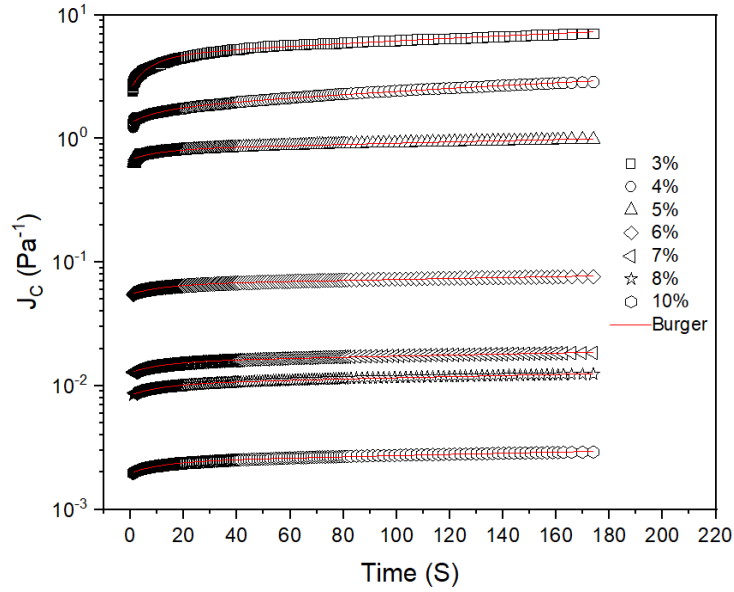


Fig. 3.15 Creep compliance as a function of time, fitted using the Burger model.

For the Kelvin representation, the retardant elastic modulus,  $G_K$ , is related to the stiffness of the fluid structure. It increases with the OHT concentration, which indicates that the complexity of the dispersion microstructure increases with its OHT concentration. Moreover, the internal viscosity,  $\eta_K$ , increases with the concentration whereas the relaxation time constant  $\tau$ ,  $\eta_K/G_K$ , seems to be independent of the OHT loading, except for the lowest concentration where we can notice a slight increase in  $\tau$  between 3 wt% and 4 wt% OHT dispersions (Fig. 3.16). Overall, the relaxation time constant takes values ranging between 10 s and 14 s.

Concentration	$G_M$ [Pa]	$G_K$ [Pa]	$\eta_M$ [Pa.s]	$\eta_K$ [Pa.s]	$R^2$
3%	0.40	0.46	65.39	4.21	0,99
4%	0,74	2,76	141,97	33,67	0,99
5%	1,47	7,32	934,60	85,97	0,98
6%	18,23	91,03	14850,19	1181,04	0,99
7%	77,95	357,86	56266,45	4914,46	0,99
8%	118,96	520,18	77873,57	7054,61	0,99
10%	509,62	2191,15	325191,14	28483,88	0,99

Table 3.3 Parameters of the Burger model obtained using Eq. 3.4.

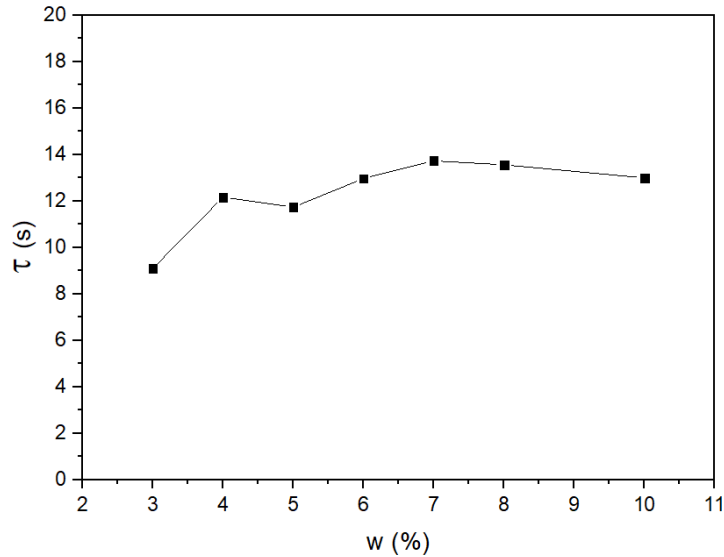


Fig. 3.16 Burger relaxation time constant as a function of the OHt loading.

In order to study the influence of the OHt concentrations on the irrecoverable strain (or viscous deformation), the recovery curves were plotted as a function of time, for the entire range of studied concentrations, and fitted using the Weibull distribution function (Fancey, 2001; Jia et al., 2011):

$$J(t) = J_{\infty} + J_{KV} \exp(-Bt^C) \quad 3.5$$

where  $J_{\infty}$  is the full recovery of the material,  $J_{KV}$  is the proper recovery of the material occurring after the instantaneous elastic recovery, and the parameters  $B$  and  $C$  are, respectively, the reciprocal of the characteristic life parameter and the shape parameter, and they describe the recovery speed of the material.

Fig. 3.17 illustrates the results of the recovery tests for the studied OHt concentrations, fitted using the Weibull distribution function. The values of  $J_{\infty}$ ,  $J_{KV}$ ,  $B$ , and  $C$  are shown in Table 3.4.

As it is illustrated in Table 3.4, both  $J_{\infty}$ , the permanent recovery resulting from the viscous deformation of the Maxwell dashpot, and  $J_{KV}$ , the viscoelastic strain recovery, decrease with the dispersion concentration, which indicates the enhancement of their elastic properties.

Furthermore, it can be noticed that the characteristic life parameter,  $1/B$ , which is inversely proportional to the recovery velocity, takes its lowest value for the 3 wt% dispersion. The shape parameter,  $C$ , on the other hand, describes the failure rate of the system.

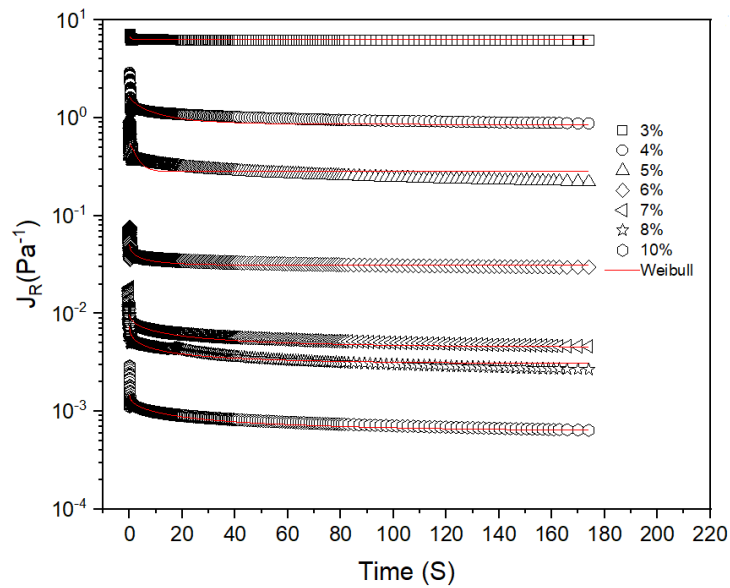


Fig. 3.17 Recovery compliance as a function of time, fitted using the Weibull distribution function.

In the case of complex fluids with macro-particles, the number of the activated bonds during the creep test is considered as a system failure. Failure rate is then the evolution, in time, of the activated bonds linking the macroparticles. If  $C > 1$ , the failure rate is increasing, and if  $C < 1$ , the failure rate is decreasing. In the case of the studied dispersions, the failure rate is decreasing, except for the 3 wt% and the 5 wt% dispersions where  $C$  shows a failure increasing tendency with time. In addition to that, for concentrations superior to 5 wt%, the failure rate seems to stabilize around the value of 0,5, which may indicate that the creep rate tends towards a constant value as the concentration of organoclays increases.

### 3.6.3 Evolution of the viscoelastic properties

Storage modulus,  $G'$ , reflects the elastic properties of the OHT dispersions, and is related to its inner structure. The evolution of  $G'$  is directly proportional to that of the attractive forces bonding the OHT platelets, and hence to the solid-like behavior of the fluid.

Concentration	$J_{\omega}$ [Pa <sup>-1</sup> ]	$J_{KV}$ [Pa <sup>-1</sup> ]	$B$ [s <sup>-c</sup> ]	$C$ [-]	R <sup>2</sup>
3%	6.31	0.44	1.48	1.46	0,99
4%	0.86	0.80	0.20	0.73	0,95
5%	0,28	0.26	0.24	1.18	0,89
6%	0,031	0,02	0.54	0.53	0,98
7%	0.0044	0.0054	0.29	0.49	0,98
8%	0.0030	0.0045	0.48	0.41	0,97
10%	6.02E-4	8.89133E-4	0.29	0.46	0,99

Table 3.4 Parameters of the Weibull distribution function obtained using Eq. 3.5.

Compliance values at  $t = \omega$  and  $t = 180s$  were calculated using Eq. 3.4 and 3.5, then the elastic index  $\Delta J$  was deduced:

$$\Delta J = J(180) - J_{\omega} \quad 3.6$$

Storage modulus values,  $G'$ , from the oscillatory measurements, at a frequency of 0,1 Hz, as well as the elastic index,  $\Delta J$ , are plotted as a function of the OHt concentration in Fig. 3.18. It can be noted that the elastic modulus,  $G'$ , undergoes a slope change at the same critical concentration,  $c^*$ , observed previously. Moreover, if we consider the relationship between  $G'$  and the inner structure of the OHt dispersion, we can conclude that a drastic change related to the network of OHt particles occurs at  $c^*$ . In addition, the curves of  $\Delta J$  exhibit a knee-point at the same critical concentration noticed earlier i.e.,  $c^* = 6 \text{ wt\%}$ .

It is worth mentioning that these results match with those of modified montmorillonite clay dispersed in xylene (Zhong and Wang, 2003), except that OHt dispersions express lower magnitudes of viscosity and of elastic modulus. Zhong and Wang (2003) described the storage modulus values,  $G'$ , of the modified montmorillonite dispersions as “sharply increasing” at low concentrations and then “leveling-off” at higher ones.

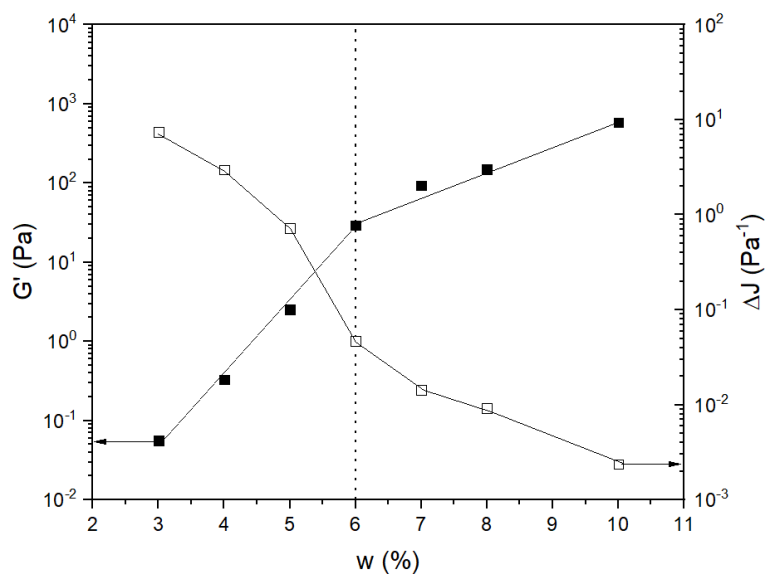


Fig. 3.18 Storage modulus and recovery elastic index as a function of organoclay loading.

### 3.7 Visual aspects

To study the relationship between the organoclay concentration and the fluid behavior, OHT in gasoil dispersions were prepared following the same protocol discussed in chapter 2. A volume of 50 ml of each concentration, was added into a graduated cylinder and kept at rest for 48 h (Fig.3.19). The volume of the gel was then measured for each concentration.

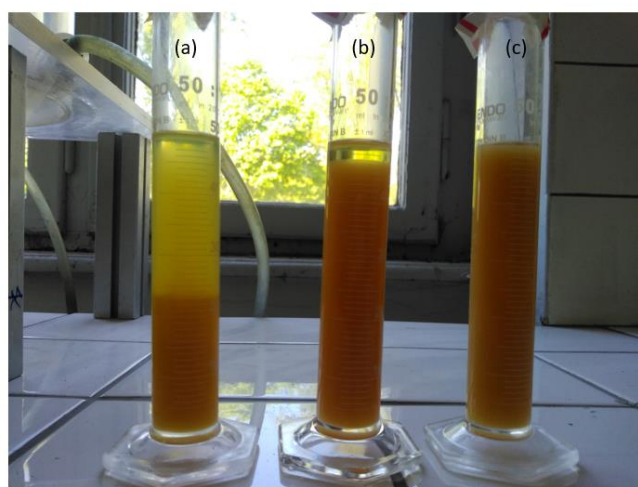


Fig. 3.19 OHT dispersions after 48 h of rest. (a): 3 wt%, (b): 6 wt%, (c): 8 wt%.

The gel volume as a function of the OHt concentration is reported in Fig. 3.20. As it can be noticed from the figure, the curve of the gel volume exhibits a slope change at 6 wt%. After this concentration, i.e.,  $c^* = 6$  wt%, the gel volume becomes constant and approaches the total volume of the dispersion. These results support our assumption about the existence of a critical concentration, and the slope change can be related to the change in the inner structure of the OHt dispersions.

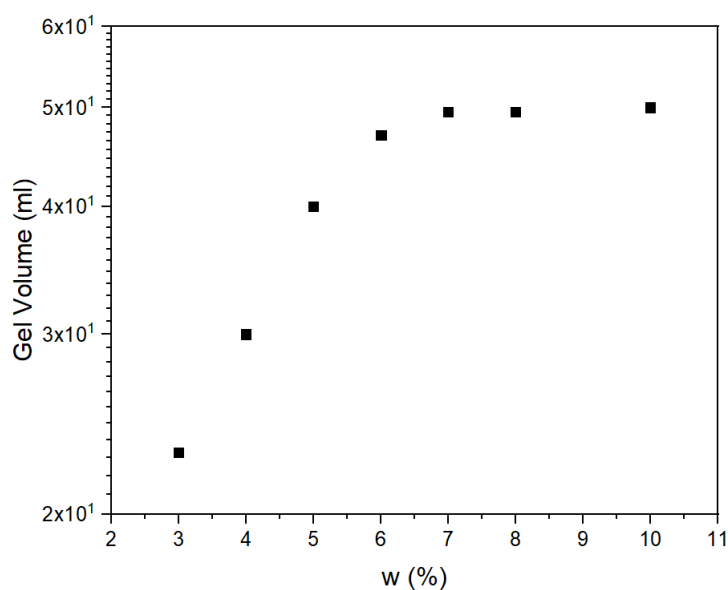


Fig. 3.20 Gel volume as a function of organoclay loading.

### 3.8 Summary to chapter

The rheological behavior of a commercial hectorite, modified with dimethyldialkyl ammonium cations, dispersed in gasoil was investigated. The viscous and the elastic properties of the organo-hectorite dispersions, at concentrations ranging from 3 to 10 wt%, were studied using a stress-controlled rheometer.

First, shear flow measurements highlighted the shear thinning behavior of the organo-hectorite dispersions. All studied concentrations exhibited a yield stress and its value increased with the concentration of the organo-hectorite. Furthermore, the yield behavior of the OHt suspensions was studied, also using shear experiments. The yield values obtained from the shear

experiments were found to be close to those of the Herschel-Bulkley model, and the yield point curve as a function of the OHT loading was found to show the same slope change at 6 wt%.

In addition to that, creep and recovery experiments allowed us to measure the compliance of the fluids and the curves of the compliance as a function of time were established. The elastic index, along with the recovery elastic modulus, were calculated and plotted as a function of the clay concentration. This curve confirmed the existence of a critical concentration,  $c^*$ , at which a change in the inner structure of the clay dispersion takes place. Moreover, gel volume measurements showed the same tendency as the rheological experiments.

Finally, and based on the results presented in this work, the following explanation can be considered: at low loadings, organo-hectorite platelets absorb the organic solvent and swell to their maximum potential with low interactions between clay aggregates. After reaching a critical concentration, the spaces between the swelled organoclay units become narrower, because of the lack of the free solvent, and thus the interactions between the swelled organoclay particles increase and a more complex structure takes place.

### 3.9 References

- Azouz, K. Ben, Dupuis, D., Bekkour, K., 2010. Rheological characterizations of dispersions of clay particles in viscoelastic polymer solutions. *Appl. Rheol.* 20. <https://doi.org/10.3933/ApplRheol-20-13041>
- Baba Hamed, S., Belhadri, M., 2009. Rheological properties of biopolymers drilling fluids. *J. Pet. Sci. Eng.* 67, 84–90. <https://doi.org/10.1016/J.PETROL.2009.04.001>
- Bekkour, K., Kherfellah, N., 2002. Linear Viscoelastic Behavior of Bentonite-Water Suspensions Abstract : *Appl. Rheol.* 12, 234–240.
- Bekkour, K., Leyama, M., Benchabane, A., Scrivener, O., 2005. Time-dependent rheological behavior of bentonite suspensions: An experimental study. *J. Rheol. (N. Y. N. Y.)* 49, 1329–1345. <https://doi.org/10.1122/1.2079267>
- Benchabane, A., 2006. Etude du comportement rhéologique de mélanges argiles - polymères. Effets de l'ajout de polymères. Thèse. Université Louis Pasteur, Strasbourg.
- Benchabane, A., Bekkour, K., 2008. Rheological properties of carboxymethyl cellulose (CMC) solutions. *Colloid Polym. Sci.* 286, 1173–1180. <https://doi.org/10.1007/s00396-008-1882-2>
- Benna, M., Kbir-Arighuib, N., Magnin, A., Bergaya, F., 1999. Effect of pH on Rheological Properties of Purified Sodium Bentonite Suspensions. *J. Colloid Interface Sci.* 218, 442–455. <https://doi.org/10.1006/JCIS.1999.6420>
- Benslimane, A., Bekkour, K., François, P., Bechir, H., 2016. Laminar and turbulent pipe flow of bentonite suspensions. *J. Pet. Sci. Eng.* 139, 85–93. <https://doi.org/10.1016/j.petrol.2015.12.020>
- Bhatt, J., Somani, R.S., Mody, H.M., Bajaj, H.C., 2013. Rheological study of organoclays prepared from Indian bentonite: Effect of dispersing methods. *Appl. Clay Sci.* 83–84, 106–114. <https://doi.org/10.1016/J.CLAY.2013.08.012>
- Burgentzlé, D., Duchet, J., Gérard, J.F., Jupin, A., Fillon, B., 2004. Solvent-based nanocomposite coatings: I. Dispersion of organophilic montmorillonite in organic solvents. *J. Colloid Interface Sci.* 278, 26–39. <https://doi.org/10.1016/J.JCIS.2004.05.015>
- Dekany, I., Szanto, F., Weiss, A., Lagaly, G., 1986. Interactions of Hydmpdk Layer Silicates with AlcoholBenzene Mixtures I. Adsorption Isotherms 422–427.
- Dolz, M., Hernández, M.J., Delegido, J., 2008. Creep and recovery experimental investigation of low oil content food emulsions. *Food Hydrocoll.* 22, 421–427. <https://doi.org/10.1016/J.FOODHYD.2006.12.011>
- Ebagninin, K.W., Benchabane, A., Bekkour, K., 2009. Rheological characterization of poly(ethylene oxide) solutions of different molecular weights. *J. Colloid Interface Sci.* 336, 360–367. <https://doi.org/10.1016/J.JCIS.2009.03.014>
- Fancey, K.S., 2001. A latch-based weibull model for polymerie creep and recovery. *J. Polym. Eng.* 21, 489–510. <https://doi.org/10.1515/POLYENG.2001.21.6.489>
- Geng, T., Qiu, Z., Zhao, C., Zhang, L., Zhao, X., 2019. Rheological study on the invert emulsion fluids with organoclay at high aged temperatures. *Colloids Surfaces A*

- Physicochem. Eng. Asp. <https://doi.org/10.1016/j.colsurfa.2019.04.056>
- Gherardi, B., Tahani, A., Levitz, P., Bergaya, F., 1996. Sol/gel phase diagrams of industrial organo-bentonites in organic media. *Appl. Clay Sci.* 11, 163–170. [https://doi.org/10.1016/S0169-1317\(96\)00018-X](https://doi.org/10.1016/S0169-1317(96)00018-X)
- Hato, M.J., Zhang, K., Ray, S.S., Choi, H.J., 2011. Rheology of organoclay suspension. *Colloid Polym. Sci.* 289, 1119–1125. <https://doi.org/10.1007/s00396-011-2438-4>
- Herzhaft, B., Francois, I., Rousseau, L., Institut, N., Moan, M., Bretagne, U. De, 2003. Influence of Temperature and Clays / Emulsion Microstructure on Oil-Based Mud Low Shear Rate Rheology. *Soc. Pet. Eng.* 8, 3–10. <https://doi.org/10.2118/86197-PA>
- Jhon, M.S., Kwon, T.M., Choi, H.J., Karis, T.E., 1996. Microrheological Study of Magnetic Particle Suspensions. *Ind. Eng. Chem. Res.* 35, 3027–3031. <https://doi.org/https://doi.org/10.1021/ie950749w>
- Jia, Y., Peng, K., Gong, X., Zhang, Z., 2011. Creep and recovery of polypropylene/carbon nanotube composites. *Int. J. Plast.* 27, 1239–1251. <https://doi.org/10.1016/J.IJPLAS.2011.02.004>
- Jordan, J.W., 1949. Organophilic bentonites. I: Swelling in organic liquids. *J. Phys. Colloid Chem.* 53, 294–306. <https://doi.org/10.1021/j150467a009>
- Karim, B., Bekkour, K., Ern, H., Scrivener, O., 2001. Rheological characterization of bentonite suspensions and oil-in-water emulsions loaded with bentonite. *Characterization of Bentonite Suspensions and Oil-In-Water Emulsions Loaded With Bentonite. Appl. Rheol.* 11, 178–187.
- Kelessidis, V.C., Maglione, R., Tsamantaki, C., Aspirtakis, Y., 2006. Optimal determination of rheological parameters for Herschel–Bulkley drilling fluids and impact on pressure drop, velocity profiles and penetration rates during drilling. *J. Pet. Sci. Eng.* 53, 203–224. <https://doi.org/10.1016/J.PETROL.2006.06.004>
- Lagaly, G., Malberg, R., 1990. Disaggregation of alkylammonium montmorillonites in organic solvents. *Colloids and Surfaces* 49, 11–27. [https://doi.org/10.1016/0166-6622\(90\)80089-M](https://doi.org/10.1016/0166-6622(90)80089-M)
- Luckham, P.F., Rossi, S., 1999. The colloidal and rheological properties of bentonite suspensions. *Adv. Colloid Interface Sci.* 82, 43–92. [https://doi.org/10.1016/S0001-8686\(99\)00005-6](https://doi.org/10.1016/S0001-8686(99)00005-6)
- Moraru, V.N., 2001. Structure formation of alkylammonium montmorillonites in organic media. *Appl. Clay Sci.* 19, 11–26. [https://doi.org/10.1016/S0169-1317\(01\)00053-9](https://doi.org/10.1016/S0169-1317(01)00053-9)
- Mourchid, A., Levitz, P., 1998. Long-term gelation of laponite aqueous dispersions. *Phys. Rev. E* 57, R4887–R4890. <https://doi.org/10.1103/PhysRevE.57.R4887>
- Paumier, S., 2007. Impact factors on the structuration and the rheological behavior of the clay-water system for smectite dispersions, Thesis. Université de Poitiers.
- Ramos-Tejada, M.M., Arroyo, F.J., Perea, R., Durán, J.D.G., 2001. Scaling Behavior of the Rheological Properties of Montmorillonite Suspensions: Correlation between Interparticle Interaction and Degree of Flocculation. *J. Colloid Interface Sci.* 235, 251–259. <https://doi.org/10.1006/JCIS.2000.7370>
- Ramsay, J.D., 1986. Colloidal properties of synthetic hectorite clay dispersions: I. Rheology.

- J. Colloid Interface Sci. 109, 441–447. [https://doi.org/10.1016/0021-9797\(86\)90321-8](https://doi.org/10.1016/0021-9797(86)90321-8)
- Rooki, R., Ardejani, F.D., Moradzadeh, A., Mirzaei, H., Kelessidis, V., Maglione, R., Norouzi, M., 2012. Optimal determination of rheological parameters for herschel-bulkley drilling fluids using genetic algorithms (GAs). *Korea-Australia Rheol. J.* 24, 163–170. <https://doi.org/10.1007/s13367-012-0020-3>
- Slabaugh, W.H., Hiltner, P.A., 1968. The swelling of alkylammonium montmorillonites. *J. Phys. Chem.* 72, 4295–4298. <https://doi.org/10.1021/j100858a060>
- Vaia, R.A., Teukolsky, R.K., Giannelis, E.P., 1994. Interlayer Structure and Molecular Environment of Alkylammonium Layered Silicates. *Chem. Mater.* 6, 1017–1022. <https://doi.org/10.1021/cm00043a025>
- Zhang, L.-M., Jahns, C., Hsiao, B.S., Chu, B., 2003. Synchrotron SAXS/WAXD and rheological studies of clay suspensions in silicone fluid. *J. Colloid Interface Sci.* 266, 339–345. [https://doi.org/10.1016/S0021-9797\(03\)00643-X](https://doi.org/10.1016/S0021-9797(03)00643-X)
- Zhong, Y., Wang, S.-Q., 2003. Exfoliation and yield behavior in nanodispersions of organically modified montmorillonite clay. *J. Rheol. (N. Y. N. Y.)* 47, 483–495. <https://doi.org/10.1122/1.1545074>
- Zhuang, G., Zhang, H., Wu, H., Zhang, Z., Liao, L., 2017a. Influence of the surfactants' nature on the structure and rheology of organo-montmorillonite in oil-based drilling fluids. *Appl. Clay Sci.* 135, 244–252. <https://doi.org/10.1016/J.CLAY.2016.09.033>
- Zhuang, G., Zhang, Z., Jaber, M., Gao, J., Peng, S., 2017b. Comparative study on the structures and properties of organo-montmorillonite and organo-palygorskite in oil-based drilling fluids. *J. Ind. Eng. Chem.* 56, 248–257. <https://doi.org/10.1016/J.JIEC.2017.07.017>
- Zhuang, G., Zhang, Z., Peng, S., Gao, J., Jaber, M., 2018a. Enhancing the rheological properties and thermal stability of oil-based drilling fluids by synergetic use of organo-montmorillonite and organo-sepiolite. *Appl. Clay Sci.* 161, 505–512. <https://doi.org/10.1016/J.CLAY.2018.05.018>
- Zhuang, G., Zhang, Z., Sun, J., Liao, L., 2016. The structure and rheology of organo-montmorillonite in oil-based system aged under different temperatures. *Appl. Clay Sci.* 124–125, 21–30. <https://doi.org/10.1016/J.CLAY.2016.01.051>
- Zhuang, G., Zhang, Z., Yang, H., Tan, J., 2018b. Structures and rheological properties of organo-sepiolite in oil-based drilling fluids. *Appl. Clay Sci.* 154, 43–51. <https://doi.org/10.1016/j.clay.2017.12.048>



**CHAPTER 4.**  
**RHEOLOGICAL AND FLOW**  
**BEHAVIOR OF ORGANO-**  
**HECTORITE BASED EMULSIONS**



## TABLE OF CONTENTS

4.1	Introduction.....	116
4.2	Literature review .....	116
4.3	Experimental Protocol.....	120
4.4	Rheological behavior .....	121
4.4.1	Shear flow experiments.....	121
4.4.2	Viscoelastic Properties .....	124
4.4.3	Limitations of rheological measurements.....	127
4.5	Pipe-flow behavior .....	129
4.5.1	Chronological sequence of measurements.....	129
4.5.2	Flow parameters during the emulsification process.....	130
4.5.3	Flow parameters during the homogenization process .....	132
4.5.4	Verification of the flow regimes.....	133
4.5.5	Comparison between flow measurements and rheology.....	136
4.5.6	Emulsion stability .....	140
4.6	Visual aspects .....	145
4.7	Summary to chapter.....	146
4.8	References.....	148

## 4.1 Introduction

Pickering emulsions are getting a lot of attention lately because of their surfactant-free characteristics, which make them applicable in many industries such as cosmetics and food industry where solid particles can be used, instead of surfactants, to establish emulsions. Moreover, it was shown that the use solid particles to stabilize emulsions increase their stability and facilitate the control of their properties, especially of the droplet size.

Organoclays are usually used in the preparation of conventional inverse emulsions drilling fluids but not as emulsion stabilizers. Usually, these fluids are stabilized using surfactants, and then organoclays are added as viscosity modifiers.

The aim of this chapter is to study a surfactant-free solid-stabilized drilling fluid, and to discuss its rheological and pipe-flow behaviors. The use of both measurements to study the behavior of these emulsions allows to eliminate experimental errors such as centrifugal forces and wall slipping, always present in rotational rheometers. In this case, the real intrinsic rheological properties will be obtained if the results from both techniques coincide. The studied fluid is a gasoil-in-water emulsion stabilized using organo-hectorites, and the rheological behavior of organo-hectorite dispersions in gasoil was detailed in chapter 3. The reasons behind the study of a solid-stabilized drilling fluid are:

- i. It has been shown that surfactants used in inverse emulsion drilling fluids alter the wettability of petroleum reservoirs and thus their productivity (Sharma and Wunderlich, 1987; McDonald and Buller, 1992; Sanner et al., 1994; Tong and Morrow, 2006; Wang et al., 2012).
- ii. Knowing their high stability, high water to gasoil ratios Pickering emulsions were studied as an attempt to suggest a more environmentally friendly drilling fluid.

## 4.2 Literature review

Inverse emulsions drilling fluids are widely used to drill the reservoir layer of petroleum wells (Schramm, 2000; Quintero, 2002). In this type of drilling fluids, surfactants are usually used to stabilize the inverse emulsion and organoclays are used to enhance the rheological properties as well as the thermal stability of the drilling fluid (Zhuang et al., 2018).

Despite their major role in the stabilization of the inverse emulsion drilling fluids, surfactants were found to change the wettability of the reservoir rock from water-wet to oil-wet. The wettability alteration of the reservoir rock was found to decrease the productivity of petroleum reservoir (Menezes et al., 1989; McDonald and Buller, 1992; Yan et al., 1993).

Pickering emulsions have received a lot of attention lately. In this type of emulsion, the stabilizers are solid particles instead of surfactants (Chevalier and Bolzinger, 2013). The solid particles used in the preparation of Pickering emulsions should be partially wet by both phases (Chen et al., 2011). Their surfactant free characteristics make them suitable for many industrial applications such as in the cosmetics, pharmaceutical and food industries (Tang et al., 2015; Xiao et al., 2016; Yan et al., 2017; Dai et al., 2018).

One of the first studies that can be found on the rheology of solid stabilized emulsions was performed by (Abend et al., 1998). In that study, montmorillonite clay was used to stabilize an oil-in-water Pickering emulsion. The effect of the presence of a layered double hydroxide on the stability and the rheology of the emulsions was also studied. It was found that the emulsions show high yield values and high viscosity ranges with an anti-thixotropic behavior. Furthermore, the emulsions showed a high elastic behavior which was linked to the formation of a clay network in the continuous phase (water). It was also shown that the layered double hydroxide contributes to the increase of the storage modulus of the emulsion by acting as “hinges” in the clay network (Thienne et al., 1999).

In a second work, the rheology of silicone oil in water Pickering emulsions was studied (Sugita et al., 2008). In this case the solid stabilizer was silica particles modified using hydroxypropyl methylcellulose (HPMC). The results of this study showed that the rheology of the emulsions was dependent on the viscosity of the silicone oil and the amount of the HPMC used to modify the silica surfaces. The effects of the silica and the oil concentrations were not studied as they were kept fixed. It was found that the storage modulus of the emulsion increases with the amount of the HPMC used to modify the silica surfaces. This is due to the hydrophobicity of the HPMC compared to the silica particles which enhances the adsorption of the particles of the oil/water interface. Unlike the study of (Abend et al., 1998), the emulsion was found to be thixotropic, which leads to the assumption that the time dependency of Pickering emulsions depends on the type of the materials used in its preparation. In a similar study, Morishita and Kawaguchi (2009), studied the rheological behavior of silicone oil in water emulsions stabilized using fumed silica suspensions pre-adsorbed poly(N-isopropylacrylamide) (PNIPAM) at two different molecular weights. It was shown that the high hydrophobicity of the PNIPAM leads

to a higher adsorption of the silica particles on the oil/water interface, a smaller droplet size and a higher emulsified oil fraction. This results in an increase in the viscosity and the elastic modulus of the emulsion.

Guillot et al. (2009) on the other hand, showed that, unlike surfactant stabilized emulsions, the droplet size is independent of clay loading; therefore, a minimal clay loading is sufficient to stabilize the emulsion and an excess of clay particles in the continuous phase would increase its viscosity, by forming a network between clay platelets. This 3D structure can enhance the stability of the emulsion. Bellalta et al. (2012) explained the power law thixotropic behavior of the emulsions by the rearrangement of the oil droplets in the continuous phase during the flow procedure.

Malkin et al. (2017) studied the rheological behavior of crude oil in water emulsions. The emulsions were prepared using both surfactants and solid particles (silica and montmorillonites). Adding water to the crude oil significantly decreased its viscosity and improved its transportation. The emulsions exhibited a yield stress and a gel-like behavior which was related to the presence of the solid particles.

Looking at the recent interest in Pickering emulsions, only few studies can be found on their pipe-flow behavior. Most of these studies are applications in the petroleum industry because of the need to transport solid stabilized emulsions such as water in crude oil emulsions stabilized with natural asphaltenes and inverse emulsion drilling fluids. Malkin et al. (2017) studied the pipeline behavior of heavy crude oil in water emulsion. The goal of this innovative study was to reduce the high viscosity of heavy crude oils to make their transportation less energy consuming. It was found that the viscosity measured in a capillary viscosimeter is different from the one measured in a rotational rheometer. In large tubes, the rheological measurements would better coincide with the pipe flow measurements. Agarwal et al. (2013) studied the behavior of water-in-oil invert emulsion drilling fluids. The Pickering emulsions were prepared using organophilic silica powders. It was found that the behavior of the prepared Pickering emulsions was similar to the surfactant-based invert emulsions. The author proposed to model the behavior of the Pickering emulsions using the Casson model.

Several studies can be found on the flow of water/Crude oil emulsions without emulsifying additives in the literature (Aguilera et al., 2010; Lim et al., 2015; Wong et al., 2015). This type of emulsions can be considered Pickering emulsions looking at the presence of asphaltenes in crude oils. Asphaltenes can form an interfacial film around the water droplets and stabilize the

emulsion (Aguilera et al., 2010). Because of the hydrophobicity of asphaltenes, the created emulsion would be a water-in-oil inverse emulsion. The water in crude oil emulsions were found to have the same rheological behavior as the rest of Pickering emulsions (viscoelastic exhibiting yield stress) and following the Hershel-Bulckley model (Ariffin et al., 2016). Plasencia et al. (2013) studied the flow behavior of salted water in different crude oils inside a flow loop. The stabilization was achieved through continuous circulation. Homogenous water-in-oil emulsion was observed before the phase inversion. After the phase inversion, multiple water-in-oil-in-water emulsion was noticed. In a similar study, Wong et al. (2018) studied the pipe flow behavior of water in crude oil emulsions. The stabilization was reached using a diameter restriction at one of the flow-loop elbows.

Many studies were dedicated to the flow of non-Newtonian fluids. Flow behaviors of viscous yielding fluids were largely studied in the literature, both experimentally and numerically (Malin, 1998; Escudier et al., 2005; Founargiotakis et al., 2008; Esmael et al., 2010; Kelessidis et al., 2011; Podryabinkin et al., 2013; Benslimane et al., 2016).

Benslimane (2013) studied the rheological and the flow behavior of bentonite suspensions and bentonite-polymer mixtures. These fluids have a similar flow behavior to that of the drilling fluids (Benslimane et al., 2016). The rheological curves of the fluids were successfully fitted using the Herschel-Bulckley model. The flow behavior was in a good correlation with the rheological measurements in the laminar flow. In the transitional flow, the fluids exhibited the same asymmetry noticed by several authors in the case of shear thinning fluids (Peixinho et al., 2005; Esmael and Nouar, 2008). A drag reduction was also observed during the turbulent flow which was related to the shear thinning nature of the fluids (Benslimane et al., 2013, 2016).

To our knowledge, no studies have been conducted on the pipe-flow of inverse emulsions stabilized with organoclays. In this work, a surfactant-free model inverse emulsion drilling fluid is prepared using only organoclays to stabilize the emulsion i.e., a Pickering emulsion. The rheological behavior of organoclay suspensions used in this work was discussed in the previous chapter. Both rheological and flow behaviors of the prepared emulsions were studied. The aim of this chapter is to give a detailed characterization of organoclay-stabilized Pickering emulsions using rheological and pipe-flow measurements.

### 4.3 Experimental Protocol

Water-in-gasoil Pickering emulsions were stabilized using organo-hectorite clay. An emulsification system, composed of two diaphragms (Fig. 2.4-8), was used to stabilize the inverse emulsions. The preparation process is detailed in chapter 2. Six different gasoil/water ratios are studied in this chapter: 100/0 (B3), 90/10 (B3-10H<sub>2</sub>O), 80/20 (B3-20H<sub>2</sub>O), 70/30 (B3-30H<sub>2</sub>O), 60/40 (B3-40H<sub>2</sub>O) and 50/50 (B3-50H<sub>2</sub>O).

Rheological measurements were conducted on all the concentrations. A fresh sample of each emulsion was taken from the hydraulic loop immediately after its preparation and their rheological behavior was studied using a stress-controlled rheometer (AR2000, TA Instruments), equipped with a cone-and-plate geometry (diameter: 40 mm; angle: 4°). All the measurements were conducted at a constant temperature of 20.0 ± 0.1 °C using a Peltier system.

Shear flow experiments were conducted as an attempt to apply the same shear stress ranges reached in the hydraulic loop. To do so, the maximum wall shear stress achieved at the maximum flow rate in the hydraulic loop and its corresponding time were used as a reference for the rheological measurements. The experimental protocol was defined to simulate the pipe-wall shear history during flow. An increasing shear stress was applied for 1 min, followed by a plateau, at the maximum wall shear stress measured in the flow loop, applied for 3 min. Finally, a decreasing shear stress for 1 min was applied. Viscoelastic measurements were conducted following the same experimental protocol discussed in chapter 3.

Regarding the pipe-flow behavior, a flow loop, equipped with velocity and pressure measuring systems (see chapter 2), was used to measure the velocity profiles as well as the linear pressure losses of the prepared fluids. The measuring system is composed of two pressure sensors (GS Sensors XPM) (Fig. 2.4 (5)) and an Ultrasound Pulsed Doppler Velocimeter (Fig. 2.4 (6)). Two pressure sensors located at 4.36 m and 8 m from the inlet of the flow loop were used to calculate linear pressure losses. This placement was chosen to ensure having an established flow at the measuring section. The pressure sensors are calibrated before and after each experiment (for the calibration method, see chapter 2).

Velocity profiles are obtained using the non-intrusive Ultrasound Pulsed Doppler Velocimetry. Particle velocity is calculated using the following expression (Benslimane et al., 2016):

$$u = \frac{c_w f_D}{2f_E \cos \theta} \quad 4.1$$

where  $c_w$  is the acoustic wave celerity in water at a given temperature,  $f_D$  is the Doppler shift frequency,  $f_E$  is the emission frequency and  $\theta$  is the angle between the axis of the UPDV transducer and the flow direction.

In the current study  $\theta = 73,8^\circ$ . This angle was selected as a compromise between:

- i. The range of the measured velocities, as the measurable velocity values is proportional to the angle between the axis of the UPDV transducer and the flow direction.
- ii. The experimental errors which are also proportional to the angle between the axis of the UPDV transducer and the flow direction.

#### 4.4 Rheological behavior

The rheological properties of inverse Pickering emulsions, at water ratios inferior to 50 wt%, were studied at both high and low deformations. A conditioning procedure was in order to ensure having a comparable structural state for all the samples and to avoid adding other variables to the equation such as memory effects. The same conditioning protocol as chapter 3 was used (a preshear of  $100 \text{ s}^{-1}$  for 1 min followed by a rest of 2 min).

Furthermore, the aging behavior of the emulsions was studied, and it was found that the rheological behavior of water-in-gasoil emulsions, stabilized using 3 wt% OHT in the continuous phase, stays stable during the current study, especially for the lowest water concentrations. This indicates the structural stability of the studied emulsions.

##### 4.4.1 Shear flow experiments

Shear flow measurements of gasoil in water Pickering emulsions, at different gasoil/water ratios are plotted in a linear scale (Fig. 4.1). The data is acquired by applying an increasing linear shear stress followed by a constant shear stress at its maximum value, and finally a decreasing linear shear stress. The values of the maximum applied shear stress and the duration of each step are kept similar to the values measured in the flow loop.

The flow curves, i.e., shear stress as a function of the shear rate, in Fig. 4.1 show that the inverse Pickering emulsions exhibit a shear thinning behavior with a yield stress. They also show that

the mass concentration of water in the inverse emulsion has an important influence on the rheological behavior of the emulsions. At very low concentrations, i.e., B3 to B3-30 H<sub>2</sub>O, yield stress values are low, the emulsion is very fluid-like, and the increasing and the decreasing flow curves overlap, which indicates the absence of time-dependency of the emulsions. The same behavior was noticed in highly concentrated organo-hectorite suspensions (chapter 3). In high concentrated emulsions, the confinement of the dispersing medium and the narrow spaces between water droplets increase the possibility of interactions between organoclay platelets, which can lead to the formation of a complex 3D structure.

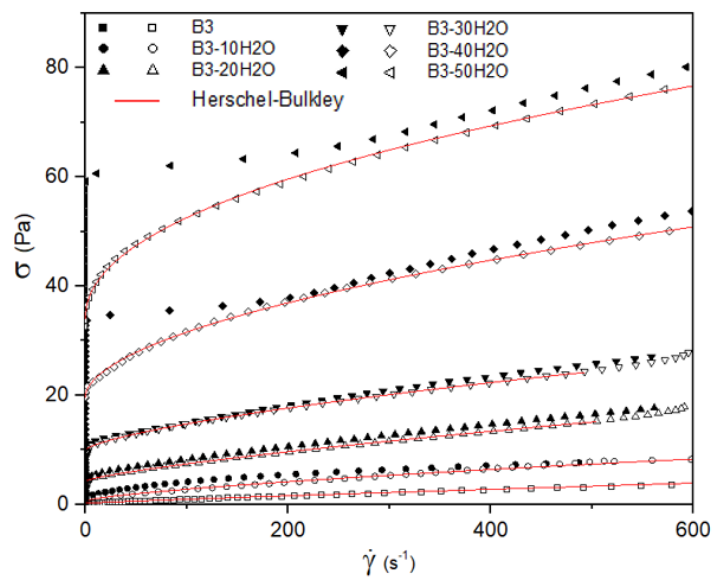


Fig. 4.1 Cyclic flow curves of inverse Pickering emulsions correlated using the Herschel-Bulckley Model. Full symbols: increasing ramp, empty symbols: decreasing ramp.

The decreasing shear stress flow curves are fitted using the Herschel-Bulckley model, in solid lines, and the corresponding parameters of the model are listed in Table 4.1. This model is widely used for rheological behavior of drilling fluids as well as Pickering emulsions and organoclay suspensions.

It was chosen to fit the decreasing shear stress curves in order to have similar conditions to those found in the flow loop, particularly for the high-water concentrations (B3-40 H<sub>2</sub>O and B3-50 H<sub>2</sub>O).

Concentration	n [-]	K [Pa sn]	$\sigma_y$ [Pa]	R2
<b>B3</b>	0,91	0,01	0,23	0,99
<b>B3-10H2O</b>	0,87	0,04	2,62	0,99
<b>B3-20H2O</b>	0,76	0,09	4,25	0,99
<b>B3-30H2O</b>	0,62	0,33	9,08	0,99
<b>B3-40H2O</b>	0,53	1,00	19,60	0,99
<b>B3-50H2O</b>	0,49	1,91	34,49	0,99

Table 4.1. Rheological parameters of the Herschel-Bulckley model.

Yield stress as a function of water mass concentration is plotted in Fig. 4.2. It can be observed that, at the range of the studied water concentrations, the evolution of yield stress values of the emulsions is exponential following the equation:

$$\sigma_y = 1.25e^{0.067C} \quad 4.2$$

$C$  being the mass concentration of water in the Pickering emulsion.

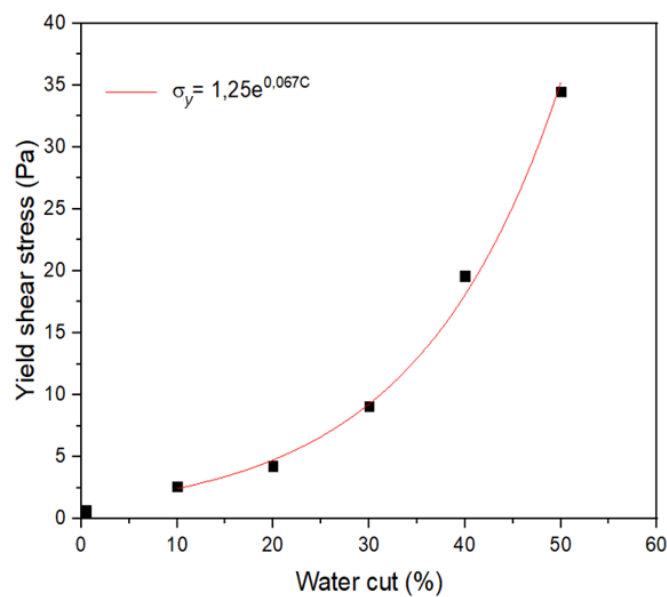


Fig. 4.2. Yield stress as a function of the mass concentration of water.

#### 4.4.2 Viscoelastic Properties

In the following, the experimental results of oscillatory shear measurements, conducted on the Oht Pickering emulsions, are presented. The aim of these experiments is to study the behavior of the emulsions at a near-to-rest undamaged inner structure, and to verify the following hypothesis:

- At rest and at high water/gasoil ratios, the small spaces between water droplets permit an interaction between Oht platelets (Fig. 4.3). This explains the high yield stress values and the hysteresis at the beginning of the flow at high water concentrations.

##### 4.4.2.1 Stress sweep measurements

An oscillatory shear stress ranging from  $2 \cdot 10^{-3}$  Pa to  $10^2$  Pa was applied on all the concentrations, at fixed frequencies ranging from  $10^{-3}$  Hz to  $10^2$  Hz. These experiments are performed to define the viscoelastic linearity domain of each sample.

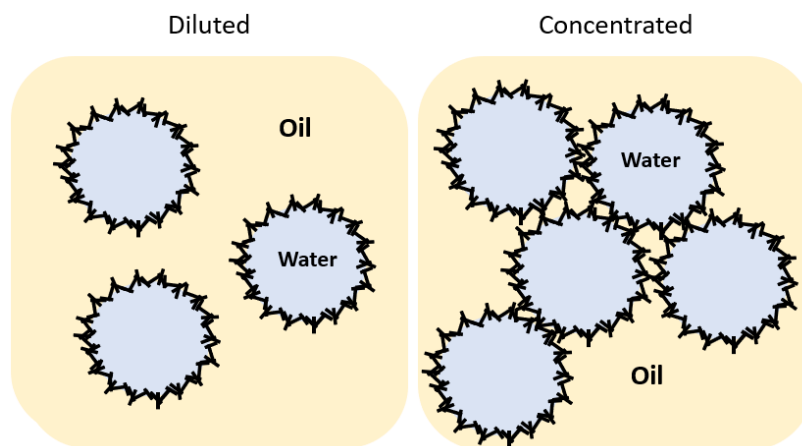


Fig. 4.3. Schematic representation of a diluted and a concentrated Pickering emulsion.

Fig. 4.4 illustrates the evolution of the storage modulus as well as the loss modulus as a function of the applied stress on the concentrations B3-10 H<sub>2</sub>O and B3-50H<sub>2</sub>O, at a fixed frequency,  $f = 0,1$  Hz.

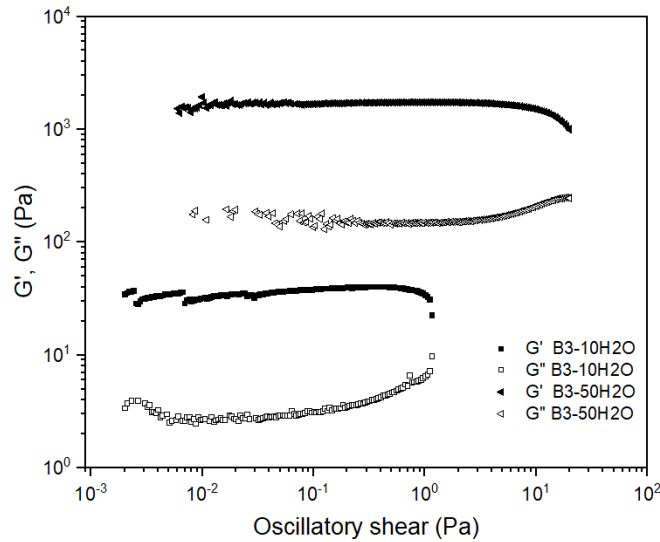


Fig. 4.4. Storage and loss moduli as a function of oscillatory shear at 0,1 Hz.

It can be noticed that  $G'$  and  $G''$  curves are flat on a wide range of the applied shear stress compared to the OHT dispersions in chapter 3. Viscoelastic linearity domain corresponds to the range for which  $G'$  and  $G''$  are independent of the applied oscillatory shear.

Strain curves as a function of the applied shear is illustrated in Fig 4.4, and were used to confirm the linearity domain defined earlier. The linear domain corresponds to the elastic behavior of the material where the slope of the strain curve on a log-log scale is equal to the unity (Fig. 4.5).

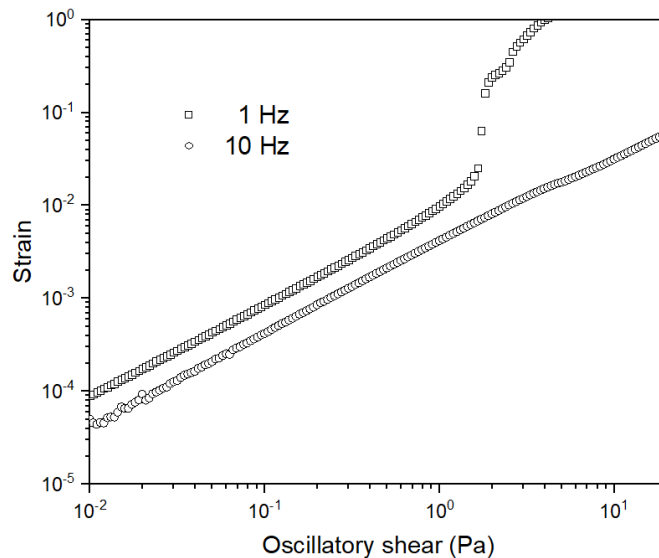


Fig. 4.5. Strain as a function of oscillatory shear at 1 Hz and 10 Hz (B3-20H2O).

#### 4.4.2.2 Frequency sweep measurements

Once the viscoelastic linearity domain defined, frequency sweep measurements were conducted by applying a constant stress for each concentration (0.1 Pa, 0.2 Pa, 0.5 Pa, 1 Pa, 1.5 Pa), and a continuous descending frequency sweep. Fig. 4.6 (a) shows the evolution of the storage modulus as a function of the frequency for all the studied water/gasoil ratios. Fig. 4.6 (b) on the other hand, compares storage and loss moduli curves for three different concentrations.

It is worth noticing that the storage modulus,  $G'$ , is independent of the applied frequency for the range of the studied concentrations. This indicates that at small deformations, OHT stabilized Pickering emulsions exhibit a solid-like behavior even at small water concentrations. Furthermore, the storage modulus,  $G'$ , is always greater than the loss modulus,  $G''$ , which means that the elastic properties of the emulsions are much higher than their viscous properties.

In order to investigate deeper the hypothesis proposed above, storage and loss moduli of a 3 wt% OHT suspension and those of B3-10H<sub>2</sub>O were plotted in Fig. 4.7. The figure illustrates the important differences between the elastic as well as the viscous behaviors of the B3 suspension and the B3-10H<sub>2</sub>O inverse emulsion. It should be pointed out that both fluids were prepared through a continuous circulation in the hydraulic loop. The B3 suspension contains a 3 wt% of organo-hectorite in gasoil whereas the B3-10H<sub>2</sub>O emulsion is prepared by adding a 10 wt% of water to the B3 suspension.

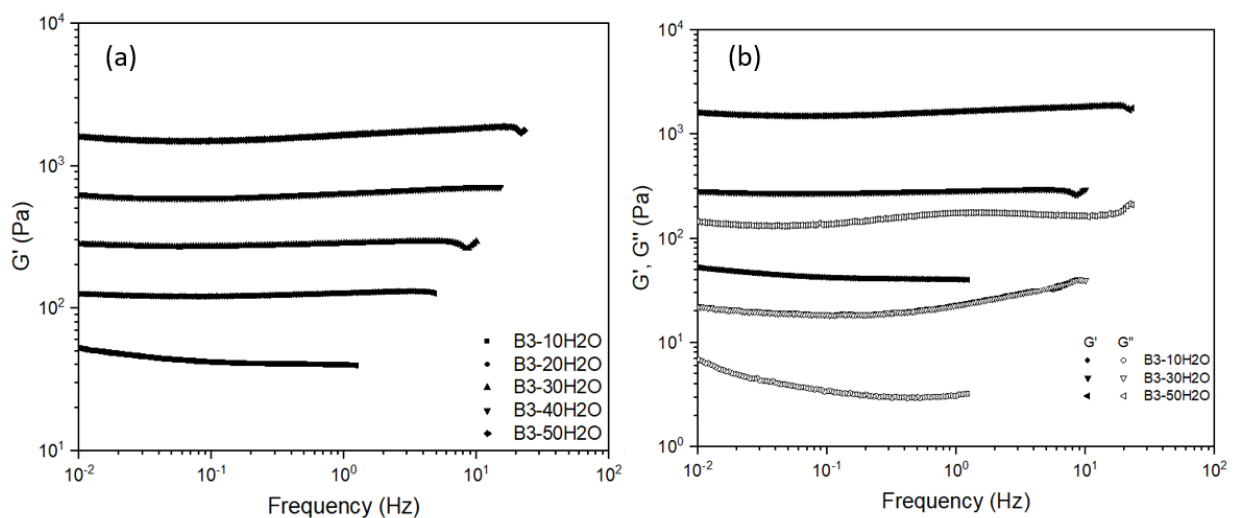


Fig. 4.6. Storage and loss moduli as a function of frequency.

Knowing that the water droplets are surrounded with OHt platelets, and that a similar viscoelastic behavior was noticed in the case of concentrated OHt dispersions (chapter 3), one possible explanation is that the water in these emulsions occupy the free volume in the continuous phase, and thus increases the possibility of interactions between the clay platelets. The latter explanation supports the hypothesis proposed earlier.

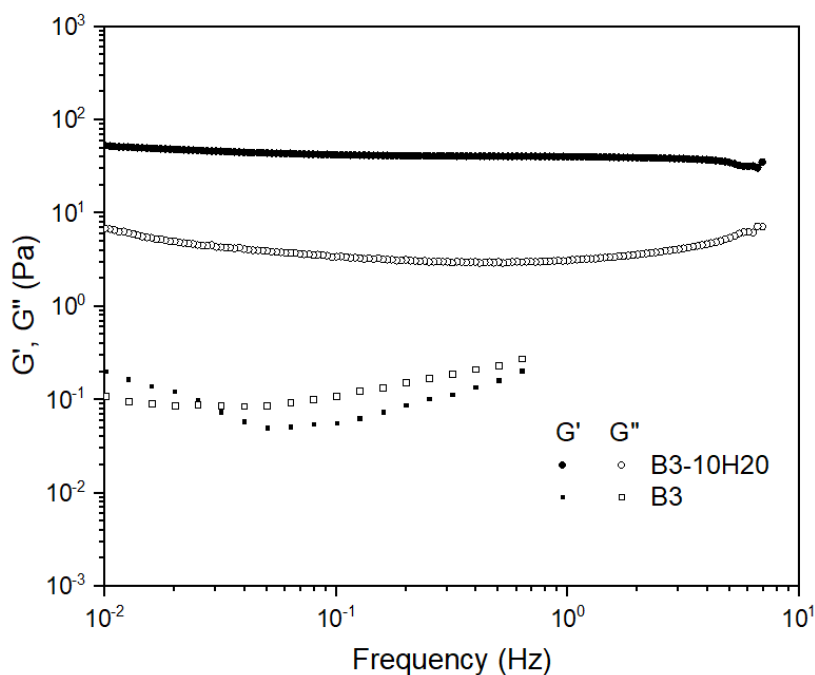


Fig. 4.7. Storage and loss moduli as a function of frequency for a OHt suspension and a OHt stabilized Pickering emulsion.

#### 4.4.3 Limitations of rheological measurements

In the case of surfactant-based emulsions, both rheological and flow measurements are possible until reaching the phase inversion concentration, where the dispersed phase become continuous.

In our case, a separation of a small water (dispersed phase) volume was noticed, but the initial formed emulsion stayed stable (Fig.4.8). This can be explained by the fact that at concentrations higher than 50 wt% of water, a multiple emulsion takes place (Plasencia et al., 2013):

- i. A stable water-in-gasoil emulsion, initially present from the precedent concentration.
- ii. A phase of free water that separates at rest.

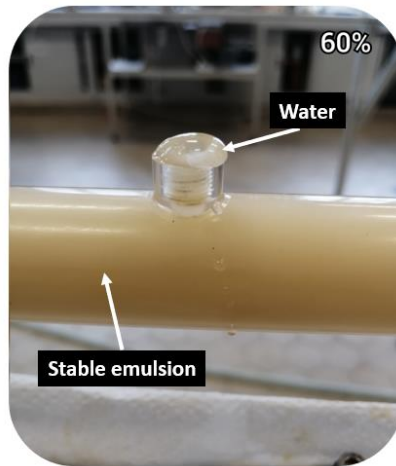


Fig. 4.8. B3-60H<sub>2</sub>O emulsion after 24 h of rest.

Fig. 4.9 shows a cyclic flow shear measurement performed on the sample B3-60H<sub>2</sub>O. Multiple experiments were proceeded using different rheometric geometries, in order to obtain reproducible results, without success. As it can be noticed, after rest, and at the increasing shear stress step, the sample is non homogenous, and a wall slipping phenomenon occurs at the beginning of the experiment, for shear rates lower than 150 s<sup>-1</sup>. At high shear rates, the homogenization of the sample begins and it continues during the shear stress plateau, where a constant shear stress of 60 Pa is applied for 3 min. At the decreasing shear stress ramp, a similar flow curve to the one of the B3-50H<sub>2</sub>O emulsion is established.

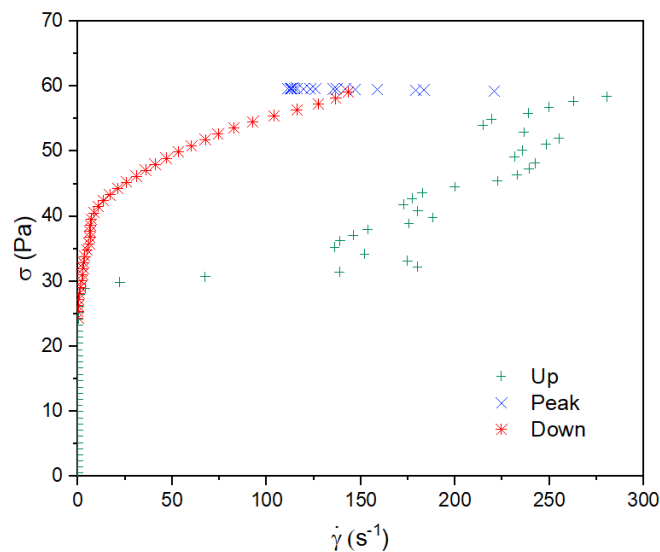


Fig. 4.9. Cyclic shearing (increasing – plateau – decreasing shear stress) of the B3-60H<sub>2</sub>O emulsion.

It should be notice that, although rheological measurements were limited for water concentrations greater that 60%, pipe flow measurements stayed possible for concentrations up to 80%. This can be explained by the presence of two diaphragms in the flow loop that assure a fast homogenization of the emulsions. Flow behavior of emulsions with concentration superior to 50% will be discussed in chapter 5.

## **4.5 Pipe-flow behavior**

In the following, the flow behavior of organo-hectorite (OHt) based emulsions, at water in gasoil concentrations inferior to 50 wt%, is discussed. As it was mentioned in chapter 2, the preparation of the emulsions and the measurements of their flow parameters were both proceeded using the same flow loop.

### **4.5.1 Chronological sequence of measurements**

For a better understanding of the process, a chronological description of the experimental protocol is presented in Fig 4.10.

A total of eight different tests separated by different rest times were conducted on the studied emulsions. Data from all the tests will be discussed in the following sections. Fig. 4.10 illustrates the experimental protocol conducted on each concentration:

- i. For each concentration, we start with a homogenized B3 dispersion i.e., a 3 wt% of OHt in gasoil dispersion.
- ii. Water is than added to the B3 suspension and an in-line emulsification process begins. The in-line emulsification (1) consists of a continuous flow at the maximum flow rate until reaching constant values of velocity and wall shear stress.
- iii. Once the emulsification is reached, the fluid is kept at rest for 24 H (2).
- iv. After 24 H, the emulsion is homogenized through a continuous pipe-flow for 20 min at the maximum flow rate (3).
- v. Six different velocity plateaus are than applied for 3 min (4). 10 min of rest separate each two tests.

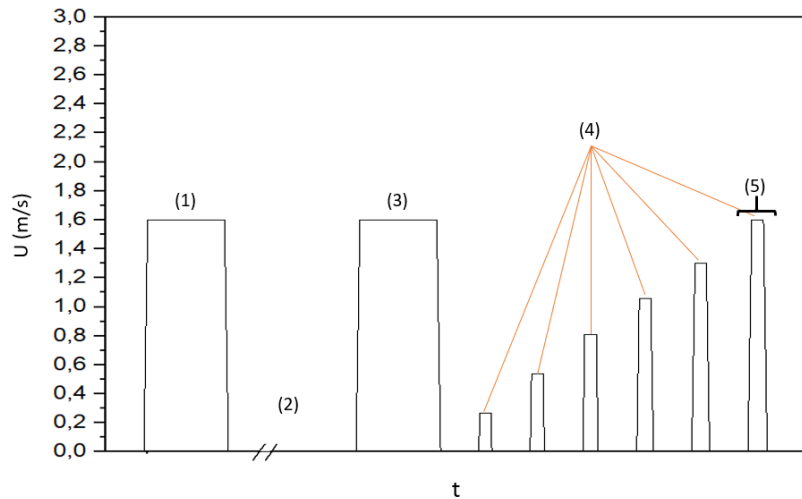


Fig. 4.10. Chronological order of the flow-loop experimental protocol.

It is worth mentioning that both pressure and velocity values are registered during this whole procedure.

#### 4.5.2 Flow parameters during the emulsification process

The preparation of organoclay-stabilized Pickering emulsions was achieved through an in-line continuous flow using two different diaphragms at the end of the flow loop (chapter 2). In order to monitor the emulsification process, flow parameters were registered during the in-line continuous flow (Fig. 4.10-1). In this section, the efficacy and the duration of the emulsification system will be discussed.

The parameters of the B3-50 H<sub>2</sub>O emulsion were followed as a function of time during the emulsification process. Using the pressure data, wall shear stress was calculated.

For unidirectional, axisymmetric pipe-flow, shear stress ( $\sigma_w$ ) at the wall is given as follows:

$$\sigma_w = \frac{R \Delta P}{2 L} \quad 4.3$$

where  $R$  (m) is the pipe radius,  $\Delta P/L$  (Pa/m) is the pressure loss over a pipe length  $L$ .

Wall shear stress as well as the velocity at the pipe center are plotted during the preparation of the B3-50H<sub>2</sub>O emulsion (Fig. 4.11). At the beginning of the emulsification process, the organic

and the non-organic phases are totally separated and the tested fluid is non homogenous; hence, the oscillations in the curves of Fig. 4.11 at the beginning of the flow. Low velocity and high wall shear stress values correspond to the passage of plugs from the precedent concentration (B3-40H2O in this case) and, in the same way, high velocity and low wall shear stress values indicate the passage of water plugs.

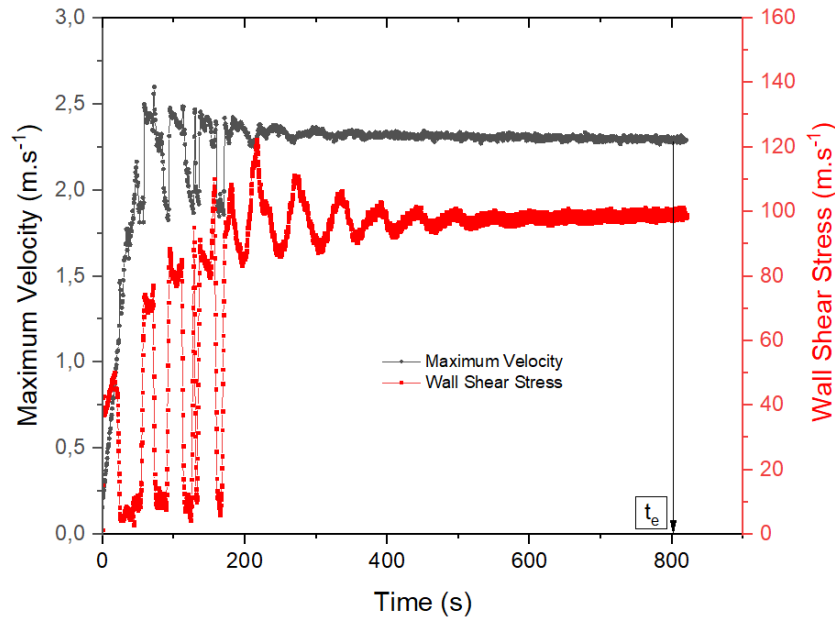


Fig. 4.11. Maximum velocity and wall shear stress as a function of time during the emulsification process of B3-50H2O emulsion.

The magnitude of the oscillation decreases with time until the equilibrium is reached. Once the flow parameters reach the equilibrium, the emulsification is considered to be reached and the fluid is supposed homogenous (Fig.4.12). It was found that in the case of B3-50H2O, the emulsification time,  $t_e$ , is about 800 s.

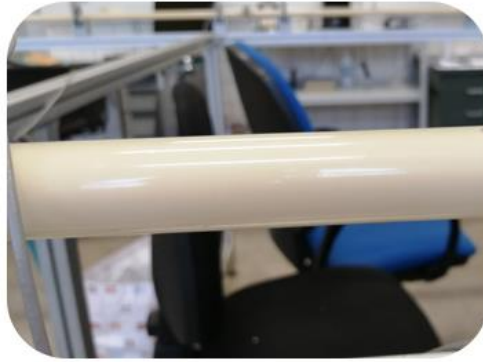


Fig. 4.12. Picture of the B3-20H2O emulsion, taken immediately after the emulsification process.

#### 4.5.3 Flow parameters during the homogenization process

Before each series of test measurements, a continuous pipe-flow at the maximum velocity delivered by the pump is conducted to assure the homogenization of the emulsions after a period of rest (Fig. 4.10-3).

The experimental protocol corresponding to the homogenization process is as follows:

- i. An increasing flow rate during 60 s.
- ii. A 20 min plateau at the maximum flow rate.
- iii. A decreasing flow rate during 60 s.

Fig. 4.13 shows the temporal evolution of the flow parameters of a B3-10H2O emulsion at a mean velocity of  $U = 1,53 \text{ m} \cdot \text{s}^{-1}$ , after 24 H of rest. It should be noticed that a similar behavior was noticed for all the concentrations studied in this chapter.

Starting from a structured fluid, the wall shear stress curve, in green, shows a stress peak in the beginning of the flow followed by a sudden drop. After that, and starting from a non-zero value due to fluid's yield stress, shear stress increases gradually in the same time as the velocity does. Finally, shear stress value slightly decreases until reaching a constant value during the mean velocity plateau.

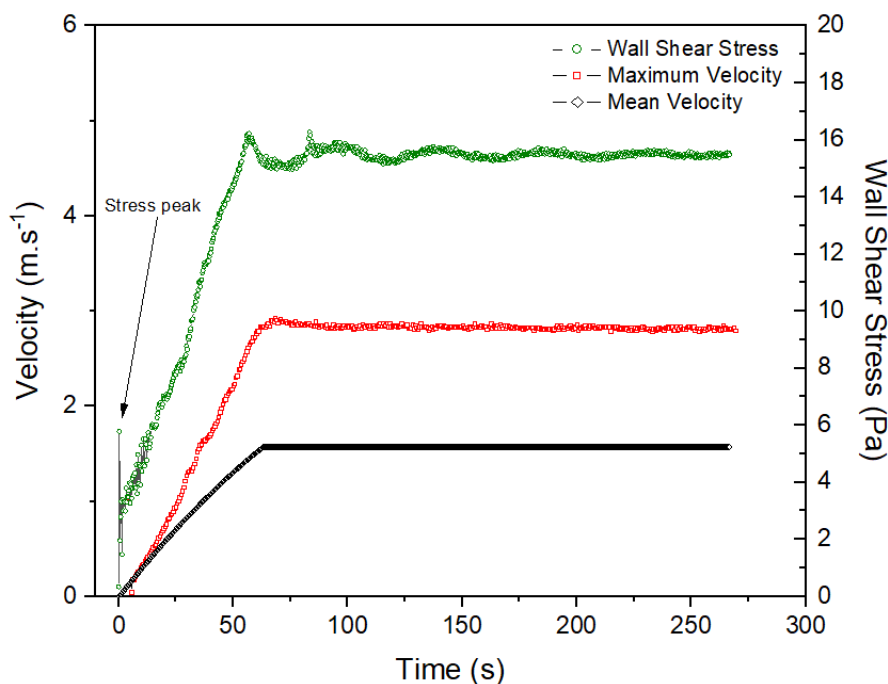


Fig. 4.13. Flow parameters after 24 H of rest of B3-10H<sub>2</sub>O emulsion.

It can be noticed that, overall, the emulsion is very stable in time. Even after 24 H of rest, small temporal changes in the flow parameters are noticed. Furthermore, both wall shear stress and maximum velocity curves illustrate the fact that a complex inner structure takes place at rest. This means that, at rest, the surfaces of water droplets interact with each other and weak bonds are developed between them.

It is worth mentioning that in the case of classic emulsions, concentration dependency of yield stress does not occur for concentrations lower than 75% (Derkach, 2009). This means that the complex behavior of the studied emulsions is probably related to the presence of OHT particles on the surfaces of the water droplets.

#### 4.5.4 Verification of the flow regimes

In this section, flow regimes of the studied emulsions will be investigated. To do so, friction factors and velocity profiles of the prepared concentrations were calculated for the range of flow rates delivered by the pump of our set-up.

#### 4.5.4.1 Using friction factors

The evolution of the friction factor,  $f$ , as a function of the wall Reynolds number,  $Re_w$ , for the studied concentrations, is presented in Fig. 4.14. The used Reynolds number is calculated using the equation:

$$Re_w = \frac{\rho U D}{\mu_w} \quad 4.4$$

where  $Re_w$  is the wall Reynolds number,  $\rho$  is the density of the emulsion,  $U$  is the mean velocity of the fluid,  $D$  is the pipe diameter and  $\mu_w$  is the wall viscosity.

The wall viscosity is the ratio between wall shear stress and wall shear rate:

$$\mu_w = \frac{\sigma_w}{\dot{\gamma}_w} \quad 4.5$$

Wall shear stress is given by Eq. 4.3, and wall shear rate can be calculated by substituting the Herschel-Bulckley model in the velocity expression:

$$\dot{\gamma}_w = \left( -\frac{du(r)}{dr} \right)_{r=R} = -\frac{nR}{n+1} \left( \frac{\sigma_w - \sigma_c}{K} \right)^{\frac{1}{n}} \left( 1 - \frac{\sigma_c}{\sigma_w} - \frac{n+1}{nR} \right) \quad 4.6$$

In the laminar regime, wall Reynolds number satisfies the Hagen–Poiseuille equation (Benslimane et al., 2016):

$$f = \frac{16}{Re_w} \quad 4.7$$

where  $f$  is the fanning friction factor and it can be calculated using the experimental data using the expression:

$$f = \frac{2\sigma_w}{\rho U^2} \quad 4.8$$

In Fig.4.14, the experimental data appear to be well correlated by the Hagen–Poiseuille equation in the laminar regime (solid line). It can be noticed that, except for the B3 suspension, all the concentrations are fully in the laminar regime. Regarding the B3 suspension, the critical Reynolds number can be defined as the deviation of the experimental data from the Hagen–Poiseuille equation. At values superior to the critical Reynolds number, the turbulent regime is observed.

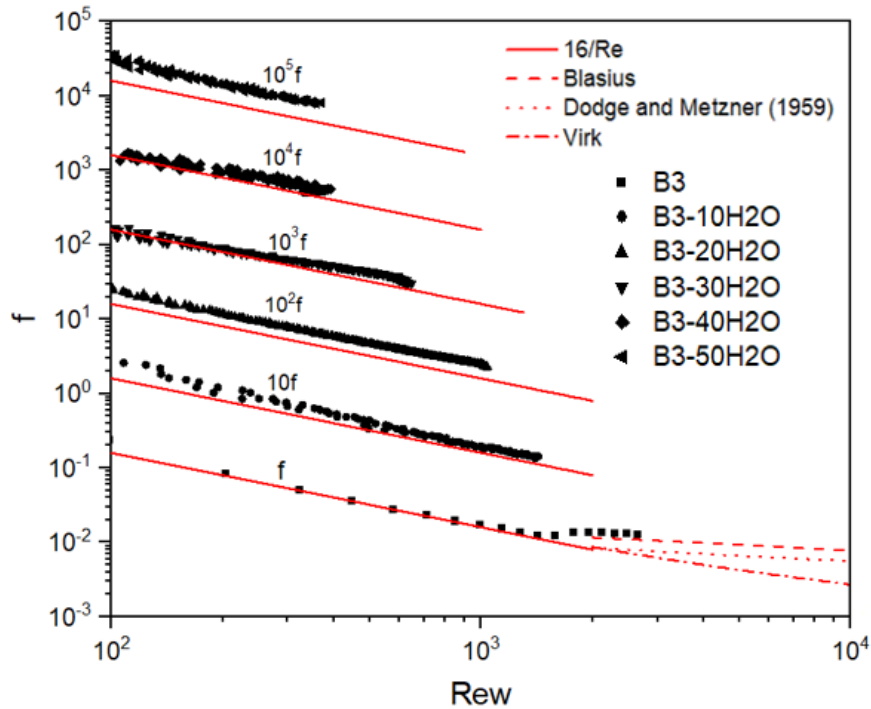


Fig. 4.14. Fanning friction factor as a function of wall Reynolds number in laminar and turbulent regimes.

In the turbulent regime, the experimental data is correlated using the Blasius, the Dodge and Metzner (1959) and the Virk equations. It can be observed that the curve is best fitted using the empirical Blasius equation (dashed line). The empirical Blasius equation was developed to simulate the friction factor of Newtonian fluids at the turbulent regime. This result can be explained by the fact that the yield stress value of the B3 suspension is very low and that its flow index is close to unity (see Fig. 4.1 and 4.2), which makes the behavior of the fluid similar to that of a Newtonian fluid.

#### 4.5.4.2 Using velocity profiles

Fig. 4.15 shows the velocity profiles of the B3 (a) and the B3-30H<sub>2</sub>O (b) emulsions at different mean velocities. The curves of Fig. 4.15 were obtained using the experimental protocol showed in Fig. 4.10-4. Both laminar and turbulent behaviors can be noticed for the B3 emulsion. For the rest of concentrations, only laminar velocity profiles can be obtained.

The laminar theoretical velocity profiles were calculated using the rheological Herschel-Bulckley parameters and the following expression (Benslimane et al., 2016):

$$u(r) = \begin{cases} \frac{R}{\sigma_w k n^{\frac{1}{n}} (\frac{1}{n} + 1)} \left[ (\sigma_w - \sigma_c)^{\frac{1}{n} + 1} - \left( \frac{\sigma_w r}{R} - \sigma_c \right)^{\frac{1}{n} + 1} \right], & R_c \leq r \leq R \\ \frac{R}{\sigma_w k n^{\frac{1}{n}} (\frac{1}{n} + 1)} \left[ (\sigma_w - \sigma_c)^{\frac{1}{n} + 1} \right] & , r \leq R_c \end{cases} \quad 4.9$$

The first equation is used for  $R_c \leq r \leq R$ ,  $R_c$  being the plug radius, where the applied shear is superior to the yield stress and the second equation is used for  $r \leq R_c$  where the applied shear stress is inferior to the yield stress and the fluid exhibits a solid-like behavior.

The transition to turbulence was estimated when the experimental data deviated from the Herschel-Bulckley model since it is applicable only in the laminar regime. Turbulence was observed only in the case of B3 concentration, which is a 3 wt% organo-hectorite suspension. The latter signifies that the maximum mean velocity generated by the pump was not sufficient to reach the turbulent regime for any of the studied emulsions due to their high viscosity.

Furthermore, the Herschel-Bulckley model describes well the flow behavior of the fluids in the laminar regime.

## 4.5.5 Comparison between flow measurements and rheology

### 4.5.5.1 Wall shear stress

The pipe flow behavior of the emulsions is mainly governed by its rheological behavior. In this section, wall shear stresses obtained from the equilibrium pipe flow pressure drop measurements (Fig. 4.10-4) as well as calculated wall shear stresses, using the parameters of the rheological model (Table 4.1), are compared.

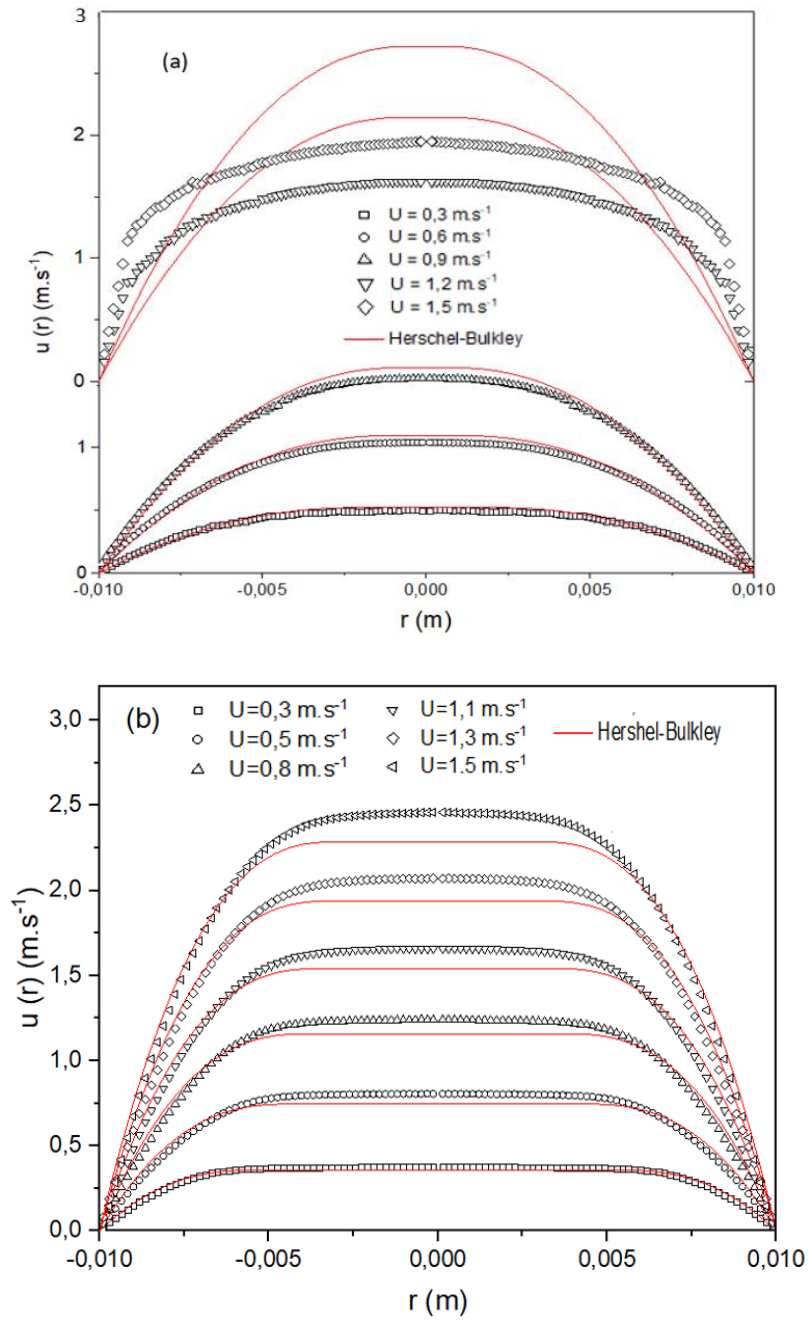


Fig. 4.15. Velocity profiles at the equilibrium at different velocities for the B3 (a) and the B3-30H<sub>2</sub>O (b) samples.

Wall shear stress, in the case of a unidirectional, axisymmetric pipe-flow is given by Eq. 4. 3.

The theoretical wall shear stress in laminar regime was obtained by resolving the following equation:

$$U = \frac{R}{K^{\frac{1}{n}} \left(\frac{1}{n}+1\right)} (\sigma_w - \sigma_c)^{\frac{1}{n}} \left[ \left(1 - \frac{\sigma_c}{\sigma_w}\right) - \frac{2\left(1 - \frac{\sigma_c}{\sigma_w}\right)^2}{\frac{1}{n}+2} + \frac{2\left(1 - \frac{\sigma_c}{\sigma_w}\right)^3}{\left(\frac{1}{n}+2\right)\left(\frac{1}{n}+3\right)} \right] \quad 4.10$$

where  $U$  is the mean velocity through a cross section of the pipe,  $R$  is the pipe radius,  $\sigma_w$  is the wall shear stress,  $K$ ,  $n$  and  $\sigma_c$  are the Hershel-Bulckley rheological parameters.

Eq. 4.10 was expressed by substituting the shear rate expression from the Hershel-Bulckley equation in the Rabinowitsch-Mooney equation, which is usually used to calculate the local wall shear rate and shear stress (Munoz et al., 1996; Benslimane et al., 2016):

$$\frac{Q}{\pi R^3} = \frac{1}{\sigma_w^3} \int_0^{\sigma_w} \sigma^2 f(\sigma) d\sigma \quad 4.11$$

where  $Q$  is the volumetric flow rate,  $R$  is the radius of the pipe,  $\sigma$  and  $\sigma_w$  are the shear stress and the wall shear stress, respectively.

The experimental wall shear stress at equilibrium and the theoretical wall shear stress calculated using the Hershel-Bulckley model parameters, at different water/gasoil ratios, are plotted as a function of the mean velocity in Fig. 4.16. In the range of flow rates generated by the pump, all the concentrations, except for B3, exhibit only a laminar flow regime. For the B3 fluid, laminar regime is noticed for mean velocities inferior to  $1 \text{ m}\cdot\text{s}^{-1}$ . Eq. 4.10 was used to calculate the theoretical wall shear stress in the laminar regime (solid line).

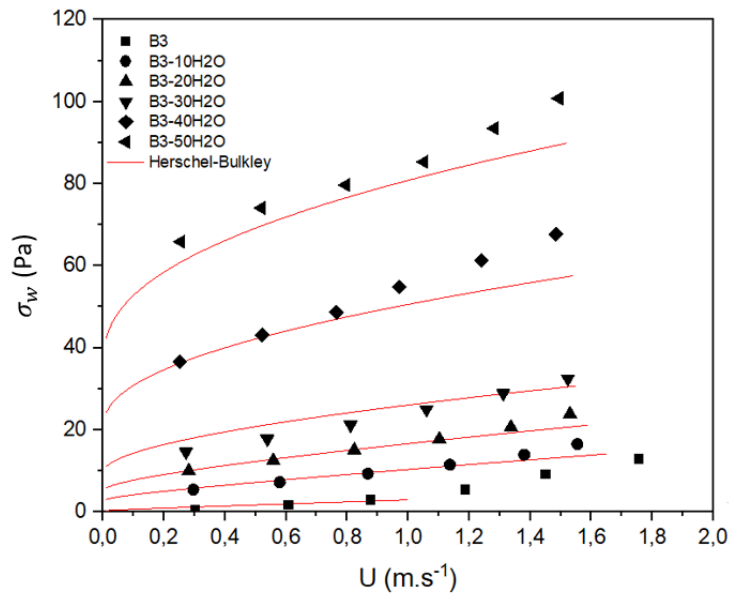


Fig. 4.16. Equilibrium experimental and theoretical wall shear stress as a function of the mean velocity.

Despite using two different measuring systems, the equilibrium shear stress values seem to be well simulated using the Herschel-Bulckley model. The latter indicates that the rheological parameters given through rheology describe well the rheological behavior of the emulsions. Several parameters can induce differences between the data collected from both techniques such as the scale difference, wall slipping effects and the difference between measuring geometries. It should be as well noticed that the used rheometer is stress controlled and the hydraulic loop is shear controlled. At high concentrations i.e., B3-40H<sub>2</sub>O and B3-50H<sub>2</sub>O, a deviation from the Herschel-Bulckley model is observed at high shear rates. This may be related to the presence of the diaphragms and the continuous emulsification of the emulsions during the tests.

#### 4.5.5.2 Velocity profiles

Fig. 4.17 illustrates the dimensionless laminar velocity profiles of the B3, B3-20H<sub>2</sub>O, and the B3-50H<sub>2</sub>O water in gasoil Pickering emulsions. All the profiles are measured at constant mean velocity plateaus after a velocity increasing ramp (Fig. 4.10-4).

It can be noted that velocity profiles get flatter as water concentration increases. This is related to the increase in the yield stress values. The plug radius of the B3 fluid is the smallest and this can be explained by the small yield stress value (0,23 Pa) of the B3 fluid (Table 4.1).

The theoretical velocity values as a function of the radius were calculated using the Herschel-Bulckley rheological parameters and plotted in solid lines (Fig. 4.17). It can be noticed that the rheological measurements are in a good correlation with the flow-loop measurements for the wide range of the prepared concentrations. The small differences between the curves can be due to several factors. One of these factors is the sampling method of the emulsions from the flow loop. It is worth noting that a sample of each concentration is taken from the flow loop for rheological measurements. A small homogeneity problem can cause errors in the rheological measurement, where a 2 ml sample is used. Another factor can be the temperature difference. In the rheometer, a Peltier system is used for the regulation of the temperature ( $T = 20.0 \pm 0.1$  °C). In the flow-loop, on the other hand, many parameters can influence the temperature such as the linear and the singular frictions (elbows, diaphragms, pump) which make temperature control more difficult than in rheology ( $T = 20.0 \pm 2.0$  °C).

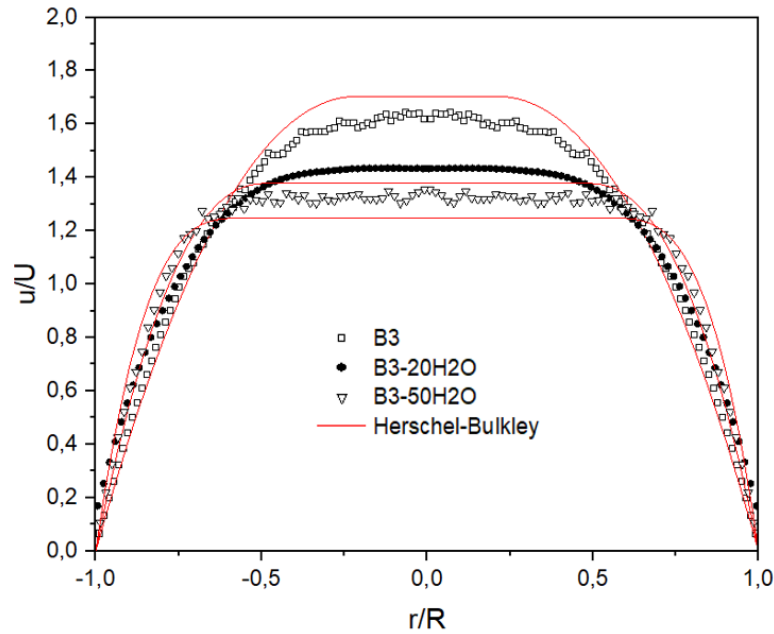


Fig. 4.17. Dimensionless laminar velocity profiles at equilibrium for the emulsions: B3, B3-20H<sub>2</sub>O and B3-50H<sub>2</sub>O.

## 4.5.6 Emulsion stability

### 4.5.6.1 Short term stability

Short term stability is a key factor used to determine the possibility of an industrial application of the studied emulsions. First, the wall shear stress, during a continuous increasing ramp, an equilibrium plateau and a continuous decreasing ramp of flow rate, was studied. This experiment is the test (5) illustrated in Fig.4.10. All concentrations were tested. The experimental wall shear stress was calculated using Eq. 4.3 and the theoretical wall shear stress was calculated using the Eq. 4.10.

Fig. 4.18 represents the evolution of wall shear stress as a function of the mean velocity. At low concentrations i.e., water concentrations under 30 wt%, the increasing (full symbols) and the decreasing (empty symbols) curves of experimental wall shear stress seem to overlap. This indicates that the rheological parameters of the emulsions are not influenced by the plateau shearing time (3 min). At higher concentrations, a small hysteresis is noticed between the increasing and the decreasing shear ramps. As it can be noticed in Fig. 4.18, for the B3-40H<sub>2</sub>O

and the B3-50H2O, the decreasing ramp is located above the increasing ramp which indicates the presence of a shear-thickening behavior.

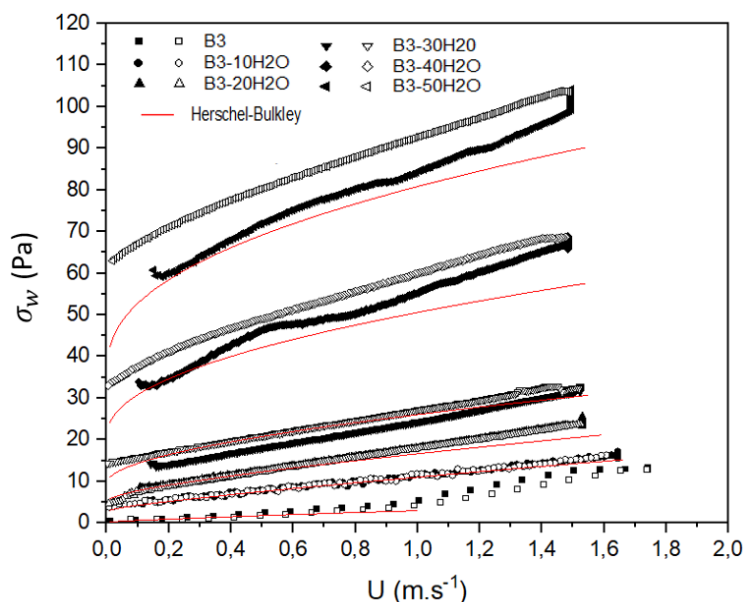


Fig. 4.18. Experimental and theoretical wall shear stress as a function of the mean velocity at increasing and decreasing velocity ramps. Full symbols: increasing ramp, empty symbols: decreasing ramp

Fig. 4.18. also shows that rheology data (solid line) coincides well with the experimental data from the flow-loop (full symbols). It should be noticed that the flow-loop measurements were not performed at the same time as the rheometric measurements. The agreement between the two types of measurements, considering the possible experimental errors coming from the fluid sampling and the small quantity used to carry out the rheometric measurements, shows the stability and the homogeneity of the emulsions as well as the absence of any memory effects. It also indicates that the wall slipping was controlled in both geometries and that the use of the Herschel-Bulckley model was adequate to fit the flow curves in Fig. 4.1.

As shown in Fig. 4.18 and Fig. 4.1, an increase in water concentration leads to an increase in yield stress and in viscosity. This can be related to the increase in the interactions between water droplets and organoclay particles and the formation of complex structures at rest.

In addition to the wall shear stress, velocity profiles can be used to study the short-term stability of the emulsions. The shape of velocity profiles depends on the rheological behavior and the internal structure of the studied fluid. It was shown, in the precedent sections, that the studied

Pickering emulsions do not show any thixotropy, for water concentration lower than 30 wt%. Thixotropy is not the only possible type of time-dependency. Time-dependency can be as well related to irreversible microstructural changes in time (aging effect) and macrostructural changes in time as in the case of emulsion phase separation.

In Fig. 4.19, velocity profiles of the B3-10H2O emulsion are represented at different velocities after 10 min of rest. This test corresponds to the increasing ramp of test (5) illustrated in Fig. 4.10. According to previous tests, the B3-10H2O emulsion is in the laminar regime at the studied velocities. The velocity profiles have the typical shape of that of yield stress fluids. They are characterized by a plug flow at the center of the pipeline where the resulting shear stress is inferior to the yield stress. The dimensions of the plug depend on the applied shear stress and hence on the mean velocity of the flow. The theoretical velocity profiles using the Herschel-Bulckley model parameters were also represented in Fig. 4.19. It can be noticed that unlike the case of equilibrium (Fig. 4.17), in an increasing ramp, there is a difference between the experimental measurements and the Herschel-Bulckley model. This difference diminishes as the mean velocity increases and becomes negligible at the highest velocity ( $U = 1,58 \text{ m} \cdot \text{s}^{-1}$ ) which is reached after 60 s from the beginning of the flow. This indicates that, at low water concentration  $s$  and after a short time rest, 1 min of continuous flow is sufficient to reach an equilibrated structural state of the emulsions.

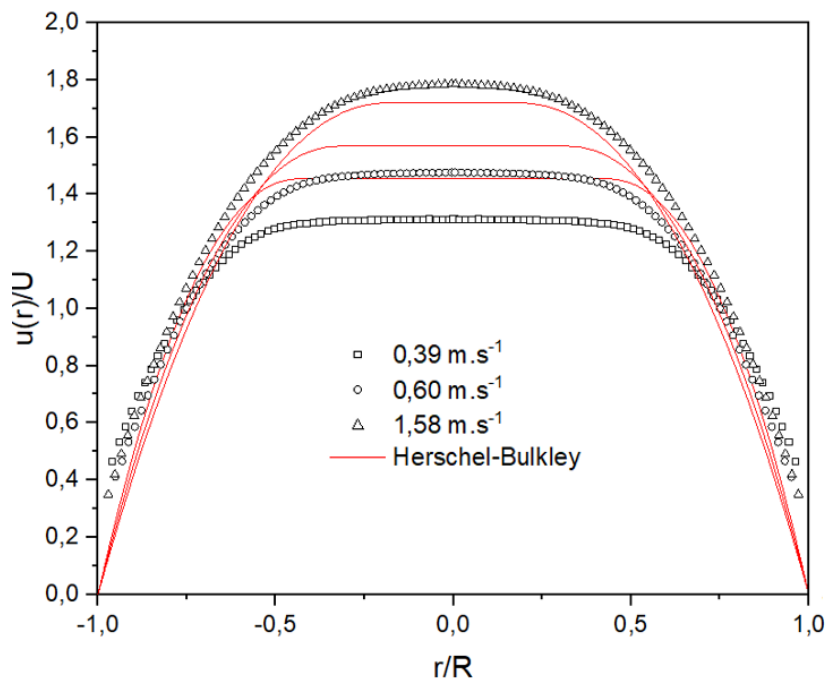


Fig. 4.19. Dimensionless velocity profiles of B3-10H2O emulsion after 10 min of rest at a mean velocity increasing ramp.

#### 4.5.6.2 Stability after 24 H of rest

The effect of a daily rest on the rheological behavior of the studied emulsions is investigated. The velocity profiles of the B3-10H2O emulsion, discussed in the precedent section at the same mean velocities as in Fig. 4.19, are studied after 24 H of rest.

Fig. 4.20 shows that after 24 H of rest, the B3-10H2O emulsion exhibits a flat velocity profile at the beginning of the flow. Looking at the absence of thixotropy in the case of the B3-10H2O emulsion (Fig. 4.1 and Fig. 4.18), a possible explanation of the solid-like flow of the B3-10H2O emulsion at the beginning of the flow can be the separation and the presence of a thin gasoil film on the pipe walls, which induces a wall slipping in these conditions. The continuous in-line circulation and the permanent presence of the diaphragms increase the shear of the outer layers as well as the homogenization of the fluid, and thus decrease the width of the gasoil film. Similar to the case of a 10 min rest (Fig. 4.19), a 1 min circulation was found to be sufficient to homogenize the emulsion and to reach an equilibrium state after 24 H of rest.

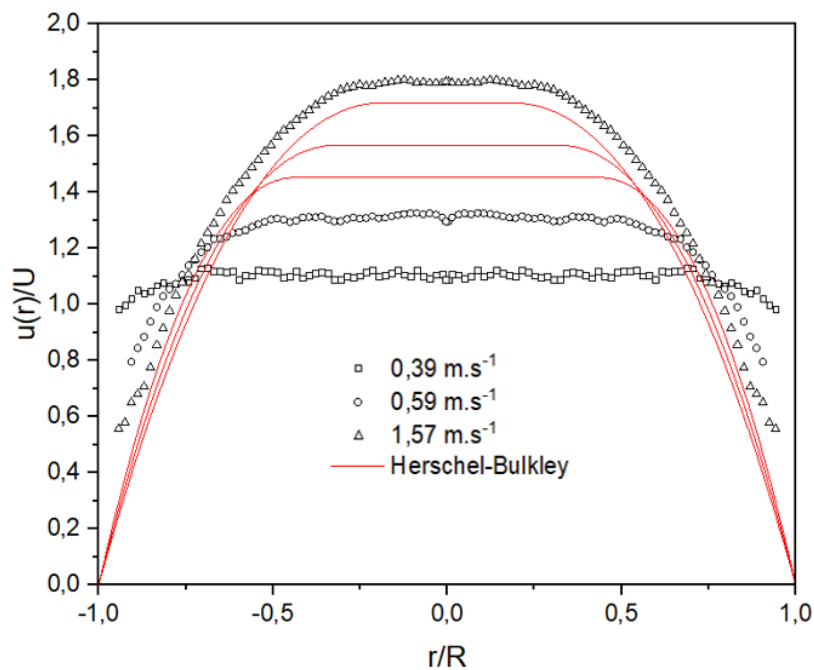


Fig. 4.20. Dimensionless velocity profiles of B3-10H2O emulsion after 24 H of rest.

#### 4.5.6.3 Stability after long-term rests

Long-term stability of the emulsions was studied by comparing the velocity profiles of freshly prepared samples and after several days of rest. The B3-50H2O emulsion was kept at rest for 5 days and the B3-20H2O was kept at rest for 30 days.

Fig. 4.21 shows that the overall behavior of the B3-50H2O emulsion stays the same after 5 days of rest. It can also be noticed that the maximum velocity slightly diminishes and the profile becomes flatter which indicates a small increase in the yield stress. This increase might be due to a further emulsification of the fluid during the homogenization step before starting the actual tests (Fig. 4.10-3).

Fig. 4.22 illustrates the velocity profiles of the B3-20H2O emulsion immediately after emulsification and after 30 days of rest. It can be noticed that the B3-20H2O velocity profiles are more rounded than those of the B3-50H2O emulsion, which can be explained by the difference of the yield stress values between the two emulsions. Fig. 4.22 also shows the overlapping of the velocity profiles of the fresh and the aged (30 days of rest) B3-20H2O emulsions, which confirms the stability of the emulsions over a month of rest.

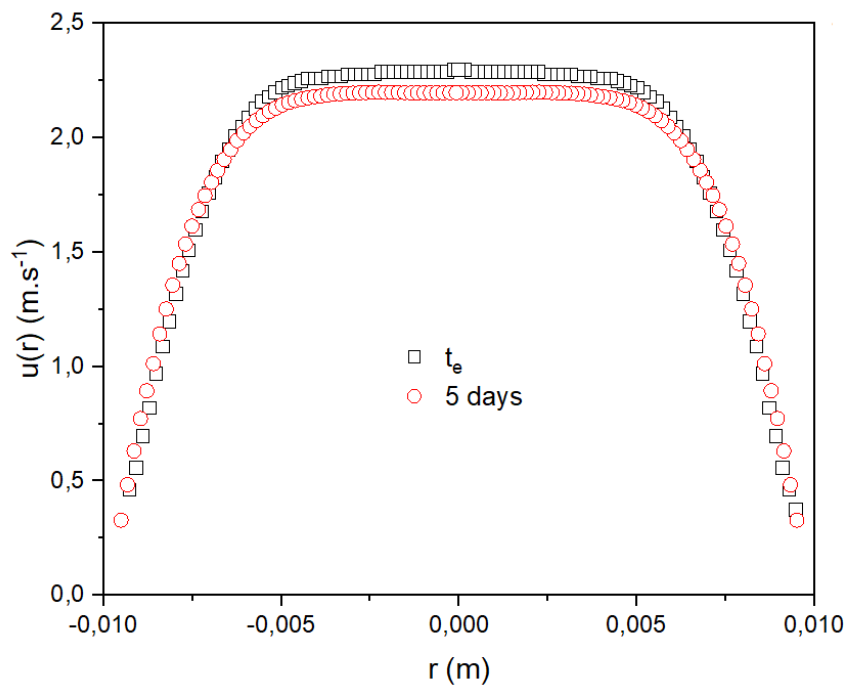


Fig. 4.21. Velocity profiles of a fresh,  $t_e$ , and a 5-day old B3-50H2O emulsion at  $U = 1,5 \text{ m.s}^{-1}$ .

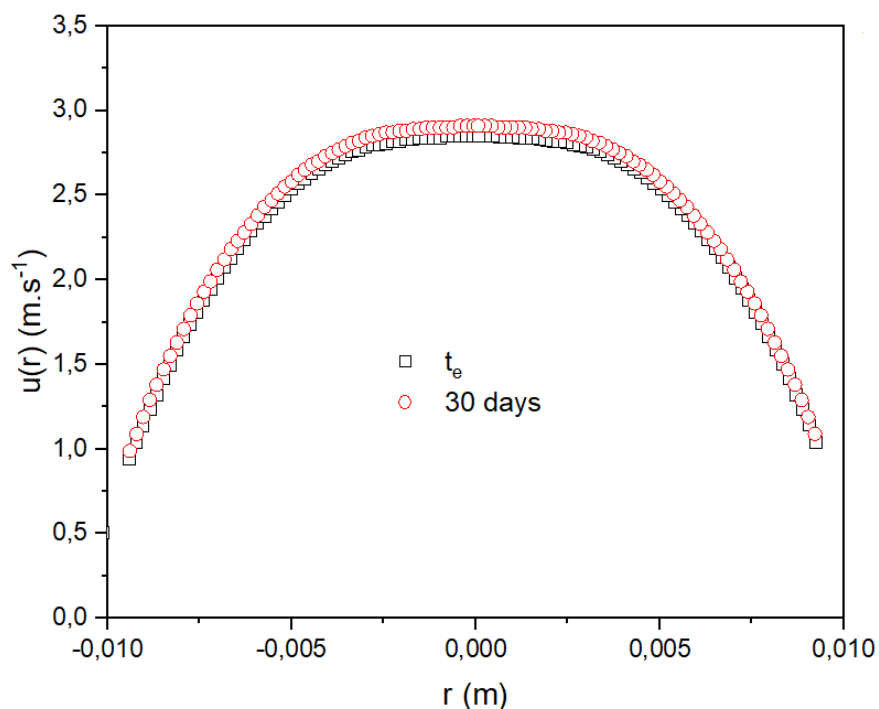


Fig. 4.22. Velocity profiles of a fresh,  $t_e$ , and a 30-day old B3-20H2O emulsion at  $U = 1,53$   $\text{m.s}^{-1}$ .

#### 4.6 Visual aspects

The same volume of 50 ml of each emulsion was poured into a graduated cylinder each and kept at rest for 4 months at a constant temperature of  $20^\circ\text{C}$  (Fig. 4.23).

For all concentrations, except for the B3-50H2O, no free water was observed. In the case of the B3-50H2O, a separated water droplet was observed attached to the cylinder wall. For concentrations under B3-50H2O, a separated gasoil layer was observed at the top of the emulsion. The quantity of the free gasoil decreased as the water concentration increased. This free gasoil layer can be homogenized into the emulsion through a simple mechanical stirring. The latter observation confirms the hypothesis announced earlier, regarding wall slipping at the beginning of the flow due to the presence of a thin gasoil film at the pipe walls (Fig. 4.20).

In the same way, wall slipping may explain the deviation from the Herschel-Bulckley behavior of the B3-10H2O after 10 min of rest (Fig. 4.19). The observed shear thickening behavior and the flow curve hysteresis at high concentrations in Fig. 4.18 can as well be explained by the re-

emulsification of the free water droplets due to the presence of the diaphragms during the increasing ramp and the plateau circulation phases.

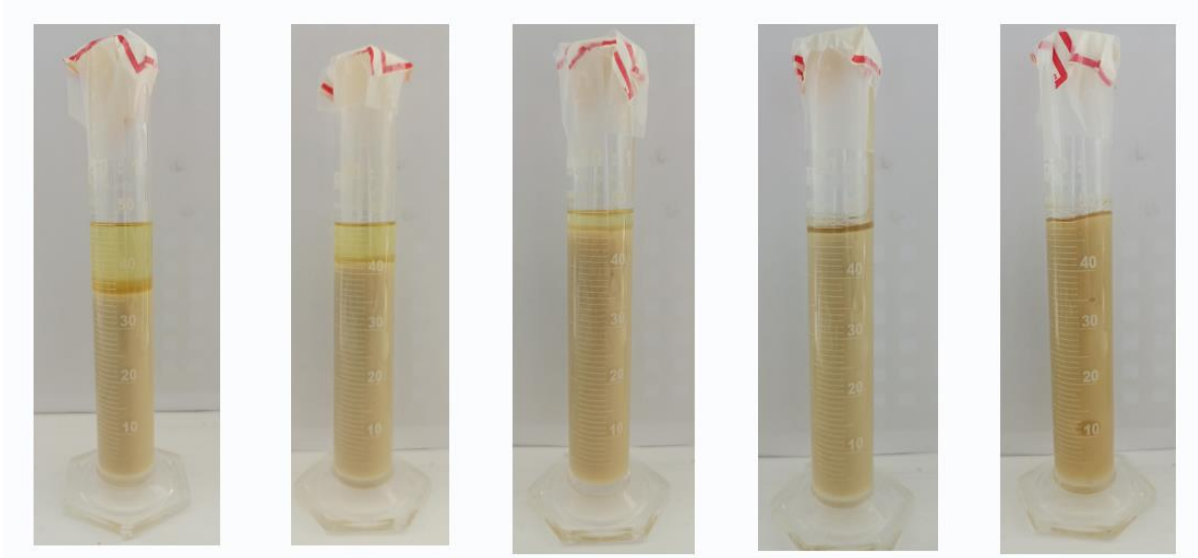


Fig. 4.23. Pickering emulsions at different concentrations after 4 months of rest. From left to right: B3-10H<sub>2</sub>O, B3-20H<sub>2</sub>O, B3-30H<sub>2</sub>O, B3-40H<sub>2</sub>O and B3-50H<sub>2</sub>O.

#### 4.7 Summary to chapter

An in-line emulsification system, using two diaphragms, was tested, and used to prepare inverse Pickering emulsions stabilized with organo-hectorite clay. The emulsification system showed its ability to prepare homogenous and stable, in time, Pickering emulsions. 800 s were necessary to completely emulsify the fluids, and sound celerity measurements were used to verify the homogeneity and the water concentrations of the prepared emulsions. The used emulsification system seemed to be suitable for an in-situ emulsion preparation. This concept can as well be used for a continuous in-line quality control of emulsions, thus avoiding the multiple in-situ sampling and testing.

Using the latter method, Pickering emulsions with five water concentrations were prepared. A sample of each emulsion was extracted and rheologically tested using a stress-controlled rotational rheometer. It was found that the Pickering emulsions exhibit a shear-thinning with

yield stress behavior that was successfully fitted using the Hershel-Bulckley model. The evolution of the yield stress as a function of water concentration showed that the phase inversion point was not yet reached for the studied concentrations.

Furthermore, viscoelastic measurements illustrated the gel behavior of the emulsions at low deformations. A comparison between the B3 and the B3-10H<sub>2</sub>O storage and viscous moduli showed the major difference in the viscoelastic properties between the two fluids. The B3-10H<sub>2</sub>O emulsion has a behavior similar to that of concentrated OHT suspensions, studied in chapter 3. Therefore, the elastic behavior of the emulsions was related to the interaction between clay platelets present on their surfaces.

In a second part, the flow behavior of the prepared emulsions was studied through a pipe-flow circulation, by the means of velocity and pressure measurements. All emulsions were found to behave in the laminar regime. Pipe wall shear stresses showed the same rheological behavior found in rheology, and its curves coincided well with the Hershel-Bulckley model extracted from the flow curves. The comparison of the experimental laminar velocity profiles with the simulated profiles using the Hershel-Bulckley parameters showed a good correlation, particularly at established flow.

Moreover, short, daily and long-term stability was studied. It was found that after rest times ranging from a few minutes to a few days, an in-line homogenization of 1 min is sufficient to reach the structural equilibrium of the emulsions. For longer rest times, yield stress values as well as the viscosity of the emulsions were found to slightly decrease.

Based on the results presented in this chapter, two main perspectives can be suggested for future research:

- i. The emulsification system should be further studied for the preparation of both solid-stabilized and surfactant-stabilized emulsions for in-situ emulsion preparations.
- ii. Pickering emulsions show a high potential for an application in drilling fluids, given their stability in time, their surfactant-free characteristics, and their rheological and flow properties similar to those of drilling fluids.

## 4.8 References

- Abend, S., Bonnke, N., Gutschner, U., Lagaly, G., 1998. Stabilization of emulsions by heterocoagulation of clay minerals and layered double hydroxides. *Colloid Polym. Sci.* 276, 730–737. <https://doi.org/10.1007/s003960050303>
- Agarwal, S., Phuoc, T.X., Soong, Y., Martello, D., Gupta, R.K., 2013. Nanoparticle-stabilised invert emulsion drilling fluids for deep-hole drilling of oil and gas. *Can. J. Chem. Eng.* 91, 1641–1649. <https://doi.org/10.1002/cjce.21768>
- Aguilera, B.M., Delgado, J.G., Cárdenas, A.L., 2010. Water-in-oil emulsions stabilized by asphaltenes obtained from venezuelan crude oils. *J. Dispers. Sci. Technol.* 31, 359–363. <https://doi.org/10.1080/01932690903196144>
- Ariffin, T.S.T., Yahya, E., Husin, H., 2016. The rheology of light crude oil and water-in-oil-emulsion. *Procedia Eng.* 148, 1149–1155. <https://doi.org/10.1016/j.proeng.2016.06.614>
- Bellalta, P., Troncoso, E., Zúñiga, R.N., Aguilera, J.M., 2012. Rheological and microstructural characterization of WPI-stabilized O/W emulsions exhibiting time-dependent flow behavior. *LWT - Food Sci. Technol.* 46, 375–381. <https://doi.org/10.1016/j.lwt.2011.12.017>
- Benslimane, A., 2013. Rhéologie et écoulement de fluides chargés : application aux réseaux d'assainissement urbains : étude expérimentale et modélisation. Thèse. Université de Strasbourg.
- Benslimane, A., Bekkour, K., François, P., 2013. Effect of addition of carboxymethyl cellulose (CMC) on the rheology and flow properties of bentonite suspensions. *Appl. Rheol.* 23, 1–10. <https://doi.org/10.3933/ApplRheol-23-13475>
- Benslimane, A., Bekkour, K., François, P., Bechir, H., 2016. Laminar and turbulent pipe flow of bentonite suspensions. *J. Pet. Sci. Eng.* 139, 85–93. <https://doi.org/10.1016/j.petrol.2015.12.020>
- Chen, J., Vogel, R., Werner, S., Heinrich, G., Clause, D., Dutschk, V., 2011. Influence of the particle type on the rheological behavior of Pickering emulsions. *Colloids Surfaces A Physicochem. Eng. Asp.* 382, 238–245. <https://doi.org/10.1016/j.colsurfa.2011.02.003>
- Chevalier, Y., Bolzinger, M.-A., 2013. Emulsions stabilized with solid nanoparticles:

- Pickering emulsions. *Colloids Surfaces A Physicochem. Eng. Asp.* 439, 23–34.  
<https://doi.org/10.1016/J.COLSURFA.2013.02.054>
- Dai, L., Sun, C., Wei, Y., Mao, L., Gao, Y., 2018. Characterization of Pickering emulsion gels stabilized by zein/gum arabic complex colloidal nanoparticles. *Food Hydrocoll.* 74, 239–248. <https://doi.org/10.1016/j.foodhyd.2017.07.040>
- Derkach, S.R., 2009. Rheology of emulsions. *Adv. Colloid Interface Sci.* 151, 1–23.  
<https://doi.org/10.1016/J.CIS.2009.07.001>
- Escudier, M.P., Poole, R.J., Presti, F., Dales, C., Nouar, C., Desaubry, C., Graham, L., Pullum, L., 2005. Observations of asymmetrical flow behaviour in transitional pipe flow of yield-stress and other shear-thinning liquids. *J. Nonnewton. Fluid Mech.* 127, 143–155. <https://doi.org/10.1016/J.JNNFM.2005.02.006>
- Esmael, A., Nouar, C., 2008. Transitional flow of a yield-stress fluid in a pipe: Evidence of a robust coherent structure. *Phys. Rev. E - Stat. Nonlinear, Soft Matter Phys.* 77, 2–5.  
<https://doi.org/10.1103/PhysRevE.77.057302>
- Esmael, A., Nouar, C., Lefèvre, A., Kabouya, N., 2010. Transitional flow of a non-Newtonian fluid in a pipe: Experimental evidence of weak turbulence induced by shear-thinning behavior. *Phys. Fluids* 22, 1–5. <https://doi.org/10.1063/1.3491511>
- Founargiotakis, K., Kelessidis, V.C., Maglione, R., 2008. Laminar, transitional and turbulent flow of Herschel-Bulkley fluids in concentric annulus. *Can. J. Chem. Eng.* 86, 676–683.  
<https://doi.org/10.1002/cjce.20074>
- Guillot, S., Bergaya, F., de Azevedo, C., Warmont, F., Tranchant, J.F., 2009. Internally structured pickering emulsions stabilized by clay mineral particles. *J. Colloid Interface Sci.* 333, 563–569. <https://doi.org/10.1016/j.jcis.2009.01.026>
- Kelessidis, V.C., Dalamarinis, P., Maglione, R., 2011. Experimental study and predictions of pressure losses of fluids modeled as Herschel–Bulkley in concentric and eccentric annuli in laminar, transitional and turbulent flows. *J. Pet. Sci. Eng.* 77, 305–312.  
<https://doi.org/10.1016/J.PETROL.2011.04.004>
- Lim, J.S., Wong, S.F., Law, M.C., Samyudia, Y., Dol, S.S., 2015. A Review on the Effects of Emulsions on Flow Behaviours and Common Factors Affecting the Stability of Emulsions. *J. Appl. Sci.* <https://doi.org/10.3923/jas.2015.167.172>

- Malin, M.R., 1998. Turbulent pipe flow of Herschel-Bulkley fluids. *Int. Commun. Heat Mass Transf.* 25, 321–330. [https://doi.org/10.1016/S0735-1933\(98\)00019-0](https://doi.org/10.1016/S0735-1933(98)00019-0)
- Malkin, A.Y., Mironova, M. V., Ilyin, S.O., 2017. Flow of heavy crude oil-in-water emulsions in long capillaries simulating pipelines. *J. Pet. Sci. Eng.* 157, 117–123. <https://doi.org/10.1016/j.petrol.2017.07.024>
- McDonald, J.A., Buller, D.C., 1992. The significance of formation damage caused by the adsorption oil-based mud surfactant. *J. Pet. Sci. Eng.* [https://doi.org/10.1016/0920-4105\(92\)90062-6](https://doi.org/10.1016/0920-4105(92)90062-6)
- Menezes, J., Yan, J., Sharma, M.M., 1989. The Mechanism of Wettability Alteration Due to Surfactants in Oil-Based Muds. *Soc. Pet. Eng. SPE* 18460, 17–29.
- Morishita, C., Kawaguchi, M., 2009. Rheological and interfacial properties of Pickering emulsions prepared by fumed silica suspensions pre-adsorbed poly(N-isopropylacrylamide). *Colloids Surfaces A Physicochem. Eng. Asp.* 335, 138–143. <https://doi.org/10.1016/j.colsurfa.2008.10.048>
- Munoz, Jose C, Leong Yeow, Y., Munoz, J C, Leong, Y.Y., 1996. Applications of maximum entropy method in capillary viscometry. *Rheol Acta* 35, 76–82.
- Peixinho, J., Nouar, C., Desaubry, C., Théron, B., 2005. Laminar transitional and turbulent flow of yield stress fluid in a pipe. *J. Nonnewton. Fluid Mech.* 128, 172–184. <https://doi.org/10.1016/J.JNNFM.2005.03.008>
- Plasencia, J., Pettersen, B., Nydal, O.J., 2013. Pipe flow of water-in-crude oil emulsions: Effective viscosity, inversion point and droplet size distribution. *J. Pet. Sci. Eng.* 101, 35–43. <https://doi.org/10.1016/J.PETROL.2012.11.009>
- Podryabinkin, E., Rudyak, V., Gavrilov, A., May, R., 2013. Detailed Modeling of Drilling Fluid Flow in a Wellbore Annulus While Drilling Distributed Sensors View project Tip-clearance cavitation and development of the means for its suppression: experimental and numerical modeling View project. *Can. ENERGY Technol. Innov.* 1, 27–36. <https://doi.org/10.1115/OMAE2013-11031>
- Quintero, L., 2002. An Overview of Surfactant Applications in Drilling Fluids for the Petroleum Industry. *J. Dispers. Sci. Technol.* 23, 1–3. <https://doi.org/10.1080/01932690208984212>

- Sanner, D.O., Petroleum, P., Norway, C., Azar, J.J., 1994. Alteration of Reservoir Rock Wettability and Its Flow Properties Caused by Oil-Based and Water-Based Drilling Muds. SPE Int. Symp. 7–10.
- Schramm, L.L., 2000. Surfactants: Fundamentals and Applications in the petroleum industry, Cambridge. ed.
- Sharma, M.M., Wunderlich, R.W., 1987. The alteration of rock properties due to interactions with drilling-fluid components. *J. Pet. Sci. Eng.* 1, 127–143.  
[https://doi.org/10.1016/0920-4105\(87\)90004-0](https://doi.org/10.1016/0920-4105(87)90004-0)
- Sugita, N., Nomura, S., Kawaguchi, M., 2008. Rheological and interfacial properties of silicone oil emulsions prepared by polymer pre-adsorbed onto silica particles. *Colloids Surfaces A Physicochem. Eng. Asp.* 328, 114–122.  
<https://doi.org/10.1016/j.colsurfa.2008.06.044>
- Tang, J., Quinlan, P.J., Tam, K.C., 2015. Stimuli-responsive Pickering emulsions: Recent advances and potential applications. *Soft Matter*. <https://doi.org/10.1039/c5sm00247h>
- Thienne, J., Abend, S., Lagaly, G., 1999. Aggregation in Pickering emulsions. *Colloid Polym. Sci.* 260, 257–260.
- Tong, Z., Morrow, N.R., 2006. Variations in wetting behavior of mixed-wet cores resulting from probe oil solvency and exposure to synthetic oil-based mud emulsifiers. *J. Pet. Sci. Eng.* 52, 149–160. <https://doi.org/10.1016/j.petrol.2006.03.006>
- Wang, D., Butler, R., Zhang, J., 2012. Wettability Survey in Bakken Shale Using Surfactant Formulation Imbibition. Eighteenth SPE Improv. Oil Recover. Symp. 1–13.  
<https://doi.org/10.2118/153853-PA>
- Wong, S.F., Dol, S.S., Wee, S.K., Chua, H.B., 2018. Miri light crude water-in-oil emulsions characterization – Rheological behaviour, stability and amount of emulsions formed. *J. Pet. Sci. Eng.* 165, 58–66. <https://doi.org/10.1016/j.petrol.2018.02.013>
- Wong, S.F., Lim, J.S., Dol, S.S., 2015. Crude oil emulsion: A review on formation, classification and stability of water-in-oil emulsions. *J. Pet. Sci. Eng.* 135, 498–504.  
<https://doi.org/10.1016/j.petrol.2015.10.006>
- Xiao, J., Wang, X., Perez Gonzalez, A.J., Huang, Q., 2016. Kafirin nanoparticles-stabilized Pickering emulsions: Microstructure and rheological behavior. *Food Hydrocoll.* 54, 30–

39. <https://doi.org/10.1016/j.foodhyd.2015.09.008>

Yan, H., Chen, X., Song, H., Li, J., Feng, Y., Shi, Z., Wang, X., Lin, Q., 2017. Synthesis of bacterial cellulose and bacterial cellulose nanocrystals for their applications in the stabilization of olive oil pickering emulsion. *Food Hydrocoll.* 72, 127–135.

<https://doi.org/10.1016/j.foodhyd.2017.05.044>

Yan, J.N., Menezes, J.L., Sharma, M.M., 1993. Wettability Alteration Caused by Oil-Based Muds and Mud Components. *SPE Drill. Complet.* 35–44.

Zhuang, G., Zhang, Z., Peng, S., Gao, J., Jaber, M., 2018. Enhancing the rheological properties and thermal stability of oil-based drilling fluids by synergetic use of organo-montmorillonite and organo-sepiolite. *Appl. Clay Sci.* 161, 505–512.

<https://doi.org/10.1016/J.CLAY.2018.05.018>



**CHAPTER 5.**  
**FLOW BEHAVIOR OF**  
**CONCENTRATED ORGANO-**  
**HECTORITE BASED**  
**EMULSIONS**



**TABLE OF CONTENTS**

5.1	Introduction.....	157
5.2	Literature review .....	157
5.3	Experimental Protocol.....	161
5.3.1	Emulsification process.....	161
5.3.2	Homogenization process.....	164
5.3.3	Verification of oil/water fractions.....	166
5.4	Flow behavior of concentrated Pickering emulsions.....	168
5.4.1	Stable emulsion.....	170
5.4.2	Unstable emulsion.....	173
5.4.2.1	Static instability.....	173
5.4.2.2	Dynamic instability.....	175
5.4.2.3	Visual observation.....	178
5.5	Attenuation measurements.....	179
5.6	Summary to chapter.....	181
5.7	References.....	182

## 5.1 Introduction

The aim of this chapter is to study the behavior of OHT stabilized emulsions with water concentrations superior to 50 wt%. To do so, the flow behavior of emulsions with high water fractions, i.e., concentrated emulsions, is presented and discussed in the following sections. As it was mentioned in the previous chapter, the emulsions show an instable behavior at around 60 wt% of water concentration, from which rheological measurements become not possible.

In the first part of the current chapter, the flow behavior of each concentration will be presented and their stability conditions will be identified. The purpose of this section is to discuss the rheological behavior of the emulsions and to compare it with the results from the previous chapter.

Second, the instability domain will be identified, presented, and discussed as an attempt to understand its causes and the structural phenomena responsible for this behavior.

## 5.2 Literature review

Looking at the current interest in Pickering emulsions, many recent works can be found in the literature (Geng et al., 2019; Bizmark et al., 2020; Feng et al., 2020; Jiang et al., 2020; Li et al., 2020). Most of this research discuss topics related to:

- i. Preparation and surface modification of the solid particles used to stabilize Pickering emulsions (Pandey et al., 2018; Maaref et al., 2019).
- ii. The influence of surface modifiers on the prepared emulsion (Kaptay, 2006; Hu et al., 2015; Zhang et al., 2015).
- iii. Emulsion stability and its droplet size (Derakhshandeh et al., 2018; Yang et al., 2020).
- iv. The influence of solid content on the properties of Pickering emulsions (Frelichowska et al., 2010; Jahandideh et al., 2018).
- v. The influence of experimental conditions and preparation protocol (PH, temperature, etc.) on droplets coalescence (Sharma et al., 2015; Araiza-Calahorra and Sarkar, 2019; Geng et al., 2019).

Wei et al. (2019) studied the influence of the surface modification as well as the concentration, in the continuous phase, of the solid particles on the stability of Pickering emulsions. First, it

was shown that a minimum of 3 wt%, in the continuous phase, of unmodified silica is necessary to stabilize the emulsion (Fig. 5.1).

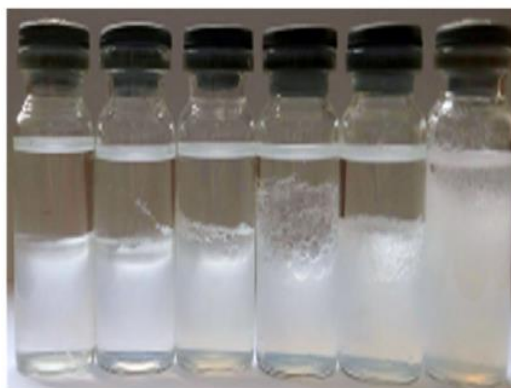


Fig. 5.1 Oil in water emulsion stabilized by nano silica. From left to right:  $[\text{SiO}_2] = 0.05 \text{ wt\%}$ ,  $0.1 \text{ wt\%}$ ,  $0.5 \text{ wt\%}$ ,  $1 \text{ wt\%}$ ,  $2 \text{ wt\%}$ , and  $3 \text{ wt\%}$ , respectively (Wei et al., 2019).

Second, and in the case of modified silica, it was found that the type of surfactants and their surface distribution have a major influence on the droplet size, and therefore on the emulsion stability (Fig. 5.2). It should be mentioned that the critical surfactant concentration noticed in Fig. 5.2 depends on multiple variables such as the nature of the solid particles, the type of the surfactants, and the length of its alkyl chains. Therefore, a generalized rule does not yet exist, and each solid-surfactant couple must be studied individually.

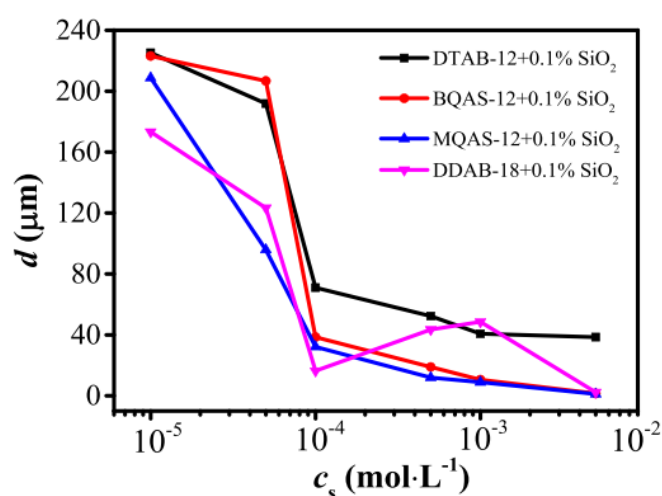


Fig. 5.2 Droplet size as a function of the concentration of surface modifiers (Wei et al., 2019).

Furthermore, unlike classic emulsions, phase inversion phenomenon is not systematic in Pickering emulsions. Its presence is governed by the type of surfactants used in the solid surface modification especially the length of its the alkyl chains. Moreover, it was shown that an irreversible adsorption of the solid particles on the oil/water interface is possible in some cases at high emulsification energy.

Dong et al. (2014) showed that the point of phase inversion in modified montmorillonite clay stabilized Pickering emulsions is controlled by the concentration of the surfactant on clay surfaces as well as the fraction of the dispersed phase. For instance, the fraction at which a phase inversion was noticed increased from 0.35 to 0.75 by increasing the hydrophobicity of the modified clay particles.

This result is in a good agreement with those of Kaptay (2006), where the phase inversion phenomena, termed “catastrophic phase inversion”, was related to:

- i. The change in the disperse phase fraction.
- ii. The change in the particle concentration
- iii. The change in the contact angle of the solid particles.

Another interesting phenomenon, related to Pickering emulsions, that was reported in literature is oil (or water) *spill*. In the latter, a volume of the dispersed phase is spilled (separated) after rest under certain conditions, especially at high temperatures (Yang et al., 2020).

The type of the emulsion is mainly controlled by the wettability and the contact angle of the solid stabilizers, which in turn is related to the type and surface concentration of the surface modifier. To prepare a water in oil emulsion, a contact angle superior to  $90^\circ$  is necessary (Briggs et al., 2018).

Moreover, the influence of solid stabilizers concentration in the continuous phase as well as the dispersed phase volume was detailed in the study of Yang et al. (2020), where particles concentration was found to be inversely proportional to the droplet size, and the dispersed phase concentration was found to be proportional to the droplet size (Fig. 5.3). The reason may be that a certain concentration of solid particles can only be adsorbed on a limited oil/water interface, this is why droplets size increases with the dispersed phase volume and decreases with the increase of the solid particles' concentration.

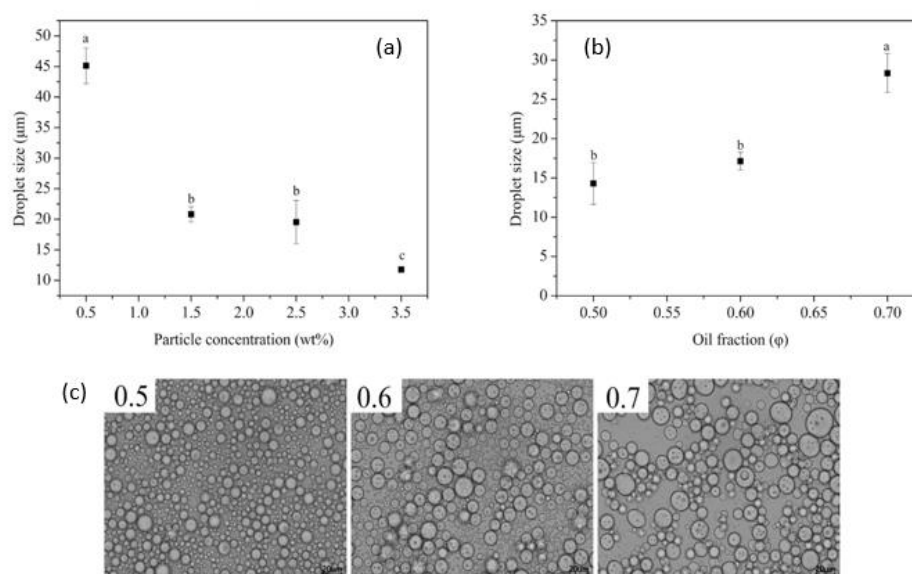


Fig. 5.3 Droplet size as a function of the particle concentration, at a fixed dispersed phase concentration after 20 days of rest (a). Droplet size as a function of the dispersed phase concentration at a fixed solid particle concentration after 20 days of rest (b). Optical microscopy images of freshly prepared Pickering emulsions at different fractions of the dispersed phase ( $\phi = 0.5\text{--}0.7$ ) (Yang et al., 2020).

During the present literature review, it became apparent that most of the recent studies are focusing on the static stability of Pickering emulsions (droplet size, microscopy, etc.) and their preparation protocol. The dynamic stability, on the other hand, was much less studied, and mostly focusing on the rheological behavior of Pickering emulsions (Xiao et al., 2016; Griffith and Daigle, 2018; Zhang et al., 2019). One of the rare papers discussing the flow behavior of Pickering emulsions is that of Griffith and Daigle (2020), where the stability of Pickering emulsions under different flow conditions was studied. It is worth mentioning that the latter is a small-scaled study where the internal diameter of the testing tube is 0,75 mm.

In the following, the experimental data registered during the preparation and the flow of concentrated Pickering emulsions will be shared and detailed. An attempt to understand the instabilities as well as the microstructure of the emulsions at water concentrations superior to 50 wt% will be as well presented.

### 5.3 Experimental Protocol

Water-in-gasoil Pickering emulsions were prepared using the same protocol as in chapter 4. The emulsification system (Fig. 2.4) and the preparation protocol are detailed in chapter 2. Five different gasoil/water ratios are studied in this chapter: 40/60 (B3-60H<sub>2</sub>O), 35/65 (B3-65H<sub>2</sub>O), 30/70 (B3-70H<sub>2</sub>O), 25/75 (B3-75H<sub>2</sub>O), and 20/80 (B3-80H<sub>2</sub>O).

The flow behavior of the emulsions was studied using an Ultrasound Pulsed Doppler Velocimeter (Fig. 2.4-6) for velocity measurements and pressure sensors (Fig. 2.4 -5) for linear pressure loss measurements. More details on the particle velocity calculation were presented in chapter 4.

It should be mentioned that the acoustic attenuation of the medium increases with water concentration. The velocity profile measurements were possible until 60 wt% of water concentration, above which the high energy loss of sound propagation obliged us to bring the sensor very close to the wall. As a result, it was not possible to measure the first points of the velocity profile, and because of the high acoustic attenuation, it was as well experimentally impossible to measure the second half of the velocity profile. This is why, the only possible and correct measurement, using our experimental set, was the velocity at the pipe center, or in other words the maximum velocity, that will be presented in the following sections.

To investigate the type of the emulsion at water concentrations superior to 50 wt%, and to study whether the reason behind the noticed instabilities is phase inversion, some visual experiments were performed. A small volume of each emulsion was diluted in both water and silicone oil. If the emulsion is water-in-oil, it is miscible with silicone oil and immiscible with water, and vice versa.

#### 5.3.1 Emulsification process

All the emulsions were prepared through an in-line continuous circulation at the maximum flow rate delivered by our volumetric pump and using two different diaphragms at the end of the flow loop. The velocity at the pipe center as well as the linear pressure loss were recorded and are presented in Fig. 5.5.

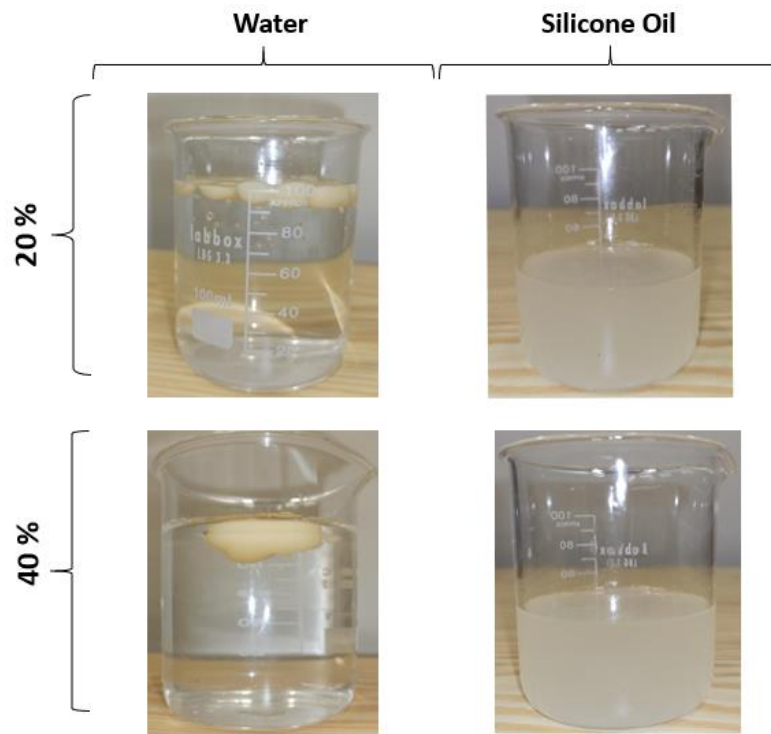


Fig. 5.4 B3-20H2O and B3-40H2O emulsions dispersed in both water (left-hand side) and silicone oil (right-hand side).

Fig. 5.5 shows the evolution of the maximum velocity, the wall shear stress, and the ratio of the maximum velocity to the mean velocity ( $U_{max}/U$ ), as a function of time, during the emulsification process for the B3-70H2O emulsion. Overall, the evolution of the flow parameters during the emulsification looks not very different from that of the B3-50H2O emulsion (Fig.4.11). The emulsification time, on the other hand, is longer in the case of B3-70H2O and its oscillations' amplitudes are higher.

The oscillation of the flow parameters at the beginning of the emulsification process can be explained by the passage of two different fluids (Fig 5.6-b):

- i. A complex fluid that induces high linear pressure losses and therefore high wall shear stress values. This fluid can be nothing but the emulsion from the precedent concentration that adheres to the pipe walls. Furthermore, the low maximum velocity peaks can be explained by the yielding behavior of the emulsions, as yielding fluids exhibit lower maximum velocity than Newtonian fluids, at the same mean velocity (flat velocity profile around the pipe center).

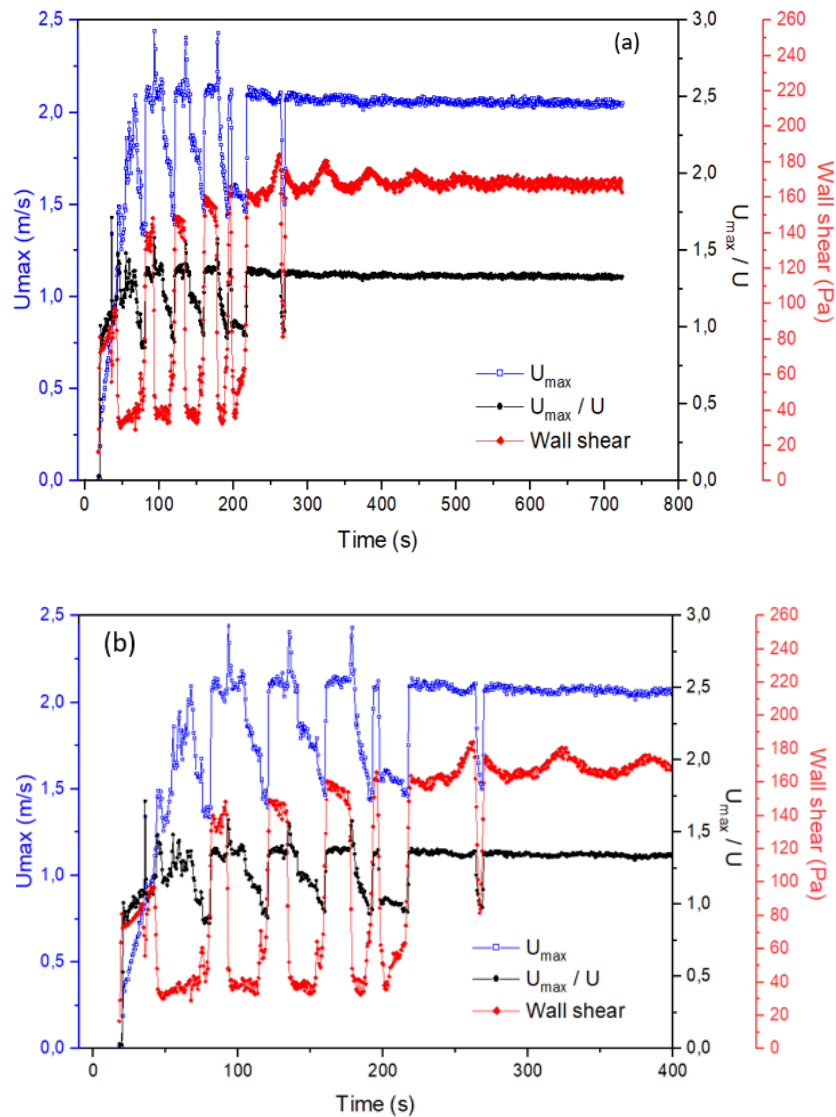


Fig. 5.5 Flow parameters as a function of time during the emulsification process of the B3-70H2O emulsion (a). Zoom in of the beginning of the emulsification process (b).

- ii. A Newtonian fluid, probably water, that can be easily identified using the  $U_{max}/U$  ratio. As it can be noticed in the figure, at high maximum velocity peaks and low shear stress peaks, the ratio  $U_{max}/U = 1$ , which indicates the passage of a Newtonian fluid (water plugs).

The circulation continuous for 20 min until reaching the equilibrium of the measured values. It can be noticed that, at the end of the emulsification process, the ratio  $U_{max}/U$  is near in value to that of the previous emulsion, found at the beginning of the emulsification. This means that

the rheological behavior of the freshly prepared emulsions is similar to that of the previous emulsion.

The same emulsification process was conducted on all the studied emulsions. It was possible to prepare stable emulsions (at least during continuous circulation) until reaching the 20/80 oil to water mass ration, at which stabilizing the emulsion was no more possible. Fig. 5.6 shows a photo of the B3-80H<sub>2</sub>O after 2 H of continuous circulation where it can be noticed that the added water could not be dispersed into the B3-75H<sub>2</sub>O emulsion. Two fluids can be noticed at this concentration:

- i. A stable flocculated emulsion.
- ii. A free water phase.

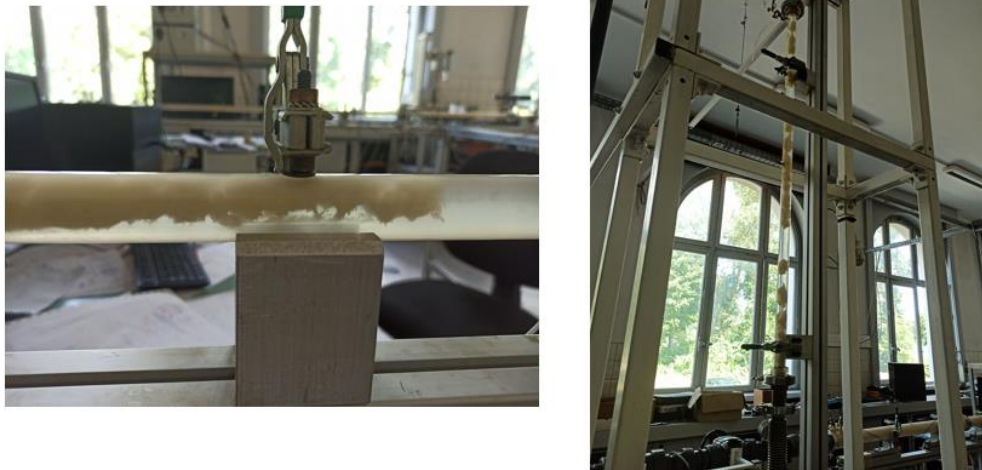


Fig. 5.6. B3-80H<sub>2</sub>O after 2 H of continuous circulation.

### 5.3.2 Homogenization process

After 24 H of rest, a homogenization process was always proceeded before the measuring sequence (Fig. 4.10-3). The aim of this process is to homogenize the emulsion and to ensure that the measurements are proceeded on an equilibrated and stable fluid.

Fig. 5.7 shows the temporal evolution of the flow parameters during the homogenization process for a B3-70H<sub>2</sub>O emulsion, after 24 H of rest, at a mean velocity of  $U = 1,50 \text{ m} \cdot \text{s}^{-1}$ .

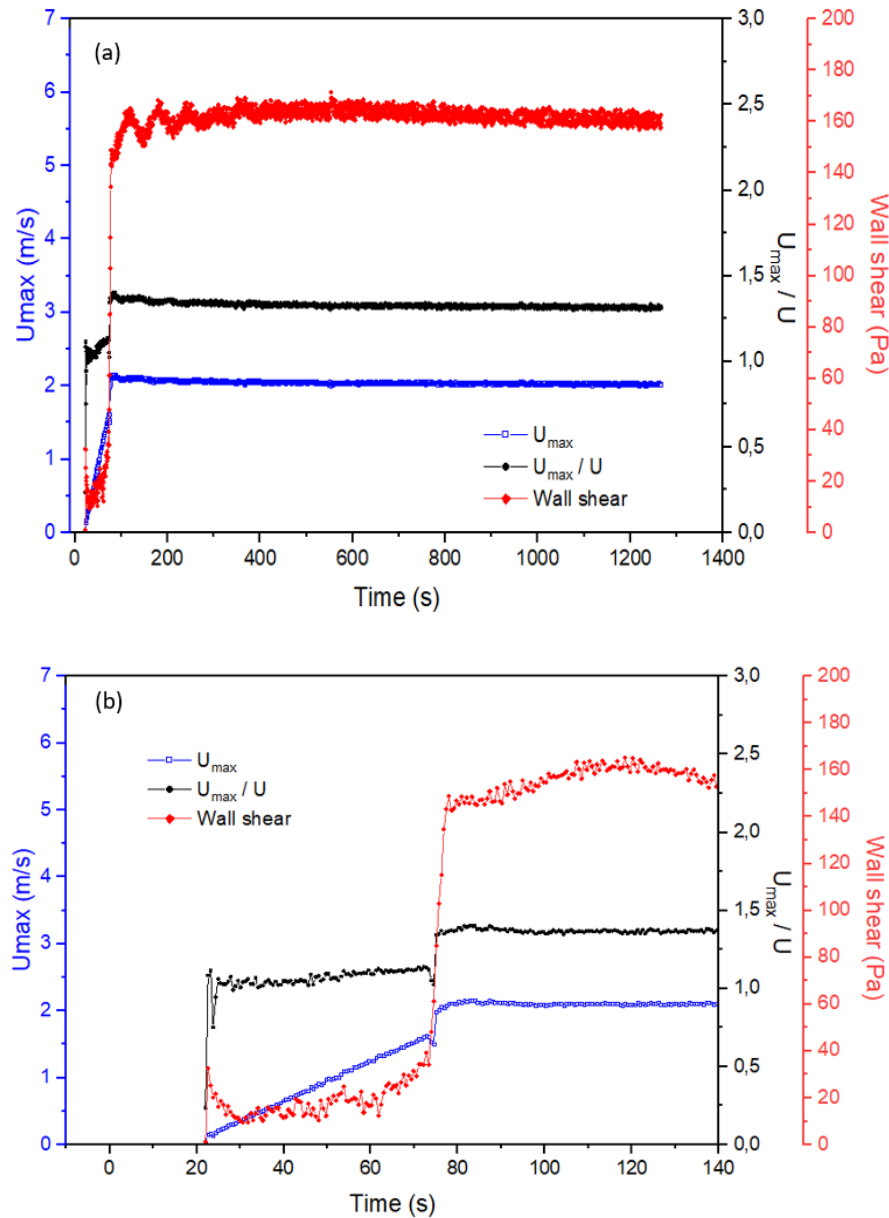


Fig. 5.7. Flow parameters after 24 H of rest of a B3-70H<sub>2</sub>O emulsion.

As it can be noticed from the figure, the emulsion exhibits two distinct behaviors during the homogenization:

- i. At the beginning of the flow (Fig. 5.7-b), a shear stress peak is noticed, followed by a gradual decrease of the wall shear stress value for about 10 s. After that, the wall shear stress value stays very low for 30 s, then it gradually increases for 10 s. Finally, a shear stress peak is noticed after about 60 s of continuous circulation.

The maximum velocity to the mean velocity ratio,  $U_{max}/U$ , on the other hand, is in a good coherence with wall shear stress values. First, at very low shear stress values,

$U_{max}/U = 1$  which is an indicator to the flow of a Newtonian fluid (water in our case). Then, the ratio slightly increases when the wall shear stress value increases, which may correspond to the beginning of the homogenization of the circulating fluid.

The maximum velocity shows a gradual increase during this phase until the peak after about 60 s of circulation. The incoherence between wall shear stress values and maximum velocity values shows that two different behaviors took place at the beginning of the circulation: a non-stable fluid at the pipe wall and a more stable fluid at the pipe center. More details on this instability will be presented in section (5.5.2).

- ii. After 60 s of continuous circulation (Fig. 5.7-a), a sudden increase in the wall shear stress as well as in the maximum velocity values is noticed, followed by homogenization curves like those of B3-50H20 (Fig. 4.13). The corresponding  $U_{max}/U$  curve decreases slightly at the beginning of this phase until reaching a constant value of  $U_{max}/U = 1,3$ .

### 5.3.3 Verification of oil/water fractions

Measuring the sound velocity was performed using the same UPDV transducer used to measure the local velocities in the flow loop. Knowing the sound velocity in water at a given temperature, a sample of tap water was used to measure the distance between the transducer and the bottom of the container. The propagation time of acoustic waves in the different emulsions is measured and its corresponding sound velocity is then calculated.

The aims of these measurements are:

- i. Correcting the measured velocities in the flow loop using the following equation:

$$u = u^* * \frac{c_e}{c_w} \quad 5.1$$

where  $u$  is the corrected velocity,  $u^*$  is the measured velocity,  $c_e$  is the sound velocity in the studied emulsion, and  $c_w$  is the sound velocity used to measure  $u^*$ .

- ii. Verifying the homogeneity and the water/gasoil ratios of the emulsions.

The theoretical sound velocity,  $c$ , on the other hand, is calculated using the following expression:

$$c = \left(\frac{\chi}{\rho}\right)^{1/2} \quad 5.2$$

where  $\chi$  is the module of compressibility and  $\rho$  is the density of the medium.

In the case of a two-phase emulsion, the compressibility module can be theoretically calculated using the following equation:

$$\chi = \frac{\frac{\delta_s}{1-\delta_s} \frac{1}{\rho_w} + \frac{1}{\rho_o}}{\frac{\delta_s}{1-\delta_s} \frac{1}{\rho_w \chi_w} + \frac{1}{\rho_o \chi_o}} \quad 5.3$$

where  $\delta_s$  is the mass fraction of the emulsion,  $\rho_w$  is the density of the aqueous phase,  $\rho_o$  is the density of the organic phase,  $\chi_w$  is the theoretical compressibility model of the aqueous phase at a given temperature and  $\chi_o$  is the theoretical compressibility model of the organic phase at a given temperature.

Sound velocity depends on the composition of the traversed medium. Using this definition, it is possible to verify the homogeneity and the composition of an emulsion. In a homogenous medium, the measured sound velocity is equal to its theoretical value.

To verify the homogeneity of the emulsions, theoretical sound velocity was plotted as a function of the measured sound velocity, for each concentration, in Fig. 5.8. The data can be fitted using the x graph.

Taking into consideration experimental errors, the measured sound velocity is overall equal to its theoretical value. It can be noticed from Eq. 5.2. and Eq. 5.3. that the mass fraction of the emulsion as well as the densities of gasoil and water were used to calculate the theoretical sound velocity. The results of these equations can thus verify the water/gasoil ratio, the homogeneity, and the preparation protocol of the emulsions. The homogeneity of the emulsions is an indicator of their stability between their preparation date the sound velocity measurement date (about 2 months).

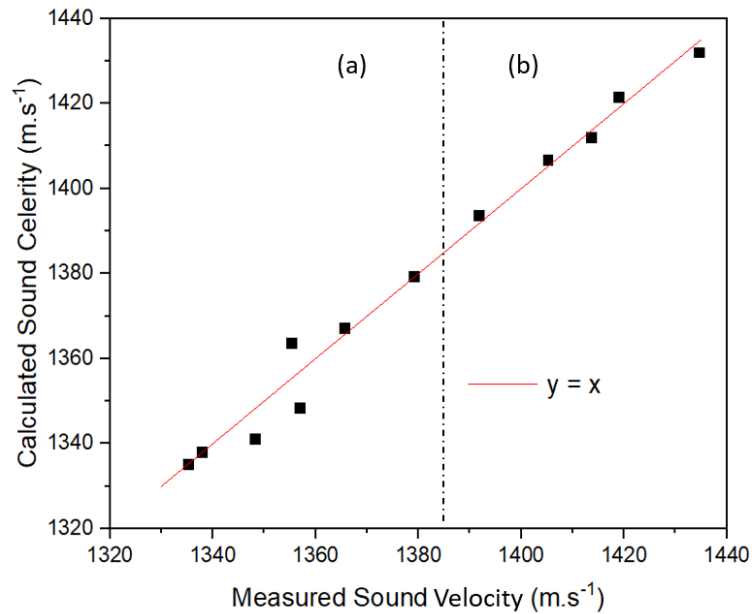


Fig. 5.8. Theoretical sound velocity as a function of the measured sound velocity. (a):  $[H_2O] \leq 50 \text{ wt\%}$ . (b):  $[H_2O] > 50 \text{ wt\%}$ .

#### 5.4 Flow behavior of concentrated Pickering emulsions

Velocity and local pressure measurements were performed after the homogenization process, in respect to the chronological sequence illustrated in Fig. 4.10-4.

Unlike emulsions with water concentration inferior to 50 wt%, where the fluid was found to be stable during the measuring process for all concentrations and under different conditions (Fig. 4.18), different behaviors were noticed for emulsions with water concentrations superior to 50 wt%:

- i. Stable emulsions: where the flow parameters i.e., local velocity and pressure, were found to be stable during a continuous circulation.
- ii. Partially stable emulsions: where both stable and unstable emulsions were noticed at certain velocity and flow time conditions.
- iii. Unstable emulsions: where the emulsion was found to be inhomogeneous during the flow measurements.

Fig. 5.9 represents the evolution of the wall shear stress as a function of the mean velocity corresponding to the B3-60H<sub>2</sub>O (a) and the B3-65H<sub>2</sub>O (b) emulsions. As it can be noticed from

the figure, the measurements were performed during an increasing velocity ramp (red symbols) followed by a constant plateau (empty symbols), then a decreasing velocity ramp (blue symbols).

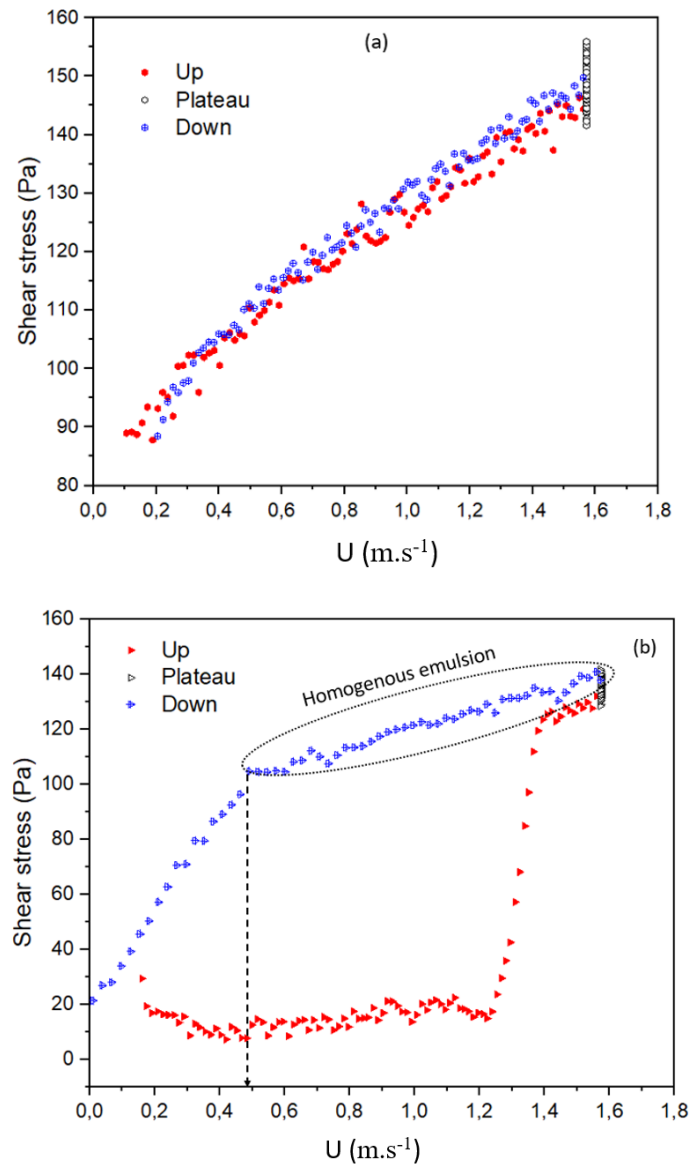


Fig. 5.9. Experimental wall shear stress as a function of mean velocity at increasing and decreasing velocity ramps for the emulsions: B3-60H2O (a) and B3-65H2O (b).

First, for the B3-60H2O, no hysteresis was noticed between the increasing and the decreasing wall shear stress curves. They overlap on the total range of the applied flow rates, which may indicate the stability as well as the homogeneity of the emulsion during the measurements.

Furthermore, it should be recalled that the rheological measurements were not possible for the B3-60H<sub>2</sub>O emulsion because of its instability under the rheometer geometry (Fig. 4.9). This result may be due to two reasons:

- i. The resulting shear rates during the rheological measurements were not sufficient to maintain the emulsion stable, compared to the high shear rates induced by the two diaphragms at the end of the flow loop.
- ii. The scale difference between the rheological measurements (1 to 2 ml) and the flow loop (70 L) may as well influence on the results as a small sampling error may falsify the rheological measurements.

Second, for the B3-65H<sub>2</sub>O emulsion, an important hysteresis was noticed between the increasing and the decreasing velocity ramps. Different behaviors were as well identified.

- During the increasing velocity ramp:
  - i. A close to zero wall shear stress plateau at the beginning of the flow and at velocities inferior to  $U = 1,2 \text{ m} \cdot \text{s}^{-1}$  which may be an indicator to wall slipping.
  - ii. A sudden jump in the shear stress value at a critical velocity followed by a wall shear stress curve like that of stable emulsions.
- During the decreasing velocity ramp:
  - i. A flow curve like that of a homogenous fluid for velocities superior to  $U = 0,5 \text{ m} \cdot \text{s}^{-1}$ .
  - ii. A sudden decrease of the fluid viscosity indicating a change in the emulsion structure.

In the following, the flow measurements of both stable and unstable emulsions will be presented and analyzed to understand the structural behavior of concentrated inverse Pickering emulsions.

### 5.4.1 Stable emulsion

It is particularly important to identify the stability domain of each studied emulsion to analyze its rheological behavior. A stability domain is the conditions under which the emulsion is homogenous, and the flow measurements are representative of the overall rheological behavior of the fluid. Moreover, it should be noticed that in the current chapter, we are studying the

dynamic stability of the emulsions under the conditions of the experimental set presented in chapter 2.

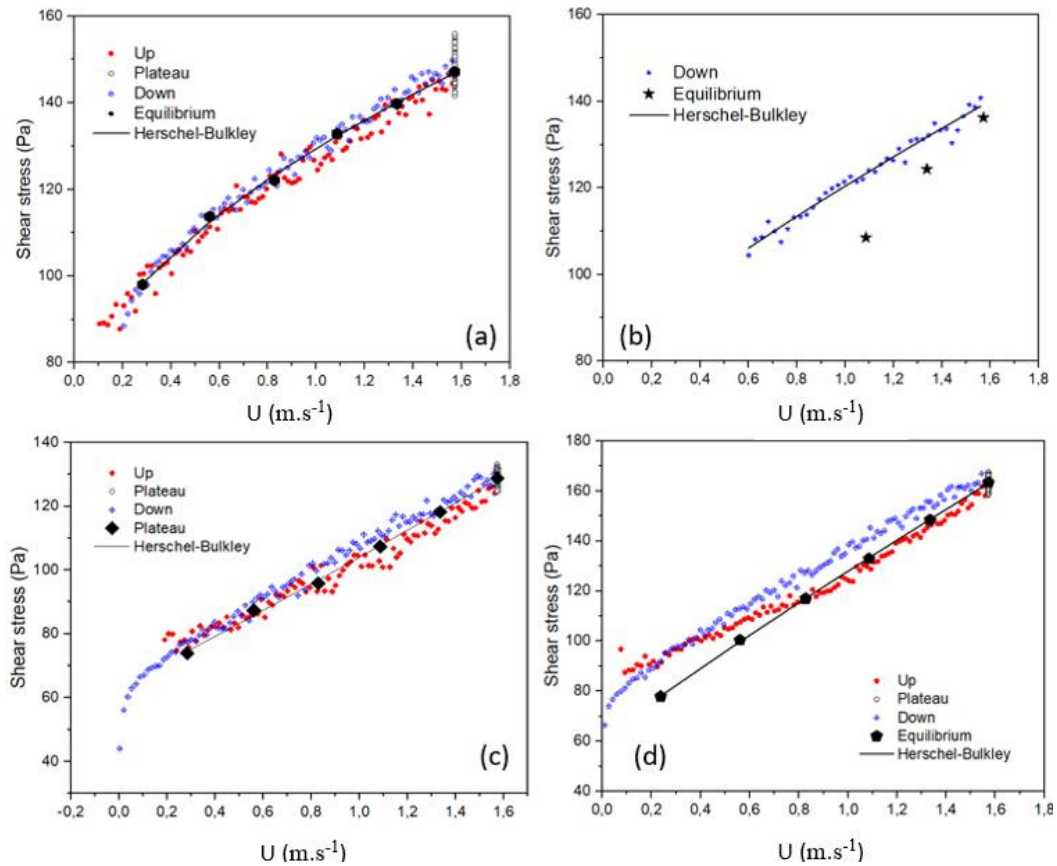


Fig. 5.10. Wall shear stress as a function of the mean velocity for the concentrations: B3-60H<sub>2</sub>O (a), B3-65H<sub>2</sub>O (b), B3-70H<sub>2</sub>O (c), and B3-75H<sub>2</sub>O (d).

Fig. 5.10 shows the wall shear stress evolution as a function of the applied mean velocity for the different studied emulsions. The results of the continuous velocity ramps are plotted in red symbols for the increasing ramp, in blue symbols for the decreasing ramp, and in empty symbols for the velocity plateau. Equilibrium shear stress values correspond to the mean wall shear stress during constant velocity plateaus and are represented in Fig. 5.10 in black full symbols. In addition to that, the Herschel-Bulkley model was used to correlate the experimental flow curves, in solid lines. The corresponding parameters of the model are listed in Table 5.1.

As it can be noticed from Fig. 5.10, the flow curves during the increasing and the decreasing velocity ramps overlap for all emulsions, except for the B3-65H<sub>2</sub>O, which indicates that the B3-

60H2O, the B3-70H2O, and the B3-75H2O emulsions were successfully homogenized before the measurements were taken. The emulsions exhibit the same rheological behavior noticed in the case of water concentrations inferior to 50 wt%.

<b>Concentration</b>	<b>n [-]</b>	<b>K [Pa.s<sup>n</sup>]</b>	<b><math>\sigma_y</math> [Pa]</b>	<b>R2</b>
<b>B3-60H2O</b>	0,54	63,38	66,12	0,99
<b>B3-65H2O</b>	0,81	41,94	78,50	0,97
<b>B3-70H2O</b>	1,05	40,15	63,91	0,99
<b>B3-75H2O</b>	0,92	68,00	59,97	0,99

Table 5.1. Rheological parameters of the Herschel-Bulckley model.

Furthermore, the equilibrium wall shear stress values are in a good agreement with the ramp values, especially for the B3-60H2O where the equilibrium and the ramp shear stress values overlap. For the B3-70H2O and the B3-75H2O emulsions, the equilibrium values at low velocities slightly deviate from the continuous ramp curves. This can be explained by the fact that equilibrium measurements (Fig. 4.10-4) were performed before the continuous ramp measurements (Fig. 4.10-5). Thus, a longer circulation time is necessary to homogenize the emulsions.

The B3-65H2O emulsion, on the other hand, exhibited a quite different behavior. It was impossible to obtain a stable and homogenous emulsion during the increasing velocity ramp, even at high flow rates and long circulation times. It was however possible to identify a small velocity interval during which the emulsion was homogenous (blue symbols in Fig. 5.10-b).

Fig. 5.11 shows the evolution of yield stress as a function of water mass concentration. It can be observed that the B3-60H2O emulsion follows the same exponential trend exhibited by emulsions with water concentrations inferior to 50 wt%. In addition, a yield stress peak is noticed at B3-65H2O, followed by a sudden decline at higher concentrations. This shows that a major structural change takes place at the 65 wt% concentration, and explains the instability presented in Fig. 5.9-b. In the case of surfactant-based emulsions, a similar phenomenon occurs at the phase inversion point, would it be the same for our Pickering emulsions?

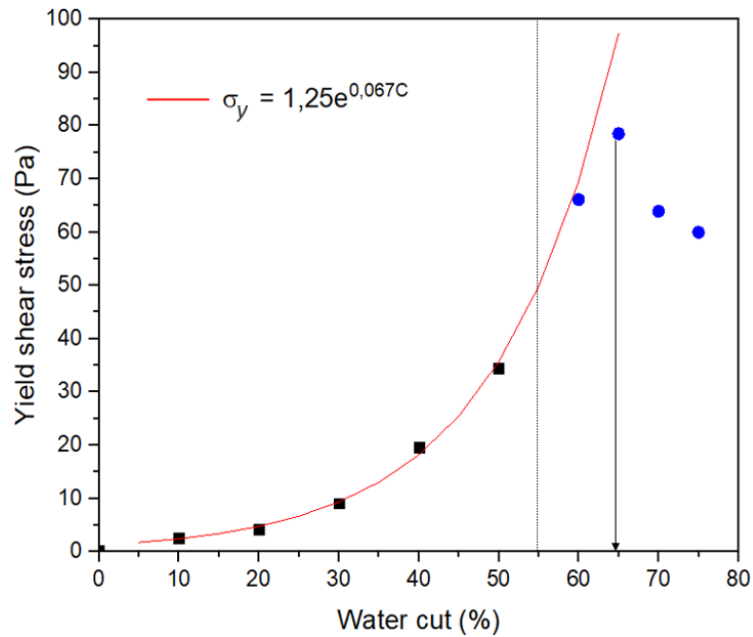


Fig. 5.11. Yield stress as a function of the mass concentration of water.

## 5.4.2 Unstable emulsion

As it was mentioned earlier, unstable emulsions were noticed at different flow conditions. In the following, a discussion of the main experimental results registered during the flow of inhomogeneous Pickering emulsions will be presented.

### 5.4.2.1 Static instability

As it was mentioned in chapter 4, the visual appearance of Pickering emulsions with water concentrations inferior to 50 wt% did not change even after 12 months of rest (Fig. 5.12). However, in the case of Pickering emulsions with water concentrations superior to 50 wt% (Fig. 4.8), volumes of water spill were noticed even after short rest times (Yang et al., 2020).

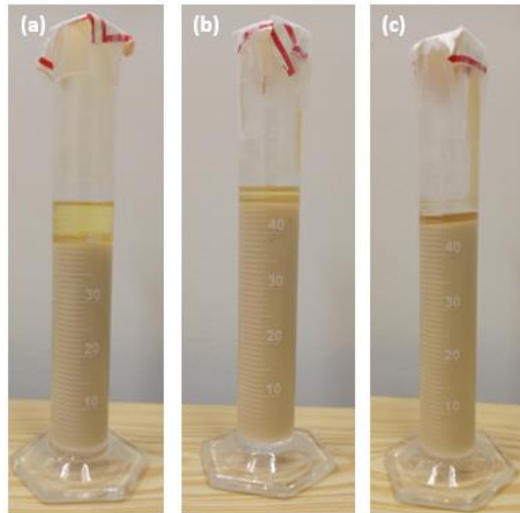


Fig. 5.12. O/Ht based Pickering emulsions after 12 months of rest at 20 °C. (a) B3-10H<sub>2</sub>O, (b) B3-20H<sub>2</sub>O, (c) B3-30H<sub>2</sub>O.

As depicted in Fig. 5.13-a, B3-60H<sub>2</sub>O emulsion lost its initial equilibrium after 5 months of rest and a phase separation took place. Unlike classic emulsions, the sample was not fully demulsified, and two phases were noticed:

- A free water phase that, preferentially, settles near to the recipient wall without forming a continuous water layer (Fig. 5.13-a). It is worth mentioning that the same behavior was as well noticed when the emulsions were kept at rest inside the flow loop (Fig. 5.14).
- An emulsion that stays stable even after a continuous mechanical agitation (5.14-b).

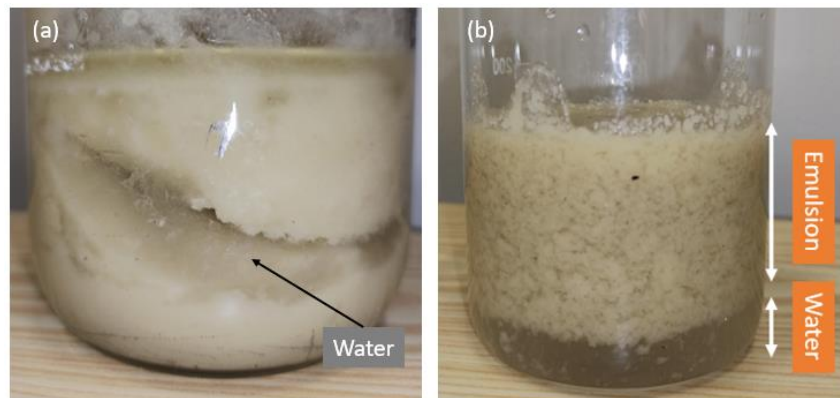


Fig. 5.13. B3-60H<sub>2</sub>O emulsion after 5 months of rest. (a) before and (b) after agitation.

### 5.4.2.2 Dynamic instability

Unstable flow behavior was noticed under different flow conditions for the OHT stabilized Pickering emulsions.

First, at the flow start-up, and after only 10 min of rest, a wall shear stress peak followed by a near-to-zero plateau were noticed for all emulsions with water concentrations superior to 50 wt%. This behavior was already illustrated in Fig. 5.7-b for the B3-70H2O emulsion and was explained by the presence of a wall slipping phase at the beginning of the flow due to the presence of a water film at the pipe wall. It can be noted that:

- i. A shear stress peak is noticed before the near-to-zero shear stress plateau. This may indicate the presence of the emulsion at the pipe wall before the flow started. After that, the shear stress curve diminishes gradually until reaching a plateau corresponding to the wall slipping.
- ii. The inconsistency between the wall shear stress and the  $U_{max}/U$  curves, at the beginning of the flow, shows that the composition and the microstructure of the fluids at the pipe wall and at the pipe center are different.

A possible explanation to this behavior can be the presence of isolated water aggregations attached to the pipe wall at rest (Fig. 5.14), that are connected to form a water film during the first 10 s of flow, at low velocities.

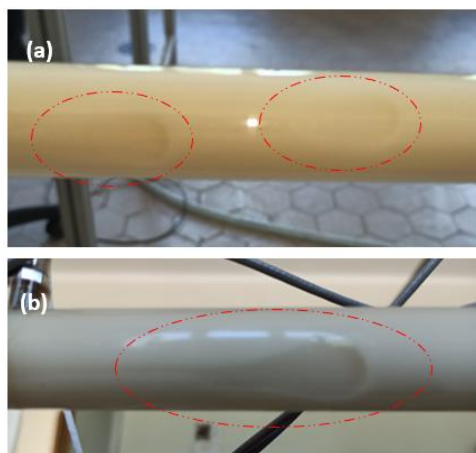


Fig. 5.14. B3-70H2O (a) and B3-75H2O (b) emulsions after 10 min of rest.

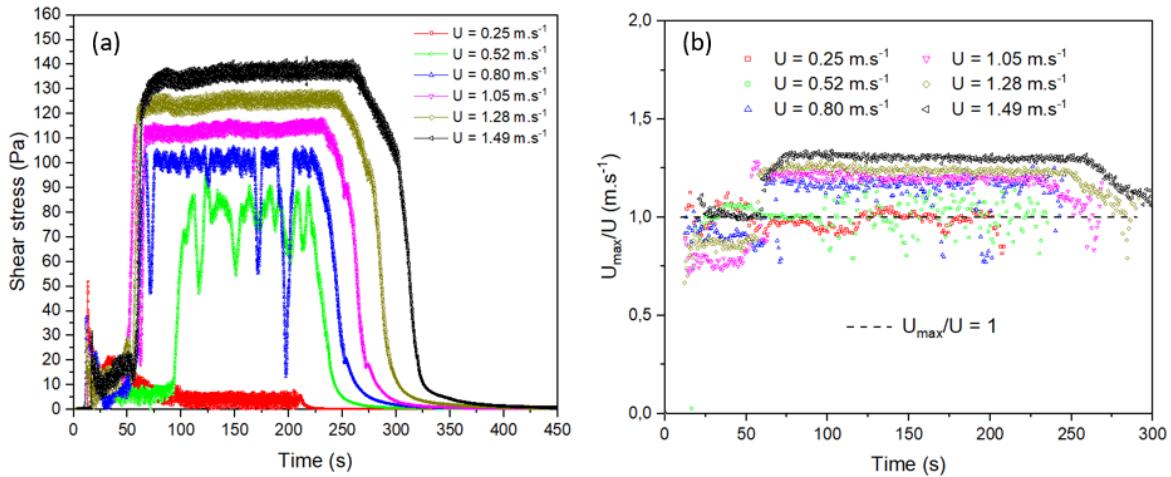


Fig. 5.15. Flow parameters as a function of time for the B3-65H<sub>2</sub>O emulsion.

Second, all emulsions, except for the B3-65H<sub>2</sub>O, exhibited a short term (60 s) wall slipping followed by a homogenous-fluid behavior when velocity ramps were applied. The B3-65H<sub>2</sub>O on the other hand, shows a specific behavior. Fig. 5.15 illustrates the temporal evolution of the wall shear stress and of the  $U_{max}/U$  ratio, for the B3-65H<sub>2</sub>O emulsion at 6 different mean velocity plateaus ranging from 0,25 m.s<sup>-1</sup> to 1,49 m.s<sup>-1</sup>. It should be mentioned that a homogenization process, followed by a 10 min of rest, was proceeded before performing the tests illustrated in Fig. 5.15.

As it can be noticed, a critical velocity can be identified, under which the emulsion cannot be homogenized. Like the rest of emulsions studied in this chapter, the wall shear stress curves exhibit a peak at the beginning of the flow, followed by a near-to-zero plateau. Overall, three regions can be noticed:

- i. First, at the lowest velocity,  $U = 0,25 \text{ m. s}^{-1}$ , a null wall shear stress value is registered until the end of the experiment. The corresponding velocity ratio  $U_{max}/U = 1$ , which is an indicator of a plug flow that can be explained by the film of water at the pipe wall that induces wall slipping.
- ii. Second, at  $U = 0,52 \text{ m. s}^{-1}$  and  $U = 0,80 \text{ m. s}^{-1}$ , after the null shear stress plateau, oscillations in the shear stress and the velocity ratio curves were noticed which denotes the flow of an unstable emulsion (Fig. 5.16).
- iii. Third, for higher velocities, the flow curves are like those of the other emulsions and a dynamic stability is observed.

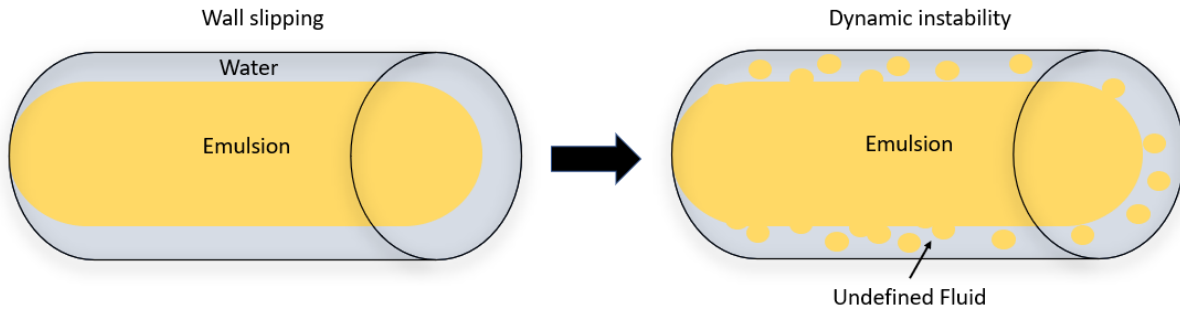


Fig. 5.16. Schematic representation of wall slipping and unstable flow behaviors.

Fig. 5.17 illustrates the temporal evolution of the wall shear stress at different distances from the loop entry. The pressure values were registered simultaneously and at a mean velocity  $U = 0,80 \text{ m} \cdot \text{s}^{-1}$ . It is quite interesting to see the evolution of the wall slipping region at different locations from the loop entry. It can be noticed that the wall slipping region lasts between 40 s and 60 s, depending on the distance between the pressure sensors and the loop entry. Using this information, the velocity of the fluid at the near-to-wall region was calculated and found to be  $0,53 \text{ m} \cdot \text{s}^{-1}$ , which is different than the mean velocity  $U = 0,80 \text{ m} \cdot \text{s}^{-1}$ . This result confirms the explanation illustrated in Fig. 5.16 which evokes the existence of two distinct fluid regions during the unstable behaviors.

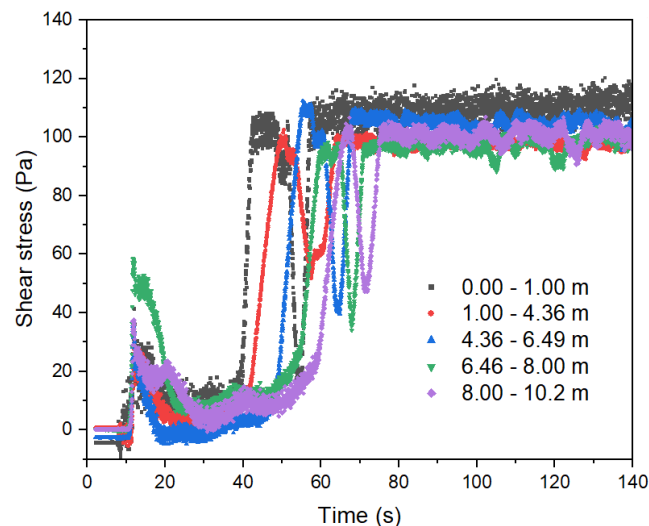


Fig. 5.17. Wall shear stress as a function of time at different distances from the loop entry for the B3-65H2O emulsion. at  $U = 0,80 \text{ m} \cdot \text{s}^{-1}$ .

### 5.4.2.3 Visual observation

To investigate the type of the emulsion (direct or inverse emulsion) around the critical concentration, visual experiments described in section 5.3 was conducted. Fig. 5.18 shows the results of the experiments when a small volume of each emulsion was diluted in both water and silicone oil. Unlike emulsions with water concentration inferior to 50 wt% (Fig. 5.4), the results in the case of concentrated emulsions did not allow to determine the type of the emulsions. It is certain that the structural change around B3-50H<sub>2</sub>O is not, only, due to phase inversion like in the case of surfactant-based emulsions. Furthermore, the following observations were drawn:

- B3-60H<sub>2</sub>O, B370H<sub>2</sub>O, and B3-75H<sub>2</sub>O emulsions are mostly oil miscible with some oil-immiscible aggregations.
- The affinity of B3-65H<sub>2</sub>O was not clear. It was found to be neither water-wet nor oil-wet.

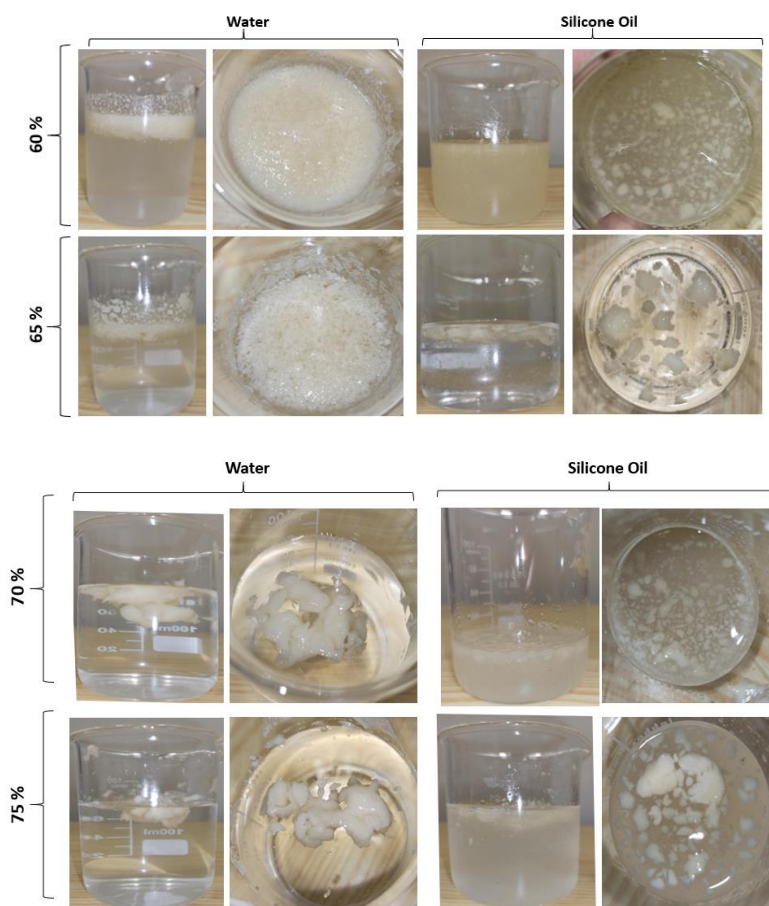


Fig. 5.18. Visual observation of concentrated Pickering emulsions stabilized by OHt clay.

Further tests need to be conducted to define the nature of the studied emulsions. A possible hypothesis is that the fluid is composed of 2 fluids:

- Water that is free at rest and temporarily emulsified during flow, as shown in Fig. 5.19.
- An emulsion with an unknown structure, that can possibly be a multiple emulsion (Pal, 2011).

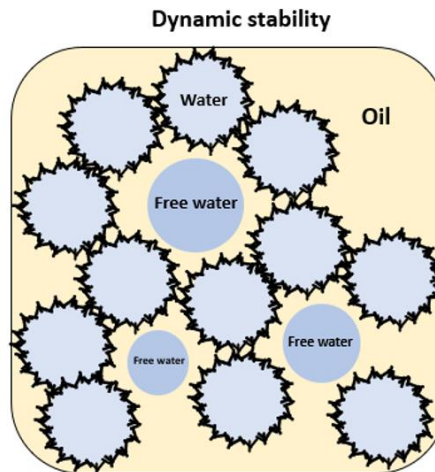


Fig. 5.19. Schematic representation of dynamic stability.

## 5.5 Attenuation measurements

The amplitude and intensity of ultrasound waves diminishes as they travel through fluid. This phenomenon is known as attenuation. Attenuation is mainly affected by the thermal conductivity as well as the viscosity of the travelled medium, if a fixed propagation source is used.

In the following, the measured and theoretically calculated attenuation coefficients are compared for each concentration. The experimental linear attenuation coefficient,  $\alpha$ , is calculated using the following expression:

$$I = I_0 e^{-\alpha \cdot x} \quad 5.4$$

where  $I$  is the beam intensity at a distance  $x$ ,  $I_0$  is the initial intensity, and  $x$  is the distance travelled by the ultrasound wave.

The theoretical attenuation coefficient was calculated based on the following assumption:

- At a water concentration of 50 wt%, the solid particles are fully adsorbed on oil/water interfaces.

The mass concentration,  $S_a$ , of the adsorbed OHt particles is then:

$$S_a = W_f * \frac{S_t}{W_c} \quad 5.5$$

where  $W_f$  is water fraction,  $S_t = 1,5 \text{ g/l}$  is OHt mass concentration in the total volume of B3-50H2O, and  $W_c = 0,5$  is water mass fraction in the B3-50H2O emulsion.

The mass concentration of free OHt particles was then deduced and the theoretical attenuation coefficient was calculated using the previous OHt mass concentrations and the experimental  $\alpha$  values at B3 and B3-50H2O.

Fig. 5.20 shows the evolution of the experimental and theoretical attenuation coefficient as a function of water concentration. As it can be noticed, both curves follow the same trend with small differences around 50 wt%. The theoretical curve predicts a peak at B3-50H2O while the experimental curve expresses a quasi-plateau between B3-30H2O and B3-50H2O. Overall, and taking into consideration the experimental errors, the experimental and the theoretical curves were successfully fitted with an order 2 polynomial trendline.

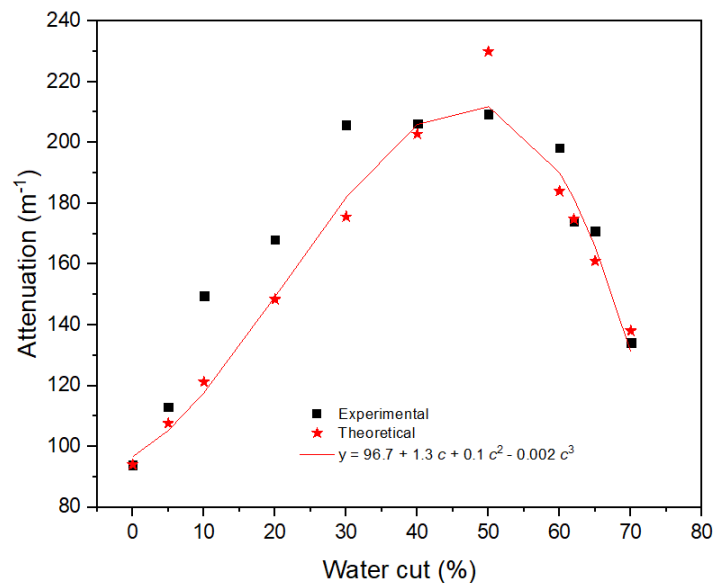


Fig. 5.20. Attenuation as a function of water concentration of Pickering emulsions stabilized by OHt clay.

## 5.6 Summary to chapter

This chapter is a continuation to chapter 4 with the aim to study the flow behavior of concentrated emulsions. Concentrated emulsions are the ones to which a continuous circulation is necessary for their homogenization. As their dynamic stability requires high shear rates, rheological measurements were not possible for emulsions with water mass concentrations superior to 50 wt%. Furthermore, because of the high medium attenuation, we were not able to measure the totality of the velocity profiles. This is why, the only represented velocity measurement, in this chapter, is the maximum velocity, which is the velocity value at the pipe center.

Concentrated emulsions were found to exhibit both stable and unstable behavior during flow, depending on many parameters such as the emulsification process, the static rest time before the measurements, the position of the measuring system in the flow loop, the applied velocity value, and most importantly their water mass concentration.

In a first part, the stability conditions were identified for all emulsions, in order to study their rheological behavior during dynamic stability. It was found that the flow curves of concentrated emulsions follow, as well, the rheological model of Herschel-Bulckley, and the yield shear stress curve as a function of water concentration showed that the emulsions exhibit a critical concentration around B3-60H<sub>2</sub>O.

In a second part, the structural change inducing the latter critical concentration was investigated. To do so, flow behavior of unstable emulsions was studied. Three main instability behaviors were noticed:

- i. A shear stress peak at the beginning of the flow, that was explained by the presence of 2 fluids attached to the pipe wall: aggregations of free water and a stable emulsion.
- ii. A wall slipping behavior at low velocities due to the presence of a free water film at the pipe wall.
- iii. The behavior of the B3-65H<sub>2</sub>O emulsion, that was found to be stable only at very high flow rates and after long times of continuous circulation.

Finally, it was shown that the structure change observed around the critical concentration was not due to a phase inversion, as a free water phase along with a stable emulsion were found to coexisted in the studied fluids.

## 5.7 References

- Araiza-Calahorra, A., Sarkar, A., 2019. Pickering emulsion stabilized by protein nanogel particles for delivery of curcumin: Effects of pH and ionic strength on curcumin retention. *Food Struct.* 21, 100113. <https://doi.org/10.1016/j.foostr.2019.100113>
- Bizmark, N., Du, X., Ioannidis, M.A., 2020. High Internal Phase Pickering Emulsions as Templates for a Cellulosic Functional Porous Material. *ACS Sustain. Chem. Eng.* 8, 3664–3672. <https://doi.org/10.1021/acssuschemeng.9b06577>
- Briggs, N., Raman, A.K.Y., Barrett, L., Brown, C., Li, B., Leavitt, D., Aichele, C.P., Crossley, S., 2018. Stable pickering emulsions using multi-walled carbon nanotubes of varying wettability. *Colloids Surfaces A Physicochem. Eng. Asp.* 537, 227–235. <https://doi.org/10.1016/j.colsurfa.2017.10.010>
- Derakhshandeh, M., Pilapil, B.K., Workman, B., Trifkovic, M., Bryant, S.L., 2018. Analysis of network formation and long-term stability in silica nanoparticle stabilized emulsions. *Soft Matter* 14, 4268–4277. <https://doi.org/10.1039/c7sm02457f>
- Dong, J., Worthen, A.J., Foster, L.M., Chen, Y., Cornell, K.A., Bryant, S.L., Truskett, T.M., Bielawski, C.W., Johnston, K.P., 2014. Modified montmorillonite clay microparticles for stable oil-in-seawater emulsions. *ACS Appl. Mater. Interfaces* 6, 11502–11513. <https://doi.org/10.1021/am502187t>
- Feng, X., Dai, H., Ma, L., Fu, Y., Yu, Y., Zhou, H., Guo, T., Zhu, H., Wang, H., Zhang, Y., 2020. Properties of Pickering emulsion stabilized by food-grade gelatin nanoparticles: influence of the nanoparticles concentration. *Colloids Surfaces B Biointerfaces* 196, 111294. <https://doi.org/10.1016/j.colsurfb.2020.111294>
- Frelichowska, J., Bolzinger, M.A., Chevalier, Y., 2010. Effects of solid particle content on properties of o/w Pickering emulsions. *J. Colloid Interface Sci.* 351, 348–356. <https://doi.org/10.1016/j.jcis.2010.08.019>
- Geng, J., Pu, J., Zhao, Y., Lin, B., Bai, B., Thomas, S.P., 2019. pH-Responsive crude oil-in-water Pickering emulsion stabilized by polyacrylamide nanogels. *Fuel* 258, 116159. <https://doi.org/10.1016/j.fuel.2019.116159>
- Griffith, C., Daigle, H., 2020. A comparison of the static and dynamic stability of Pickering

- emulsions. *Colloids Surfaces A Physicochem. Eng. Asp.* 586, 124256.  
<https://doi.org/10.1016/j.colsurfa.2019.124256>
- Griffith, C., Daigle, H., 2018. Manipulation of Pickering emulsion rheology using hydrophilically modified silica nanoparticles in brine. *J. Colloid Interface Sci.* 509, 132–139. <https://doi.org/10.1016/j.jcis.2017.08.100>
- Hu, Z., Ballinger, S., Pelton, R., Cranston, E.D., 2015. Surfactant-enhanced cellulose nanocrystal Pickering emulsions. *J. Colloid Interface Sci.* 439, 139–148.  
<https://doi.org/10.1016/j.jcis.2014.10.034>
- Jahandideh, H., Ganjeh-Anzabi, P., Bryant, S.L., Trifkovic, M., 2018. The Significance of Graphene Oxide-Polyacrylamide Interactions on the Stability and Microstructure of Oil-in-Water Emulsions. *Langmuir* 34, 12870–12881.  
<https://doi.org/10.1021/acs.langmuir.8b02288>
- Jiang, H., Liu, L., Li, Y., Yin, S., Ngai, T., 2020. Inverse Pickering Emulsion Stabilized by Binary Particles with Contrasting Characteristics and Functionality for Interfacial Biocatalysis. *ACS Appl. Mater. Interfaces* 12, 4989–4997.  
<https://doi.org/10.1021/acsami.9b16117>
- Kaptay, G., 2006. On the equation of the maximum capillary pressure induced by solid particles to stabilize emulsions and foams and on the emulsion stability diagrams. *Colloids Surfaces A Physicochem. Eng. Asp.* 282–283, 387–401.  
<https://doi.org/10.1016/j.colsurfa.2005.12.021>
- Li, S., Zhang, B., Li, C., Fu, X., Huang, Q., 2020. Pickering emulsion gel stabilized by octenylsuccinate quinoa starch granule as lutein carrier: Role of the gel network. *Food Chem.* 305, 125476. <https://doi.org/10.1016/j.foodchem.2019.125476>
- Maaref, S., Kantzas, A., Bryant, S.L., 2019. The effect of silanization assisted nanoparticle hydrophobicity on emulsion stability through droplet size distribution analysis. *Chem. Eng. Sci.* 201, 175–190. <https://doi.org/10.1016/j.ces.2019.02.034>
- Pal, R., 2011. Rheology of simple and multiple emulsions. *Curr. Opin. Colloid Interface Sci.* <https://doi.org/10.1016/j.cocis.2010.10.001>
- Pandey, A., Derakhshandeh, M., Kedzior, S.A., Pilapil, B., Shomrat, N., Segal-Peretz, T., Bryant, S.L., Trifkovic, M., 2018. Role of interparticle interactions on microstructural

- and rheological properties of cellulose nanocrystal stabilized emulsions. *J. Colloid Interface Sci.* 532, 808–818. <https://doi.org/10.1016/j.jcis.2018.08.044>
- Sharma, T., Kumar, G.S., Chon, B.H., Sangwai, J.S., 2015. Thermal stability of oil-in-water Pickering emulsion in the presence of nanoparticle, surfactant, and polymer. *J. Ind. Eng. Chem.* 22, 324–334. <https://doi.org/10.1016/j.jiec.2014.07.026>
- Wei, X.Q., Zhang, W.J., Lai, L., Mei, P., Wu, L.M., Wang, Y.Q., 2019. Different cationic surfactants-modified silica nanoparticles for Pickering emulsions. *J. Mol. Liq.* 291, 111341. <https://doi.org/10.1016/j.molliq.2019.111341>
- Xiao, J., Wang, X., Perez Gonzalez, A.J., Huang, Q., 2016. Kafirin nanoparticles-stabilized Pickering emulsions: Microstructure and rheological behavior. *Food Hydrocoll.* 54, 30–39. <https://doi.org/10.1016/j.foodhyd.2015.09.008>
- Yang, H., Su, Z., Meng, X., Zhang, X., Kennedy, J.F., Liu, B., 2020. Fabrication and characterization of Pickering emulsion stabilized by soy protein isolate-chitosan nanoparticles. *Carbohydr. Polym.* 247, 116712. <https://doi.org/10.1016/j.carbpol.2020.116712>
- Zhang, S., Zhou, Y., Yang, C., 2015. Pickering emulsions stabilized by the complex of polystyrene particles and chitosan. *Colloids Surfaces A Physicochem. Eng. Asp.* 482, 338–344. <https://doi.org/10.1016/j.colsurfa.2015.06.029>
- Zhang, Y., Cui, L., Xu, H., Feng, X., Wang, B., Pukánszky, B., Mao, Z., Sui, X., 2019. Poly(lactic acid)/cellulose nanocrystal composites via the Pickering emulsion approach: Rheological, thermal and mechanical properties. *Int. J. Biol. Macromol.* 137, 197–204. <https://doi.org/10.1016/j.ijbiomac.2019.06.204>



**CONCLUSIONS  
AND  
PERSPECTIVES**

## CONCLUSIONS AND PERSPECTIVES

## A. Conclusions

In this thesis, the mechanical behaviors of organoclay suspensions and Pickering emulsions were investigated in order to study the potential of Pickering emulsions stabilized by organoclay particles to be used as a base for drilling fluids preparations. Organo-hectorite particles as solid stabilizers for water-in-gasoil inverse emulsions showed some promising results, and were able to stabilize emulsions with high water ratios. In the following, the main conclusions drawn based on this work are listed:

- Modified clays, or organoclays, are getting a lot of attention lately because of their use as fillers in the preparation of nanocomposites, and more recently as emulsion stabilizers. For the latter application, they are first dispersed in organic media before adding the discontinuous aqueous phase. The mechanical behavior of organoclay dispersions in organic media can then have a major influence on the behavior of Pickering emulsion. This hypothesis was confirmed in our work when rheological behaviors of organo-hectorite dispersions and organo-hectorite stabilized Pickering emulsions were studied. We found that the rheological behavior of the studied Pickering emulsions is similar to that of concentrated OHt suspensions. These results can be explained by the fact the added water, to OHt suspensions, occupies the free spaces between OHt particles and thus enables the interactions between them. Hence, the yielding behavior exhibited by the studied Pickering emulsions is nothing but the result of the interactions between OHt platelets, that increase with the increase in water to gasoil ratio.
- Our in-house emulsifying set, used to prepare the studied emulsions, showed a satisfying potential to prepare large quantities of Pickering emulsions with a surprising high long-term stability. The cost of this apparatus is very low as it only requires the integration of two diaphragms to the flow loop (few Euros for each diaphragm VS 5000 Euros at least for a turbine). Therefore, an in-line emulsification section can be added to any existing circulation system without imposing any specific changes. Such simple and low-priced solution can be very attractive for industrial use.
- Emulsions were found to lose their static stability when water mass concentration exceeds 50 wt%. In this case, two different fluids were noticed at rest: (i) a stable

emulsion and (ii) a free water phase. Using the results shared in chapter 5, we can conclude that the prepared emulsion with water concentrations lower than 50 wt% are irreversible. Furthermore, a free water phase starts being noticed when the solid particles, dispersed in gasoil, are completely adsorbed on the surfaces of water droplets (water/gasoil interfaces). This might be a very probable explanation to the observed behavior (absence of phase inversion, simultaneous presence of free water and stable emulsion, at high water fractions).

- Even at high water fractions, dynamic stability can be reached under certain conditions like high flow rates and long homogenization processes.
- The quality of the studied emulsions was verified using our in-line pressure and velocity systems. This method can be very interesting to be used as a non-intrusive in-line quality control system for industrial applications (hydrocarbon fields, water treatment, food industry, etc.,).
- Long-term stabilized Pickering emulsions with high water fractions may be achieved if the following parameters are better optimized: (i) the solid particles content, (ii) the three-phase contact angle, and (iii) the emulsification time and energy.
- Pickering emulsions stabilized with OHT particles were found to have a comparable flow behavior to that of inverse-emulsion drilling fluids. In addition to that, we were able to prepare emulsions with high static and dynamic stability, and with water volume concentrations up to 45 % (Annex 2). Therefore, the main objective of this thesis, being optimizing surfactant-free highly-stable Pickering inverse-emulsions with high water fractions, has then been successfully achieved.

## B. Perspectives

Based on the obtained results and the previous conclusions, some propositions, for future research, can be suggested:

- Looking at its low cost and high efficacy, the emulsification system described in this work merits further attention in future works. The effects of the diaphragms number, their imposed diameter restriction, and their placement can be interesting for industrial applications and in-set emulsion preparation.
- It is as well very interesting to study the influence of:
  - Temperature
  - pH
  - The type of solid particles and their wettability
  - The continuous phase composition
 on the stability and flow behavior of Pickering emulsions.
- To understand better the interactions between the solid particles, it would be interesting to further investigate on the microstructure of organoclay dispersions and Pickering emulsions, especially at high water concentration.
- Even though we were more interested in preparing long-term stable Pickering emulsions, dynamic instability at high water fractions and low mean velocities can be interesting as well, for instance, in the case of long-distances fluid transportation. It was seen in chapter 5 that, under some conditions, the emulsions exhibited plug flow behaviors with near-to-zero wall shear stress values (energy efficient flows).

Finally, our contribution to the experimental study of flow behavior of Pickering emulsions revealed a good potential of modified clay particles to be useful as solid stabilizers for inverse emulsion drilling fluids as well as for many other applications where shear-thinning, irreversible, inverse-emulsions with yielding behavior are envisaged.

## CONCLUSIONS AND PERSPECTIVES

# **Annexes**



## Résumé étendu en Français

Ce travail a été financé par l'Université de Strasbourg, au sein du Laboratoire des Sciences de l'Ingénieur, de l'Informatique et de l'Imagerie - ICube, par l'Université de Boumerdes, au sein du Laboratoire du Génie Physique des Hydrocarbures, et par le ministère des Affaires Etrangères Français, dans le cadre de la bourse franco-algérienne Profas B +. La présente thèse est une contribution expérimentale à l'étude rhéologique et en écoulement des émulsions de type Pickering. La préparation de ces systèmes dans un dispositif de circulation continue et l'étude de leurs comportements dans un circuit hydraulique est une des valeurs ajoutées de ce travail, car pour l'instant encore très peu étudié.

Une vinaigrette, une crème hydratante, une perfusion médicale, un joint d'étanchéité ou encore un fluide de forage à émulsion inverse sont tous des émulsions largement exploitées, soit par le grand public, soit en milieu industriel. Ces émulsions sont classiquement stabilisées par des surfactants (molécules tensioactives). Leur préparation, ainsi que leur stabilité sont connues et largement documentées. Malgré les problèmes d'instabilité liés aux émulsions classiques, la part du marché des surfactants reste l'une des plus grandes dans le marché des molécules chimiques, avec une valeur de 42120,3 M€ et une consommation mondiale de 380 kg par seconde<sup>1</sup> ! Au-delà de son impact économique, l'utilisation massive des tensioactifs est néfaste pour l'environnement et pour la santé de l'être humain<sup>2</sup>.

Si on arrivait à produire des émulsions plus stables dans le temps (voir irréversibles), en utilisant des produits moins chers, tout en contrôlant la taille des gouttelettes de la phase dispersée, ne serait pas-t-il intéressant ?

En effet, ces dernières années, un intérêt majeur a été porté sur les émulsions stabilisées par des particules solides. Connues sous le nom de « Pickering », ces émulsions sont stabilisées par l'adsorption de particules solides, qui possèdent des propriétés à la fois lipophiles et lipophobes, à l'interface entre l'huile et l'eau.

L'objectif principal de cette thèse est de préparer des émulsions inverses, stabilisée par des particules d'argile modifiée, et d'étudier leur comportement rhéologique et mécanique en écoulement à différentes concentrations de phase dispersée. Le type d'émulsions étudié est

appelé « inverse » (eau dans l'huile) et est utilisé dans plusieurs applications industrielles, parmi lesquelles les fluides de forage.

C'est dans ce contexte que s'inscrit le travail de cette thèse, en préparant de grandes quantités (50 L) d'émulsions inverses, stabilisées par des particules d'argile lipophile, à l'aide de deux diaphragmes montés près de la sortie d'un système de circulation hydraulique. Ce système a été utilisé, non seulement pour la préparation des émulsions, mais également pour étudier leur comportement mécanique, en utilisant un vélocimètre ultrasonore Doppler pulsé et des capteurs de pression. En ce qui suit, un résumé synthétique des chapitres de ce travail sera présenté.

## Chapitre 1 : Bases Théoriques

Dans un premier chapitre bibliographique, nous présentons les bases théoriques nécessaire pour la compréhension de l'ensemble des travaux et résultats expérimentaux reportés dans ce manuscrit.

D'abord, nous commençons par détailler les principes de mesures rhéologiques et en écoulement utilisées dans ce travail avant de nous attarder sur les processus de modification d'argiles étudiées et de leur utilisation en tant que stabilisateurs d'émulsions Pickering (Fig. 1).

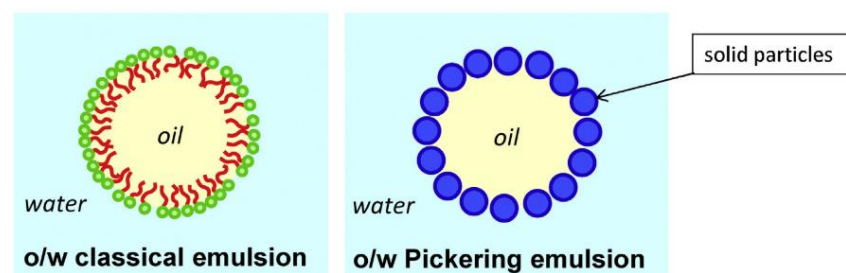


Fig. 1. Mécanismes de stabilisation d'émulsions classiques (gauche) et Pickering (droite).

Le comportement rhéologique des fluides étudiés (suspensions d'argile modifiée et émulsions inverses Pickering) a été représenté par le modèle de Herschel-Bulckley (Eq. 1) :

$$\sigma = \sigma_y + K\dot{\gamma}^n \quad 1$$

Où  $K$  est la consistance du fluide,  $n$  son indice d'écoulement et  $\sigma_y$  sa contrainte seuil.

Ce modèle, fréquemment utilisé en littérature pour simuler le comportement rhéologique des suspensions de bentonite, permet d'évaluer la contrainte seuil et le comportement rhéofluidifiant du fluide.

Un deuxième modèle rhéologique, celui de Carreau-Yasuda, a été utilisé pour présenter les propriétés intrinsèques des fluides étudiés :

$$\frac{\eta(\dot{\gamma}) - \eta_\infty}{\eta_0 - \eta_\infty} = [1 + (\tau\dot{\gamma})^a]^{\frac{n-1}{a}} \quad 2$$

Où  $\eta_0$  et  $\eta_\infty$  sont les viscosités à cisaillements nul et infini, respectivement,  $\tau$  est le temps caractéristique de relaxation,  $n$  est l'exposant de la loi de puissance et  $a$  est le facteur de transition adimensionnel.

L'écoulement en conduite des fluides de type Herschel-Bulckley est caractérisé par un profil de vitesse composées de deux zones : i) une zone iso-vitesse au centre de la conduite, où la contrainte imposée est inférieure à la contrainte seuil du fluide et ii) un gradient de vitesse près de la paroi, où le fluide suit une loi de puissance et la contrainte imposée est supérieure à la contrainte seuil.

## Chapitre 2 : Matériel et Méthodes

Dans le deuxième chapitre, nous décrirons, dans une première partie, les techniques de mesures rhéologiques utilisées. Puis, nous présentons la boucle hydraulique conçue au laboratoire ICube, ainsi que le système d'émulsification, utilisé pour la préparation des fluides étudiés, et les deux chaînes de mesure de pression et de vitesse (Fig. 2). Enfin, nous terminons ce chapitre par une description des protocoles de préparation des différents systèmes étudiés, notamment les suspensions d'argile modifiée et les émulsions inverses de type Pickering.

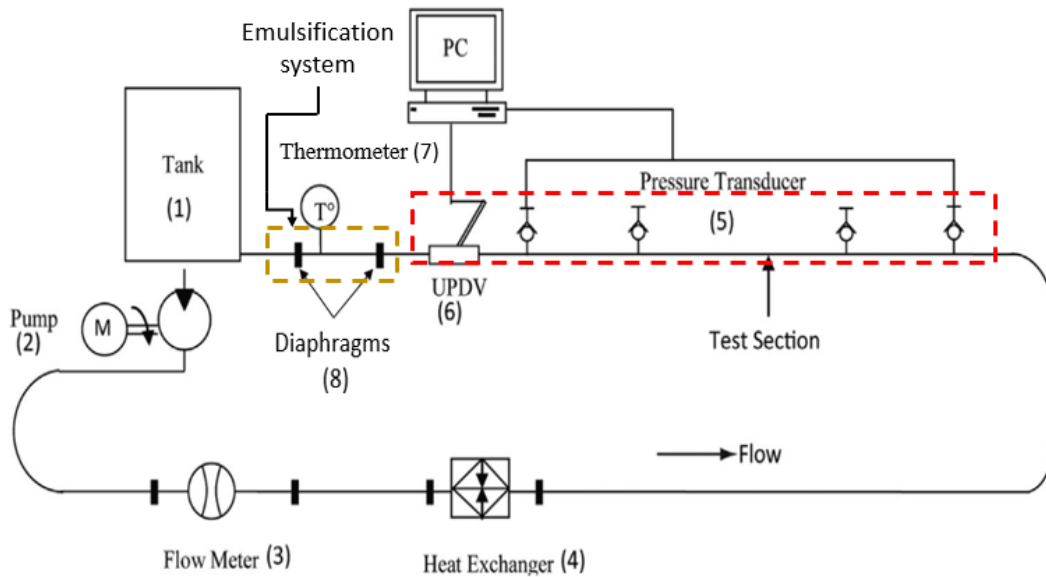


Fig. 2. Différents composants de la boucle hydraulique.

### Chapitre 3 : Comportement rhéologique des suspensions d'argile modifiée

Etant donné qu'une suspension d'argile lipophile est utilisée dans la préparation de nos émulsions, nous avons commencé notre étude expérimentale par un chapitre détaillant le comportement rhéologique des suspensions d'hectorite modifiée dans le gasoil à différentes concentrations massiques (3 % à 10 %). La rhéologie de ces suspensions a été étudiée en utilisant un rhéomètre à contrainte imposée, équipé d'une géométrie cône-plan (AR2000).

Tout d'abord, les mesures en écoulement ont mis en évidence le comportement rhéofluidifiant des suspensions d'hectorite modifiée. Toutes les concentrations étudiées présentent un comportement à seuil, avec une valeur qui augmente avec la teneur en argile. Les résultats d'essais rhéologiques en écoulement ont été modélisés par les modèles de Herschel-Bulckley et de Carreau-Yasuda. En outre, les valeurs expérimentales de la contrainte seuil ont été trouvées proches de celles du modèle d'Herschel-Bulckley, et la courbe de la contrainte seuil en fonction de la concentration d'argile modifiée a subi un changement de pente à 6 wt%.

De plus, les expériences en fluage nous ont permis de mesurer le coefficient de compliance des fluides étudiés, et les courbes de ce coefficient en fonction du temps ont été établies. L'index de recouvrance élastiques a été calculés et tracés, sur le même graphe avec le module élastique,

en fonction de la concentration d'argile (Fig. 3.). Cette courbe a confirmé l'existence d'une concentration critique,  $c^*$ , à laquelle un changement dans la structure interne des dispersions d'argile a eu lieu. En outre, les mesures de volume de gel ont montré la même évolution présentée par les mesures rhéologiques.

Enfin, et en se basant sur les résultats présentés dans ce travail, l'explication suivante a été proposée : après avoir atteint une concentration critique, les espaces entre les particules d'argile gonflées deviennent plus étroits, en raison de l'absence du solvant libre, et donc les interactions entre ces particules deviennent plus importantes et une structure plus complexe se forme. Les résultats de ce chapitre ont été publiés dans le *Journal of Applied Clay Science*.

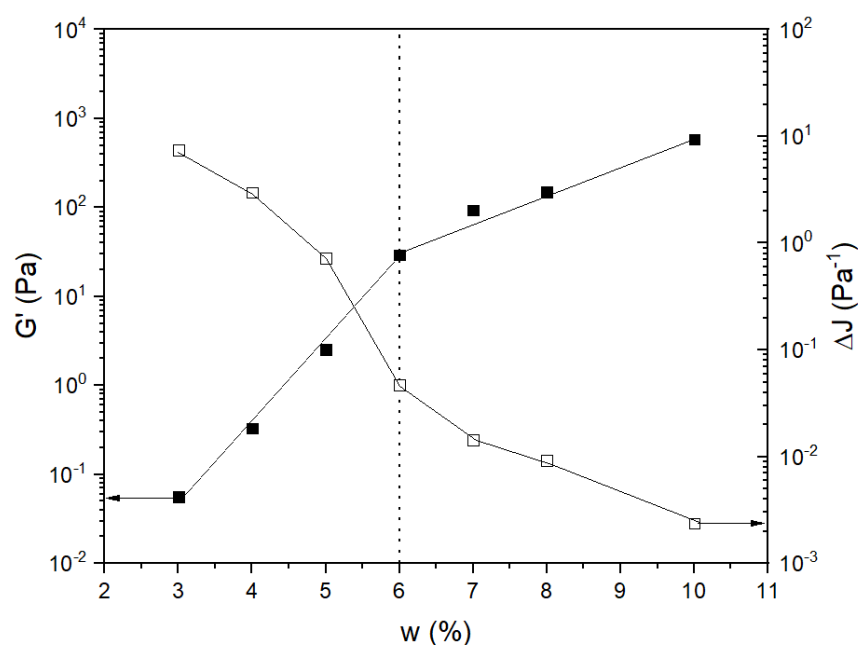


Fig. 3. Le module élastique et l'index de recouvrance élastique en fonction de la concentration d'hectorite modifiée.

## **Chapitre 4 : Comportement Rhéologique et en Ecoulement des Emulsions Pickering à Faibles Concentrations d'eau.**

Le but de ce chapitre étant d'étudier le comportement mécanique, rhéologique et en écoulement, d'émulsions inverses stabilisées par des particules solides (hectorite modifiée). La comparaison des mesures rhéologiques et celles en écoulement ont permis d'éliminer les erreurs expérimentales telles que les forces centrifuges et le glissement aux parois, souvent présents au niveau des rhéomètres rotationnels. Dans ce cas, les propriétés rhéologiques intrinsèques réelles seront obtenues si les résultats des deux techniques coïncident.

Un système d'émulsification en ligne, utilisant deux diaphragmes, a été testé et utilisé pour la préparation d'émulsions inverses de type Pickering. Le système d'émulsification a montré un grand potentiel pour la préparation des émulsions homogènes et stables dans le temps. 800 s de circulation continue a été suffisante pour émulsionner complètement les fluides, et des mesures de la vitesse sonore ont été utilisées pour vérifier leur homogénéité et les concentrations d'eau dans chaque émulsion préparée.

En utilisant cette méthode, des émulsions Pickering avec 5 concentrations d'eau ont été préparées. Le comportement rhéologique, en écoulement et viscoélastique a été étudié pour chaque concentration en utilisant le même rhéomètre rotatif à contrainte imposée utilisé dans le Chapitre 3. Nous avons constaté que les émulsions Pickering présentent un comportement rhéofluidifiant à contrainte seuil qui suit la loi de Herschel-Bulckley. L'évolution du seuil en fonction de la concentration d'eau a montré que le point d'inversion de phase n'est pas encore atteint pour les concentrations étudiées (inférieures à 50 %).

En outre, les mesures viscoélastiques ont mis en évidence le comportement gel des émulsions à faibles déformations. Une comparaison entre les modules élastique et visqueux des émulsions B3 (0 % H<sub>2</sub>O) et B3-10H<sub>2</sub>O (10 % H<sub>2</sub>O) a montré que le comportement rhéologique des émulsions évolue du domaine visqueux au domaine élastique lorsque la concentration en eau augmente, à une fréquence donnée. L'émulsion B3-10H<sub>2</sub>O a un comportement similaire à celui des suspensions d'argile concentrées, étudiées dans le Chapitre 3. Par conséquent, le comportement élastique des émulsions est lié à l'interaction entre les plaquettes d'argile présentes sur les interfaces eau-huile. Dans une deuxième partie, le comportement des émulsions préparées dans des conduites cylindriques horizontales a été étudié grâce aux essais

sur la boucle hydraulique (Chapitre 2). Toutes les mesures de vitesse et de pression ont été réalisées dans le régime laminaire. Ces mesures ont permis de calculer les contraintes pariétales  $\sigma_w$  et d'obtenir les courbes de comportement rhéologique en conduite ( $f(U) = \sigma_w$ ) pour chaque émulsion étudiée, ce qui a permis de comparer les mesures en écoulement et celles en rhéomètre mais aussi de voir l'effet de la concentration de la phase dispersée (eau) sur le comportement des émulsions Pickering. Une étude détaillée de l'évolution de profils de vitesse pour les différentes concentrations, avec notamment une comparaison des résultats en écoulement avec les paramètres du modèle de Herschel-Bulckley, extraits des mesures en rhéomètre, a été présentée (Fig. 4).

D'autre part, la stabilité des émulsions à court, moyen et à long terme a été étudiée, en comparant les profils de vitesse à l'équilibre avant et après le repos. Il a été constaté qu'après des temps de repos allant de quelques minutes à quelques jours, une homogénéisation, en écoulement, de 1 min est suffisante pour atteindre l'équilibre structurel. Pour de plus longues périodes de repos, une légère diminution de la contrainte seuil et de la viscosité a été remarquée. En général, de faibles variations ont été constatées au niveau du comportement mécanique des émulsions Pickering même après de longs temps de repos (jusqu'à une année), une caractéristique très attractive pour de diverses applications industrielles.

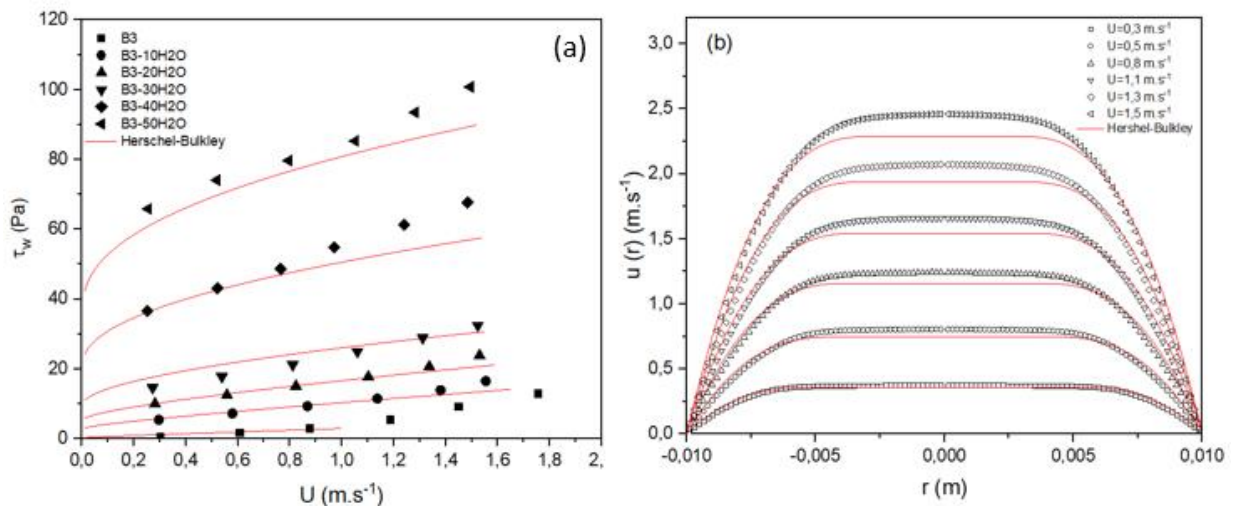


Fig. 4 Comparaison des résultats rhéologiques (ligne continue) et des résultats en écoulement (symboles). (a) : l'évolution de la contrainte pariétale en fonction de la vitesse. (b) : les profils de vitesse pour une émulsion Pickering à 30 wt% d'eau.

## **Chapitre 5 : Comportement Rhéologique et en Ecoulement des Emulsions Pickering à Hautes Concentrations d'eau.**

La dernière partie de cette thèse, a été consacrée pour l'étude en écoulement des émulsions Pickering concentrées (concentrations massiques en eau de 60 % à 80%), présentant des instabilités au repos. Ce chapitre est une continuation du Chapitre 4 qui a comme but de comprendre les mécanismes structuraux assurant la stabilité dynamique des émulsions Pickering concentrées.

Les émulsions concentrées sont celles qui nécessitent une circulation continue pour rester « stables ». Comme leur stabilité dynamique exige des taux de cisaillement élevés, les mesures rhéologiques ne sont pas possibles à cause des effets importants du glissement aux parois. En outre, en raison de leur atténuation moyenne élevée, la seule mesure de vitesse représentée, dans ce chapitre, est la vitesse maximale, qui est la valeur de vitesse au centre de la conduite. Des discussions détaillées de chacun des phénomènes d'instabilité rencontrés ont été présentées. Ces derniers sont schématisés dans la Fig. 5.

La partie expérimentale a commencé par une identification des conditions de stabilité de chaque concentration, ce qui a permis d'étudier leur comportement rhéologique et de le comparer avec celui des émulsions stables (Chapitre 4). Nous avons constaté que les courbes d'écoulement des émulsions concentrées suivent, aussi bien, le modèle rhéologique de Herschel-Bulckley, et la courbe de la contrainte seuil en fonction de la concentration d'eau a montré une concentration critique autour de B3-60H<sub>2</sub>O. De plus, nous avons pu identifier les conditions expérimentales menant à l'instabilité, ce qui nous a permis de discuter les causes et les phénomènes structurels responsables de ce comportement. Trois comportements ont été identifiés :

- Un pic de contrainte pariétale au démarrage, que nous avons expliqué par la présence de 2 fluides différents en contact avec la paroi de la conduite : des poches d'eau libre et des agrégations d'émulsions stables.
- Un glissement à la paroi, à faibles vitesses d'écoulement, dû à la présence d'un film d'eau libre à la paroi de la conduite.
- Un comportement inattendu de l'émulsion B3-65H<sub>2</sub>O, qui ne se stabilise qu'à des vitesses de circulation très élevées et de longues périodes de circulation continue.

Enfin, nous avons montré que le changement structurel observé autour de la concentration critique (60%) n'est pas lié au phénomène d'inversion de phase mais à une coexistence de deux phases immiscibles : une émulsion eau-dans-huile stable et une phase d'eau libre (Fig. 5).

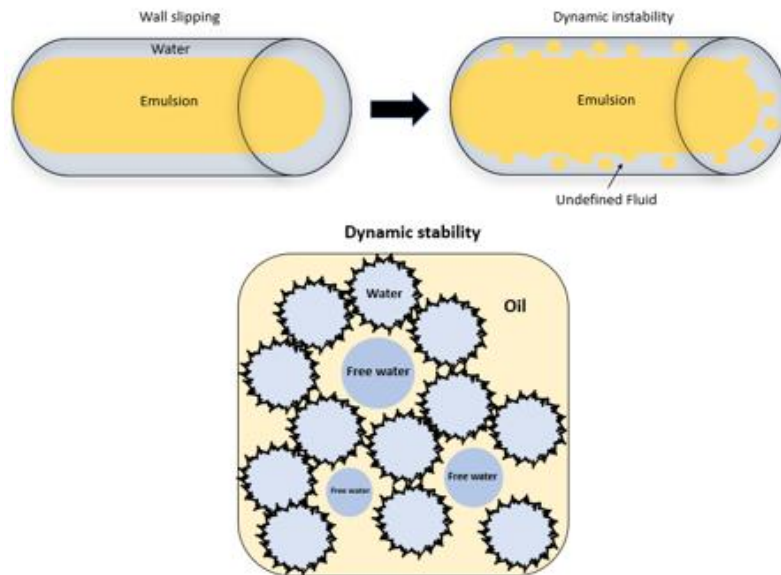


Fig. 5 Représentation graphiques des phénomènes d'instabilité et de stabilité dynamiques.

### Conclusions et Perspectives :

Le comportement mécanique des suspensions d'argile modifiée et des émulsions de type Pickering a été étudié dans le but de déterminer leur potentiel d'être utilisée comme base pour les fluides de forage à émulsion inverse. Dans ce qui suit, nous présentons les principales conclusions tirées de cette étude expérimentale :

- Le comportement mécanique des émulsions Pickering est principalement contrôlé par les interactions entre les particules solides, présentes sur les interfaces huile-eau, et leur concentration dans la phase continue.
- Le système d'émulsification que nous avons proposé dans ce travail a démontré sa capacité à préparer de grands volumes d'émulsions Pickering, très stables dans le temps, voire irréversibles.

- Les émulsions étudiées ont présenté un comportement en conduite comparable à celui des fluides de forage à émulsion inverse. De plus, nous avons pu préparer des émulsions stables avec des concentrations d'eau allant jusqu'à 45% (Annexe 2). Par conséquent, l'objectif principal de cette thèse, étant d'optimiser la composition d'émulsions Pickering à hautes fractions d'eau a été atteint avec succès.

Ce travail pourrait être complété par une étude approfondie de la microstructure des suspensions d'argile modifiée et leur influence sur le comportement des émulsions Pickering. Aussi, l'étude de l'influence de divers paramètres tels que la température, le pH, l'angle de contact des particules solides et la composition de la phase continue sur le comportement mécanique des émulsions pourrait expliquer les phénomènes d'instabilité présents à hautes concentrations d'eau.

Deux travaux ont été publiés dans le cadre de cette thèse :

Merad, B., Bekkour, K., Francois, P., Gareche, M., Lawniczak, F., 2021. Rheological and Flow Behavior of Water-in-Oil Pickering Emulsions Stabilized with Organo-Hectorite clay. J. Pet. Sci. Eng. 108780. <https://doi.org/10.1016/j.petrol.2021.108780>

Merad, B., Bekkour, K., Francois, P., Gareche, M., Lawniczak, F., 2021. Rheological and Flow Behavior of Water-in-Oil Pickering Emulsions Stabilized with Organo-Hectorite clay. J. Pet. Sci. Eng. 108780. <https://doi.org/10.1016/j.petrol.2021.108780>

**CONVERSION TABLE: FROM MASS TO VOLUME WATER CONCENTRATION**

<b>Emulsion</b>	<b>Water mass concentration (wt%)</b>	<b>Water volume concentration (%)</b>
<b>B3</b>	0	0
<b>B3-10H2O</b>	10	8,16
<b>B3-20H2O</b>	20	16,67
<b>B3-30H2O</b>	30	25,53
<b>B3-40H2O</b>	40	34,78
<b>B3-50H2O</b>	50	44,44
<b>B3-60H2O</b>	60	54,55
<b>B3-65H2O</b>	65	59,77
<b>B3-70H2O</b>	70	65,12
<b>B3-75H2O</b>	75	70,59
<b>B3-80H2O</b>	80	76,19

Water volume concentrations were calculated using the following equation:

$$[H_2O] (\%) = \frac{[H_2O] (wt\%)*100}{[H_2O] (wt\%)+\frac{100-[H_2O] (wt\%)}{\rho_g}} \quad A1.1$$

with:  $[H_2O] (\%)$  being the volume concentration of water,  $[H_2O] (wt\%)$  being the mass concentration of water, and  $\rho_g$  being the density of gasoil ( $\rho_g = 0,8 \text{ kg.l}^{-1}$ )









